KINETICS OF THE METHANE-STEAM REFORMING PROCESS

A THESIS SUBMITTED BY

SUHA ATAMER

FOR THE DEGREE OF DOCTOR OF PHILOSOPHY

AUGUST 1972

THE UNIVERSITY OF ASTON IN BIRMINGHAM

DEPARTMENT OF CHEMICAL ENGINEERING

ACKNOWLEDGEMENTS

It is a pleasure to acknowledge the following debts of gratitude:

The first is to Mr. A.R. Cooper, my supervisor, for the many long hours of consultation and his support throughout.

I am specially indebted to Professor G.V. Jeffreys for giving me the opportunity to work in the research school of the Department of Chemical Engineering.

I wish to thank my colleagues at the Middle East Technical University, Ankara, for their assistance in willingly taking over my teaching work for my three years leave of absence.

I am also grateful to U.N.E.S.C.O. for the financial support which made this investigation possible, and to Miss E. Czaykowska of the British Council for her efforts in all aspects of the programme organisation.

Thanks are also due to Mr. N. Roberts, Mr. M. Lee, and the technical staff for assistance during the construction of the apparatus.

I would also like to express my sincere appreciation to my wife for her endless encouragement and patience during these last few years.

Finally, I am indebted to Miss N.P. Freeman, for the excellent production of the thesis which she willingly completed in a very short time.

CONTENTS

SUMMARY

A thermodynamic study of hydrocarbon-steam systems has been made and a generalised digital computer program capable of predicting equilibrium composition and gas yields for a variety of plant operation has been developed. In particular the program has been used to define the carbon deposition boundaries for a range of hydrocarbons as a function of temperature, pressure, and steam to hydrocarbon ratio.

A commercial hydrocarbon reforming catalyst (I.C.I. 46-1) has been used for the kinetic study. Experimental determinations of catalyst surface area and pore size distribution and of reaction rates over rod catalyst for a range of temperatures, pressures and steam to methane ratios have been made. In the analysis of the results consideration has been given to the various steps which might control the rate of reaction. Having established the transition region at which the gas film diffusion resistance ceased, subsequent experiments were made under conditions of negligible bulk phase mass transfer limitations. Although no exact evaluation of the catalyst's effectiveness factor was performed, it was inferred that its value could not be greater than 0.1 and hence, as would be expected from the determined pore sizes, there is appreciable pore diffusion resistance. Experiments over a range of pressure and initial reactant concentrations provided evidence that adsorption of none of the reactants was rate controlling. Two semi-empirical expressions were developed for the initial rate of the reaction, and a further correlation as a 'best fit' of the integral rate data.

LIST OF FIGURES.

LIST OF TABLES.

LIST OF PLATES

CHAPTER I

INTRODUCTION

1. INTRODUCTION

The catalytic reforming of hydrocarbons in the presence of steam has developed in the past thirty years into one of the most important industrial processes. Its broad applications range from the production of hydrogen required for ammonia synthesis and hydrogenation processes to the use of the products as town gas. In consequence, the reforming reaction has been extensively investigated. However, in common with many heterogeneous catalytic reactions its mechanism seems to be extremely complex. The conclusions reached regarding the kinetic mechanism and rate of reactions involved appear to be largely contradictory and the determinations of detailed mechanisms inconclusive.

Direct comparison between the results obtained by individual workers is hardly ever possible, since information on the detailed nature and composition of the catalysts used and the applied operating parameters is rarely complete. Even if analytic figures were available, the complex effects of particle size and molecular surface structure caused by previous treatment of the catalyst or by the presence of some constituents as promoters for certain side reactions make comparison under widely different experimental conditions of doubtful validity.

The fundamental principles and the main technological aspects of various reforming processes are outlined by Padovani (118), Andrew (6,7), and well described in relevant literature (6,27,31, 34, 35, 40, 43, 48, 85, 164, 168).

The steam-hydrocarbon reforming reaction (oxygenolysis) may be represented by the overall stoichiometry :

$$C_pH_q + \alpha\, H_2O \longrightarrow a\, CH_4 + b\, H_2O + c\, CO + d\, CO_2 + e\, H_2$$

which, when carried out over an active nickel catalyst at high temperatures, is very fast giving complete conversion of the feedstock

with methane as the only surviving hydrocarbon in the product. The composition of the product stream is controlled by the equilibria of the two reactions:

Methane reforming $CH_4 + H_2O \rightleftarrows CO + 3\ H_2$

Water gas shift $CO + H_2O \rightleftarrows CO_2 + H_2$

which permit the exit compositions to be predicted entirely on the thermodynamic basis from a knowledge of operating conditions alone. It is claimed that in the production of hydrogen rich gas with modern catalysts, the heat transfer requirements for the highly endothermic reforming reaction is more of a limiting factor than catalyst activity, provided that poisoning effects are reduced to a low level (7, 164).

The primary object of the present work was a direct evaluation of some kinetic parameters in the steam reforming of methane at low temperatures (540 - 700^{o} C) and atmospheric pressure in an isothermal, integral flow reactor, using a commercial reforming catalyst developed and manufactured by Imperial Chemical Industries Ltd. It was hoped, as a further object, that some clarification of the existing discrepancies would be achieved.

CHAPTER 2

THE THERMODYNAMICS OF REFORMING

2.1 INTRODUCTION.

In spite of the conflicting results which have been obtained by many investigators to elucidate the kinetic mechanism of the hydrocarbon reactions with or without steam, in the presence or absence of a catalyst, the thermodynamic treatment of hydrocarbon-steam systems has led to unique conclusions which are of great value for industrial practice. The reasons for this fact are, in the first place, the very definite limitations and the exact nature of the thermodynamic method. Thus the thermodynamic analysis evaluates only the driving potentials for the chemical changes, but gives no information on the rate at which each reaction will proceed, nor does it offer any help in deciding which one of the group of possible reactions having similar potentials will be favoured. In addition to these limitations two assumptions must be made:

(i) the temperatures of the gas, the catalyst bed, and the inner walls of the reactor are identical and constant for a given region within the reactor

(ii) no matter what the space velocity or the reaction rates are the thermodynamic equilibrium corresponding to this temperature is attained.

In industrial practice, the second assumption is relevant because the reformed gas leaving reactors has in fact been found to have actual compositions which are very close to those corresponding to the simultaneous equilibria of the methane reforming reaction and the water gas shift reaction. This is true provided that there are no components in the feed which might have a poisonous effect on the catalyst nor any condition resulting in deposition of carbon on the catalyst surface causing a reduction in its activity.

2.2 POSSIBLE REACTIONS.

The thermodynamic aspects of the reforming, both for methane or light hydrocarbons as feedstock, have been studied by a number of researchers (50, 52, 79, 101, 104, 111, 121, 130, 131, 149, 154, 179). These studies cover:

(i) The free energy relationships of all plausible reactions and the use of the numerical value of the standard free energy change of each reaction as a criterion for its feasibility (179).

(ii) The elimination of the least probable and selection of the most probable reactions taking place under any set of conditions of interest to reforming (52, 53, 154, 179).

(iii) The derivation of equations for the equilibrium constants as functions of temperature for the relevant reversible reactions (52,179).

(iv) The calculation of equilibrium compositions based on ideal gas behaviour (31, 51,154), and also allowing for the fugacities of components present in the equilibrium mixture (101,179).

In the thermodynamic analysis of hydrocarbon reforming the approach common to all researchers is the listing of all simultaneous and consecutive reactions which may possibly take place. For the case of methane as feedstock, with the exception of equilibrium reaction (2), the following list is given by Dodge (52) and Somer (154):

$$CH_4 + H_2O \rightleftharpoons CO + 3H_2 \qquad (1)$$

$$CH_4 + CO_2 \rightleftharpoons 2CO + 2H_2 \qquad (2)$$

$$CH_4 + 2H_2O \rightleftharpoons CO_2 + 4H_2 \qquad (3)$$

$$CH_4 \rightleftharpoons C + 2H_2 \qquad (4)$$

$$2CH_4 \rightleftharpoons C_2H_6 + H_2 \quad (5)$$

$$C_2H_6 \rightleftharpoons C_2H_4 + H_2 \quad (6)$$

$$CO + H_2O \rightleftharpoons CO_2 + H_2 \quad (7)$$

$$C + H_2O \rightleftharpoons CO + H_2 \quad (8)$$

$$CO_2 + C \rightleftharpoons 2CO \quad (9)$$

$$CO_2 \rightleftharpoons C + O_2 \quad (10)$$

$$2CO \rightleftharpoons 2C + O_2 \quad (11)$$

$$H_2O \rightleftharpoons H_2 + \tfrac{1}{2}O_2 \quad (12)$$

In addition, Woodcock (179) has considered the following reactions:

$$C_2H_4 + 2\,H_2O \rightleftharpoons 2CO + 4H_2 \quad (13)$$

$$C_2H_2 + 2H_2O \rightleftharpoons 2CO + 3\,H_2 \quad (14)$$

$$C_2H_4 \rightleftharpoons 2C + 2\,H_2 \quad (15)$$

$$C_2H_2 \rightleftharpoons 2C + H_2 \quad (16)$$

If the hydrocarbon feed is light naphtha represented by the general formula C_pH_q, then the following four reactions have to be added to the above series:

$$C_pH_q + p\,H_2O \rightleftharpoons p\,CO + (\tfrac{q}{2} + p)\,H_2 \quad (17)$$

$$C_pH_q + 2pH_2O \rightleftharpoons p\,CO_2 + (\tfrac{q}{2} + 2p)H_2 \quad (18)$$

$$C_pH_q + \frac{(4p - q)}{4}\,H_2O \rightleftharpoons \frac{(4p + q)}{8}\,CH_4 + \frac{(4p - q)}{8}\,CO_2 \quad (19)$$

$$C_pH_q \rightleftharpoons m\,CH_4 + n\,H_2 + (p - m)\ \text{olefins.} \quad (20)$$

It must be noted, however, that since this list is concerned with the products which can be present at equilibrium, it does not include any of the radical forming reactions, although it is a well-established fact that the reforming reaction proceeds with the formation of certain radicals (methyl, methylene, etc.) some of which initiate chain reactions. In addition, reactions such as those between C_p H_q and steam are most unlikely to occur directly, since this would require the simultaneous and extremely improbable collision of (1 + p) molecules; in the case of heptane, for

example, $(1 + p) = 8$. Undoubtedly, the reactions of hydrocarbons heavier than methane must proceed in a sequence of formation and interaction of some intermediate products resulting ultimately in methane, carbon monoxide, carbon dioxide, hydrogen, and unreacted steam. The application of the standard free energy change concept as the criterion of the feasibility for any of the reactions listed above implicitly assumes that the intermediate products formed during the course of the reforming are so unstable and consumed at such a high rate that their concentrations at equilibrium are negligible in comparison with those of the main products. In fact, the results obtained in a number of investigations concerning the steam-reforming of naphtha justify this assumption. Schnell (146), for example, found that even at very short contact times, the steam-butane reaction at 600° C over an alkalised nickel catalyst gave only minute quantities of olefins, C_2H_4, along with the main components CH_4, CO, CO_2, H_2 and H_2O.

This complex system can be simplified to a certain extent by recognising that some of the reactions are not independent and can be eliminated on this basis; thus,

$$(2) = (1) - (7)$$

$$(3) = (1) + (7)$$

$$(8) = (7) + (9)$$

$$(11) = (10) + (9)$$

$$(4) = (1) - [(7) + (9)]$$

$$(15) = (13) - 2\,[(7) + (9)]$$

$$(16) = (14) - 2\,[(7) + (9)]$$

$$(5) + (6) = 2\,(1) - (13)$$

As a result of these relations, reactions (3), (8), (11), (4), (15), (16), and (6) can be eliminated. Hence, the reactions representing

the components which may be present at equilibrium in a steam-hydrocarbon system can be reduced to the following:

$$CH_4 + H_2O \rightleftarrows CO + 3\,H_2 \qquad (1)$$

$$2\,CH_4 \rightleftarrows C_2H_6 + H_2 \qquad (5)$$

$$CO + H_2O \rightleftarrows CO_2 + H_2 \qquad (7)$$

$$CO_2 + C \rightleftarrows 2\,CO \qquad (9)$$

$$CO_2 \rightleftarrows C + O_2 \qquad (10)$$

$$H_2O \rightleftarrows H_2 + \tfrac{1}{2}\,O_2 \qquad (12)$$

$$C_2H_4 + 2\,H_2O \rightleftarrows 2CO + 4\,H_2 \qquad (13)$$

$$C_2H_2 + 2\,H_2O \rightleftarrows 2CO + 3\,H_2 \qquad (14)$$

$$C_pH_q + p\,H_2O \rightleftarrows p\,CO + \left(\frac{q}{2} + p\right) H_2 \qquad (17)$$

$$C_pH_q + 2p\,H_2O \rightleftarrows p\,CO_2 + \left(\frac{q}{2} + 2p\right) H_2 \qquad (18)$$

$$C_pH_q + \frac{(4p - q)}{4} H_2O \rightleftarrows \frac{(4p + q)}{8} CH_4 + \frac{(4p - q)}{8} CO_2 \qquad (19)$$

$$C_pH_q \rightleftarrows m\,CH_4 + n\,H_2 + (p - m)\ \text{olefins} \qquad (20)$$

At this stage, a study of the standard free energy change of each reaction will give the necessary indication of its thermodynamic feasibility. The values for standard free energy changes of these reactions are listed in Table 2.1 for a temperature range relevant to the operating range for various steam-reforming processes where C_pH_q is represented by n - heptane.

The free energy change for a reaction

$$a\,A + b\,B + \ldots\ldots \rightleftarrows r\,R + s\,S + \ldots\ldots$$

is related to the equilibrium constant by the equation

$$\Delta G_T^o = - R_g T \ln K_a$$

where ΔG_T^o = the standard free energy change, cal/mole. of the reaction at temperature T ^oK

R_g = the gas constant, cal/(mole) (deg K)

T = the temperature of the mixture at equilibrium, ^oK

K_a = the equilibrium constant in terms of activities.

TABLE 2.1.

VALUES FOR STANDARD FREE ENERGY CHANGE (ΔG_T^o) *
(cal/mole)

Reaction	Temperature, °C					
	427 (700°K)	527 (800°K)	627 (900°K)	727 (1000°K)	827 (1100°K)	927 (1200°K)
(1)	+11,437	+ 5,516	- 479	- 6,522	- 12,573	- 18,644
(5)	+17,000	+17,020	+ 16,980	+ 16,910	+ 16,840	+ 16,750
(7)	- 3,058	- 2,219	- 1,413	- 632	+ 126	+ 862
(9)	+11,444	+ 7,185	+ 2,946	- 1,274	- 5,469	- 9,645
(10)	+94,496	+94,539	+ 94,578	+ 94,610	+ 94,637	+ 94,661
(12)	+49,912	+48,918	+ 46,344	+ 43,731	+ 41,100	+ 38,445
(13)	- 5,904	-14,558	- 23,288	- 32,061	- 40,846	- 49,656
(14)	-27,726	-33,246	- 38,816	- 44,416	- 50,025	- 55,655
higher** hydro-carbons						
(17)	-11,378	-58,938	- 94,699	-136,562	-178,421	- 220,331
(18)	-32,784	-68,471	- 104,590	-140,986	-177,539	- 214,297
(19)	-78,863	-86,605	- 94,195	-101,672	-109,136	- 116,557
(20)	- 5,956	-20,582	- 35,184	- 49,757	- 64,301	- 78,821
carbon reactions						
(4)	+ 3,050	+ 550	- 2,010	- 4,610	- 7,220	- 9,850
(8)	+ 8,386	+ 4,966	+ 1,533	- 1,906	- 5,343	- 8,783
(9)	+11,444	+ 7,185	+ 2,946	- 1,274	- 5,469	- 9,645
(15)	-22,676	-24,490	- 26,354	- 28,249	- 30,160	- 32,090
(16)	-44,498	-43,178	- 41,882	- 40,604	- 39,339	- 38,089

* Reference states for components are taken as 25° C and 1 atm abs. pressure, water being in the vapour state. Carbon, where involved, is in the form of β- graphite.

** $C_p H_q$ is n-heptane

References: (156, 165, 179).

and

$$K_a = \frac{(^aR)^r\ (^aS)^s\ \ldots.}{(^aA)^a\ (^aB)^b\ \ldots..}$$

Accordingly, values of $\Delta G_T^o \leqslant 0$ will result in such values of K_a that the concentrations of the products at equilibrium are high or finite quantities. On this basis, Dodge (53) has suggested approximate, but useful criteria for the feasibility of chemical reactions and considered reactions having a standard free energy change greater than + 10,000 cal/mole as unfavourable for the given temperature levels.

It can be seen from Table 2.1 that reactions (10) and (12) have extremely high positive standard free energy change values which make the presence of the respective reaction products at equilibrium almost impossible. In fact, Mayland and Hays (104) have calculated the concentration of oxygen in the equilibrium mixture in a thermodynamic study of synthesis gas production from methane by the autothermic partial oxidation process, and found that at 21.4 atm abs. and 1093^o C, a synthesis gas comprising 200 moles of hydrogen, 100 moles of carbon monoxide, 5 moles of carbon dioxide, 2.3 moles of steam, and 3.7 moles of methane could contain only (3.9) (10^{-11}) moles of oxygen.

Reaction (5) exhibits a ΔG_T^o value of + 17,020 cal/mole at 527^o C which would correspond to finite, but exceedingly small quantities of ethane in the equilibrium mixture. Due to the thermodynamic instability of ethane in the presence of steam and an active catalyst, these minute concentrations can readily be consumed to give CO and H_2. Therefore, reaction (5) can also be eliminated.

The reactions of hydrocarbons higher than methane with steam are represented by reactions (13), (14), (17), (18), (19), and (20). Although they do not describe the intermediate steps and the mode of degradation of the hydrocarbon molecule before equilibrium, thermodynamically they are equally valid. Since reaction (18) is

equivalent to reactions (17) and (7) taking place in succession, it does not need further consideration. A comparison of the standard free energy changes involved in these reactions (n - $C_7 H_{16}$ is selected as the hydrocarbon) with that of the methane reforming one will immediately lead to the conclusion that within the temperature region pertinent to reforming processes, methane can be the only stable hydrocarbon in equilibrium with steam and the other reaction products. It is worthy of note that the magnitudes of the standard free energy changes of reactions (17) and (19) are of the same order. They are even almost equal at 627°, namely - 94,699 and - 94,195 cal/mole, respectively. This fact underlies one of the main reasons for the diversity of opinion concerning the primary reaction which exists in the field of hydrocarbon reforming. Since a discussion on a solely thermodynamic basis is not sufficient to identify the intermediate steps involved in the approach to the equilibrium state, it is not possible to assign one of them as the preferred reaction. All three of the following extreme assumptions could equally well be justified:

(1) The reaction $C_p H_q$ proceeds stepwise producing at every step carbon monoxide and hydrogen and a lower hydrocarbon and representing a steady degradation of hydrocarbon until methane remains at equilibrium concentration:

$$C_p H_q + H_2O \rightleftarrows CO + H_2 + C_{p-1} H_{q-2} \qquad (17\text{-a})$$

$$C_p H_q + (p-1) H_2O \rightleftarrows (p-1) CO + \left[(p-1) + \left(\frac{q-4}{2}\right)\right] H_2 + CH_4 \qquad (17\text{-b})$$

Simultaneously, carbon monoxide and steam equilibrate according to the water gas shift reaction.

(2) The hydrocarbon reacts with steam in an identical manner to that indicated above, but methane is being formed not as the final product of hydrocarbon breakdown, but rather by synthesis from carbon monoxide and hydrogen (125).

(3) The hydrocarbon is completely decomposed by steam to give methane and carbon dioxide, i.e. reaction (19), called the initial methanation reaction, takes place, and the methane so formed then reacts with further steam to yield carbon monoxide and hydrogen (100).

Giving preference to any one of them on the basis of their respective standard free energy changes or their endothermic or exothermic character would be thermodynamically unsound.

Reaction (20) represents the general cracking reaction of a hydrocarbon giving methane, hydrogen and unsaturated hydrocarbons as products. For the case of heptane, the values of standard free energy change of the reaction at relevant temperatures favour high concentrations of products at equilibrium.

The reactions which form carbon at equilibrium merit separate consideration since they cause the undesirable deactivation of catalyst. The deposition of carbon on active sites may be reversible (5, 16, 17, 31) but continuous formation resulting in agglomeration of the carbon as deposited is considered to be irreversible, and thus, detrimental to the catalyst bed, and reforming yields (26). Carbon can be formed by the pyrolysis of hydrocarbons [reactions (4), (15), and (16)], by the heterogeneous water gas reaction (8), the Boudouard reaction (9), and by reactions (10) and (11). Reaction (10) has been eliminated due to the very high positive value of the standard free energy change. Reaction (11) has been shown not independent within the group of possible reactions; moreover, its standard free energy change is of the same order of magnitude as reaction (10). In considerations of the thermodynamic equilibrium, all three of the pyrolysis reactions (4), (15), (16), together with the heterogeneous water gas reaction (8) can be omitted, since they are not independent.

Consequently, the only reaction remaining and the one which is responsible for the deposition of carbon at equilibrium is the Boudouard reaction (9).

However, attention has to be drawn to the fact that within the temperature range 527 - 827° C, the standard free energy change values of reactions (8), (4), and more particularly (15) and (16), favour carbon deposition. It is not inconceivable therefore, that for a methane-steam system approaching the equilibrium state, carbon may be deposited according to one of the carbon-forming reactions, but consumed either by another in the reverse direction or by the Boudouard reaction. Whether there will be an accumulation of carbon on the catalyst surface at any particular temperature will depend upon the kinetics and relative rates of the individual reactions.

2.3 EQUILIBRIUM COMPOSITION AND CARBON FORMATION BOUNDARIES.

It has been established in the previous section that an analysis of the steam-hydrocarbon system on a thermodynamic basis leads to the general conclusion that the composition of the reformed gas at equilibrium is governed by the two reactions:

$$CH_2 + H_2O \rightleftarrows CO + 3\,H_2 \qquad (1)$$

$$CO + H_2O \rightleftarrows CO_2 + H_2 \qquad (7)$$

Hence, the mole fractions of methane, carbon monoxide, carbon dioxide, hydrogen, and unreacted steam can be calculated by the simultaneous solution of five equations, i.e. three element balances and two equilibrium relationships. The gas temperature, the pressure, the steam : hydrocarbon ratio and/or carbon dioxide : hydrocarbon ratio in the feed, the hydrogen : carbon atomic ratio of the hydrocarbon, and hydrogen : carbon monoxide ratio of the product gas are the parameters in such calculations.

The results thus obtained can also be used to define the carbon deposition boundaries for sets of operating conditions at any temperature simply by comparing the value of p^2_{CO}/p_{CO_2} corresponding to the equilibria of reactions (1) and (7) with the equilibrium constant of the Boudouard reaction at that temperature (31, 47, 52, 79, 101, 130, 154, 155, 179). When the calculated value of p^2_{CO}/p_{CO_2} is less than the thermodynamic equilibrium constant, carbon will not be in equilibrium with the system. If the value is greater than the constant, then the system itself is not at equilibrium, and carbon will start to form. The carbon deposition boundary is the locus of the points when carbon first appears in equilibrium with the system. Since the system is not in equilibrium when carbon is being deposited, it is, of course, not then possible to predict the composition of the reformed gas leaving the flow reactor.

Compositions have been developed from the computer solution of algebraic equations with a variety of parameters. Thus, Reitmeier and co-workers (130) gave a series of equations and plots which make possible the selection of reacting mixtures of methane, steam and/or carbon dioxide to produce synthesis gas for a preset ratio of H_2:CO, thereby preventing the danger of carbon deposition on the catalyst. However, in order to simplify the computation, they assumed that no methane remained unreacted in the synthesis gas. Since this condition could never actually exist, they developed another equation for estimating the moles of methane remaining unreacted. According to the authors, the error involved in the estimation depended on the quantity of unreacted methane present, and varied between 1 and 10% ; there is, however, no correction made for the effect which this error would have on the percentage of the other constituents. Nevertheless, they claimed that the results obtained from pilot plant scale work,

closely confirmed their theoretical findings. Holland and Wan (79) have combined in their computational investigation the methane-steam reforming in the primary reformer and the partial oxidation taking place in the secondary reformer and presented in graphical form the range of permissible temperatures for carbon-free operation at one atm abs. pressure. Somer (154) has tabulated the equilibrium gas composition of the steam-methane system for the following range of parameters :

H_2O : CH_4 molar ratio	:	1.5, 2.0, 2.5, 3.0, 4.0, 5.0;
temperature	:	750^o, 800^o, 850^o, 900^o, 950^o C;
pressure	:	2 and 11 psig ;

and included the possibilities of carbon deposition and suppression of methane slip by using CO_2 recycle.

A graphical trial-and-error method for the simultaneous solution of equations has been developed by Lihou (101) for the reforming of paraffinic hydrocarbons ($C_n H_{2n+2}$) with steam. He also considered the correction necessary when fugacities of the components were used instead of partial pressures, and found that even at the worst possible conditions for a deviation from ideal gas behaviour, i.e. at 127^o C and 50 atm pressure, the correction for non-ideality was insignificant and could be neglected. This was supported by Woodcock (179) who performed digital computational solutions for methane-steam and heptane-steam reactions; for the case of methane reforming with steam : methane molar ratio of 3 at 50 atm pressure and 527^o C, he obtained the following differences in gas composition:

	Solution using partial pressures	Solution using fugacities
CO, %	0.88	0.88
CO_2, %	4.24	4.20
CH_4, %	17.03	17.07
H_2, %	21.28	21.14
H_2O, %	56.57	56.71

A series of parametric plots are also given by Bridger and Chinchen in the recently published Catalyst Handbook (31) for steam-reforming of methane and light naphtha, although the molecular formula of the latter is not indicated. The authors point out that over the range of parameters plotted, the gas compositions can be read from the graphs to within ± 5% for any combination of temperature, pressure and steam-hydrocarbon ratio.

A number of authors have applied the same calculation principles to oxygen-hydrocarbon and air-hydrocarbon systems (79, 104, 111, 131). Montgomery et al. (111) have studied the equilibrium stoichiometry of synthesis gas production by the partial oxidation of methane with pure oxygen for isothermal operation (727 - 1227° C). For given H_2 : CO ratios in the exit gas they calculated the minimum O_2 : CH_4 ratio in the feed to produce a maximum yield of synthesis gas and established the carbon formation boundaries corresponding to the respective operating conditions. Mayland and Hays (104) analysed the adiabatic oxygen-methane and air-methane autothermic systems at different feed ratios, and defined the carbon deposition region for 1000° F preheat temperature, 1600 - 2500° F equilibrium temperatures, and 1-20 atm pressures.

In all these works, with the exception of Woodcocks (179), the Boudouard constant for any temperature level has been calculated or taken from published thermodynamic data based on standard free

energies of CO, CO_2 and β-graphite. However, it has been pointed out by Dent et al.(47) that the numerical values of the Boudouard constant were not identical with the constants obtained by direct equilibrium measurements over a nickel containing catalyst at different temperatures and different initial CO : CO_2 ratios. The functional relationship between temperature and equilibrium constant is reproduced in Fig. 2.1, curve 2, which shows that towards the lower end of the temperature range, there is an increasing difference between the experimentally obtained values of p_{CO_2}/p^2_{CO} and those calculated from β - graphite (curve 1).

In addition to Dent's work, Nicklin and Whittaker (115) have found that the p_{CO_2}/p^2_{CO} ratio at the point of carbon formation is even lower with uranium oxide as a constituent of the catalyst (Fig. 2.1, curve 3). These differences indicate that the initiation of the carbon deposition on the catalyst requires a still higher concentration of carbon monoxide then is predicted by the thermodynamic Boudouard equilibrium, and is equivalent to a reduction in the minimum steam : hydrocarbon ratio necessary to prevent the formation of carbon.

From this review of the relevant literature it may be concluded that the majority of the data available at present for the prediction of the equilibrium gas composition and the carbon laydown in steam/carbon dioxide reforming or partial oxidation processes are restricted to methane or some saturated aliphatics as feedstocks. Due to the large number of parameters affecting the calculation, it is not possible to obtain the results and ascertain the optimum operating conditions from generalised graphs which would eliminate elaborate calculations. The use of three dimensional graphs (79) for methane or parametric plots for saturated hydrocarbons (101) have the major drawback of having

Fig: 2.1

The Equilibrium Constants of the Boudouard Reaction

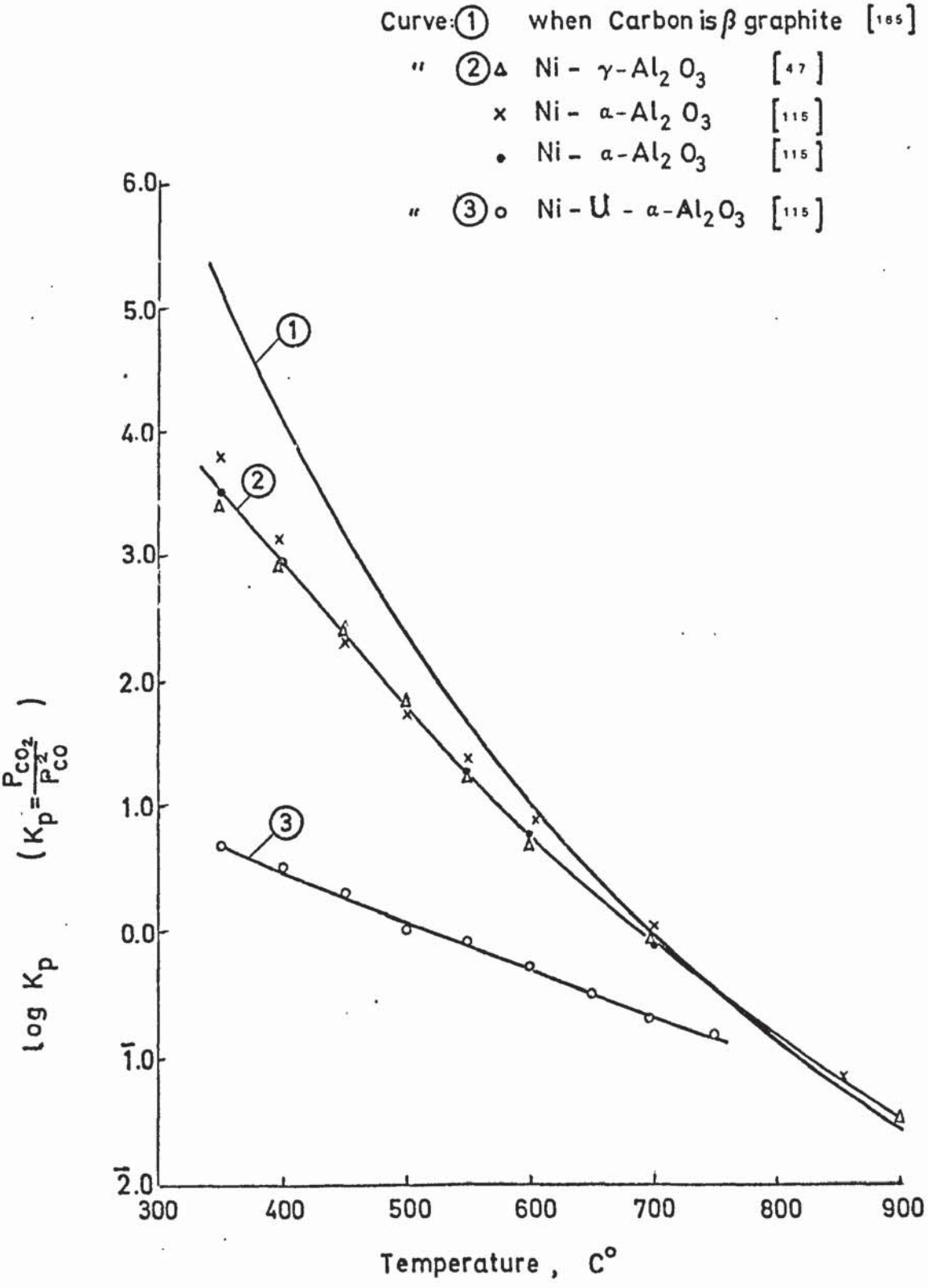

limited accuracy and applicability.

It is the opinion of the author that these calculations have to be carried our for each type of feedstock and for a given range of operating variables. Subsequently the optimum conditions for the process can be selected from an analysis of the results obtained. Therefore it has been considered worthwhile to develop a generalised machine-computational procedure to cover the use of any kind of hydrocarbon (C_pH_q) as feedstock in combination with any type of oxidising agent at any temperature and pressure. The method developed is outlined briefly in the next section.

2.4 MATHEMATICAL TREATMENT.

The calculation of the gas composition at equilibrium for any type of process and for any set of operating variables can be carried out according to the following development:

Feedstock	:	A hydrocarbon whose molecular formula is represented by C_pH_q
Oxidising Agent	:	Steam and/or carbon dioxide and/or oxygen or air
Equilibrium temperature	:	t^oC
Operating pressure	:	P_T atm abs.

(H_2O : $C_p H_q$) molar ratio in the feed: α

(CO_2 : $C_p H_q$) molar ratio in the feed: β

(O_2 : $C_p H_q$) molar ratio in the feed: γ

Then taking 1 mole of hydrocarbon feed as the basis of calculation, the input is:

hydrocarbon	:	1 mole
steam	:	α moles
carbon dioxide	:	β moles
oxygen	:	γ moles

For carbon-free operation, let the output be:

carbon monoxide	:	a moles,
carbon dioxide	:	b moles,
methane	:	d moles,
hydrogen	:	c moles,
steam	:	e moles.

The element balances give the following relations:

C-atoms balance: $p + \beta = a + b + d$ (2.1)

H_2-mole balance: $\frac{1}{2} q + \alpha = 2d + c + e$ (2.2)

O-atoms balance : $\alpha + 2\beta + 2\gamma = a + 2b + e$ (2.3)

From Equations (2.1), (2.2), and (2.3), c, d, and e can be eliminated, and the number of moles of hydrogen, methane, and unreacted steam in the reformed gas expressed in terms of the moles of oxides of carbon, a and b. Thus,

H_2 : $c = \frac{1}{2}q - 2p - 4\beta - 2\gamma + 3a + 4b$ (2.4)

CH_4: $d = p + \beta - a - b$ (2.5)

H_2O : $e = \alpha + 2\beta + 2\gamma - a - 2b$ (2.6)

The total number of moles of reformed gas is then

$$N_T = \tfrac{1}{2}q - p + \alpha - \beta + 2a + 2b \qquad (2.7)$$

The equilibrium constants of reactions (1) and (7) based on partial pressures of the constituents provide the simultaneous equations to be solved. By definition:

$$K_1 = \frac{P_{CO}\ P_{H_2}^{3}}{P_{CH_4}\ P_{H_2}} \quad \text{and} \quad K_7 = \frac{P_{CO_2}\ P_{H_2}}{P_{CO}\ P_{H_2O}}$$

Assuming ideal gas behaviour for all components, and using Dalton's Gas Law, the final form of the equations can be written as follows:

$$K_1 = \frac{(a)\ (\frac{1}{2}q - 2p - 4\beta - 2\gamma + 3a + 4b)^3\ (P_T^{\,2})}{(p + \beta - a - b)\ (\alpha + 2\beta + 2\gamma - a - 2b)\ (N_T)^2} \qquad (2.8)$$

$$K_7 = \frac{(b)\ (\frac{1}{2}q - 2p - 2\gamma - 4\beta + 3a + 4b)}{(a)\ (\alpha + 2\beta + 2\gamma - a - 2b)} \qquad (2.9)$$

The roots $\bar{a}$ and $\bar{b}$ of the simultaneous equations (2.8) and (2.9) can be obtained by applying Newton's iterative technique (96) which starts with an initial guess for $\bar{a}$ and $\bar{b}$, and converges through the iteration to the desired root in a finite number of steps. Writing both equations in the form : $F(a, b) = 0$ and $G(a, b) = 0$ and expanding the functions in a Taylor series in terms of arbitrary initial estimates $a^{(0)}$ and $b^{(0)}$ of the exact roots $\bar{a}$ and $\bar{b}$, there results:

$$F(\bar{a}, \bar{b}) = 0 = F(a^{(0)}, b^{(0)}) + (\bar{a} - a^{(0)}) \frac{\delta}{\delta a} F(a^{(0)}, b^{(0)}) + (\bar{b} - b^{(0)}) \frac{\delta}{\delta b} F(a^{(0)}, b^{(0)}) + \ldots\ldots\ldots$$

and

$$G(\bar{a}, \bar{b}) = 0 = G(a^{(0)}, b^{(0)}) + (\bar{a} - a^{(0)}) \frac{\delta}{\delta a} G(a^{(0)}, b^{(0)}) + (\bar{b} - b^{(0)}) \frac{\delta}{\delta b} G(a^{(0)}, b^{(0)}) + \ldots\ldots\ldots$$

Defining $\bar{a} - a^{(0)} = \Delta_a$ and $\bar{b} - b^{(0)} = \Delta_b$ as the differences between the desired roots and the initial estimates, and truncating the Taylor series after the first derivative:

$$F(a^{(0)}, b^{(0)}) + \Delta_a \frac{\delta}{\delta a} F(a^{(0)}, b^{(0)}) + \Delta_b \frac{\delta}{\delta b} F(a^{(0)}, b^{(0)}) = 0 \qquad (2.10)$$

$$G(a^{(0)}, b^{(0)}) + \Delta_a \frac{\delta}{\delta a} G(a^{(0)}, b^{(0)}) + \Delta_b \frac{\delta}{\delta b} G(a^{(0)}, b^{(0)}) = 0 \qquad (2.11)$$

These simultaneous equations are solved for Δ_a and Δ_b corresponding to $a^{(0)}$ and $b^{(0)}$, and the iteration process can be set up as:

$$a^{(r+1)} = a^{(r)} + \Delta_a^{(r)} \qquad (2.12)$$

$$b^{(r+1)} = b^{(r)} + \Delta_b^{(r)} \qquad (2.13)$$

Thus for the present situation:

$$F = F(a, b) = 0 = (a)(c)^3 (P_T)^2 - (K_1)(d)(e)(N_T)^2 \qquad (2.14)$$

$$G = G(a, b) = 0 = (b)(c) - (K_7)(a)(e) \qquad (2.15)$$

The partial derivatives of F(a, b) with respect to a and b are:

$$FA = [c^3 + 9ac^2](P_T)^2 - (K_1)[4de(N_T) - (d + e)(N_T)^2] \qquad (2.16)$$

$$FB = [12ac^2 (P_T)^2] - (K_1)[4de(N_T) - (2d + e)(N_T)^2] \qquad (2.17)$$

The partial derivatives of G(a, b) with respect to a and b are:

$$GA = 3\,b - (K_7)\,(e - a) \tag{2.18}$$

$$GB = (c + 4\,b) + (K_7)\,(2a) \tag{2.19}$$

From the simultaneous solutions of Equations (2.10a) and (2.11a):

$$F + \Delta_a FA + \Delta_b FB = 0 \tag{2.10a}$$

$$G + \Delta_a GA + \Delta_b GB = 0 \tag{2.11a}$$

Δ_a and Δ_b are calculated to give:

$$\Delta_a = \frac{(F)\,(GB) - (G)\,(FB)}{(FB)\,(GA) - (FA)\,(GB)} \tag{2.20}$$

and

$$\Delta_b = \frac{(G)\,(FA) - (F)\,(GA)}{(FB)\,(GA) - (FA)\,(GB)} \tag{2.21}$$

As can be seen from the mathematical development, this treatment can be applied to a wide range of hydrocarbon feedstocks. The composition of the reformed gas can also be calculated for hydrocarbons higher than methane in the special case of their incomplete decomposition. This case would correspond to operation at extremely high space velocities, where the reaction rate for the breakdown of the hydrocarbon to give methane and other reaction products is rather low compared with the rates of equilibration reactions (1) and (7). For setting up the computation scheme, the following assumptions have to be made:

(i) The reacting system is at equilibrium with respect to reactions (1) and (7),

(ii) The only hydrocarbon present in the reformed gas besides methane is unreacted feedstock $C_p H_q$.

Since the unreacted feedstock is now another unknown, a further parameter must be introduced for the solution. This parameter is taken as the moles of hydrocarbon in the feed which is reacted to give CO, CO_2, and CH_4 per mole of hydrocarbon feed, and called conversion, x. Choosing 1 mole of hydrocarbon fed as the basis of calculation, the equilibrium gas will be composed of:

carbon monoxide : a moles

carbon dioxide : b moles

methane : d moles

hydrogen : c moles

unreacted steam : e moles

unreacted hydrocarbon C_pH_q : g moles

The element balances are:

C - atom balance $p + \beta = a + b + d + (p)\ (g)$ (2.1a)

H_2 - mole balance $\frac{1}{2}q + \alpha = 2\,d + c + e + (\frac{1}{2}q)\ (g)$ (2.2a)

O - atom balance $\alpha + 2\beta + 2\gamma = a + 2\,b + e$ (2.3a)

where $g = (1 - \frac{x}{100})$. (2.22)

From these balance equations:

H_2 : $c = (\frac{1}{2}q - 2\,p)\ (\frac{x}{100}) - 4\beta - 2\gamma + 3a + 4\,b$ (2.4a)

CH_4 : $d = p\ (\frac{x}{100}) + \beta - a - b$ (2.5a)

H_2O : $e = \alpha + 2\beta + 2\gamma - a - 2\,b$ (2.6a)

2.5 COMPUTER PROGRAM.

The equilibrium gas compositions have been established by means of a computer program written in Fortran - IV and run on the ICL - 1905 computer at the University of Aston. A print-out of the program and of the results is given in Appendix(A-2.1). The results apply to a hydrocarbon C_pH_q, where p = 1.0 and q = 2.0 which would represent any feedstock $C_n\ H_{2n}$ or $(CH_2)_n$ being equivalent to $(CH_{q/p})_p$. The only difference in the results would be that for p = 1.0, the steam : hydrocarbon molar ratio, α , would become moles of steam per atoms of carbon in the hydrocarbon, α' . While there would be no change in composition of the reformed gas, the moles of product gases, printed-out in terms of per atom of carbon in the feedstock, would have to be multiplied by (p) to obtain the moles of product gases per mole of hydrocarbon fed.

The program as given in Appendix (A-2.1) consists of four loops, one for the iteration, and three for pressure, temperature, and steam:

hydrocarbon ratio, respectively. Other parameters such as CO_2 : hydrocarbon molar ratio and/or O_2 : hydrocarbon molar ratio in the feed, could be added to the program as additional loops or as input data. Since the execution of the program for ten pressure and eight temperature levels with nine steam : hydrocarbon ratios requires more than 14,000 of lines of output, the cases of steam-carbon dioxide - oxygen - hydrocarbon mixtures have not been separately calculated. The applicability of the program can easily be extended to any $C - H_2O - O_2 - CO - CO_2 - H_2$ system, since the relevant equilibration reactions remain the same. However, the primary objective of the computer program was to define the boundaries of equilibrium - carbon deposition over a given range of operating parameters.

The computer results comprised the following information:

(i) Operating variables

(ii) Per cent composition of dry gas

(iii) Moles of products per mole of hydrocarbon fed

(iv) Check of the equilibrium constants, computed from the partial pressures of the constituents, with the thermodynamic equilibrium constants

(v) Carbon deposition possibility on the basis of the comparison of given and computed equilibrium constants of reactions (9) and (4)

(vi) Different ratios among the constituents

(vii) The final values of Δ_a and Δ_b accurate to 4 decimal places

(viii) The number of iterations needed for convergence.

The following information is required for input data:

(i) p and q of the hydrocarbon $C_p H_q$

(ii) Steam : hydrocarbon molar ratio,

(iii) Temperatures and the corresponding thermodynamic equilibrium constants for reactions (1), (7), (9), and (4)

(iv) The error limits for the equilibrium constants K_1 and K_7.

The data in (iii) and (iv) are summarized in Table 2.2.

The equilibrium constants used in the computations to establish the carbon deposition boundaries were the usual value obtained from thermodynamic data rather than those given by Dent, Hebden, and Nicklin and co-workers (47, 76,115). The value of p_{CO}^2/p_{CO_2} at the point of carbon formation is reported (47) to depend on the nature of the catalyst surface and its internal structure, as well as on the corresponding properties of the carbon (115), and it is because of this uncertainty that classical thermodynamic data, which will give conservative results for carbon formation, has been used. The graphs representing the variations of equilibrium constants with temperature are given in Fig. A-2.2.1 to Fig. A-2.2.4 in Appendix (A-2.2).

2.6 DISCUSSION OF THE COMPUTER RESULTS.

The following ranges of parameters as input data was selected as representative of steam reforming processes :

hydrogen : carbon atomic ratios of feedstocks, $\frac{q}{p}$, : 1.9 to 4.0,

moles of steam per atom of carbon in the hydrocarbon, α' ,
: 0.625 to 3.00,

temperature : 427 to 816° C in increments of 55 deg. C,

pressure : 1 to 25 atm abs. in increments of 3 atm.

The effect of temperature on the equilibrium concentrations of the reformed gas components at different pressures and steam : hydrocarbon ratios outside the range of carbon deposition and embracing the operating conditions that are used industrially for methane, heptane or light naphtha as feedstocks has been considered fully by numerous authors (31, 47, 48, 79, 155, 179). No detailed account of this work is presented here, but some of the main features are discussed below:

The parametric plots show that, no matter what the $\frac{q}{p}$ - ratio of the feedstock is, the equilibrium concentration of methane decreases as the temperature and steam : hydrocarbon ratio are increased and as

TABLE 2.2

THERMODYNAMIC INPUT DATA FOR COMPUTER PROGRAM.

Temperature			Ther. Equil. Const. reaction (1) $K_1 = \frac{P_{CO} \cdot P_{H_2}^3}{P_{CH_4} \cdot P_{H_2O}}$	Error Limits for K_1	Therm. Equil. Const. reaction (7) $K_7 = \frac{P_{CO_2} \cdot P_{H_2}}{P_{CO} \cdot P_{H_2O}}$	Error Limits. for K_7	Ther. Equil. Const. reaction (9) $K_9 = \frac{P_{CO}^2}{P_{CO_2}}$	Ther. Equil. Const. reaction (4) $K_4 = \frac{P_{H_2}^2}{P_{CH_4}}$
^oK	^oC	^oF						
700	427	800	0.000269	0.000001	9.0170	0.0180	0.000267	0.1115
755	482	900	0.004338	0.000009	5.6100	0.0112	0.002355	0.3283
811	538	1000	0.048866	0.000100	3.7502	0.0075	0.015435	0.8461
866	593	1100	0.40891	0.000800	2.6541	0.0053	0.079221	1.948
922	649	1200	2.6819	0.0057	1.9657	0.0040	0.33345	4.090
977	704	1300	13.269	0.0285	1.5127	0.0030	1.1868	7.947
1033	760	1400	63.430	0.127	1.209	0.0024	3.6677	14.39
1089	816	1500	242.251	0.485	0.9812	0.0019	10.067	24.55

References: (104, 165)

the pressure is decreased; this would be expected in view of the endothermic nature of the reforming reaction with an increase in moles between reactants and products. The opposite features are true for hydrogen. However, the equilibrium concentrations of the carbon oxides exhibit differences for the cases of methane reforming and naptha reforming. In the reforming of methane, the concentration of carbon dioxide has a maximum within the range 650 - 700° C, whereas for naphtha reforming within the same temperature interval no such maximum exists. This is because the decrease of the $\frac{q}{p}$ - ratio in the hydrocarbons higher than methane results in higher concentrations of carbon oxides at equilibrium if the reforming process is carried out at the same operating conditions (Table 2.3). Because of the variation of the standard free energy change of the water gas shift reaction with temperature (Table 2.1), at low temperatures (i.e. less than 650° C), equilibrium will favour the formation of carbon dioxide, whilst in the high temperature region (i.e. above 700° C), the equilibrium will be shifted in the direction of carbon monoxide formation. With naphtha as feedstock the increased amount of carbon on its break-down will, therefore, result at low temperatures in such high yields of carbon dioxide that the presence of a maximum on a plot representing the variation of CO_2 - concentration against temperature will be eliminated.

A comparison of methane or hydrogen concentration in product gas versus temperature at 2 different steam ratios for methane and heptane as feedstocks, shows that to obtain a required methane or hydrogen per cent in the product gas, the temperature necessary may be reduced if the steam ratio is increased.

The equilibrium calculations have also been used to establish the carbon deposition boundaries and to determine the minimum permissible steam : hydrocarbon ratio in the feed for carbon-free operation. Although a number of authors (47, 79, 111, 130, 154, 179) gave

TABLE 2.3

EFFECT OF $\frac{q}{p}$ - RATIO ON THE COMPOSITION OF THE REFORMED GAS.

Equilibrium temperature : 1200° F (649° C)

Operating pressure : 25 atm abs.

moles of H_2O : atom of C, α' : 2

	FEEDSTOCK		
	CH_4	C_2H_6	C_7H_{16}
Equilibrium composition of reformed gas, % (dry)			
CH_4	37.25	36.44	35.13
CO	3.23	4.33	5.21
CO_2	9.97	14.80	18.98
H_2	49.55	44.42	40.68
Moles of components present per mole of hydrocarbon feed			
CH_4	0.7384	1.3114	4.1461
CO	0.0640	0.1559	0.6142
CO_2	0.1975	0.5327	2.2397
H_2	0.9823	1.5986	4.8012
H_2O	1.5409	2.7787	8.9065
Total	3.5231	6.3772	20.7077
Moles of components present per atom of carbon in hydrocarbon feed			
CH_4	0.7384	0.6557	0.5923
CO	0.0640	0.0780	0.0877
CO_2	0.1975	0.2665	0.3200
H_2	0.9823	0.7993	0.6859
H_2O	1.5409	1.3894	1.2725
Total	3.5231	3.1886	2.9583
CO_2 : CO ratio in the reformed gas	3.09	3.42	3.64
Moles of $(CO + CO_2)$ in the reformed gas per atom of carbon in hydrocarbon feed	0.2515	0.3445	0.4077

some consideration to this very important aspect, it is considered useful to discuss and extend the conclusions.

The effect of increasing the steam : hydrocarbon ratio on the reforming process is, as would be expected, an increase of the conversion of the feedstock into reaction products. The reformed gas composition is thus affected by the variation of the steam : hydrocarbon ratio, α , such that an increase of α would result in a decrease of methane and carbon monoxide, but in an increase of hydrogen and carbon dioxide percentages. The type of reformed gas required (i.e. town gas which is rich with respect to methane, or Fischer-Tropsch synthesis or oxo-synthesis gas with H_2 : CO ratios varying within a range 2 to 3, or lean gas for ammonia synthesis) is one of the factors, in combination with other operating variables, to be considered in the selection of the steam : hydrocarbon ratio. When making town gas less steam per atom of carbon in the feed is required than for synthesis gas or lean gas production. In fact, the use of high steam ratios in town gas manufacture should be avoided since this causes more methane to react, thereby reducing the reformer temperature with less sensible heat being carried away in the gases produced. This means a decrease in the thermal efficiency of the process and represents an expense which should be avoided (7,8, 48, 179).

At the same time, higher steam ratios correspond to operation at higher space velocities or to overloading of the reformer which would restrict the approach to the equilibrium of the reactions involved. Therefore, with the exception of some special circumstances, such as increase of the reformer output at times of peak load or deliberate reduction of reformer temperature, the steam ratio is kept at the minimum limit, governed by the thermodynamics of the Boudouard reaction, which induces the deposition of carbon on the catalyst.

In order to illustrate the effect of steam ratio, combined with other operating variables, on the formation of carbon, Figs. 2.2 to

to 2.10, in which the operating pressure is plotted against the operating temperature, have been prepared, as part of the present work, for hydrocarbons ($C_p H_q$) with varying $\frac{q}{p}$ ratios, steam : hydrocarbon ratio being the parameter. For each assumed steam ratio one obtains a three-dimensional surface of which the co-ordinates are temperature, pressure and $\frac{q}{p}$ ratio. Each of the above figures is therefore a slice taken through the surfaces at a given $\frac{q}{p}$ value. The region bound within the abscissa and the boundary for any value of steam : hydrocarbon ratio, α', corresponds to the carbon deposition zone, whilst outside that region carbon-free operation can be ensured for any given set of conditions.

It should be re-emphasized here that these considerations are valid only for establishing the equilibrium carbon boundaries, and they do not involve any indication of the limiting kinetic possibilities, i.e. of the formation of carbon, its suppression or accumulation, arising from the kinetic mechanism of the reforming reactions and the catalyst behaviour.

Several general conclusions are apparent from these graphs. It can be seen that the H : C atomic ratio, $\frac{q}{p}$, of the feedstocks used in steam-hydrocarbon reforming systems has a pronounced effect in determining the limits for equilibrium carbon deposition. In the case of methane reforming, for example, it is possible to ensure carbon-free operation even at steam ratios as low as 0.50, provided that high pressures (7 - 25 atm abs.) and low temperatures (427 - 482° C) are employed. On the other hand, for a hydrocarbon having a $\frac{q}{p}$ - ratio of 3.0 ($C_2 H_6$), the steam ratio for the same range of pressure and temperature has to be a minimum of 1.125. Assuming $\frac{q}{p} = 2.20$ as the representative value for light naphtha, the minimum steam ratio corresponding to similar pressure and temperature conditions must be 1.50. The graphs reveal also the fact that the critical region for carbon laydown for different hydrocarbons is being

shifted from high temperature - low pressure operation for the larger $\frac{q}{p}$ - values, to low temperature- high pressure operation for the smaller $\frac{q}{p}$ values. This situation is shown in Fig. 2.11.

Especially at low values of $\frac{q}{p}$, i.e. using naphtha as feedstock, the steam-hydrocarbon system is very sensitive to variations of steam ratio in the reactor feed. Fig. 2.7 indicates that in a naphtha reforming plant operating at 22 - 25 atm abs. pressure and 700° C with an average steam : carbon ratio 1.40 - 1.35, even a temporary and slight decrease in steam supply would cause spontaneous deterioration of the catalyst bed by carbon deposition. Assuming that this carbon lay-down is reversible, according to Fig. 2.7 the activity of the catalyst can be restored by increasing the steam supply and reformer temperature. Only an increase in steam feed would have the adverse effect of decreasing the reactor temperature due to the heat effects of the reforming reaction which would take place to a greater extent, if the external heat supply had remained fixed. For a given $\frac{q}{p}$ value, the minimum steam ratio increases at first with the extent of reaction, but flattens out at higher temperature where a greater proportion of carbon monoxide can exist at equilibrium. This is due to the increased concentration of carbon dioxide explained previously.

In connection with the computer results, their discussion or their application to industrial equipment, particularly with respect to different operating conditions for carbon deposition or removal, it should be borne in mind that they are based on the assumption that neither temperature nor concentration gradients exist in the radial or axial directions in the reformer section to which they are applied. A further assumption is that the reforming mechanism is identical throughout a cross-sectional area perpendicular to the direction of gas flow, so that homogeneous mixtures are ensured at all times. Because of the boundary effects of both the reactor walls and catalyst mass, a perfectly uniform temperature distribution can never be achieved in the reactor where

Fig: 2.2 Carbon Deposition Regions for Hydrocarbon $C_p H_q$ (Methane) $\frac{q}{p} = 4.00$

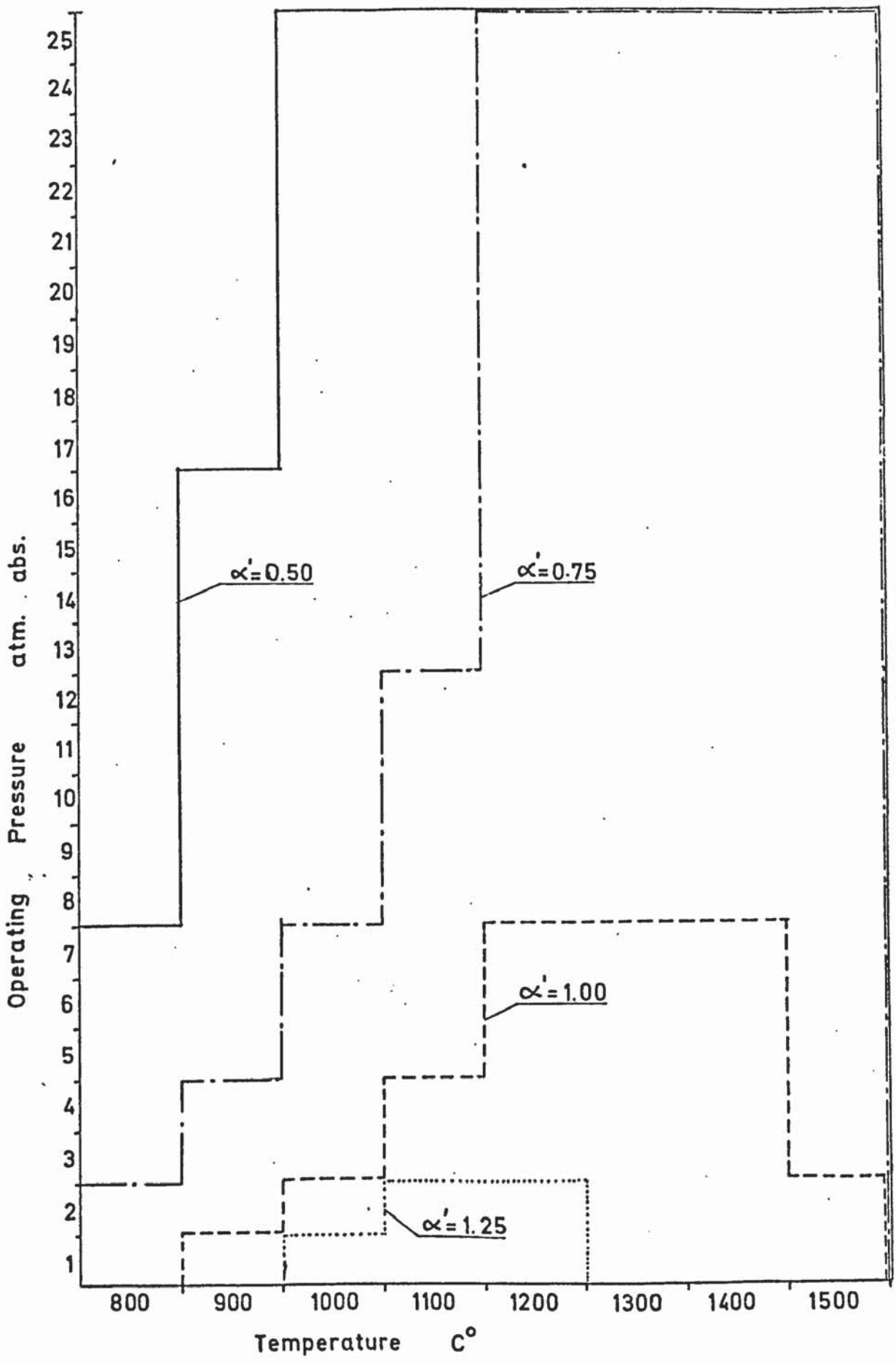

Fig:2.3 Carbon Deposition Regions for Hydrocarbon $C_p H_q$ (Ethane) $\frac{q}{p} = 3.00$

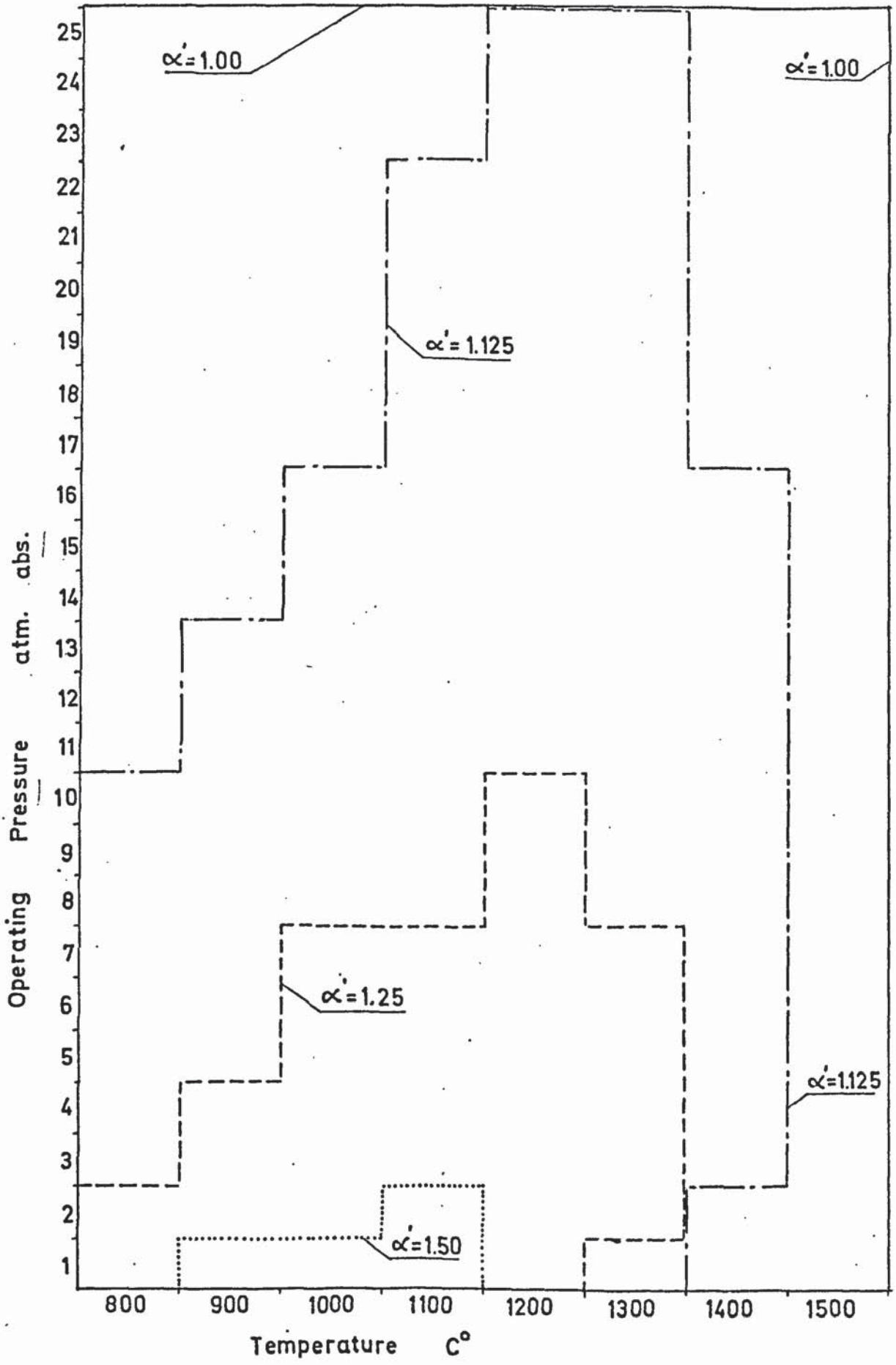

Fig:2.4 Carbon Deposition Regions for Hydrocarbon $C_p H_q$ (Propane) $\frac{q}{p}=2.667$

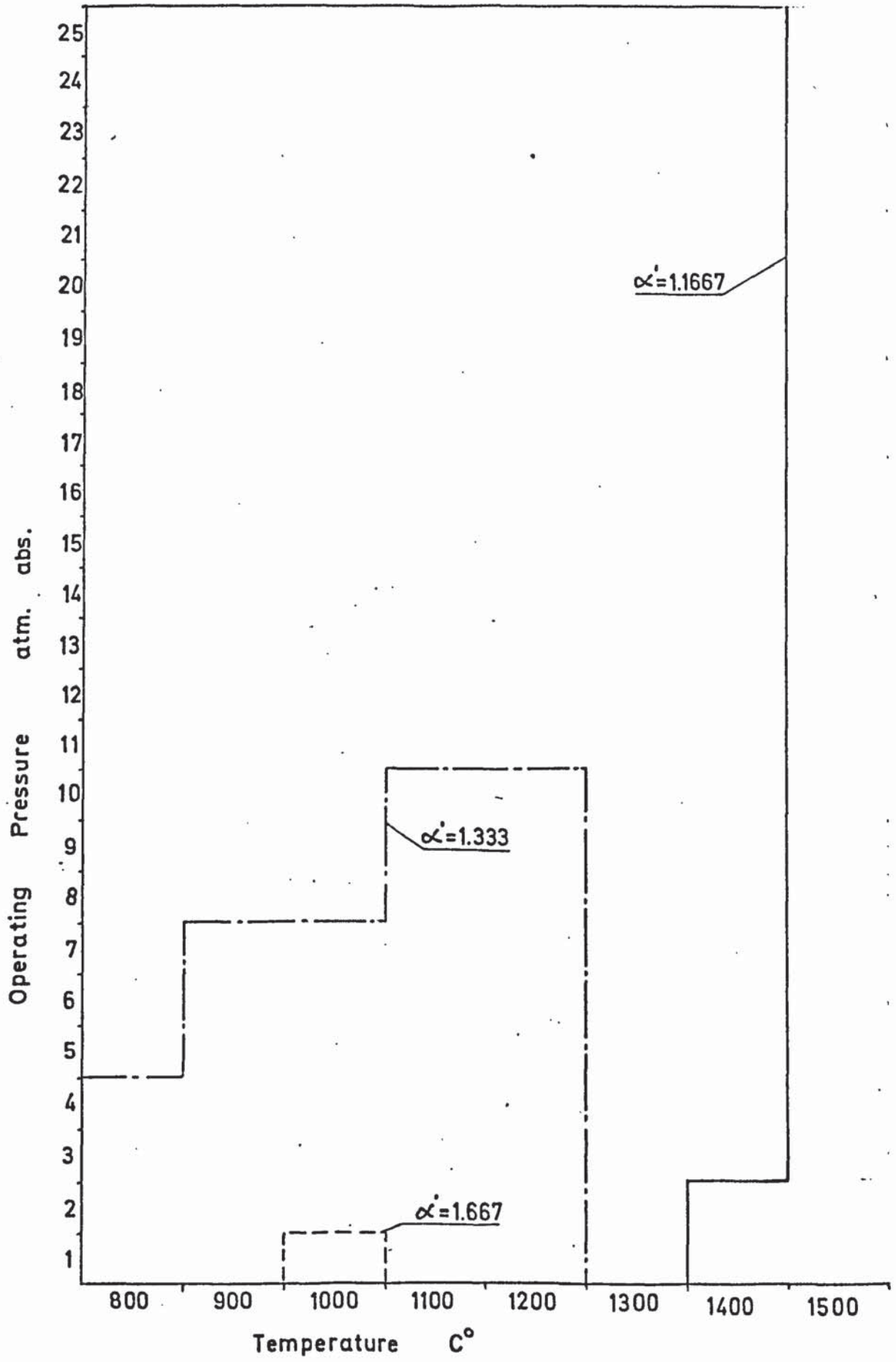

Fig. 2.5 Carbon Deposition Regions for Hydrocarbon $C_p H_q$ (Pentane) $\frac{q}{p} = 2.40$

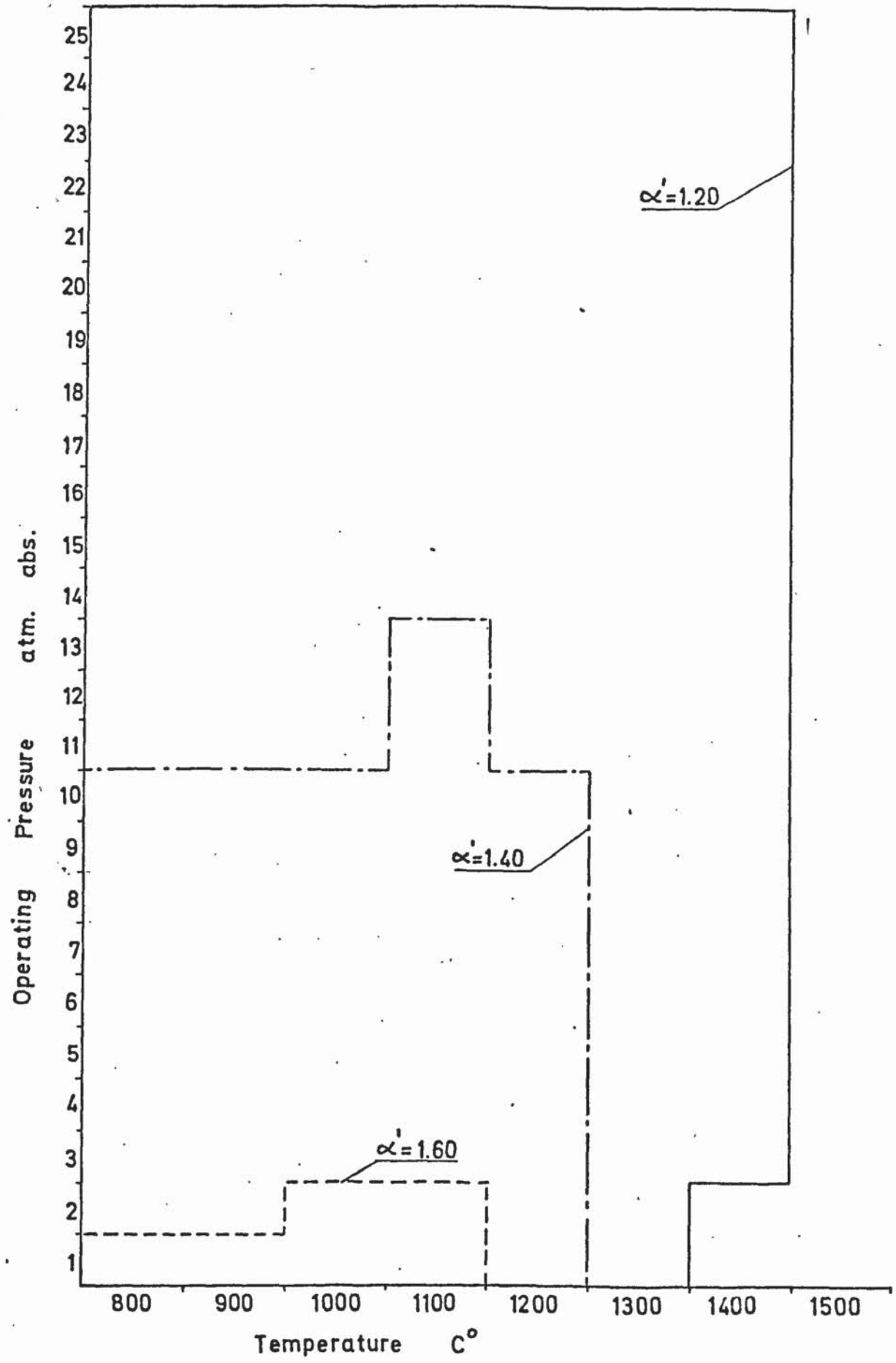

Fig: 2.6 Carbon Deposition Regions for Hydrocarbon $C_p H_q$. (Heptane) $\frac{q}{p} = 2.2857$

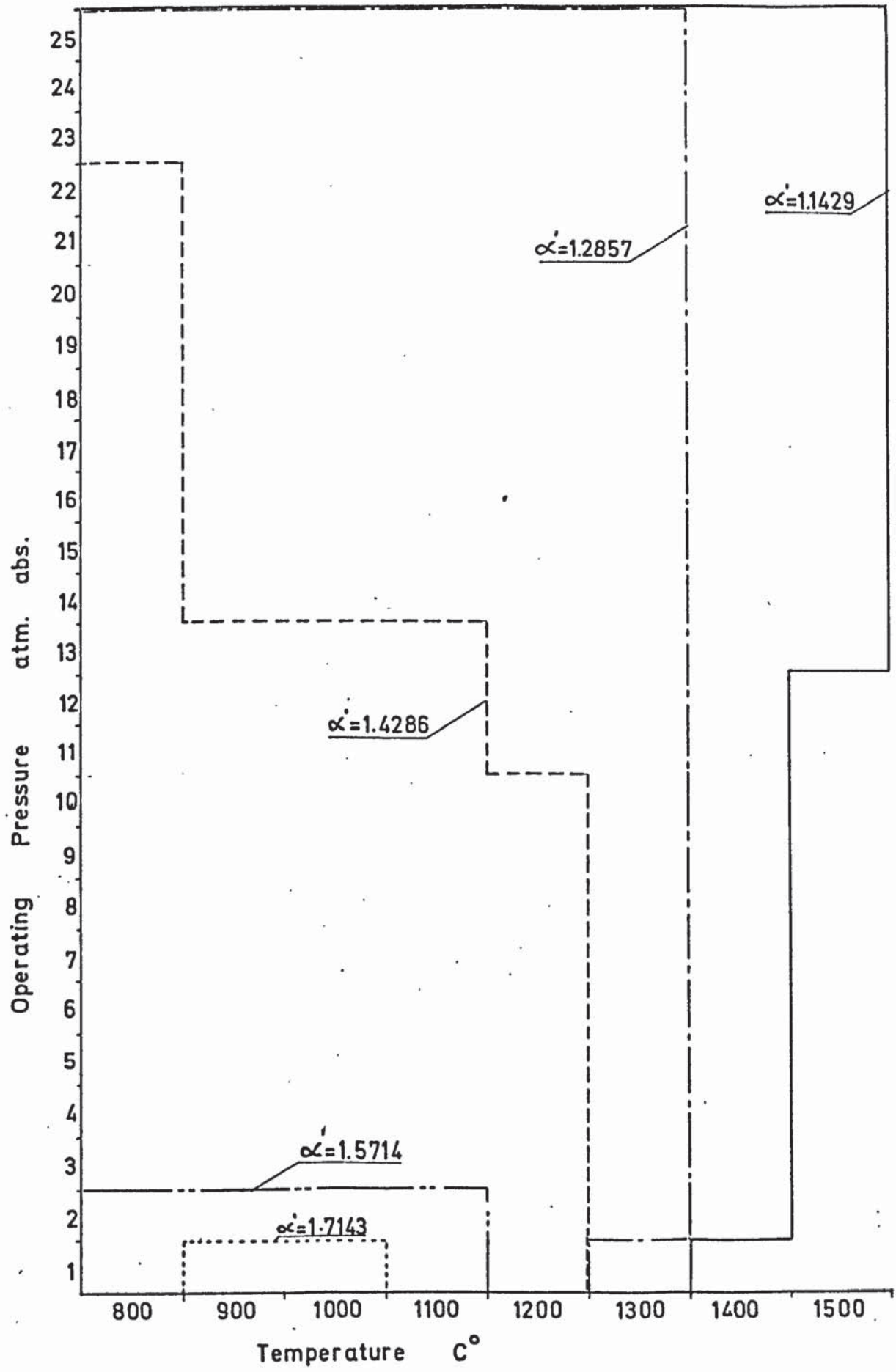

Fig: 2.7 Carbon Deposition Regions for Hydrocarbon $C_p H_q$ $\frac{q}{p} = 2.20$

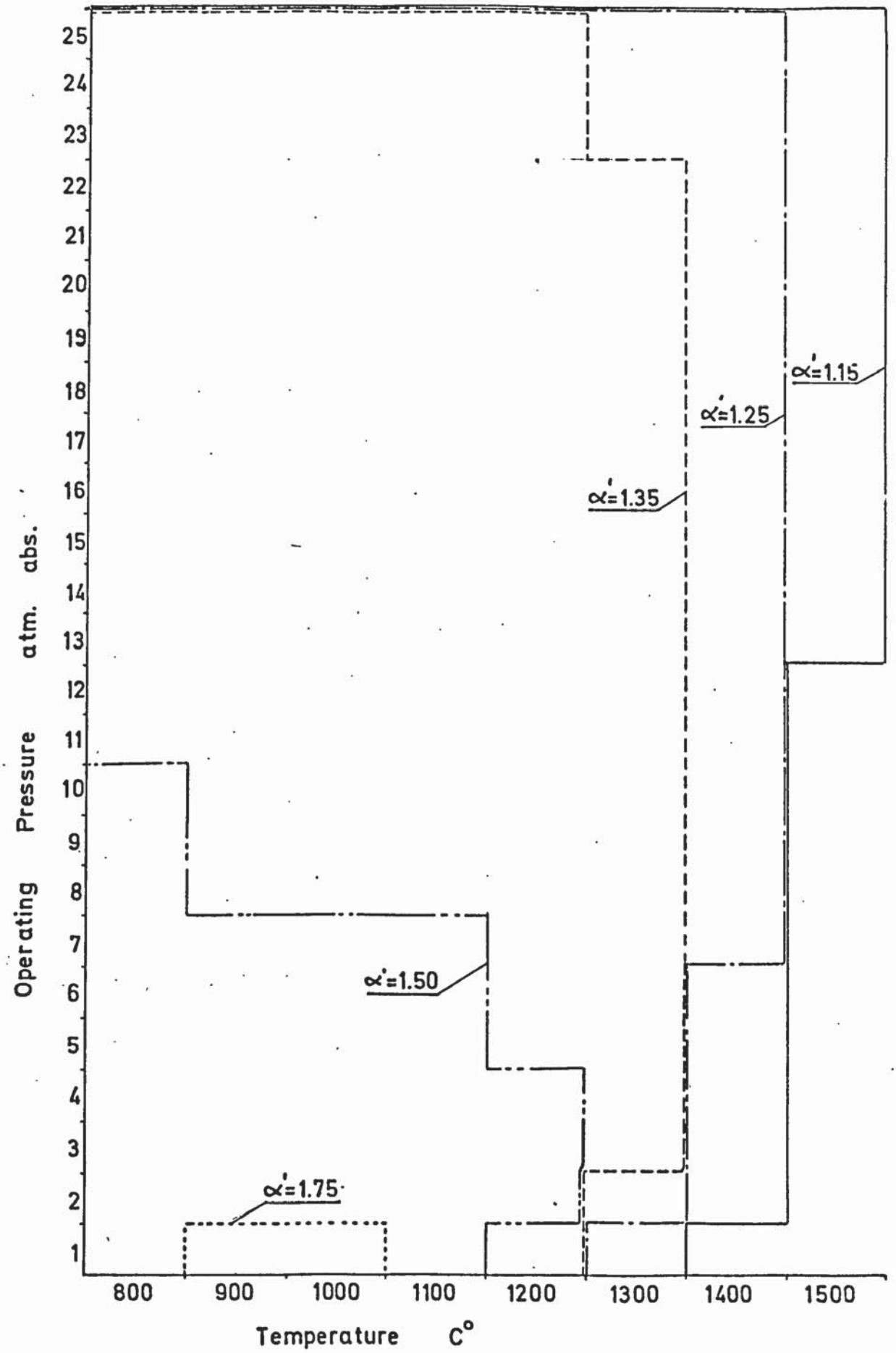

Fig: 2.8 Carbon Deposition Regions for Hydrocarbon $C_p H_q$ $\frac{q}{p} = 2.10$

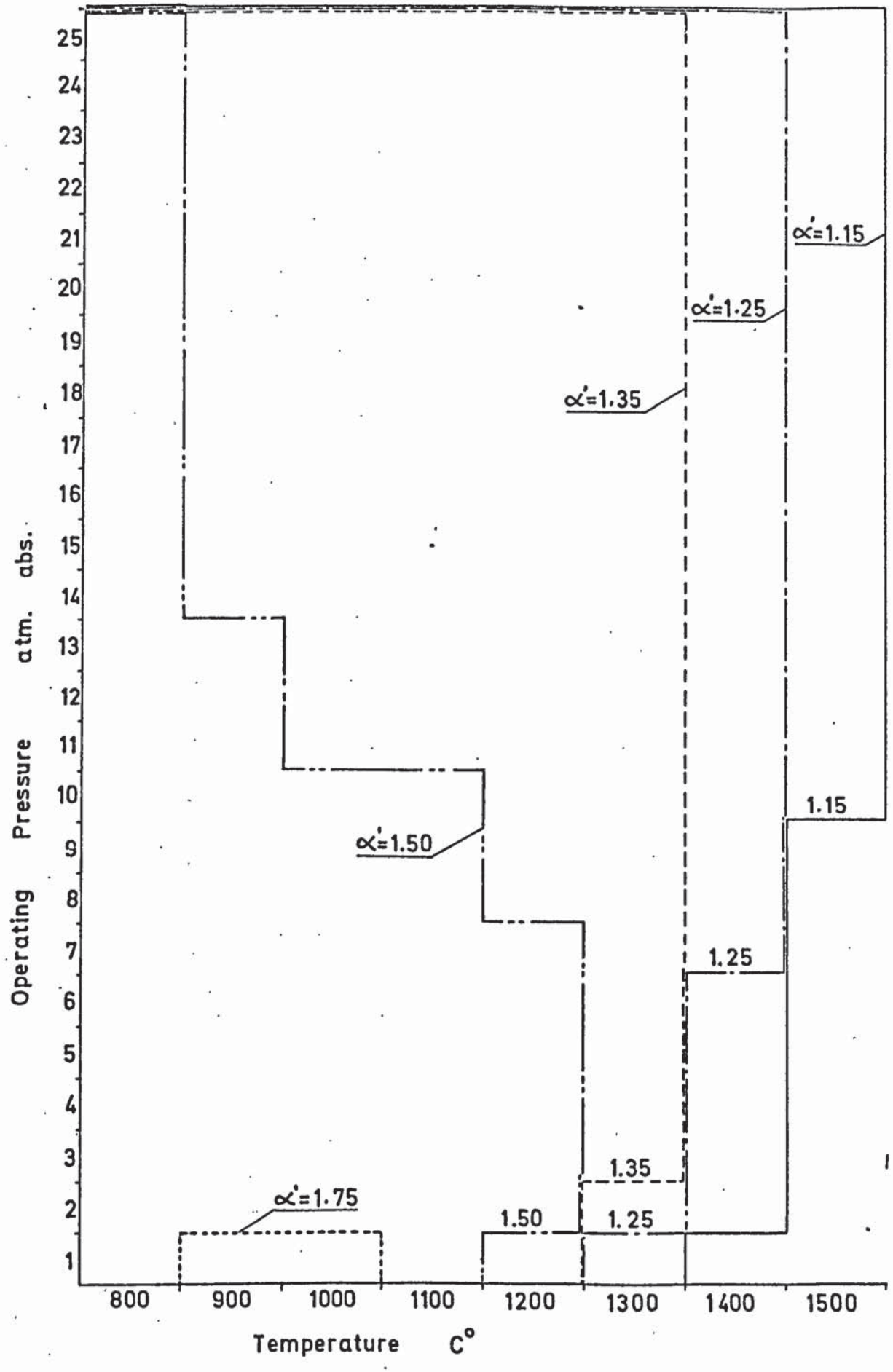

Fig:2.9 Carbon Deposition Regions for Hydrocarbon $C_p H_q$. $\frac{q}{p}=2.00$

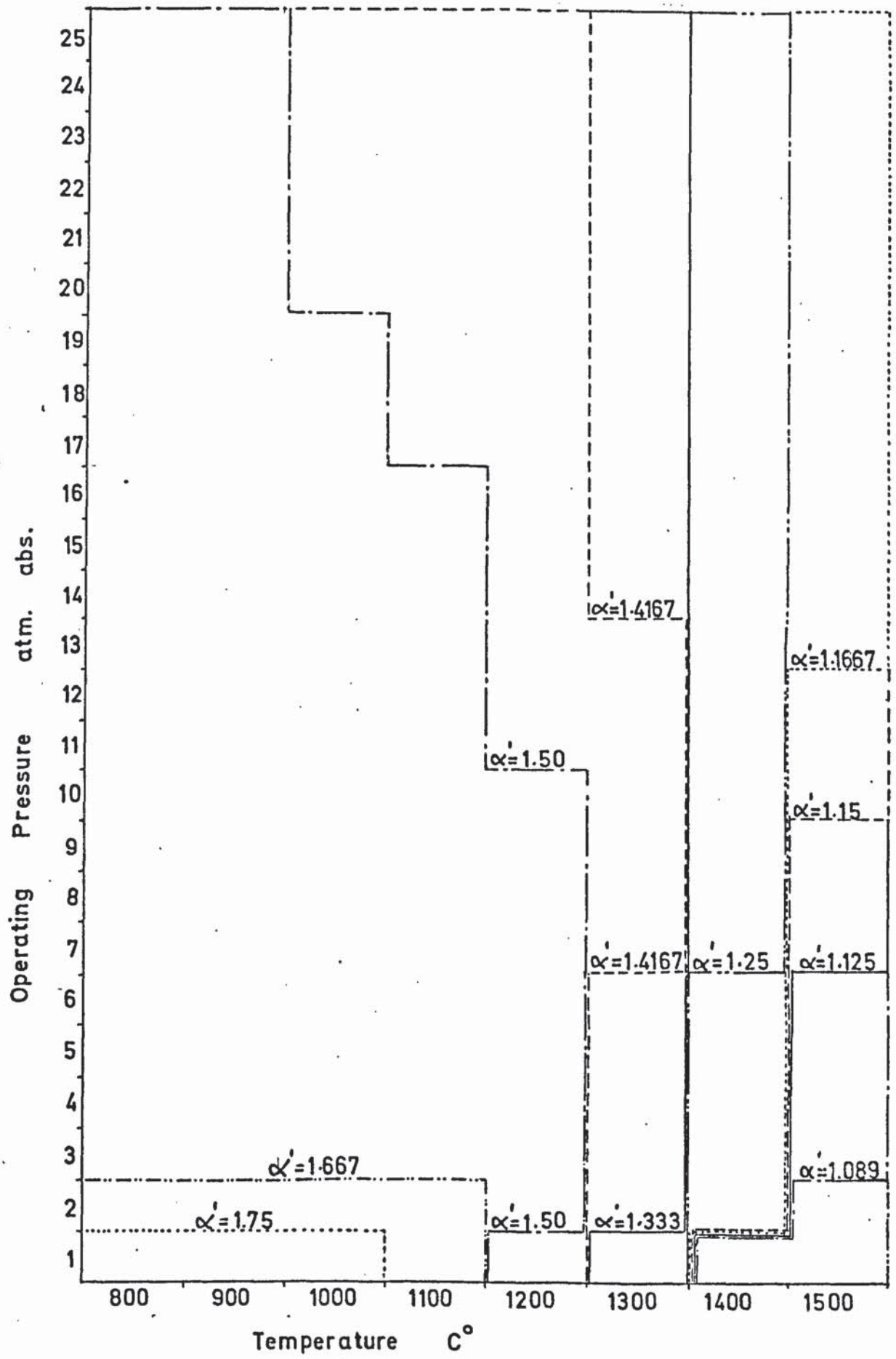

Fig: 2.10. Carbon Deposition Regions for Hydrocarbon $C_p H_q$

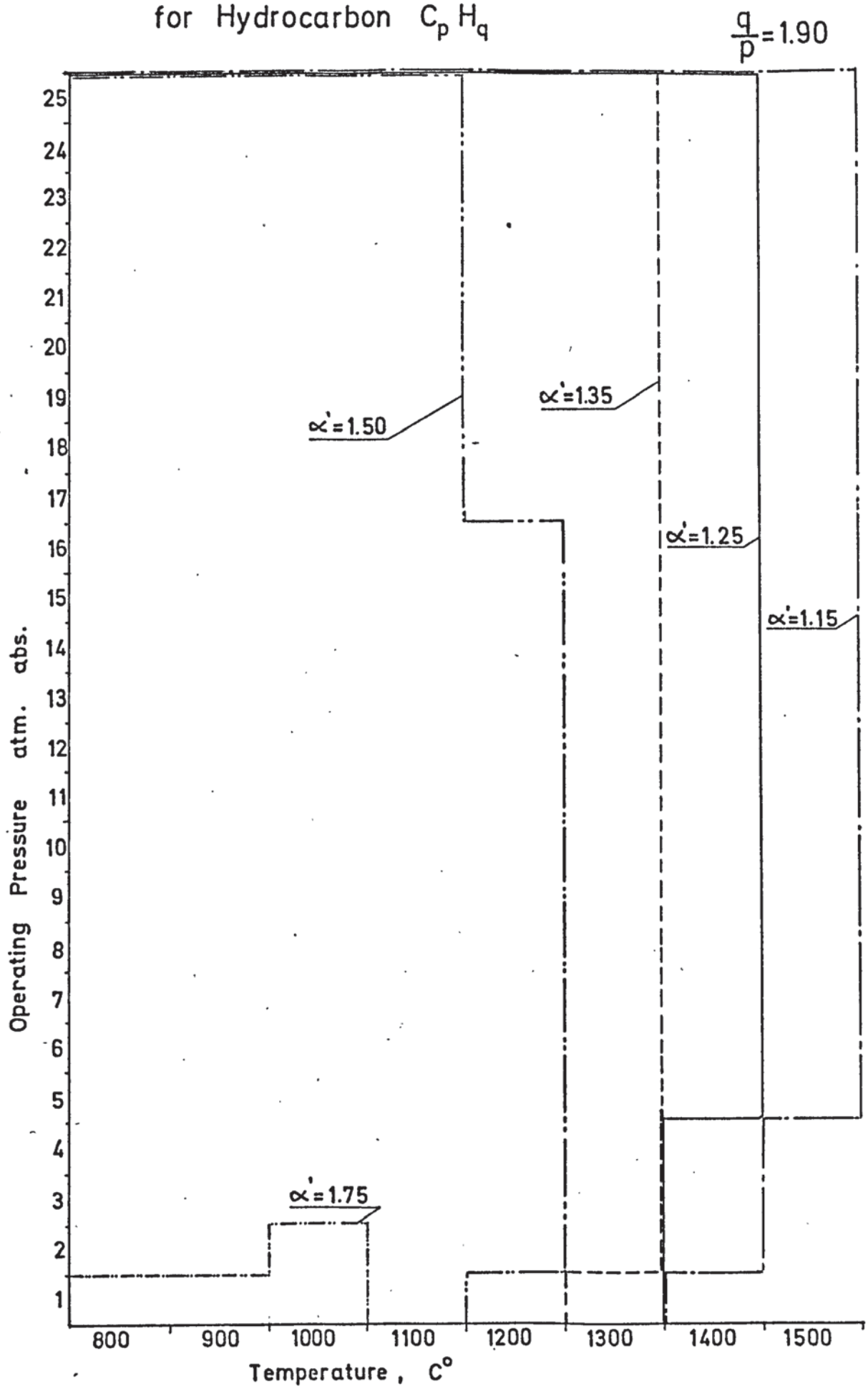

Fig: 2.11. Effect of the q/p ratio on the Carbon Deposition Boundaries

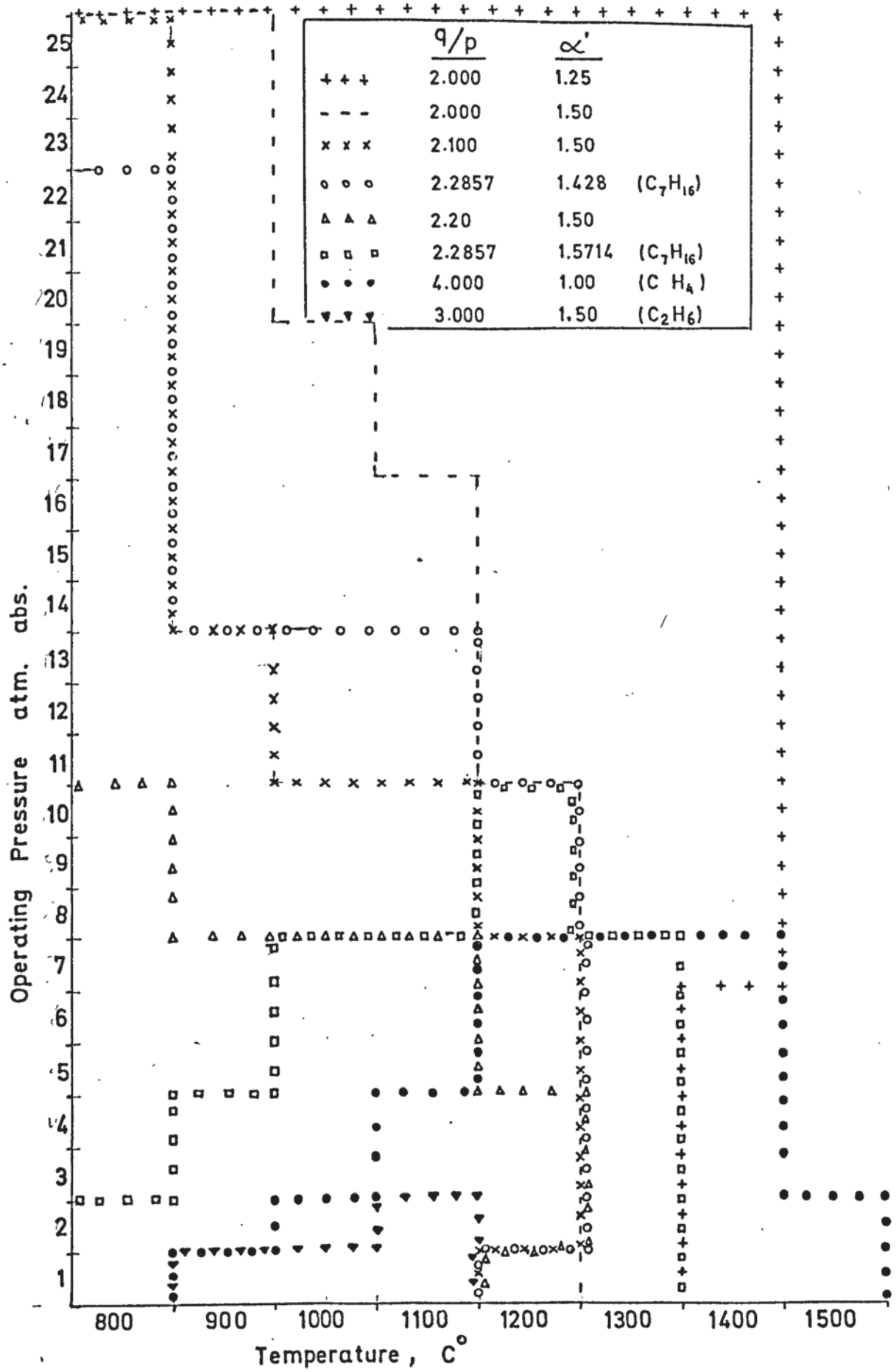

reactions with considerable heat effects are taking place. However, the high space velocities usually encountered may reduce these gradients to such an extent that they may be neglected. On the other hand, they are more severe within the catalyst pellet itself, and it is very unlikely that an isothermal profile exists therein. The maximum temperature difference that can occur in the particle pores relative to the particle surface temperature, $(T_i - T_s)/T_s$, under steady state conditions can be calculated by the heat generation function, β, of Weisz and Hicks (172):

$$\frac{T_i - T_s}{T_s} = \frac{(-\Delta H)\,(D_{eff})}{(\lambda)\,(T_s)}\, c_s \qquad (2.22)$$

where:

T_i = temperature within the pore, ^oK

T_s = temperature of the pellet surface, ^oK

ΔH = enthalpy change of reaction, cal/mole

λ = thermal conductivity of porous structure, cal/(sec)(cm^2 total cross section) (^oC/cm)

D_{eff} = effective diffusion coefficient for the catalyst based on total cross-section normal to direction of diffusion, cm^2/sec

c_s = local surface concentration of the reactant, mole/cm^3

Accordingly the temperature or gas composition may vary through the pore network of an individual catalyst particle enough to approach or cross the boundary for equilibrium carbon.

A further note has to be made of the effects of cooling on the change of the gas composition leaving the reformer at equilibrium for given conditions. It is evident that carbon formation may be encountered on cooling the reformed gas as might occur through heat exchange with the feed. Cooling is equivalent to moving horizontally across a graph at constant value of $\frac{q}{p}$. It can be seen from Figs. 2.2 - 2.11 that changes in the gas compositions and formation of carbon become thermodynamically possible in all cases as the temperature is decreased. It is most

probable that equilibrium is not maintained during the cooling process. However, since carbon formation may possibly involve surface reactions with slower rates, the whole problem of re-equilibration is mainly a kinetic one, and it can be said, at least, that carbon is not likely to form. Even if it were formed, it would not have a deleterious effect on the catalyst bed. If the reformer should operate at high pressure to take advantage of the characteristics of the carbon boundary surface, which is the case in actual practice, then there would appear to be some benefit if the products are throttled down to lower pressures as they are cooled. For instance, in reforming naphtha, $\frac{q}{p} = 2.20$, with a steam ratio of 1.35 moles of steam per atom of carbon at 22 - 25 atm abs. pressure and above 760° C, the margin of safety amounts to approximately 100° C on reduction of the pressure to 1 atm abs. The rate of carbon deposition would probably be too slow to cause blocking of the heat exchange equipment in the absence of a catalyst.

2.7 HEAT EFFECTS OF THE REFORMING REACTIONS.

It is worthwhile to discuss the heat effects of the reactions relevant to reforming processes, since they govern the longitudinal temperature profiles of the reactor and play a very important role in determining the heat load and its distribution along the length of the reformer tube. The heats of reaction are given in Table 2.4 and are based on 25° and 1 atm pressure as datum. They may be used for calculations, but correction for pressure and temperature should be carried out if accurate results are required. The principles of this correction are given in textbooks (36, 53, 82, 153). Because of the endothermicity of the steam-methane reaction, a plot of heat absorbed by the reformed gas against temperature shows that the heat to be supplied increases progressively with the extent of the reaction at higher temperatures. The same curves for light naphtha as feedstock (48) are notably different from methane. In the first place, the

TABLE 2.4

ENTHALPY CHANGE OF REFORMING REACTIONS.

			Enthalpy change* of reaction ΔH^* (cal/mole)	Ref.
$CH_4 + H_2O = CO + 3\ H_2$	complete conversion		- 49,200	(31)
$CO + H_2O = CO_2 + H_2$	" "		+ 9,840	(156)
$C + CO_2 = 2\ CO$	" "		+ 41,220	(156)
$CH_4 = C + H_2$	" "		- 18,240	(156)
$C + H_2O = CO + H_2$	" "		+ 31,400	(156)
	Equilibrium Conversion			
	Temperature ^oC	Pressure atm abs.		
$CH_{2.2} + 3\ H_2O \rightarrow 0.2\ CH_4 + 0.4\ CO + 0.4\ CO_2 + 1.94\ H_2 + 1.81\ H_2O$	800	20.4	+ 24,500	(31)
$CH_{2.2} + 3\ H_2O \rightarrow 0.35\ CH_2 + 0.25\ CO + 0.4\ CO_2 + 1.50\ H_2 + 1.95\ H_2O$	750	30.6	+ 17,900	(31)
$CH_{2.2} + 2\ H_2O \rightarrow 0.75\ CH_2 - + 0.25\ CO_2 + 0.14\ H_2 + 1.50\ H_2O$	450	30.6	- 11,400	(31)

* The enthalpy change is given for 25° C and 1 atm abs. pressure, water being in the vapour state, and carbon in form of β - graphite.

conversion of naphtha with low steam ratios at low temperature to yield methane and carbon dioxide as the main reaction products is exothermic and a negative heat absorption may result up to 500° - 550° C. Within this temperature range and corresponding to a product gas with 50 - 60% CH_4 and 15 - 20% H_2 (dry basis), the reaction is thermally neutral. At higher operating temperatures, corresponding to low methane concentrations at equilibrium, heat has to be supplied, eventually to a greater extent than with methane. This fact is attributed by Dent (48) to the reduced heat transfer in the feedstock preheater probably due to restrictions in the preheat temperatures of naphtha (maximum 500° C).

CHAPTER 3

THE KINETICS OF REFORMING

3.1 INTRODUCTION.

The reaction kinetics of light hydrocarbons either thermally or catalytically, with or without the presence of steam and/or other oxygen carrying agents, have received considerable attention over the past four decades. In spite of innumerable investigations, there still exists a significant diversity of opinion concerning the mechanism and sequence of reactions involved. The types of reactor used in the investigations, the ranges of temperature, pressure and reactant concentrations, the accuracy of analytical techniques, and the chemical, physical and crystal-lattice properties of the catalysts are the principal reasons responsible for the conflicting conclusions. The experimental observations made even in the simplest case of the thermal and non-catalytic decomposition of the very elementary hydrocarbon methane, in pure form and at low pressures, did not lead to conclusions in complete agreement.

3.2 NON-CATALYTIC AND CATALYTIC PYROLYSIS OF METHANE.

Kassel (89) studied the homogeneous pyrolysis of methane in quartz bulbs at different surface : volume ratios within the temperature range 700 - 850^{o} C and at sub-atmospheric pressures (150 - 385 mm Hg). He used a static method and followed the time rate of change of pressure. From the data obtained, he concluded that an induction period for the reaction existed and found the initial rate after this period to be first order and unaffected by any change of the surface : volume ratio. The activation energy of pyrolysis was calculated to be 79,385 cal/mole. He also observed that the hydrogen had a retardation effect on the decomposition reaction, such that if present in large quantities (10 - 75 % at 80 - 120 mm Hg), the rate became proportional to $P_{CH_4}^2 : P_{H_2}^3$. Based on the assumption that only CH_2 radicals were formed, he postulated a scheme of reversible parallel and consecutive

reactions; the formation of CH_3 and CH radicals was excluded from the sequence of reactions. Kassel (89) indicated also the presence of carbon or a carbonaceous residue formed on the reactor walls depending on the reaction time. Storch (158) investigated the pyrolysis of methane at higher temperatures (1457 - 2000° C) over carbon filaments in a static system and reached the same conclusions. Belchetz and Rideal (15) conducted experiments with methane and ethane in a dynamic system within the temperature range 1510 - 1810° C and found the same hydrocarbons (C_2H_2, C_2H_4, C_2H_6) as stable reaction products, but calculated an activation energy of 95,000 cal/mole. They explained the predominance of C_2H_4 in the product stream by the formation of CH_2 radicals as the initial step of pyrolysis. Gordon (65), on the other hand, studied the pyrolysis reaction at 1000 - 1100° C and atmospheric pressure in a flow system and, using a mass spectrometer, detected together with C_2H_2, C_2H_4, and C_2H_6, some aromatic compounds (benzene, naphthalene, phenanthrene) in the carbonaceous deposit which covered the surface of the reactor and slowed down the reaction. On interpreting the observed data, he concluded that the reaction was less than first order, homogeneously catalysed by addition of some C_2H_2 (0.72 %) to the feed, whereas C_2H_4 (1%) had no catalytic effect on the rate of pyrolysis. In contrast to Kassel's observations, he found no induction period for the reaction, but established an acceleration effect of H_2 and attributed this to the increase of C_2H_2 formation. He indicated also a pronounced catalytic effect of the surface, but restricted to the early stages of the pyrolysis reaction and concluded an auto-catalytic reaction mechanism.

The more recent studies of methane pyrolysis were conducted in tubular flow reactors or in shock tubes, in which the temperature of the methane feed was increased instantaneously to the required level at the immediate entrance of the reaction zone. In spite of the

refined techniques for quenching the reaction products and of the precise analytical instrumentation to identify the intermediates of probable reactions, the inconsistencies could not be resolved completely. In fact, Germain and Vaniscotte (64) found with tubular reactors at 1050° C and 1 atm abs. pressure with pure CH_4 feed 10% conversion in less than 1 sec, whereas Schneider (145) observed in shock tubes 8 % conversion in 16 sec. A rather generally agreed conclusion of recent studies is that C_2H_6 accelerates the reaction. The formation of a carbonaceous residue is also a common observation, but its H : C ratio differed in each case. Hydrogen inhibition was confirmed by Germain and co-workers,but not by Boudart et al. (25). Schneider (145) proposed a mechanism of chain reactions in which the formation of CH_2 radicals was considered to be the initiation step, and free H and CH_3 radicals were the constituents of the chain propagation. He solved the rate equations corresponding to each step of the mechanism with the steady-state assumption and found that the rate of methane pyrolysis should be first order at low conversions. For higher conversions, however, the rate expression had to be modified to:

$$r = k \; p_{CH_4} \left[\frac{p_{CH_4}}{p_{CH_2} + p_H} \right]$$

Eisenberg and Bliss (56) attempted to resolve the discrepancies between the results obtained from the tubular reactor (Germain) and the shock tube at higher temperatures (Schneider). They proposed another kinetic model which would fit the experimental observations at any temperature. The suggested chain mechanism excluded entirely the formation of CH_2 radicals and was based merely on H and CH_3 radicals, which together with C_2H_2, C_2H_4 and C_2H_6, were considered to be the intermediate products formed and remained in pseudo-equilibrium within the sequence of chain reactions, with C as the ultimate product. The formation of aromatic hydrocarbon was not

accounted for. From their derived correlation it was concluded that methane pyrolysis within the temperature range 1100 - 1200° C was definitely not a first order reaction, its activation energy being 84,000 cal/mole. Their isothermal conversion versus reaction time plot was of a typical growth-curve shape, exhibiting one region of rapid increase of rate, one region of constant rate, and one zone in which the rate had decreased.

This brief summary covers only very few of the many studies carried out to elucidate the kinetic mechanism of the non-catalytic pyrolysis of methane; however, it does explain the difficulty in combining the diverse conclusions, supported in each case by firm evidence obtained with different experimental techniques.

The kinetic pattern of the catalytic decomposition of methane on the surface of various catalysts is described by similar mechanisms as proposed for non-catalytic pyrolysis. Morikawa et al. (112,113) examined the catalytic decomposition of CH_4, C_2H_6, and C_3H_8, and concluded that the process proceeded via a dissociative adsorption of hydrocarbon molecules forming primarily CH_3 radicals. In the cases of C_2H_6 and C_3H_8, they found that C_2H_5 and CH_3 radicals were also formed and reacted with adsorbed hydrogen to give methane. In the limit, they found the dissociative adsorption process to proceed to the state where all of the C - H bonds were broken to yield C and H_2. In the work with ethane in the range 157 - 300° C, they found C and CH_4 as major reaction products. Kemball (90, 91) studying the exchange of hydrogen in CH_4 with deuterium on nickel films, concluded that the exchange proceeded via the formation of chemisorbed CH_3 and CH_2 radicals. Wright, Ashmore and Kemball (180) investigated the decomposition of CH_4 on the surface of nickel, forming chemisorbed CH_2 radicals and gaseous hydrogen. They concluded that the adsorption of CH_4 yielded a CH_3 radical and a H atom, with a subsequent breakdown

of the radical to form CH_2, CH, and C, the formation of CH_2 being the rate controlling step, and all dissociations contributing to the liberation of gaseous hydrogen. As the temperature was increased towards 200° C, H_2 liberation was enhanced. Galwey (62),using a supported nickel catalyst, found that hydrocarbons were irreversibly adsorbed; hydrogen, formed in the dissociative adsorption of hydrocarbon, was found to desorb partially and reversibly on heating.

3.3 NON-CATALYTIC AND CATALYTIC DECOMPOSITION OF HIGHER HYDROCARBONS.

The mechanisms of non-catalytic and catalytic cracking and dehydrogen ation-polymerization reactions become more complicated in the case of higher hydrocarbons, and yet more important for the reforming process, since the reactions of unstable and stable cracking and dehydrogen ation intermediates with each other and with steam, leading to the ultimate reaction products (CH_4, CO, CO_2, H_2, and H_2O), will compete with the pyrolysis reactions leading to carbonaceous residues or carbon deposits on the catalytic surface.

Steacie and Puddington (157) who studied the thermal decomposition of n-C_4H_{10}, iso-C_4H_{10}, and C_3H_8, in the temperature range 500 - 600° C, found that the initial products of the reaction contained H_2 and CH_4 together with other saturated and unsaturated hydrocarbons. They also detected amounts of polymer and a deposit of carbon on the quartz reactor walls. Marschner (102) found that the thermal decomposition of n-C_8H_{18} at 571° C led to a long series of products including CH_4 and H_2. Above this temperature, CH_4 and H_2 increased with the exclusion of heavier hydrocarbons. At temperatures below 571° C, CH_4 was found essentially to be stable, and its percentage was found higher than the heavier hydrocarbons. Kemball and Taylor (92) examined the decomposition of C_2H_6 in the presence or absence of H_2 over a supported nickel (15%) catalyst at about 200° C in a static reactor, and found that the decomposition products were CH_4 and C.

Their postulated mechanism involved the formation of C_2H_5 radicals. They observed, however, abnormal kinetic results for initial concentrations of C_2H_6 and H_2, if H_2 : C_2H_6 ratio was altered from above 1.0 to below 1.0. The carbon was found to be deposited reversibly and could be converted to CH_4 by treatment with H_2. Using C_2H_4 as feed of approximately 190° C they found C_2H_6 as an additional product to CH_4. These observations were supported by Mc Kee (107) who found at temperatures below 60° C, C_2H_4 self-hydrogenated to give C_2H_6; but above 60° C, CH_4 appeared in the product. Above 200° C, CH_4 was found to be the sole gaseous product accompanied by a carbon residue on the catalyst. Similarly for C_4H_{10}, Mc Kee (108) found that CH_4 and C_2H_6 were the gaseous products; the carbonaceous residue formed in this case was of variable composition.

Greensfelder and Voge (70), studying the catalytic cracking of hydrocarbons ranging from C_3 - C_{24} between 500 and 600° C over silica (86.2%) -zirconia (9.4 %) - alumina (4.3 %) catalyst, compared the results with thermal cracking data. They found that the catalytic process led to less production of CH_4 and C_2 species. Also with large paraffins, the catalysis was found to operate leaving very little cracked hydrocarbons above C_{10}, which was not the case thermally. A further conclusion they made was that the presence of catalyst accelerated the overall cracking reactions by factors of the order 5 to 60, with more pronounced acceleration for the high hydrocarbons. The rupture was found to be selective, with the first and second C-C bonds at the ends of the hydrocarbon chains relatively inert, thus accounting for the high percentage of C_3 and C_4 species. They observed also some secondary isomerization and aromatization reactions. The composition of the carbonaceous deposit formed differed in each case in H : C ratio. Anderson and Baker (5) reported that in the cracking of saturated hydrocarbons in the presence of hydrogen

(hydrogenolysis), the general mode of behaviour of all hydrocarbons over nickel or other uniform metallic films was the extensive fragmentation yielding CH_4 as the dominant product with only relatively small amounts of higher hydrocarbons. They also found that over nickel films, the rate of methane formation from hydrogenolysis was greater than the rates of adsorption - desorption established for methane alone. The authors gave no explanation for this contradiction; the only explanation would be the interaction between different adsorbed species increasing the adsorption-desorption rates and adsorbed quantities on the same active surface (Section 8.8). The H : C ratio of the chemisorbed residue resulting from hydro-cracking (hydrogenolysis) of saturated hydrocarbons, was found to be 0.9 - 1.4 over nickel, and 1.3 - 2.3 over platinium,indicating either a change in the kinetic mechanism or a different selectivity of the catalyst.

It is beyond the scope of this survey to summarize all the investigations in this field and attempt to reconcile the conflicting conclusions and rate expressions derived. Common to all workers who studied the dissociative adsorption and cracking of light hydrocarbons, in the absence or pres ence of hydrogen and on supported metallic catalyst or on uniform metallic films, is the general agreement that the kinetic mechanism was fundamentally the formation of free H and hydrocarbon radicals, with methane and a carbon-hydrogen residue as the ultimate reaction products. For straight-chained hydrocarbons, the general trend for cracking activity to fall with decreasing carbon number is also established.

3.4 KINETICS OF STEAM-METHANE SYSTEM.

Many researchers have studied the steam-methane catalytic system with the view to establishing the reaction mechanism, the effects of different reaction parameters, and in particular, the initial stable products being formed.

Leibush et al. (97, 98), working at 750° - 900° C using nickel as catalyst, suggested a chain reaction mechanism involving the formation of CH_2 radicals together with C_2H_6, C_2H_4, C_2H_2 and C. They concluded that each of these compounds reacts with H_2O independently to give the final stable reaction products. Gordon (68) investigated the same reaction in the absence of catalyst in a tubular reactor at 1000 - 1100° C and atmospheric pressure applying H_2O : CH_4 ratios 1 - 5. According to his observations, the reaction was less than first order and catalyzed by the addition of small amounts of C_2H_2. The observed rates of reaction remained unchanged with variation of H_2O : CH_4 ratio. Since the increased concentration of steam did not affect the concentration of reaction intermediates, he concluded that the steam had acted as an inert diluent until a carbonaceous deposit was formed. This view is shared by others to some extent. Thus Yarze and Lockerbie (183) who used a H_2O - C_4H_{10} mixture concluded that the hydrocarbon molecule is first adsorbed, then catalytically cracked, dehydrogenated and polymerized resulting in a carbonaceous deposit. These deposits are then removed by the adsorbed H_2O reacting to give the final products. A mechanism with intermediate carbon formation followed by a steam-carbon reaction is offered also by Dirksen and co-workers (49). A reaction mechanism based on the assumption of carbon formation was found unrealistic by Bodrov et al. (21), since they found the CH_4 pyrolysis to give C many times slower than the reaction of CH_4 with H_2O. The activation energy for the steam-methane reaction on metallic Ni-foil in the range 800 - 900° C and 1 atm abs. pressure was calculated to be 31,000 cal/mole, which coincided with that of the exchange of CH_4 with deuterium on Ni-film found by Kemball (90). Based on these considerations, together with the derived rate expression, which gave a very satisfactory fit for the experimental observations, Bodrov

and co-workers proposed a kinetic mechanism which yielded CO and H_2 via the initial step of CH_2 radical formation. This step was assumed to be rate controlling. It was also assumed that the degree of coverage of the catalytic surface by CH_2 radicals was negligible, which is hard to justify. Akers and Camp (2) favoured also a mechanism involving possibly the formation of CH_2 radicals assumed to be the rate determining step, which might have subsequently reacted with steam to give CO, CO_2 and H_2 as products. They used nickel supported on Kieselguhr catalyst at a temperature 638° C and 1 atm abs. pressure, and the activation energy was calculated to be only 9,000 cal/mole. In a recent study of the steam-methane catalytic system at 650° C and 250 psig pressure,Woodcock (179) proposed two equally plausible mechanisms which involve the reaction of adsorbed CH_4 with unadsorbed H_2O, with the chemisorption of CH_4 being the rate controlling step, and the reaction of adsorbed CH_4 with adsorbed H_2O, in which the chemical reaction between adsorbed species was the rate determining step.

Similar diversity extends into the conclusions that have been drawn on the initial stable products formed in the reforming process of hydrocarbons.

Cryder and Porter (41) investigated the H_2O - C_2H_6 reaction, catalysed and uncatalysed, and found that CO and H_2 were present as the initial products, but for a given temperature the relative amounts of each increased considerably for the catalysed reaction. They also found that the threshold temperature for pyrolysis was 600° C, but in the presence of nickel catalyst, the reaction started at 430° C. Slovokhotova et al. (151) also investigating the reaction of steam with a number of hydrocarbons (C_2H_6, C_5H_{12}, cyclo-hexane) obtained conversion at slightly lower temperatures than Cryder and co-worker, the range being 250 - 420° C. The initial products in this case

were found to be CO_2, H_2, CH_4 and C which was deposited on the catalyst. Yarze and Lockerbie (183) studied the H_2O - C_4H_{10} reaction over a nickel catalyst and found, that as well as CO and H_2, CO_2 was also an initial product. Extrapolation of their conversion curves indicated that CH_4 was not a primary product of the reaction, and was only produced when C_4H_{10} conversion exceeded 15%. They assumed, therefore, that CH_4 arises as the result of a subsequent methanation reaction. This fact was also observed by Rakovskii et al. (128), working with H_2O - C_3H_8 - C_4H_{10} mixtures over a supported catalyst. Topsøe (164) differed from Yarze and co-worker with regard to the origin of CH_4. In his work with C_3H_8, C_4H_{10} and C_5H_{12}, he found in all cases a methane concentration in excess of the thermodynamic equilibrium value, and therefore, concluded that CH_4 must be a primary product of the overall reforming reaction with higher hydrocarbons as feedstock. Bridger and Wyrwas (25) also postulated that CH_4 was an original product from thermal and catalytic cracking of the feedstock on the catalyst. These then underwent steam reforming to yield CO, CO_2, and H_2. Dent (48) supported an initial reaction between the hydrocarbon and steam yielding CH_4 and CO_2 as products. This view was shared by Lihou (101). Phillips and co-workers (124) studied the kinetics of the H_2O - C_7H_{16} and H_2O - C_6H_{14} reactions over nickel catalysts in the temperature range 350 - 500° C and at 14.7 atm pressure and found that the primary reaction products were H_2 and CO, and CH_4 was formed subsequently by the methanation reaction. Schnell (146) conducted reforming experiments at 600° C, atmospheric pressure and very low contact times, with C_3H_8 and C_4H_{10} as feedstocks, using commercial nickel-base catalysts. He established also that CO_2 appeared before any CO was detected, and explained this by a virtual reaction sequence involving the formation and decomposition of ketenes and acids.

Some differences of opinion exist even in the case of CH_4 reforming as to which of the carbon oxides is being formed. In fact, Akers and Camp (2) found that both CO and CO_2 were primary products at 638° C and 1 atm abs. pressure, and that the water gas shift reaction was either absent or was very slow. On the other hand, Bodrov et al. (21, 22) claimed that the primary oxide was CO, and the water gas shift equilibrium was always established. The rate expression derived on the basis of CO formation from CH_2 radicals gave a satisfactory fit for their experimental observations.

These different conclusions on the initial products of reforming are probably due to the relative rates of competing reactions at different operating conditions.

3.5 REFORMING MECHANISM OF HIGHER HYDROCARBONS.

The different mechanisms postulated for the reforming process of higher hydrocarbons (light naphtha) are summarized by Schnell (146) and in the Catalyst Handbook (31):

(i) initial decomposition of the hydrocarbons to carbon and hydrogen followed by the reaction of carbon with steam ;

(ii) stepwise breakdown of the hydrocarbons and direct reaction of steam with hydrocarbon fragments on the catalyst surface;

(iii) direct reaction of hydrocarbons with steam, giving oxygen-containing intermediates, possibly in the form of surface compounds on the catalyst.

On the basis of extensive experiments with paraffins, employing a small catalyst bed and high space velocities over a wide range of temperatures (500 - 800° C) and at atmospheric pressure, it is suggested that the steam reforming reaction is a combination of the homogeneous thermal cracking of hydrocarbons and the heterogeneous catalytic reaction of the hydrocarbons with steam(27,31,124,146). At high temperatures

(about 700 - 750° C), the activation energy of the paraffin-steam reaction was found to be almost identical with published values for homogeneous thermal paraffin cracking. At lower temperatures (below 650° C) the reaction had a smaller activation energy, typical of a catalysed process, and a number of different paraffins showed qualitatively similar behaviour. With respect to the kinetics of catalytic reforming of higher hydrocarbons, Schnell (146) distinguishes three major stages :

(i) catalytic cracking and dehydrogenation and, at high temperatures, thermal cracking - leading mainly to olefins of low molecular weight, CH_4, and some H_2 ;

(ii) reaction of the primary intermediates (olefins, CH_4) with steam leading initially to H_2 and CO_2 ; and

(iii) a final stage comprising the equilibration reactions between methane, steam, carbon dioxide, carbon monoxide and hydrogen.

It is claimed that the dehydrogenation in step (i) is only of importance for hydrocarbons smaller than C_4H_{10}, because with increasing chain length, cracking becomes thermodynamically more feasible than dehydrogenation (59,146,183). A scheme for the catalytic reactions between paraffins and steam is given in the Catalyst Handbook (31).

3.6 PROPOSED RATE EQUATIONS.

In view of the dissimilarities in the proposed kinetic mechanisms for the steam-methane catalytic reaction, it is inevitable that the rate expressions derived to describe the reaction will have significant discrepancies. Some of the suggested rate equations are given below:

Akers and Camp (1955) (2) :

(638° C, 1 atm abs. ; catalyst : Ni on kieselguhr)

$$r_m = k_m P_{CH_4}$$

E = 9,000 cal/mole

Obolentsev et al. (1956) (179) :

(800° C, 1 atm abs.)

$$\frac{dP_{CH_4}}{d\theta} = (P_{CH_4,i} - P_{CH_4})\, a\, b\, \theta^{b-1}$$

where:

$P_{CH_4,i}$ = initial partial pressure of CH_4 .

θ = contact time

a, b = parameters, functions of temperature.

Leibush and Lyndkovskaya (1958) (98) :

(400 - 700° C, 1 atm abs. ; catalyst : Ni on Al_2O_3, Cr - oxide)

$$r_m = k_m \left[\frac{P_{CH_4} P_{H_2O}}{(10) P_{H_2} + P_{H_2O}} \right]$$

E_a = 22,700 cal/mole

Bodrov, Apel'baum, and Temkin (1964) (20, 21, 22):

(800 - 900° C, 1 atm abs. ; catalyst : metallic Ni-foil

$$r_s = k_s \frac{P_{CH_4}}{1 + a\left[\frac{P_{H_2O}}{P_{H_2}}\right] + b\, P_{CO}}$$

(at 800° C : a = 0.5, b = 2.0

at 900° C : a = 0.2, b = 0.0

E_a = 31,000 cal/mole)

(700° C, 1 atm abs. ; catalyst : Ni on $\alpha - Al_2O_3$)

(pore diffusion controlled operation)

$$r_m = k_m \frac{P_{CH_4}}{1 + a\left[\frac{P_{H_2O}}{P_{H_2}}\right] + b\, P_{CO}}$$

(at 700° C : a = 0.5, b = 1.0

at 800° C : a = 0.05, b not determined

E_a = 19,400 cal/mole)

Topsøe (1966) (164) :

(temperature-pressure conditions and catalyst type not indicated)

$$r = k \left[p_{CH_4} - \frac{1}{K_{eq}} \frac{p_{CO_2} \; p_{H_2}^4}{p_{H_2O}^2} \right]$$

Woodcock (1971) (179) :

(650° C, 250 psig. ; catalyst : ICI, 46 - 1 commercial naphtha reforming).

$$r_m = k_m \left[\frac{p_{CH_4} - \frac{1}{K_{eq}} \cdot \frac{p_{CO} \; p_{H_2}^3}{p_{H_2O}}}{1 + A \; p_{CO} \; p_{H_2}^3 + B \; p_{CO} + C \; p_{CO_2}} \right]$$

(k = 0.00806 ; A = 0.00582 ; B = 0.0586 ; C = 3.30 ; $K_{eq.}$ = 2.794

Woodcock (1971)(179) :

(650° C, 250 psig ; same catalyst)

$$r_m = k_m \left[\frac{p_{CH_4} \; p_{H_2O} - \frac{1}{K_{eq}} \cdot p_{CO} \; p_{H_2}^3}{1 + A \; p_{CH_4} + B p_{H_2O} + C \; p_{CO} \; D p_{CO_2}} \right]$$

(k = 0.00262 ; A = 0.0426 ; B = 0.09145 ; C = 0.04595 ;

D = 2.382 ; $K_{eq.}$ = 2.794).

It is impossible to find common features of all proposed rate equations, since they are derived from different assumptions and kinetic mechanisms. The expression suggested by Akers and Camp is only a simple empirical satisfactory fit of experimental observations, while Woodcock derived his equations by a Langmuir-Hinshelwood approach. The equations given by Bodrov et al.are semi-empirical expressions which account partly for the retardation effects of the adsorbed species. The authors claim that the reaction proceeds via formation of the CH_2 radicals in the adsorbed state,but assume also that they do not

occupy any active sites. It has to be noted also that the hydrogen produced in the sequence of the proposed scheme of kinetic mechanism is assumed to be formed in the unadsorbed state, whereas White and co-workers (3, 18), who studied the reverse reaction (methanation), derived their two kinetic models (both Langmuir type rate expressions) on the assumption that the reaction takes place between adsorbed H_2 and adsorbed CO.

Some rate expressions for higher hydrocarbons for the initial reaction either on an empirical basis or by the Langmuir-Hinshelwood approach are also published (13, 16, 17, 124, 125, 127, 151, 152).

3.7 FORMATION OF CARBON.

The deposition of carbon on the catalyst during the course of the reforming process can be attributed to two sources :

(i) from non-catalytic and catalytic fragmentation of the hydrocarbon feed (kinetic carbon) and

(ii) by the effect of partial pressures of the components in the system at equilibrium (equilibrium carbon).

In both of these cases, the circumstances leading to the formation of carbon is not only a function of the operating conditions, but also of the catalyst itself. Some effects of various catalyst components in promoting the formation of kinetic carbon by the pyrolysis reaction or its removal by catalysing the steam-carbon are discussed in Chapters 2 and 6. The exact distinct mechanisms and the rate of the reactions leading to the formation and build-up of kinetic carbon by the pyrolysis in the presence of different types of catalyst are not yet established. In spite of its uneconomic consequences, the application of steam : hydrocarbon feed ratios considerably higher than the thermodynamic minimum seems to be still operational requirement to avoid carbon laydown, and consequently

the deactivation of the catalyst. There is,however, sufficient evidence available to accept that the carbon deposited on the surface of the catalyst forms relatively unstable carbides of nickel of non-ionic crystal structures (62,76,78,105,106,159). It is claimed that these carbi des react with hydrogen below 350° C whereby the carbide is quantitatively converted to CH_4 and a few per cent of C_2H_4. Above 350° C, there is extensive decomposition of the carbides to carbon. Storch (159) gave a summary of the investigations prior to 1945 and indicated that the presence of hydrogen may have a catalytic effect on metal carbide formation by forming an unstable metal hydride, which may result in sufficient distortion of the crystal lattice so that upon removal of the hydride hydrogen by decomposition or by reaction with neighbouring metal carbide or by adsorbed CO, penetration of the lattice by C is accelerated. Mc D. Baker and Rideal (105) had the same observations for diffusion of CO into the lattice. Galwey (62) proposed the theory that carbon may diffuse into the bulk catalyst and proposed a scheme by which an adsorbed CH_4 molecule formed the series of adsorbed CH_3, CH_2, CH radicals and adsorbed C together with adsorbed H in a pseudo-equilibrium state. Hebden (76) concluded also that chemisorbed C atoms formed, diffused into the catalyst solid mass to form a lattice carbide and induced a structural re-arrangement which altered the thermodynamic properties of the system causing the change of the equilibrium constant of the Boudouard reaction.

Some quantitative data has been published regarding the reaction rates of carbon-forming and removal reactions (31) :

(i) the rate of carbon formation from CO (Boudouard reaction) is 3 - 10 times faster than from the pyrolysis of CH_4 under the same conditions (66).

(ii) carbon formation from the pyrolysis of C_4H_{10} proceeds at about

the same rate as by the Boudouard reaction (66).

(iii) The rate of the steam-carbon reaction is 2 - 3 times faster than the reverse Boudouard reaction (69).

(iv) The rate of methane formation from carbon and hydrogen is about 1000 times slower than the reverse Boudouard reaction (61).

It is reported that the pyrolysis reactions are at least as fast as the Boudouard, C-H_2O, and C-H_2 reactions. It follows, therefore, as long as the removal of deposited carbon and/or carbonaceous residues by steam is continuous and at a rate equal to the deposition, the integral effect will not be detrimental to the activity and life of the catalyst. The heavier the feedstock and the more unsaturated compounds it contains, the higher the required steam : hydrocarbon ratio. It is reported (31) that the top region of a primary reformer is the most susceptible zone for carbon formation and catalyst deactivation, since the concentration of higher hydrocarbons is still appreciable in this region and the driving force for carbon removal is at its lowest value.

CHAPTER 4.

THE REFORMING APPARATUS AND PROCEDURE.

4.1 GENERAL DESCRIPTION.

The apparatus employed in this work was essentially the same as that used by Woodcock (179) for the same purpose but at different operating conditions. The construction of the equipment could enable a large range of experimental conditions related to the type of low molecular weight hydrocarbon, steam : hydrocarbon ratio, feedrate, temperature, and pressure to be obtained. One reactor, designed and used by Woodcock (179),was an integral type fixed bed flow reactor specifically to test catalyst pellets of definite external diameter made in the form of hollow cylinders (6.4 mm I.D., maximum 16.0 mm O.D), and mounted on a holder with only the external surface exposed. A second tubular reactor was developed and operated by the present author for experiments carried out with catalysts in powdered or granular form ; the modifications done and their results are explained in the respective sections. The front and rear views of the reforming apparatus are shown in Plates 4.1 and 4.2, while a schematic diagram of the arrangement is shown in Fig. 4.1.

High purity methane and hydrogen were obtained from cylinders. After pressure reduction by means of regulators, the gases were metered with rotameters within the range $(0.1)(10^{-3})$ - $(15.0)(10^{-3})$g moles/min.They then passed through a preheating furnace,where the temperature was increased to 300 - 350° C, and into the evaporator furnace which was fed with liquid water by a microfeed pump. The homogeneous mixture of hydrocarbon-hydrogen-steam then passed into two successive superheating furnaces where its temperature increased gradually to 20 - 50 deg C below the reactor temperature. A detailed description of the reactors and their operation is given in Section 4.3.1 rather than here.

On leaving the reactor the reformed gas passed into a water cooled cocurrent condenser for separation and collection of unreacted steam,

Plate No. 4.1

THE FRONT VIEW OF REFORMING APPARATUS

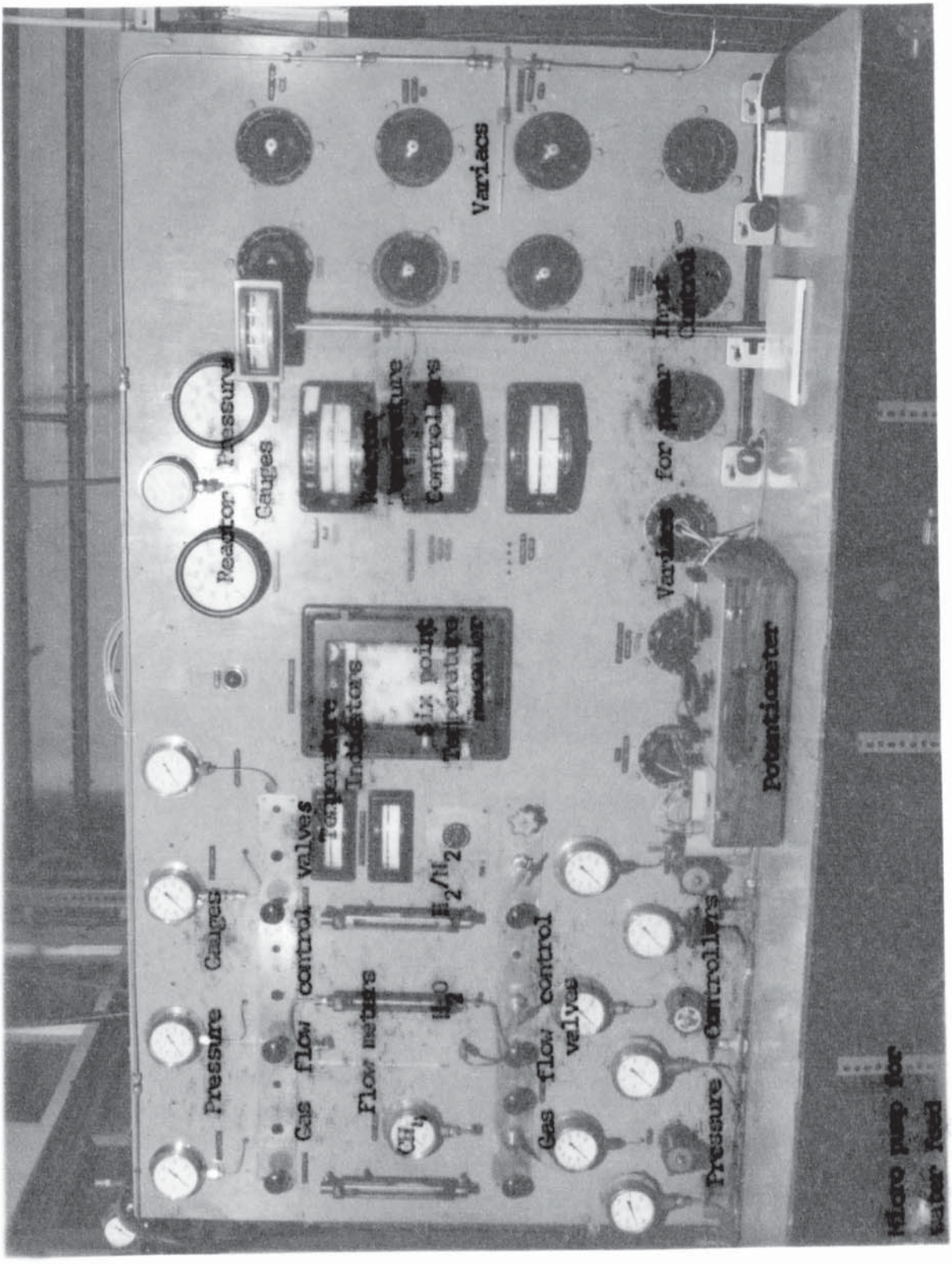

Plate No. 4.2

The Rear view of the Reforming Apparatus

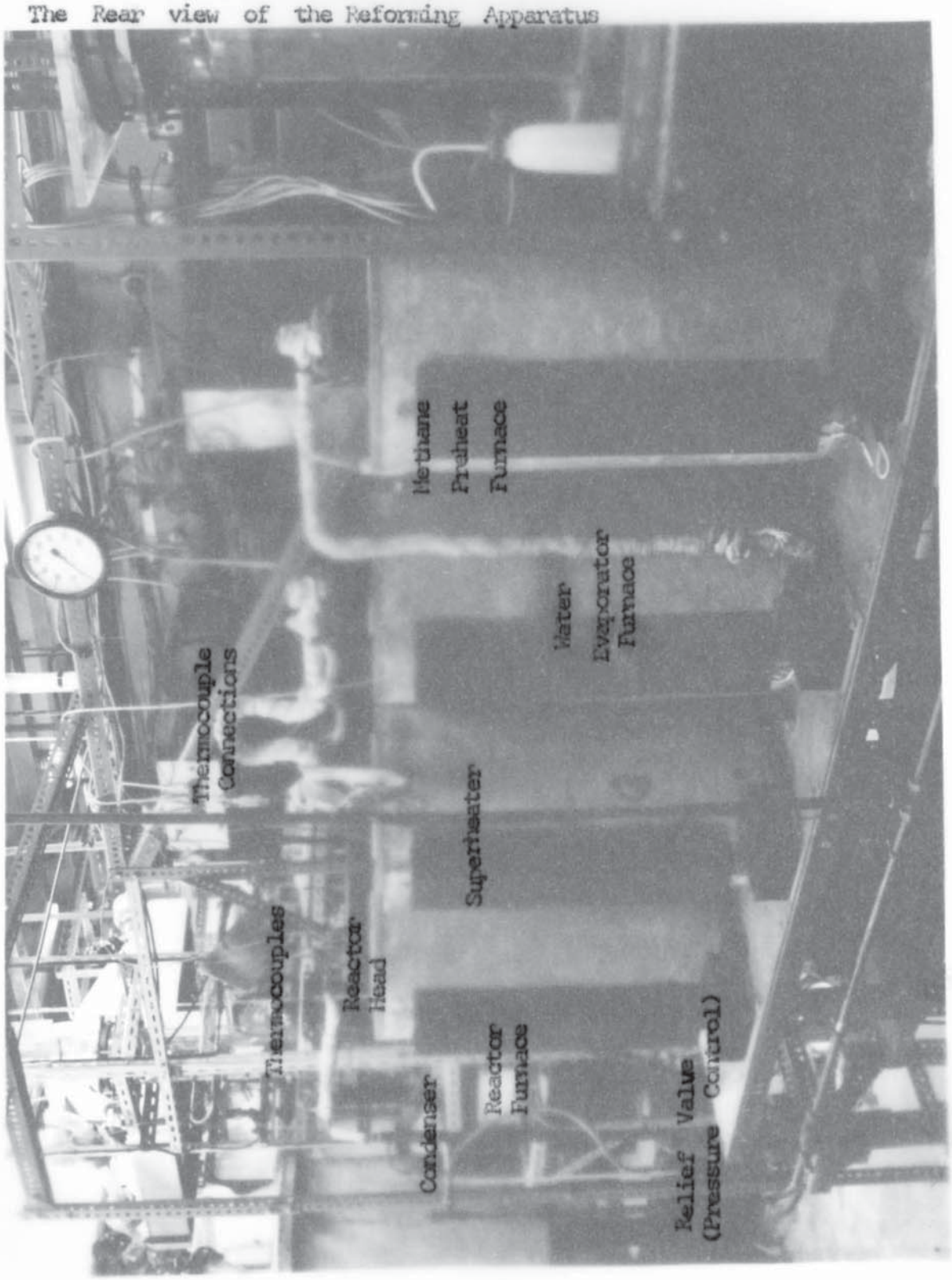

underwent a pressure reduction in cases of high pressure runs and branched into two streams, one of which led to the gas chromatograph to provide a continuous supply of sample, while the other went to the flare. The construction material was stainless steel of Type 304 throughout, with the exception of glass pipe in the water feed line prior to the micropump and glass U-tubes containing calcium chloride for drying the gas samples to be analysed. The composition of the stainless steel Type 304 was given by the manufacturer as 0.08 % C, 0.20% Si, 2.0 % Mg, 8 - 11 % Ni, and 17.5 - 20.0 % Cr.
It was confirmed by blank runs prior to the systematic study, that the catalytic effect of nickel present in the stainless steel on the pyrolysis and reforming of the feedstock at different temperature levels was negligible; only at relatively long contact times was the conversion 0.5 - 0.6 % and was coupled with deposition of carbon.

The piping system for water, feed gas, and product gas was ¼ in. or 1/8 in. in O.D. stainless steel tubing with high pressure fittings used for all joints. All the ¼ in. stainless steel tube connections between the functional equipment were wrapped with electrical heating tape and insulated with asbestos rope. The pressures at different locations of the apparatus were measured with Bourdon gauges, whereas the pressure of the sample gas to the chromatograph was measured on a U-tube water manometer. For temperature measurements chromel-alumel thermocouples were used, and the connections of the thermo-couple terminals to the controllers, recorder and indicators were made with compensating cables. The thermocouples were situated in thermo-wells within the equipment items and extended along the whole height of the feed-stock preheater, the evaporator, the super-heater, and the reactor furnace, permitting internal temperatures to be scanned. The heat loads on all of the radiation furnaces and heating tapes were adjusted by Variac type regulators controlling separately the bottom, middle, and

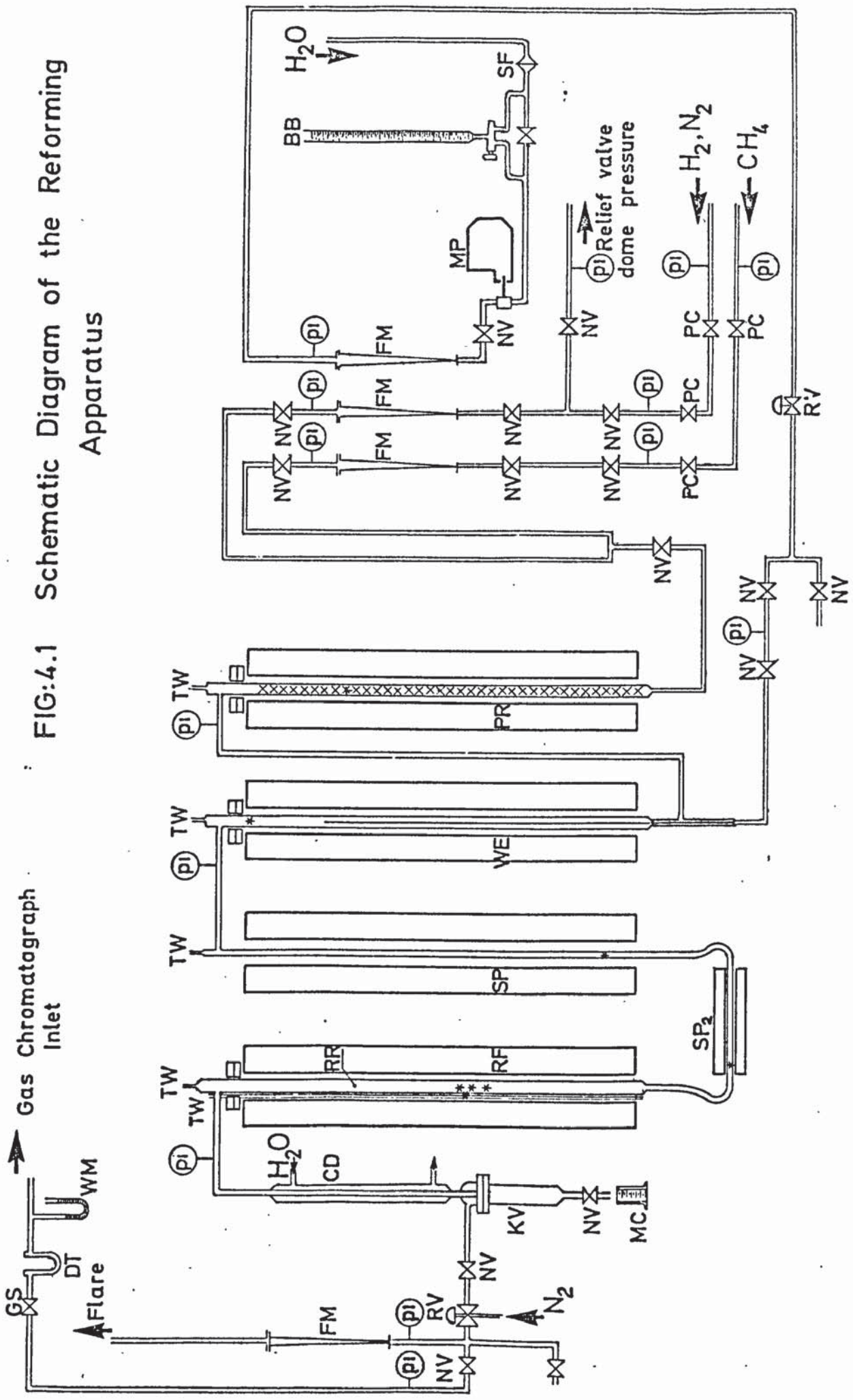

FIG:4.1 Schematic Diagram of the Reforming Apparatus

BB	Uniform-bore Burette
CD	Co-current Condenser
DT	Glass $CaCl_2$ Drying Tubes
FM	Flowmeter
GS	Glass3-way Valve
KN	Pressure Knock-out Vessel
MC	Measuring Cylinder
MP	Micro-pump
NV	Needle Valve
PC	Pressure Controller
PR	Feedstock Preheater
RF	Reactor Furnace
RV	Relief Valve
RR	Reactor
SF	Sintered Glass Filter
SP	Superheater No.1
SP2	Superheater No. 2
TW	Thermowell
WE	Water Evaporator
WM	Water Manometer
*	Temperature Control Points

top resistances wound on fused silica (vitreosil) tubes (6.50 cm I.D.) The reactor furnace had only two windings, the one carried the base load while the other was a supplementary one wound along the middle third of the silica tube. Both were equipped with Ether-Transitrol temperature controllers in addition to the voltage regulators. The temperatures were controlled manually in response to a six-point selector switch indicator and were also recorded on a six-point recorder. Reactor temperatures were measured with a two-position potentiometer accurate to 5μ V, at three internal positions and two wall temperatures, all five thermocouples being capable of movement in the vertical direction.

Detailed information concerning the catalyst employed is given in Chapter 6.

4.2 THE FEED SECTION.

4.2.1 Water feed.

Distilled water was fed from a uniform-bore precision burette (50 ml), through a No. 3 porosity filter to a F.A. Hughes Series 2 single acting reciprocating micro-pump equipped with a 20 RPM drive unit having a short stroke mechanism. The discharge rates of the pump with a single delivery head could be varied within the limits of (2) (10^{-3}) - (40) (10^{-3}) g moles/min. The pulsations in the water feed due to the mode of operation of the pump have been damped to a great extent by connecting a second delivery head 180^{o} out of phase, thereby doubling the output. An adjustable relief valve (Hale Hamilton R - Mk 5) in the pump discharge line permitted checking of the feedrate to be carried out at operating pressures. During the experiments it was adjusted to 50 psi above the working pressure of the system. The mean position and the amplitudes of the float oscillations of a Fischer and Porter (1/16 in) variable area flowmeter mounted in the pressure line served as a qualitative indication of the flowrate.

4.2.2 Methane, Hydrogen, and Nitrogen Feed.

Methane, hydrogen, and nitrogen, the latter to provide an inert atmosphere for purging purposes and for pressure testing of the equipment, were all of high purity and supplied by British Oxygen Co. Pressure reduction was obtained by means of Hale Hamilton L 15 and L 16 type pressure controllers. Gas flowrates were measured with Fischer and Porter variable area flowmeters. A large variation of the flowrates was achieved by using interchangeable flowmeters (1/16 and 1/8 in), with a combination of glass, sapphire and stainless steel floats.

4.2.3 The Feedstock Preheater.

The preheater was 742 mm in length and 18.85 mm I.D. made of stainless steel of 3.91 mm wall thickness, and was packed with fused silica chips to improve the heat transfer. It was placed concentrically in a fused silica (vitreosil) tube of 65.2 mm I.D. which was heated electrically by means of three elements wound on it. These three elements consisted of one central winding (30 ohms) running along the whole length of the silica tube, and two end windings (each 9 ohms) for compensating the heat losses at the two ends of the furnace. All three resistances were separately controlled by Variac transformers. A thermowell made of 1/8 in. O.D. stainless steel tube and running along the axis of the preheater was provided. Into the thermowell a 0.04 in. chromel-alumel thermocouple was inserted and, traversed during operation to any position along the axis, so that the heat input could be adjusted to maintain a definite temperature level.

4.2.4 The Water Evaporator.

The furnace of the water evaporator was of identical design to that used for the feedstock preheater and superheater. A detailed diagram of the evaporator itself is given in Fig. 4.2. The water feed tube (1/8 in) has been extended axially to the top of the

evaporator, i.e.beyond the height used by Woodcock (179). The water was preheated therein by the upward cocurrent flow of methane and then overflowed into the evaporator section. The annulus between the inner walls of the evaporator and the water feed pipe was densely packed with stainless steel knitted-mesh in order to provide a large heat transfer area and evaporation. The original silica chipspacking was replaced by dense knitted mesh which has proved to be more convenient with respect to uniform evaporation of water, and to give no pressure drop for the gas flows used.

4.2.5 The Superheaters.

The construction of the first superheater furnace was the same as that of the previous heating systems. The original superheater (18.85 mm I.D., stainless steel) was packed with silica chips. However, to reduce the time lag of the system for any change of the feed conditions,it was replaced by a ¼ in. O.D. stainless steel tube containing a 1/8 in. O.D. stainless steel thermowell to provide a temperature scan along the whole length.

An additional horizontal radiation heater installed between the superheater and reactor furnaces served to maintain and, if necessary, to increase the temperature of the reactant mixtures before they entered the reactor. Special care was given to the gradual and uniform increase of gas temperatures.

4.3 THE REACTOR SECTION.

4.3.1 The Reactors.

Two types of reactor were used during the experimental runs according to the form of the catalyst. Reactor No. 1, used in the previous investigation (179), was employed to study the effect of the accessible outer surface of hollow cylindrical pellets on the rates of conversion. Reactor No. 2 was developed to investigate the effects

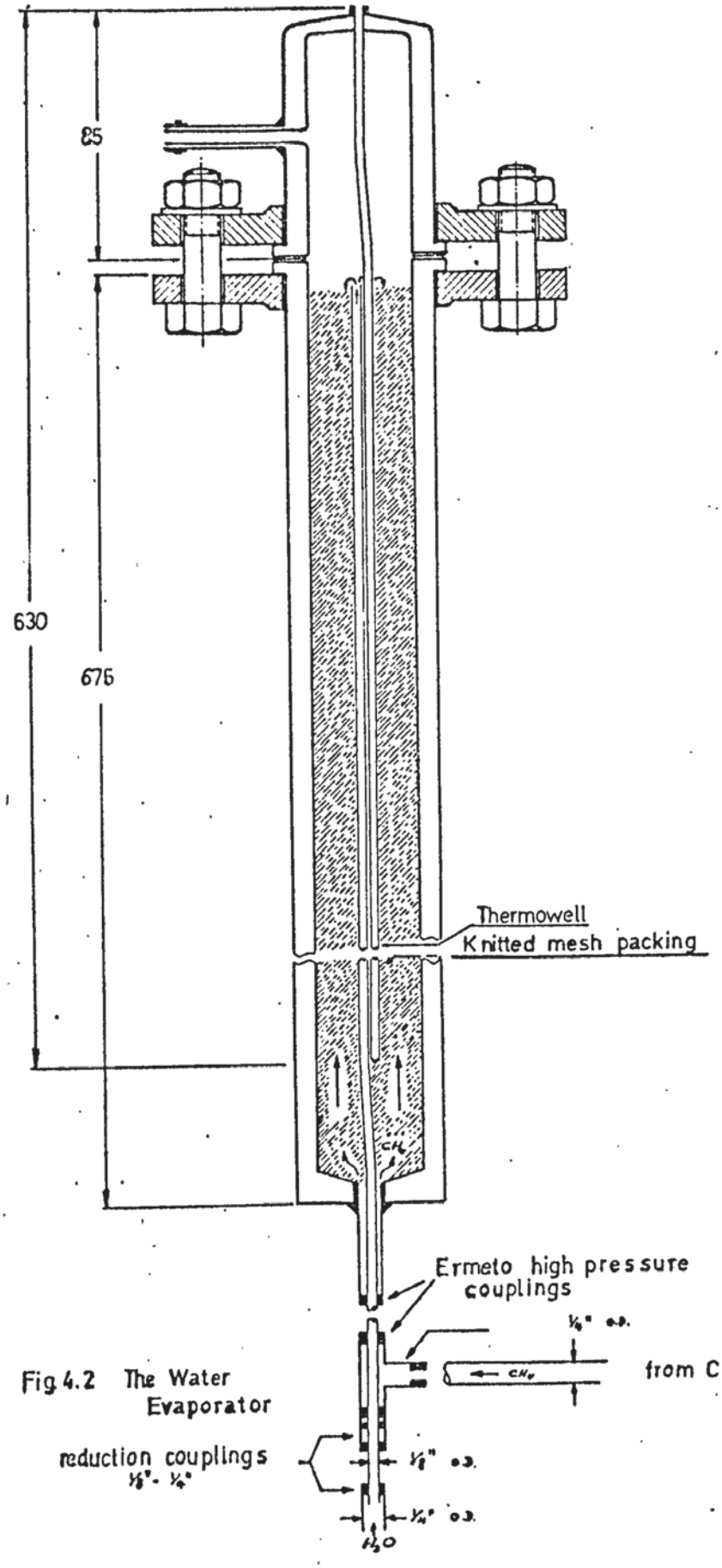

Fig 4.2 The Water Evaporator

of particle size of catalyst in granular or powdered form.

Reactor No. 1. The reactor (Figs. 4.3 and 4.3a) was a stainless steel tube of 18.3 mm I.D. A ¼ in. O.D. tube with a high pressure fitting was welded to the lower part (inlet) of the reactor, whereas a conical Rushton type metal-to-metal joint was used for the exit section. This joint and the high pressure couplings at the inlet and exit of the reactor were coated with a high temperature anti-sieze compound (Threadgard). The high pressure seal was effected by bolting down the backing flanges of the reactor main body and the lid. A ¼ in. O.D. tube welded to the lid at right angles allowed the connection of the reactor assembly to the condenser.

A ¼ in. O.D. tube, placed concentrically in the reactor main body served as the catalyst holder. The location of the catalyst pellets within the reactor could be adjusted by sliding the catalyst support which was fixed to the holder tube by means of grub screws. Another 1/8 in. O.D. tube sealed at the bottom end and welded to the top of the lid, was inserted into the holder and extended to the bottom of the reactor. Three moveable bonded-hot-junction thermocouples, (0.020 in cable diameter , Pyrotenax Ltd.) enabled the axial temperature to be measured and hence controlled throughout the whole length. The outside wall temperatures were measured with two other thermocouples (0.040 in. cable diameter) inserted into a 3/16 in. O.D. tube running along the reactor.

Reactor No. 2. Since the arrangement of Reactor No. 1 did not enable the testing of catalysts in granular or powdered form, a second reactor (Fig. 4.4) was developed. It consisted of a ¼ in. O.D. stainless steel tube, both ends fitted with high pressure joints. A layer of stainless steel wire meash (B.S. 150; nominal aperture 106 μ) was used as the catalyst support. It could be placed at any location

Fig: 4. 3. Reactor No.1

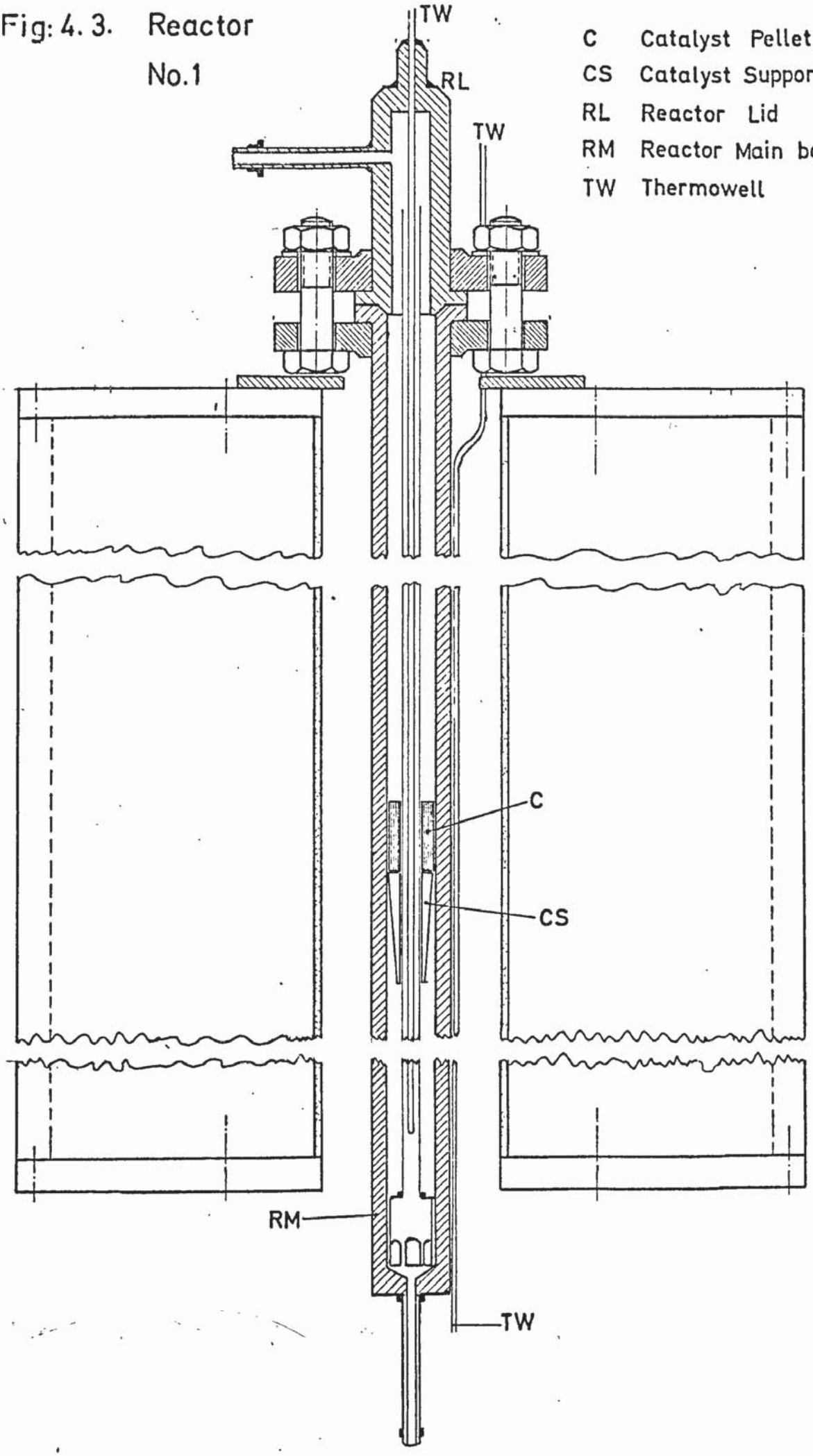

C Catalyst Pellet
CS Catalyst Support
RL Reactor Lid
RM Reactor Main body
TW Thermowell

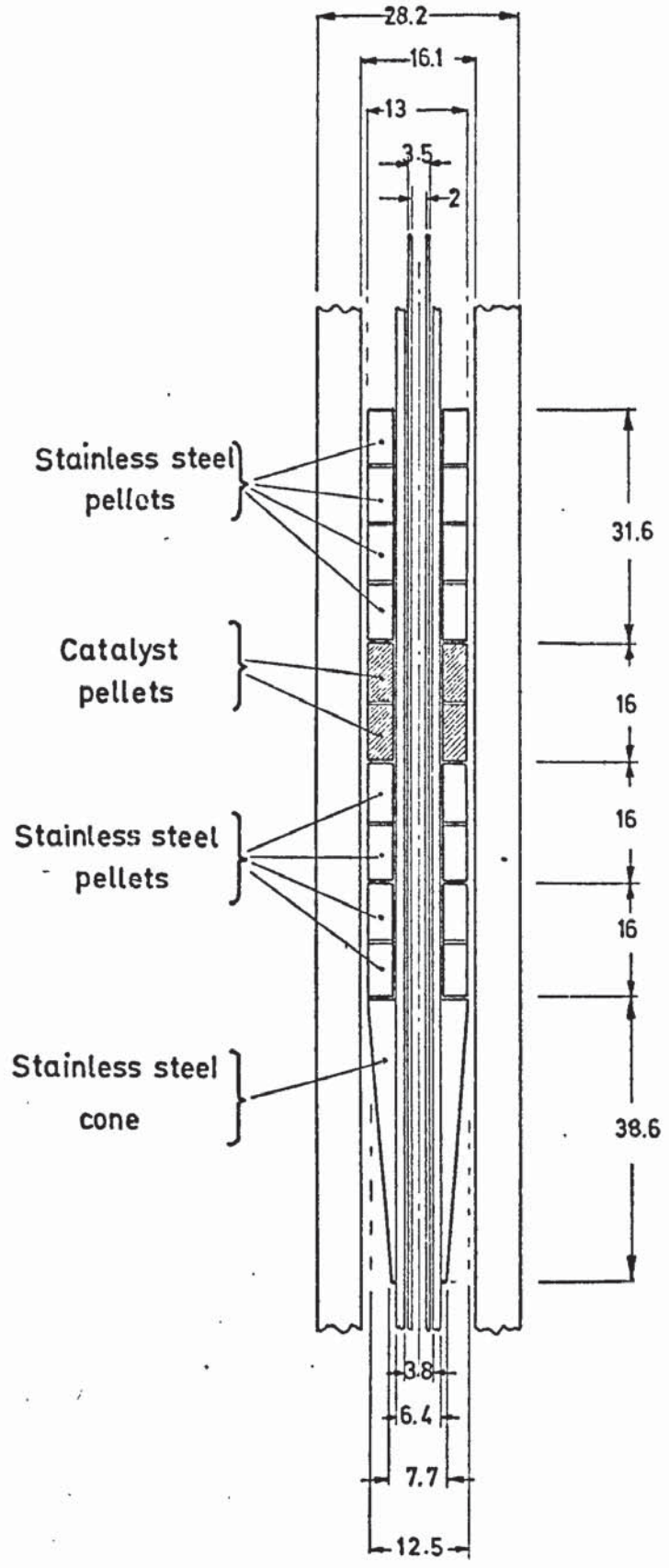

Fig:4.3a. Catalyst Bed of Reactor No:1

Fig: 4.4. Reactor No. 2

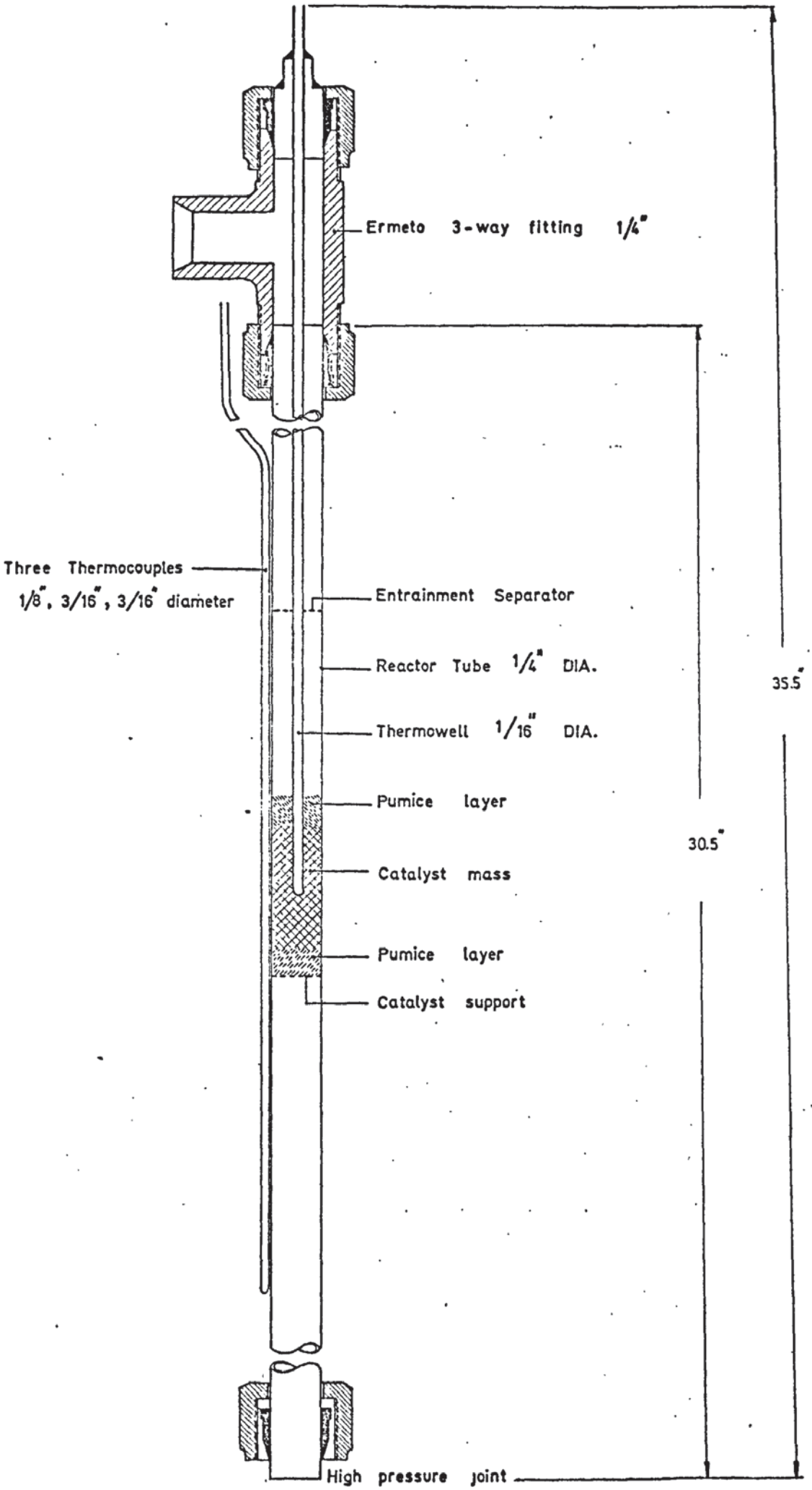

along the height of the reactor tube and was renewed after every set of runs, The top of the reactor was fitted with a "Tee" - joint, the horizontal leg of which connected the reactor to the condenser, while the vertical leg carried the thermowell (1/16 in. O.D) extending to the mid-height of the catalyst bed. Thermowells silver-soldered to the outside wall of the reactor served to measure the wall temperatures.

4.3.2 Heat Supply.

The furnace of the reactor used previously was of similar design and construction to those employed for the preheating and superheating systems. However, in operation, it was found unsatisfactory for the following reasons:

(i) The main winding running along the entire length of the vitreosil tube (620 mm O.D.) supplied heat unnecessarily to the upper part of the reactor above the catalyst bed, where the temperature had to be kept as low as possible in order to prevent any homogeneous gas phase reactions taking place. Thus the upper supplementary winding was found superfluous and even had an adverse effect ; this winding has been removed and also the main winding has been shortened to avoid heating of the upper region.

(ii) It has been proved impossible to concentrate the heat flux in the section of the reactor where the catalyst beds of varying heights were located by means of the existing arrangement. The length of the main winding (65 ohms) has therefore,been reduced to approximately the middle third of the silica tube.

(iii) The response of the system to temperature fluctuations above and below a given preset level was too slow. To improve the operation and to obtain better temperature control and uniform heat supply, the power system has been modified by replacement of the bottom winding with a new 24-gauge Ni-Cr wire (25 ohms).

In each run the mid-height of the catalyst bed was located in the reactor so that it coincided with the region where the heat generated by the two windings overlapped. The lower winding governed the base load on the furnace, whereas the upper served as the supplementary one. The control of the temperature by the heat input was achieved by two Ether-Transitrol controllers incorporated independently in the circuits of the two windings and connected to two thermocouples sensing the bottom and top catalyst bed temperatures.

4.4 THE PRODUCT SECTION.

The products leaving the reactor were made to flow through a ¼ in. O.D. stainless steel tube to a condenser (2 ft x 1 in O.D), which was operated cocurrently in order to obtain an instantaneous reduction of reformed gas temperature. The condensed water was collected in a stainless steel knock-out vessel and emptied through a dip tube fitted with a needle valve to control the condensate outflow. The permanent gases then passed through a Hale-Hamilton dome-loaded type DR-2 pressure controller which maintained the pressure of the reforming apparatus at a given relief setting. For atmospheric pressure work the DR-2 controller was removed since it caused some fluctuations (1 - 12 in WG), in the discharge gas stream. After pressure reduction the gas stream was divided into two branches. One stream, restricted to (2.0 - 2.2) (10^{-3}) g moles/min., went as a continuous sample to the gas chromatograph, while the other passed through a flowmeter and then to the flare. The pressures and temperatures of both gas streams were measured. The flowmeter placed in the flare line was used only for calibration purposes, and during runs it served as qualitative indication for uniform operation and gas flow.

4.5 CALIBRATIONS AND CONTROL.

4.5.1 The Flowmeters.

For relevant methane feedrates and operating pressures, the

"mass flowrate vs scale reading" curves for any combination of rotameter tube size and float material have been prepared by applying the method of calculation given in the Fischer and Porter Flowmeter Handbook (58). A computer program has been written and included the intermediate steps of the calculation procedure involving different levels of ambient temperature and barometric pressure. A sample calculation and one set of curves are given in Appendix A - 4.1 and Figs. A - 4.2.1 - 4.2.3, respectively.

The flowrates of methane and hydrogen obtained for given scale readings on feed flowmeters with different tube size and float material were checked with reactor exit gas and chromatograph sample gas flowmeters using the whole of the apparatus operated at ambient temperature and different pressures. In all cases the maximum deviation was found to be not greater than $\pm$ 1.2%.

4.5.2 The Water Pump.

Variation of the water feedrate was obtained by the micrometer adjustment of the plunger stroke. Calibration curves of pumping rate against micrometer setting were carried out by adjusting the relief valve in the delivery line to 50 psi above the operating pressure of the system and by-passing the water pump to atmospheric discharge. The diagrams (Appendix A - 4.2) show that the pumping rates were not greatly affected by the line pressure. In fact, they were used for approximate selection of new pump micrometer settings when feed conditions were changed. The actual water input was read from differences in burette readings in the suction line of the pump. A further, but approximate, check for the pump operation at low feedrates and for the steady functioning of the evaporator was the quantity of water condensed and collected after the cooler during the activation stage of the catalyst.

4.5.3 Reactor Temperature Control.

The most important and difficult task of the study was to ensure isothermal conditions within the catalyst bed. To achieve this the following steps were taken :

(i) The mid-height of the catalyst bed was located at a place within the reactor where the heat supplied by the two independent windings overlapped.

(ii) The Ether-Transitrol controllers incorporated into the power circuits governing the heat load to the furnace were calibrated with a potentiometer in accordance with the instructions stated in the manual. (Fig. A - 4.5).

(iii) Since the controllers employed were on/off type, the set point of the supplementary upper winding controller was arranged to be 3 - 5 degrees C higher than the bottom controller. By this means the overshoot and undershoot could be reduced considerably.

(iv) The location of the thermocouples connected to the controllers has been found very critical from the standpoint of maintaining a constant temperature region (179). Therefore, two sets of runs under actual reforming conditions, viz.540^{o} C, atmospheric pressure, and 650^{o} C, atmospheric pressure, each at varying feedrates were carried out placing the functional thermocouples inside or outside of the reactor and indicating the bottom and the top temperatures of the catalyst. In these runs the distance between the thermocouple ends was adjusted to 40 mm, corresponding to a maximum bed height. A third and a fourth moveable thermocouple, connected to the potentiometer, were inserted into the thermowells to scan the temperatures along the vertical axis inside and outside the reactor respectively.

The readings were taken every 20 minutes after the reactor bed reached steady state, i.e. approximately 3 hours after the methane-steam mixture was first fed to the system. The longitudinal temperature profiles along the central axis of the reactor and along the reactor outside wall, based on the arithmetic average, are presented in Fig. 4.5. The deviations from the set-point were of a minimum ($\pm$ 1.6), if the controller thermocouples were situated in the thermowell secured to the outside wall. The temperature differences between the central position and outside wall were found rather high in both arrangements.

As a further attempt to reduce the deviations from the set-point and to diminish the temperature differences between the central axis and the outside wall of the reactor, lagging of the middle and bottom sections of the reactor with asbestos rope was tried. The greater thermal capacity of the system had the expected adverse effect of increasing the time lag. However, by a careful adjustment of voltage input, it was possible to maintain a stabilized temperature level, as long as no appreciable disturbances in the heat balance were produced. By this means the fluctuations could be evened out to within $\pm$ 1 degree C. The variations in the feedrates or steam-methane molar ratios were effected gradually and very carefully with the appropriate very small adjustment in the Variac settings. The temperature differences between the central axis and outside wall of the reactor could be reduced to 5 - 9 degrees C. In spite of every effort made to obtain a completely uniform axial temperature distribution along the height of the catalyst bed, it was not possible to eliminate the temperature differences observed. The differences observed changed according to the bed temperature and feedrates and were a minimum (0.5 degrees C) at low temperature of operation and high feedrates, and a maximum (3.5 degrees C) at high temperature conditions and low feedrates. Fig. 4.5 represents for the two temperature levels the longitudinal temperature profile of the

Fig. 4.5. Temperature Profiles Along the Reactor

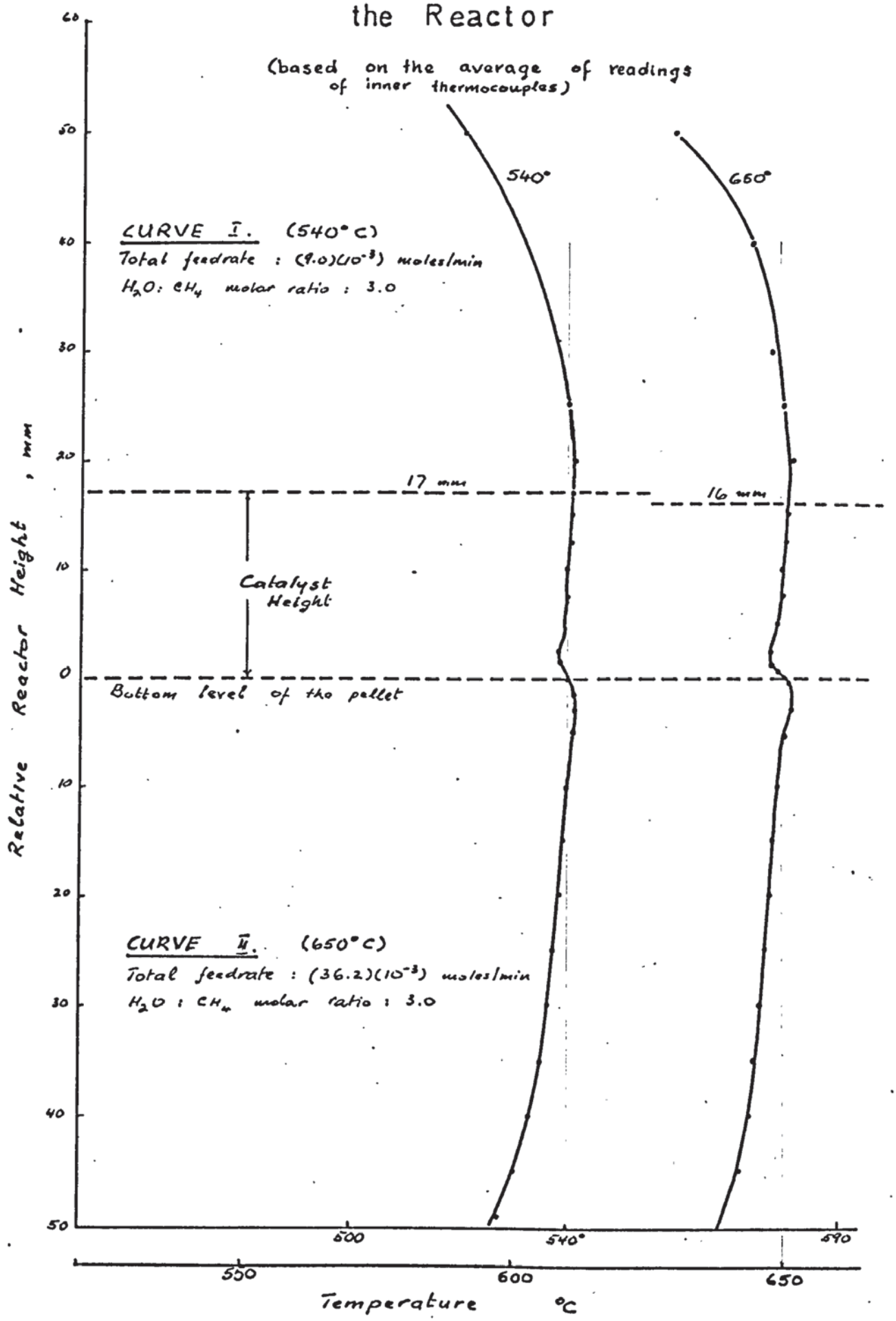

reactor, in each case showing the temperature at the catalyst centre.

The curve for 540° C of Fig. 4.5 refer to a total feedrate (9.0×10^{-3} g moles/min), which was found during the course of investigations to be close to the limiting flowrate for bulk-gas-phase diffusion. On the basis of these tests the reactor, lagged with asbestos rope, was considered satisfactory and therefore used for the subsequent work.

4.6 THE OPERATING PROCEDURE.

4.6.1 Catalyst Loading.

In the preparation of reforming runs with Reactor No. 1, Ermeto couplings on the inlet and outlet ends of the reactor were disconnected and the reactor assembly removed from the furnace. The flange connecting the lid to the reactor main body was unfastened and the lid with the thermowell and the catalyst holder carrying the catalyst pellets was removed. The pellets were then taken out of the holder and kept in a covered glass bottle for weighing and sizing. The catalyst holder and the thermowell were wiped clean of traces of carbon. The inlet and outlet tubes of the reactor were cleaned each time with a pipe cleaner, and the feed-line was cleaned by a blast of nitrogen under pressure. The required number of catalyst pellets in inactive form was measured to 0.1 mm accuracy, weighed and placed on the catalyst holder. The location of the pellets on the holder was measured and adjusted, if necessary, by sliding the catalyst support so that the mid-height of the catalyst column coincided with that section of the furnace where the two heat inputs overlapped. The distance of the bottom of the catalyst pellets from the inlet end of the reactor was also measured and then related to the top of the thermowell in order to take the temperature traverse of the bed during the runs. The reactor was then re-assembled and after relocation in the furnace, Ermeto joints were tightened, and the whole system was pressure tested at 300 psig with nitrogen. A decrease of 10 psi within 6 hours was considered acceptable. When the equipment

had proved to be pressure tight, the pipe-work joining the reactor assembly to the rest of the equipment was insulated, the thermocouples placed in their respective positions, and the system pressure released. The dome of the pressure controller DR-2 was left under nitrogen at the pressure corresponding to that intended for the runs.

The preparatory work for the runs with powdered or granular catalyst using Reactor No. 2 was the same with the exception of unloading and loading the reactor tube. For unloading, the reactor tube was separated from the "Tee"-joint, turned upside down, tapped gently and the catalyst power or granules were collected in a weighing bottle. The wire mesh serving as the catalyst support was removed by pushing it out with a stainless steel rod. The inside of the reactor tube was then cleaned with a pipe cleaner and blasted with high pressure nitrogen. For loading, a new catalyst support was inserted into the reactor and located in the position corresponding to the mass of the catalyst to be used for the runs. The height of the catalyst bed was calculated from the bulk density measurements carried out for each particle size fraction. (A - 4.4). The required quantity of catalyst power was charged into the reactor by means of a long thin stainless steel funnel. Another wire screen was fitted onto the thermowell which extended to the catalyst bed, in order to prevent any particle entrainment during the gas flow.

4.6.2 The Start-up Procedure.

The temperature control tests provided the experience to adjust the voltage input to the ancillary heating equipment to obtain the required preset temperature range within the system. The procedure was as follows:

(1) After pressure-testing the equipment with nitrogen, the dome pressure of the controller DR-2 was adjusted to a level 20 psi higher than the intended operating pressure.

(2) The system was then connected to the flare and nitrogen was

passed for 15 minutes at a pressure just sufficient to overcome the dome pressure of the DR-2 controller. The excess nitrogen pressure in the dome was then released gently until the system pressure dropped to the planned operational level.

(3) After this adjustment, nitrogen flow was stopped and hydrogen was admitted into the system. The flow pressure of hydrogen was adjusted to the system pressure by means of L-16 controllers. The hydrogen flowrate was initially regulated to (40) (10^{-3}) g moles/min. A check of the flowrate was obtained with a further flowmeter having different tube size and float material placed in the flare line.

(4) The water pump was then switched on, the delivery line pressurised by the relief vale to 50 psi higher than the operating pressure and then by-passed to atmospheric discharge. The warm-up period of the whole system was long enough to check at least four pumping rates at various pump micrometer settings against the calibration diagram.

(5) The power was switched on with the preset voltage inputs to various ancillary heating equipment. At this stage the control temperatures of the reactor were set to 400° C.

(6) The following temperatures had to be obtained before the water was introduced to the system and 2½ hours were usually required for this:

Feed preheater		200° C
Water evaporator	(bottom)	80°C
	(middle)	120° C
	(top)	150° C
Superheater I		280° C
Superheater II		300° C
Reactor (catalyst bed level)		300° C

(7) With a gradual increase of the reactor temperature to 650° C

the system would reach thermal equilibrium in 4 hours. Since every series of runs was carried out with new catalyst charges, they had to be activated in situ at 650° C in a stream of hydrogen having a definite hydrogen: steam molar ratio (Chapter 6). The activation was considered started as soon as the catalyst bed attained this temperature level. At 600° C, the hydrogen flow and the water feed were re-adjusted to $(54)(10^{-3})$ and $(6)(10^{-3})$ g moles/min (6.5 ml/h), respectively.

(8) Operation continued for 2 - 4 more hours for the rest of the day and then had to be stopped and left overnight. For this purpose the needle valve on the water feed line was closed, the water pump switched off, the valve on the flare line shut-off, the hydrogen steam turned off, the plant inlet valve closed, and the reactor temperature reduced to approximately 450 - 500° C. The power was left on.

(9) To continue with the activation on the next day, the same procedure had to be carried out in the reverse order, the reactor temperature was raised to 650° C again and held at this level for a further period of 8 - 10hours. The system was left overnight following the procedure stated as Step 8.

(10) On the following morning, the reactor control temperature was set to 12 - 15 degrees C above the intended test temperature to allow for the subsequent drop in temperature caused by the heat capacity difference between steam-methane and hydrogen-steam mixtures and by the endothermicity of the reaction. Hydrogen was again passed through the system with the reactor exit valve open to flare, and the water feed was then switched on. It was not considered necessary to wait for thermal equilibrium, since replacing the hydrogen flow with methane would, in any case, have disturbed it. Generally it took 1 - 2 hours for the reactor temperature to attain the present control temperature.

(11) As soon as the reactor temperature reached the control value, a final adjustment of water feedrate was made in the following manner:

(i) if the water rate required for the first run was smaller than the rate used for activation, then it was reduced to this level.

(ii) if the water rate required was greater than the feedrate during activation, no immediate adjustment was made. The stepwise increase of water supply was carried out later as the hydrogen flow was gradually replaced by methane.

This mode of adjustment was adoptedto prevent the probable instantaneous increase of water vapour concentration during the change-over from hydrogen to methane, which would have caused deactivation of catalyst or disturbances in steam : methane ratio.

(12) The hydrogen flow was then gradually replaced by methane.

(13) When the reator temperature attained a stable level, final adjustments of the furnace temperatures and feedrates were made. The reactor exit gas stream was then branched, with one stream going to the gas chromatograph. Stabilized operation was continued for at least two hours before data logging was started.

4.6.3 Data Logging.

Each set of runs involved a fixed catalyst mass, and generally constant temperature and pressure. Either the total feedrate was varied, the steam : methane molar ratio being held constant, or the latter was changed, while the former was held constant. In either case,after a variation of conditions, 1 - 2 hours were necessary to reach steady-state operation. The runs were arranged so that the changes were effected in ascending order, i.e. the first run was carried out with the lowest feedrate or steam : methane ratio, and continued with higher steam concentrations.

Every run lasted 30 minutes, and a specimen data log sheet is

included as Appendix A - 4.5. For the measurement of the catalyst bed temperatures three readings were taken corresponding to the top, middle, and bottom of the bed. If, for any reason, the deviation from the scheduled temperature exceeded $\pm$ 2 degrees C, the run was rejected. The gas was analysed during the period allowed for the system to attain steady-state operation after a change of operating conditions.

4.6.4 Shut-down Procedure.

It was not possible to complete a full series of runs in one day. In order to continue the runs on the next day, the methane flow was purged with hydrogen for 30 minutes using the same hydrogen : steam ratio as used during activation. After this period the equipment was shut off as described in the previous section (Step 8). The reaction conditions were restored on the following morning, and the runs were continued.

After completion of the run schedule the methane flow was replaced with hydrogen, the water pump switched off, and the power supply to the reactor furnace turned off. The rest of the equipment was left with the power on in order to shorten the time for attainment of thermal equilibrium of the preheat furnaces. The hydrogen flow was stopped overnight and the catalyst bed was kept under a hydrogen atmosphere. The next day the pressure of the system was carefully released by opening the needle valve at the exit of the unreacted steam condensate vessel, the system flushed with nitrogen (white-spot) for 15 minutes and the reactor disassembled. The catalyst was removed from the reactor, weighed and sized.

CHAPTER 5

THE ANALYTICAL EQUIPMENT AND PROCEDURE

5.1 GENERAL DESCRIPTION.

The analyses of the reaction products after the condensation of water were carried out using a Beckman GC-2 gas chromatograph in conjunction with a Honeywell-Brown potentiometric chart recorder having a one second response and one mV span. The arrangement of the analytical equipment is shown in Plate 5.1.

The Beckman GC-2 chromatograph, whose flow diagram is shown in Fig. 5.1, consisted essentially of the following elements:

- a heated sample inlet system with two sample loops,
- a carrier gas flow control system,
- a chromatographic column,
- a differential thermal conductivity cell,
- an electronically controlled heating system providing a continuously variable amount of heat to maintain the selected temperature within $\pm$ 0.01 deg. C.

A voltage regulator served to provide a constant voltage supply to the chromatograph and to the X-Y chart recorder.

Gas samples were admitted to the chromatograph by means of the stainless steel gas sampling valve. The stainless steel chromatographic column, ¼ in. O.D. and 21 ft. long, was the same as that used in the previous investigation (179). Argon was employed as the carrier gas. The column packing was Porapak Q (a porous ethyl-vinyl benzene polymer) beads sized 80 - 100 Mesh. Before each set of runs the packing was reactivated for 8 hours at 120^{o} C in an Argon gas purge.

Two sample loops were connected to the valve whose inlet was on the front of the equipment and which exhausted to atmosphere at the rear. When the valve was being changed with the sample gas, the open exhaust allowed gas to flow purging the interval volume of the

Plate No. 5.1

The Front View of the Analytical Equipment

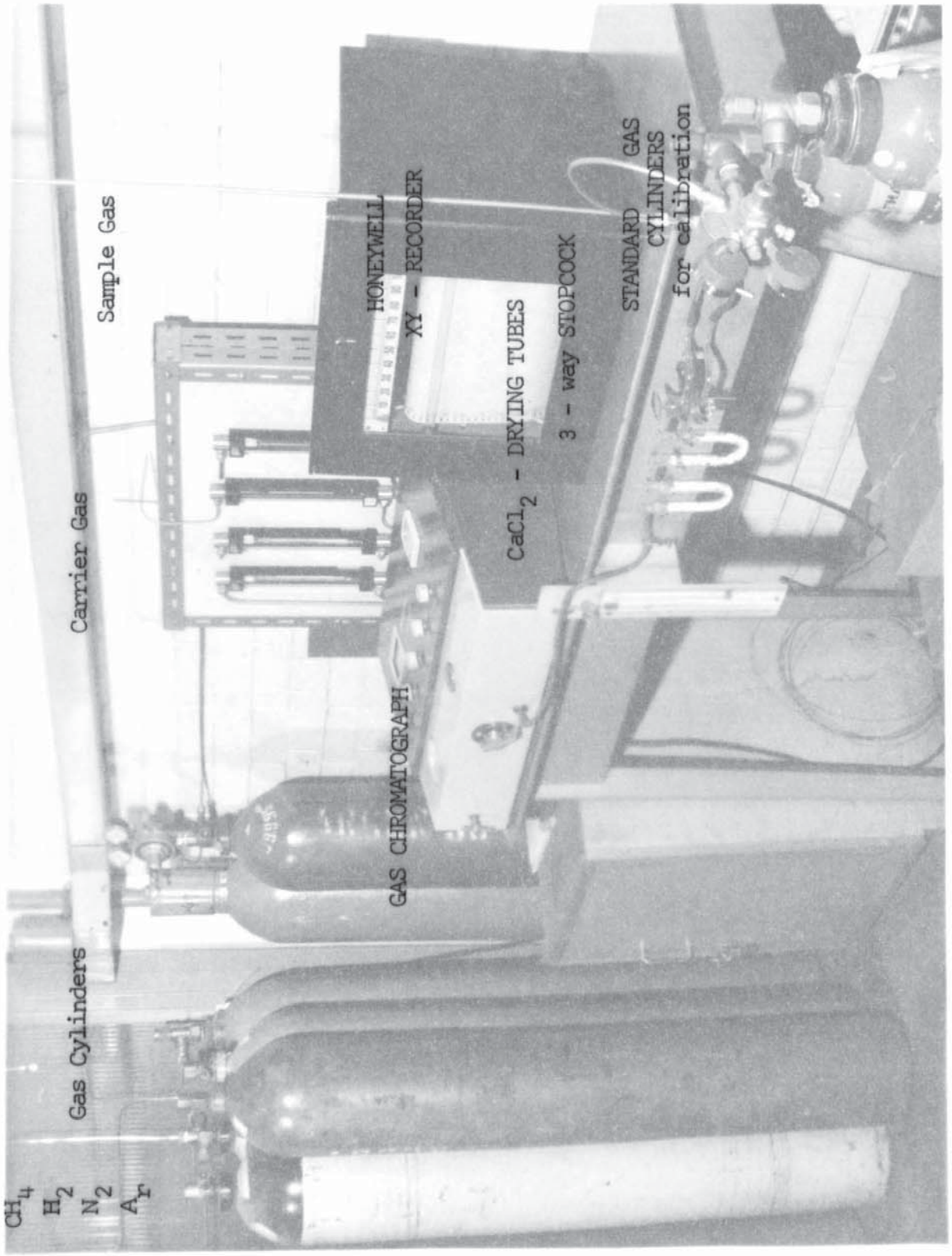

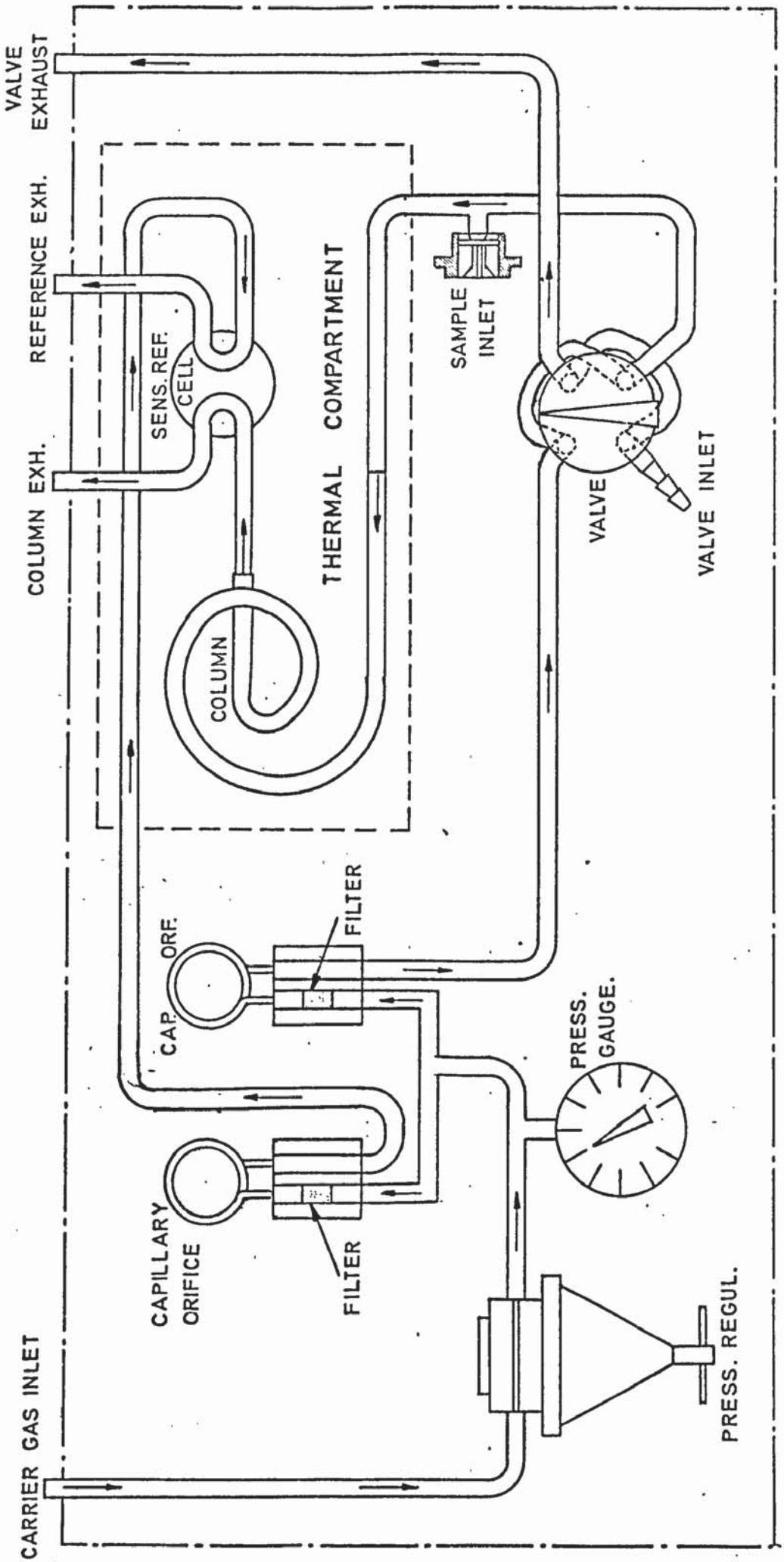

Fig: 5.1 Flow Diagram of the Gas Chromatograph Beckman GC-2

valve and one of the loops, while the other loop received carrier gas. Rotating the valve handle 90° caused the two loops to reverse position, so that the loop formerly in the sample flow system was placed in the carrier gas stream and a given quantity of sample in the loop was swept by the carrier gas into the chromatograph column. The exhaust of the gas sampling arrangement was connected to a 1/16 in. Fischer and Porter flowmeter (sapphire float) to enable a standard flow to be passed through the sampling loop.

Peak areas beneath the recorder trace were used as the quantitative measure of each component. The analyses were carried out at 40° C which was the minimum level for the controlled temperature of the chromatograph. The use of temperature programming was found to be unnecessary.

5.2 THE CALIBRATION.

Porapak Q (Waters Associates, Framingham, Massachussetts, U.S.A.) was preferred as the column packing because it was capable of separating a variety of compounds, including water, very efficiently, and enabled a complete analysis from a single injection in a reasonable length of time (80). Other factors affecting the choice of Porapak Q as the packing material are discussed in detail by Wilhite and Hollis (178) and Woodcock (179), who also studied a combination of column lengths, column temperatures, carrier gas flowrates, and detector filament currents to obtain optimum elution times and peak heights. The column operated at 30.5 psig and the analytical procedure applied in the present work differed from the previous work in the following respects:

(i) A continuous and accurate check of the carrier gas flowrate was achieved by incorporating a Fischer and Porter variable area flowmeter at the inlet of the chromatograph in addition

to the existing pressure regulating valve and dual flow controller of the chromatograph. The carrier gas flowrate was adjusted to 125 ml/min STP. A reduction of this rate to obtain a more significant separation of carbon monoxide and hydrogen was considered to be undesirable since it would have reduced the filament life of the katharometer.

(ii) The katharometer current was increased from 150 mA to 200 mA to obtain higher sensitivities.

(iii) The purge method was employed for gas sampling instead of the vacuum method.

A flowmeter, incorporated in the gas sample exhaust line and a U-tube water manometer, placed before the sampling valve, enabled control of the gas flow and gas pressure through the sampling system. The inevitable fluctuations of flowrate and gas pressure during reforming runs affecting changed in gas sample quantities were restricted by stopping the gas flow to the chromatograph and equalizing the gas pressure to barometric before the sample valve was switched to the carrier gas flow. Also the gas temperature at inlet to the chromatograph varied with the reactor operating temperature, and with the ambient temperature through which it had passed and so the mass of sample varied. Hence the calibration factors had to be determined for every temperature and barometric pressure likely to be encountered using a standard gas, before and after each series of reforming runs. For this purpose high purity CO, CO_2 and H_2 and two certified gas mixtures having the following compositions were used:

	Standard Gas No.I	Standard Gas No.II
H_2, %	50.2	37.6
CO, %	4.9	23.4
CH_4,%	34.5	19.6
CH_2,%	10.4	19.4

Two loops of different size (1 ml and 5 ml nominal volumes) were employed for sample injection. The larger size loop was found especially suited for low conversions yielding low CO and CO_2 concentrations in the reformed gas. The range of appropriate attenuator control settings for each component was established during the pre-calibration tests and summarized in Table A - 5.1 in the Appendix.

The chart speed of the recorder was adjusted to 0.5 in/min and one complete analysis lasted 24 min.

5.3 THE PROCEDURE.

The chromatograph and the chart recorder were prepared for an analysis following the steps detailed in the instruction manuals. However, the necessary warm-up periods for both instruments as indicated in the manuals were found not to be sufficient for temperature stabilization and were extended to at least four hours to obtain higher stability and to prevent base-line drifts. After this period the powerswitch was turned on to supply current to the detector filaments. For complete equilibration and elimination of recorder pen fluctuations, it was considered necessary to allow for an additional warm-up time of two hours. When the recorder trace indicated that the instruments had been completely stabilized, the base line on the strip chart was adjusted by the zero-control-knob on the chromatograph with the lowest attenuator control setting.

The sample gas connections to the inlet of the chromatograph are shown in Plate 5.2. The 3-way glass valve permitted the instantaneous shift of the gas stream from the calibration gas cylinders to the reactor exit. The water vapour was completely separated from the reformed sample gas which was saturated at the condenser temperature before it reached the column, since the elution time of water vapour was, according to the literature (81) , 2½

Plate No. 5.2

The Sample Gas Connections to the Inlet of the Gas Chromatograph

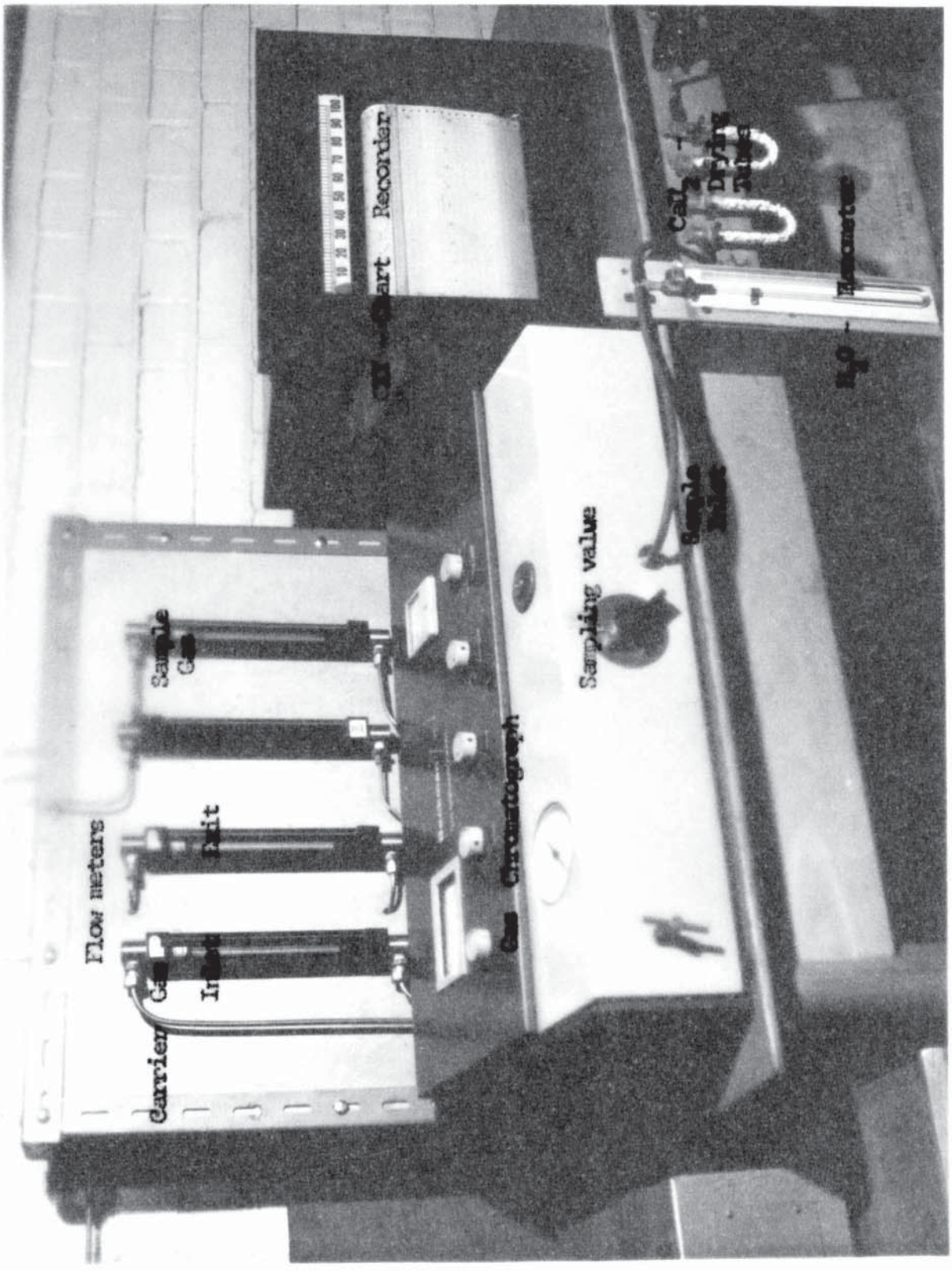

- 6 times longer than carbon dioxide, whose retention time was 20 min. The sample gas, therefore, was dried by passing it through two successive glass U-tubes loosely packed with anhydrous calcium chloride. The pressure was measured by a U-tube water manometer placed close to the sample valve inlet.

After the exit pressure of the calibration gas cylinder was reduced to 15 psig, a continuous gas stream was fed to the chromatograph with the sampling valve in either position. The flowrate and pressure of the gas stream were adjusted to (2.0 - 2.2) (10^{-3}) gmoles/min and 10 - 12 mm WG, respectively. The connection lines, drying tubes, chromatograph valve and the sampling loop were purged with the sample gas for 20 minutes. Then the gas flow was stopped, and the pressure as indicated by the water manometer allowed to adjust itself to atmospheric, since the exhaust of the loop system was open to atmosphere. This ensured accurate measurement of the sample volume for successive uninterrupted runs. The gas sample, now at barometric pressure, was admitted into the carrier gas flow system.

If the sample was injected through the 5 ml loop, hydrogen concentrations exceeding 52% caused overshooting of the recorder pen, even at the highest attenuator setting (200). In such gases, the chromatograms obtained with the 1 ml loop were used for the calculation of the gas composition. In general, the results obtained with two loops in successive analyses for the same operating conditions were checked against each other.

5.4 THE EVALUATION OF THE CHROMATOGRAMS.

It has been found (93) that for quantitative work, more accurate results are obtained by relating the concentration of the components in the gas mixture to peak areas rather than peak heights.

The almost linear relationship which is generally obtained between the peak area and the concentration or amount of sample component also allows the establishment of good calibration curves with fewer measurements (87) and, hence enables the volume per cent of each component in the gas to be found by simple calculation.

Peak areas are determined by various techniques in the field of chromatography. With the exception of expensive automatic integration which requires the least effort by the operator, all methods are dependent upon the skill of the operator and the accuracy of the measuring instrument. Planimetry, the cut-and-weigh method, and the product (peak height x width at half-peak height) were all tried in the preparation of the calibration curves. Because of possible fluctuations in the mains voltage, the effects of chart speed variations of the X - Y recorder causing erroneous peak areas were eliminated by using a constant-voltage transformer. The reproducibility of the peak area measurements with the planimeter was $\pm$ 2.0 % for five tests on identical samples of standard gas. The areas calculated as the product "height x width at half peak height" differed from the planimeter measurements by a maximum of $\pm$ 4.0 %. The accuracy limits for the planimeter were found to be 2.2 % based upon ten observations on a given peak. The cut-and-weight method gave reproducible results within $\pm$ 1.8 %, but was not used to avoid the destruction of the chromatograms.

To establish the correlation between the volume of the component in the sample and the peak area, the calibration analyses were continued, changing the calibration gases and sampling loops each time. The peak areas thus obtained for every component and converted to a base attenuation were then plotted against the volume of the component in the sample. These plots showed that, over the range of gas compositions anticipated during actual

reforming experiments, a reasonably linear relationship existed between the peak area and the quantity of component gas in the sample. However, the slopes were different because of the difference in thermal conductivities of the components.

The component elution times were:

Hydrogen	5 min ± 2 sec.
Carbon monoxide	6 min 40 sec ± 3 sec.
Methane	9 min 20 sec ± 5 sec.
Carbon dioxide	20 min ± 10 sec.

5.5 THE ANALYSIS OF THE REFORMED GAS.

After two calibration check runs (one for each sample loop) carried out prior to every set of experimental reforming runs, the calibration gas cylinder was isolated, and the reactor exit gas line from the pressure controller DR - 2 was connected to the chromatograph by means of a 3-way glass valve. The connection line, the drying tubes, and the sampling valve assembly were purged for 30 minutes with the reformed gas before the latter was analysed. The the gas flow was stopped, the gas pressure in the sample loop equalised to barometric, and the gas sampling valve turned to introduce the sample into the carrier gas stream. The reactor product gas flow was then restored to its previous rate, the second sampling loop now being purged with the reformed gas. The elution time of the first component (i.e. hydrogen, 5 min) was sufficient to re-check the stability of the base line at the maximum and minimum attenuator settings, with adjustment of the zero-control, if necessary. The attenuations had to be changed for every component and the changes were made immediately before the peak corresponding to the component started to be trac ed. However, in the case of carbon dioxide, which was the final peak and was usually traced at

the lowest attenuation, the attenuator control setting was adjusted earlier (4 - 5 min) in order to re-check the base line.

Upon completion of the analysis, the sampling valve was turned to the other position, and a second sample of reformed gas resulting from the same operating conditions of the reactor was analysed. Two typical chromatograms representing analyses of reformed gas with the 5 ml and 1 ml loops are illustrated in Fig. 5.2 and Fig. 5.3 respectively. The operating parameters for each analysis and the calculated composition for each peak are also stated.

5.6 THE CALCULATION OF THE REFORMED GAS COMPOSITION.

From a completed chromatogram the composition of the sample was calculated using the calibration curves or applying the following relationship between the reduced peak areas and volume per cent of the component:

$$x = (x_c) \frac{a_x A_x}{a_c A_c} \quad \% \qquad (5.1)$$

where:

x = Volume per cent of component x in the reformed gas,

x_c = Volume per cent of component x in the calibration gas mixture

a_x = Attenuator setting for component x in the analysis of the reformed gas,

A_x = Peak area of component x obtained in the analysis of the reformed gas,

a_c = Attenuator setting for component x in the analysis of calibration gas,

A_c = Peak area of component x obtained in the analysis of calibration gas.

A sample calculation for a reformed gas composition is given in Appendix A - 5.2 . A confirmatory check of the total volume

FIG: 5.2 CHROMATOGRAM OF A REFORMED GAS
(1 ml sample loop)

Column	:	Porapak Q, 21 ft, ¼" O.D.
Sample loop	:	5 ml (nominal)
Carrier gas	:	Argon (30.5 psig)
Carrier gas flowrate	:	125 ml (STP)/ml
Katharometer current	:	200 mAmp
Column temperature	:	40° C
Recorder chart speed	:	0.5 inch/min
Sample gas flowrate	:	$(21)\ (10^{-3})$ moles/min
Sample gas pressure	:	8 mm H_2O

Reactor operation

Temperature	:	650° C
Pressure	:	0.987 atm abs.
CH_4 - flowrate	:	$(9.70)\ (10^{-3})$ moles/min
H_2O - flowrate	:	$(29.14)\ (10^{-3})$ moles/min
H_2O : CH_4 ratio	:	3.0

Gas Composition			Attenuator Setting.
H_2	:	34.35%	(100)
CO	:	1.45%	(1)
CH_4	:	56.79%	(20)
CO_2	:	7.41%	(1)

Conversion : 13.50%

Fig.5.2.

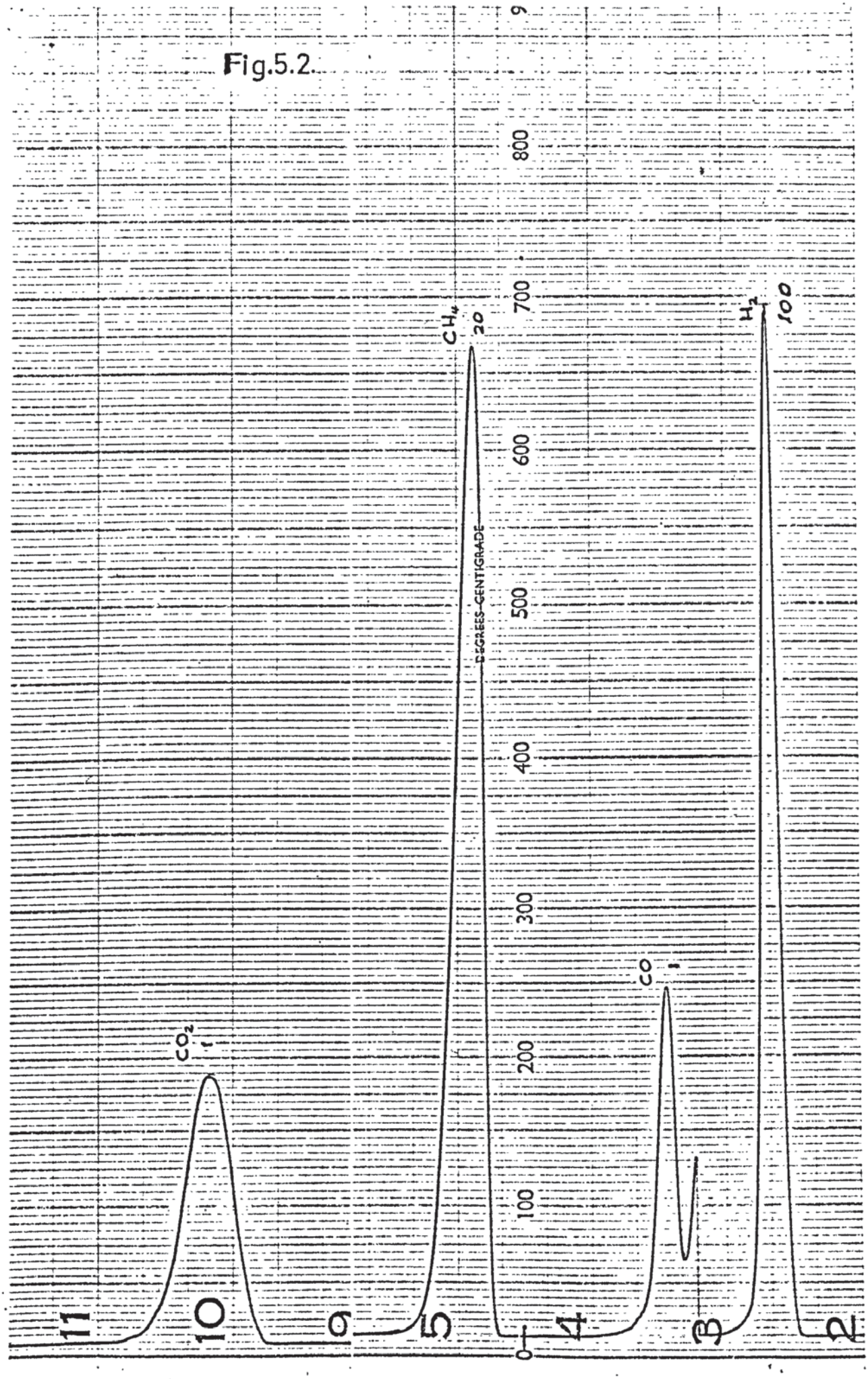
DEGREES-CENTIGRADE
CO2
CH4
CO
H2
11
10
9
5
4
3
2
1
100
200
300
400
500
600
700
800
900

FIG. 5.3 CHROMATOGRAM OF A REFORMED GAS

(5 ml sample loop)

Column	:	Porapak Q, 21 ft, ¼" O.D.
Sample loop	:	1 ml (nominal)
Carrier gas	:	Argon (30.5 psig)
Carrier gas flowrate	:	125 ml (STP)/min
Katharometer current	:	200 m Amp
Column temperature	:	40^{o} C
Recorder chart speed	:	0.5 inch/min
Sample gas flowrate	:	$(21)(10^{-3})$ moles/min
Sample gas pressure	:	10 mm H_2O

Reactor operation

Temperature	:	650^{o}C
Pressure	:	0.987 atm abs.
CH_4 flowrate	:	$(7.25)(10^{-3})$ moles/min
H_2O - flowrate	:	$(21.83)(10^{-3})$ moles/min
H_2O : CH_4 ratio	:	3.01

Gas Composition			Attenuator Setting.
H_2	:	40.87%	(200)
CO	:	1.84%	(2)
CH_4	:	48.47%	(50)
CO_2	:	8.80%	(1)

Conversion : 18.01%

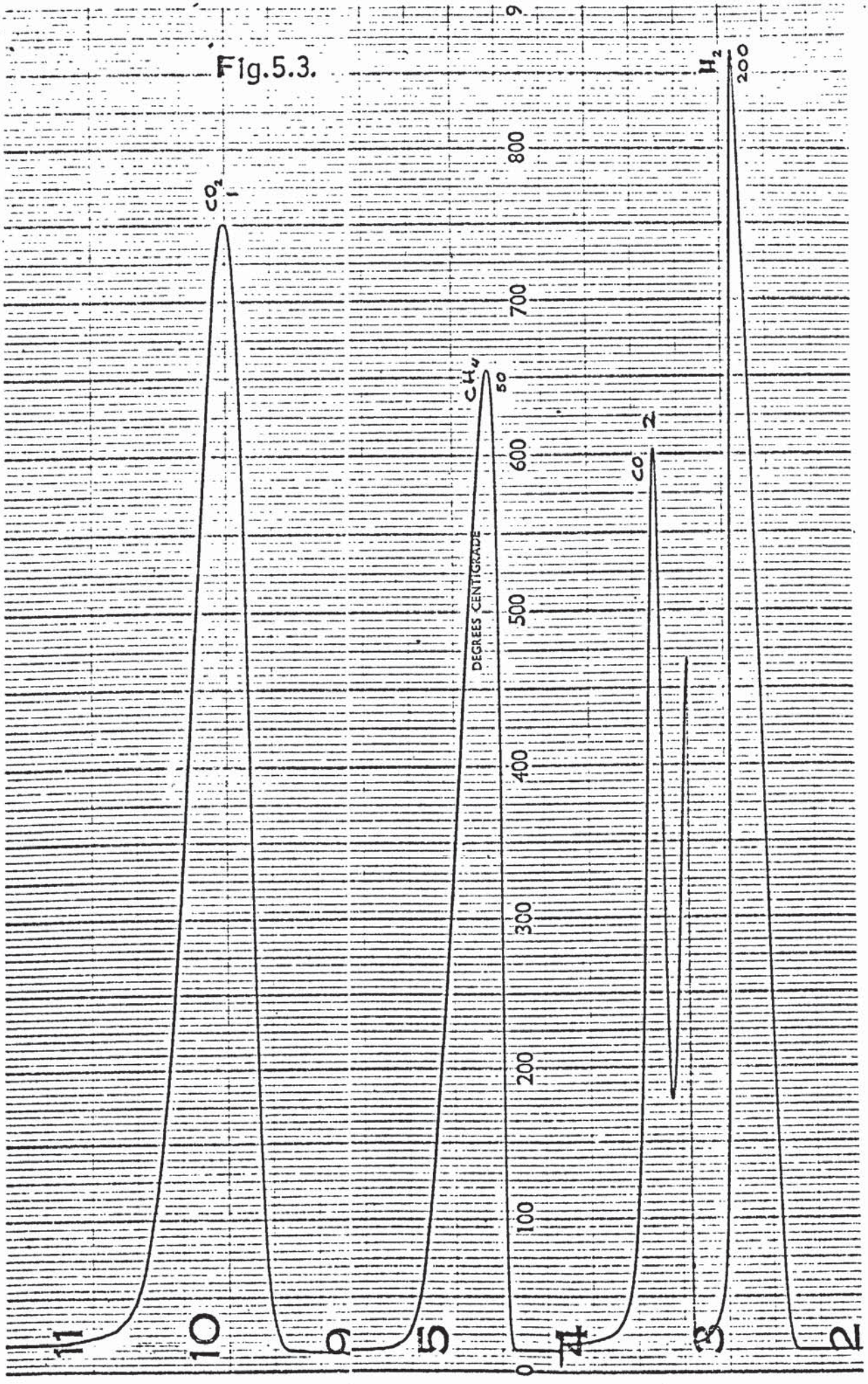
Fig.5.3.
CO_2
CH_4
CO
H_2
DEGREES CENTIGRADE
0
100
200
300
400
500
600
700
800
900
50
200
11
10
9
6
5
4
3
2

could be made by summing the individual volumes of the components.

For an analysis, and consequently a run, to be considered valid, the following criteria had to be satisfied:

(i) The sum of the volume per cent of the components should not have an error greater than $\pm$ 2%.

(ii) The massbalance check (Appendix A - 5.3) should be within the limits of $\pm$ 2%.

A computer program has been written to calculate the composition of the reformed gas and also to evaluate other information pertinent to the kinetic analysis. The computer program and a print-out of the results are given in Appendix A - 5.4. The input data of the computer program was:

Weight of the catalyst pellet, g
External surface of the pellet, cm^2
Diameter of the catalyst pellet, cm
Height of the catalyst bed, cm
Cross-sectional area of annulus between the reactor inner wall and the catalyst bed, cm^2
Operating pressure, atm abs.
Operating temperature, ^oC
Reduced area of the hydrogen peak, cm^2
Reduced area of the carbon monoxide peak, cm^2
Reduced area of the methane peak, cm^2
Reduced area of the carbon dioxide peak, cm^2
Methane feedrate, 10^{-3} moles/min
Water feedrate, 10^{-3} moles/min
The calibration coefficients allowing for temperature and pressure for H_2, CO, CH_4 and CO_2 which were continually up-dated according to the calibration runs repeated before each reforming experiment.

The computer calculated the following quantities:

The per cent composition of the reformed gas according to Equation 5.1.
The normalised per cent composition of the reformed gas
The mass balance check, (BAL1 and BAL2) (detailed procedure is given in Appendix A - 5.3)

CO_2 : ($CO + CO_2$) volumetric ratio, (RATI)

Per cent conversion $= \frac{\% CO + \% CO_2}{\% CH_4 + \% CO + \% CO_2} \times 100$, (CONV)

Individual feedrate of the reactants (FMET and FWAT)

and the total feedrate (10^{-3}) gmoles/min (FTOT)

$(W/F_T) \times 10^3$, g catalyst/(moles total feed) $(min)^{-1}$

$(S_c/F_T) \times 10^3$, cm^2 catalyst external area/(moles total feed) $(min)^{-1}$

H_2O : CH_4 molar ratio,

Flowrate of individual reaction products leaving the catalyst bed, 10^{-3} moles/min (calculation procedure is given in Appendix A - 5.4)

(FCH_4, FH2O, FCO, FCO2, FH2)

Total reformed gas, computed as the sum of the individual reaction products, (10^{-3}) moles/min, (TOTAL REF. GAS 1 and 2)

Partial pressure of the reformed gas components, atm,

(PCH4, PH2O1, PH2O2, PCO, PCO2, PH2)

Mole fraction of the reformed gas components, (YCH4, YH2O1, YH2O2, YCO, YCO2, YH2)

Check for the sum of mole fractions of components, (YTOT1 and 2)

Check for the sum of partial pressures, (PTOT1 and 2)

Moles of methane converted per mole of total feed, (SCH4)

Moles of steam reacted per mole of total feed, (SH2O1 and 2)

Moles of carbon monoxide formed per mole of total feed, (SCO)

Moles of carbon dioxide formed per mole of total feed, (SCO2)

Moles of hydrogen formed per mole of total feed, (SH2)

Volume of reformed gas, cm^3/min (detailed calculation for the figures printed out are given in Appendix A - 5.4)

Linear velocity of the reacting gas, cm/min

Contact time, (10^{-3}) min

Space velocity, min^{-1}

Density of the reformed gas, (10^{-3}) g/cm^3

Check calculation of unreacted steam as collected water, ml/mole of total feed

Viscosity of the reaction components, g/cm/sec

Viscosity of the reformed gas, g/cm/sec

(Calculation procedure is given in Appendix A - 5.4)

Superficial mass velocity of the reacting mixture, (10^{-3}) $g/(cm^2)(sec)$

(Calculation procedure is given in Appendix A - 5.4)

Reynolds number of the reacting mixture

$$N_{Re} = \frac{(D_R - D_c)\, G}{\mu}$$

Following ratios:

$(P_{CO_2})\,(P_{H_2}) : (P_{CO})\,(P_{H_2O})$, (KSHIFTI and 2)

$(P_{CO})\,(P_{H_2}) : (P_{CO_2})\,(P_{H_2})$, (KSHIFT REV 1 and 2)

$(P^2_{CO}) : (P_{CO_2})$, (KBOUDOUARD REAC.)

$(P_{CH_4}) : (P^2_{H_2})$, (KMETHANE REAC.)

$(P_{CO})\,(P^3_{H_2}) : (P_{CH_4})\,(P_{H_2O})$, (KREFORMING REAC. 1 and 2)

$(P_{CO_2})\,(P^4_{H_2}) : (P_{CH_4})\,(P^2_{H_2O})$, (KCOMB.REFOR. REAC. 1 and 2)

CHAPTER 6

THE CATALYST

6.1 INTRODUCTION.

The chemical composition and physical properties of the commercial catalysts used for steam-reforming of hydrocarbons differ in general, according to the type of feedstock and the operating conditions, which cover a wide range of temperature (400 - 1200^{o} C) and pressure (1 - 35 atm). This is associated mainly with the tendency of different hydrocarbons to form carbon as a result of their kinetic behaviour which is affected by the catalytically active species as well as by the components of the support. Innumerable investigations have been undertaken in the past four decades to develop a catalyst formulation which could be applied effectively to any type and at any stage of reforming. However, it has not proved possible to completely satisfy with a single formulation the conflicting requirements in the general properties of reforming catalysts such as:

(i) high activity, i.e. high surface area of the active component

(ii) long range stability, i.e. prevention of crystal growth or sintering

(iii) physical strength to withstand the severe reforming conditions of high partial pressures of steam and hydrogen at comparatively high temperatures

(iv) catalyst shapes which would minimise pressure drop in the reformer

(v) and, of course, the direct economic requirement of low production costs.

Especially with the higher hydrocarbon feedstocks, carbon laydown even at steam: hydrocarbon feed ratios well above the thermodynamic minimum was the major limitation which could only be overcome by using extremely high steam ratios resulting in uneconomic operation. The kinetic formation of carbon from methane and hydrocarbons below butane by pyrolysis did not seem a critical problem even at thermodynamic minimum

steam ratios (11, 26, 31).

6.2 CHEMICAL COMPOSITION OF REFORMING CATALYSTS.

6.2.1 The Effect of Chemical Composition on Activity.

Common to all type of commercial catalysts is the use of nickel as the active component, although in different percentages. Several mixtures of nickel oxide with cupric oxide did not improve the catalytic activity in methane reforming (84). Pease and Chesebro (121) reported that they could attain the equilibrium state very rapidly with methane-steam mixtures at 500° C and 1 atm abs. with a catalyst prepared by impregnating diatomite brick with nickel nitrate and thorium nitrate solution. Metallic nickel in wire mesh form has also been used (21) in steam and carbon dioxide reforming methane, but was limited to laboratory scale kinetic investigations and only to eliminate the interference of pore diffusional effects. Elemental nickel in the form of shot or screens is reported to exhibit relatively less activity because of low porosity and low surface area (11). Oxidation of methane in fluidised beds of group VIII metals at 30 psig and 1530° F is claimed to produce 92 per cent H_2 and CO in the ratio of 2 : 1 (154). Cobalt catalysts, prepared from cobalt nitrate and corundite (75), or in combination with cupric oxide and alumina (84) were found in some cases entirely unsatisfactory (75), and furthermore to be less effective and more expensive (31). Lewis (100) employed cupric oxide as catalyst in a fluidised bed and indicated an effective oxidation of methane at 1700° F. The noble metals platinum, palladium, iridium, rhodium, and ruthenium were found to be more active per unit weight of active component than nickel, but the cost of catalyst per unit activity outweighed this advantage. At the same time, these metals did not eliminate the difficulties associated with the formation and deactivating effects of carbon arising from dehydrogenation-polymerization reactions of higher hydrocarbons.

The catalytically active component, nickel, is supported on a complex mixture of oxides such as Al_2O_3, MgO, CaO and SiO_2, whose main functions are to provide a non-sintering surface for the active species even at the severe reforming conditions as well as adequate physical strength to prevent disintegration. Extensive studies have been carried out to elucidate the effects of the support components on the initiation and extent of the cracking reactions, when higher hydrocarbons (C_5 - C_{10}) are being processed, and on the stability of the catalyst, i.e. the preservation of the nickel surface area and the suppression of crystal growth induced by high partial pressures of steam and high temperature. From the results obtained it has been concluded that the presence of silica, which acted as binder in the form of aluminum silicates had to be avoided as much as possible for two reasons. In the first place, the volatility of silica in steam, particularly at high pressures, as orthosilicic acid, $Si(OH)_4$, was found to be significant so that it was slowly removed from the catalyst bed and deposited downstream in cooler parts; consequently a change in the crystal structure of the support was evident. Secondly, and of more importance with respect to the formation of non-equilibrium (kinetic) carbon, is its catalytic effect as an acidic component on the cracking of higher hydrocarbons. It has been well-established that in steam reforming of higher hydrocarbons the tendency for carbon formation increases with the increase of Lewis acidity of the support, which is consistent with the fact that acidic silica-alumina gels are good hydrocarbon cracking catalysts (70, 71, 160).

In fact, the minimum steam ratios, moles of H_2O : atoms of C, to suppress the non-equilibrium carbon deposition in steam-naptha reforming could be diminished for nickel catalysts from 10 when supported on china clay, to 4.30 when supported on α-alumina, and to 3.7 when supported on magnesia (8); however, these values are

still outside the range of economic operation. For the neutralization of the incompletely co-ordinated ions (Al^{+++}, Mg^{++}) on the catalytic surface, which take on acidic character at high temperatures and high steam concentrations and give rise to the formation of carbon, some basic refractory oxides, in particular UO_2, have been incorporated in the α-Al_2O_3 support. There is as yet no full agreement about the effects of uranium oxide. Thus while Andrew (8) indicates that UO_2 had virtually no activity, other workers (115, 116, 117) claim, on the basis of direct experimental evidence, that carbon deposition could be suppressed in a very efficient way. The introduction of uranium oxide to the catalyst formulation was found to increase the activity in terms of gas composition, i.e. by obtaining a closer approach to equilibrium, and to result in the stabilization of active nickel sites by preventing sintering and encapsulation with carbonaceous deposits arising from the cracking reactions. It is interesting to note that the addition of uranium oxide (U_3O_8 = 7.2 %) decreased the specific surface of α - Al_2O_3 support from 3.5 m^2/g (bare support) to 1.0 m^2/g, whereas the specific surface of a sample containing 6.2 % NiO on the same support was 7.0 m^2/g. On the other hand, a mixture of nickel oxide(Ni= 2.7 %) and urania(U = 2.95 %) on the same α-Al_2O_3 resulted in an increase of specific surface to 12.0 m^2/g (114). They concluded from these facts that the uranium is either reducing the crystallite size of nickel atoms or is combining with nickel to form a compound of high surface area, thought to be nickel uranate NiO.3 UO_3, the fragmentation of which might have probably produced additional boundary surfaces. This compound is also considered responsible for an enhanced adsorption and dissociation of H_2O molecules to give them a high activity against carbon or carbonaceous deposits. It is also remarkable that the presence of uranium in the catalyst has proved to have important effects on the kinetics of the reactions involved. In fact, the initial reaction

rate between n-butane and steam on a (15 %) nickel catalyst supported on γ - alumina over the temperature range 420 - 480° C has been given by Bhatta and Dixon (16) as zero-order with respect to butane and first-order with respect to water with an activation energy of 13,000 cal/mole, whereas the same workers report later (17) that with a catalyst composed of 13% nickel, 12.1 % uranium, 0.3 % potassium, supported on corundum, the initial reaction rate could be described by the equation:

$$r_o = k.p_{C_4H_{10}} \cdot p_{H_2O}^{-0.6}$$

at 450° C, where the apparent activation energy, obtained over a temperature range 404 - 491° C, had a value of 24,000 cal/mole.

The mechanism responsible for this radical change in kinetic parameters of the same reaction for given initial feed composition is still not completely elucidated. On the basis of X-ray examinations, active pore area measurements, and differential thermal analyses for hydrogen adsorption of urania incorporated catalysts(114), there is sufficient evidence to conclude that the surface structure is modified by re-arrangements and development of new surface phases and crystallite structures, but is not sufficient to explain the change in the reaction orders. The responsibility of the preferential adsorption of steam on the urania containing catalyst for the reduction of reactor order with respect to H_2O, is attributed to the effects of different types of uranium oxides ranging from UO_2 via U_3O_8 to UO_3. It has been reported by Dowden et al. (55) that oxygen-deficient oxides may favour the dissociative adsorption of steam to form a higher oxide and hydrogen (45, 116)Bhatta and Dixon (17) indicate the possibility of the formation at the nickel-urania-interface of a complex which is active for both the breakdown of hydrocarbon and for the dissociative adsorption of steam, which then acts as a source for the supply of oxygenated species to the nickel surface for the subsequent reforming reactions.

Whatever the mechanism, it is apparent that uranium oxide functions as a structural promoter for the creation and stabilization of accessible active sites on the catalyst surface.

Another important component considered in the catalyst formulation is the alkali metal, potassium, in the form of hydroxide, carbonate, or acetate. Its structural function is twofold:

(i) the neutralisation of acidic sites of the support and thus the prevention of the polymerixation of dehydrogenation products of cracking (8, 31, 109).

(ii) the catalysis of the carbon oxidation reaction, thereby preventing the active sites on the surface becoming covered with coke which might be produced from an advanced pyrolysis by non-acidic routes (120).

It is known that potassium oxide has the effect of catalysing the oxidation reaction of carbon (120). However, the exact mechanism by which the alkali inhibits the formation of non-equilibrium carbon is still not completely clear.

Comparing the relative activities of the low melting point alkali carbonates with those of the more refractory alkaline earth carbonates for the oxidation of carbon to carbon oxides, and taking into account the substantially improved experimental results obtained when using a nickel (supported on china-clay magnesia) catalyst with incorporated potassium, Andrew (8) concluded that the effect of potassium can be attributed to the mobility of alkali ions which are capable of migrating and reacting with Lewis acidic sites on the support, enhancing at the same time the carbon removal reaction. Consequently the mobility of alkali ion appears to be the key factor to ensure carbon-free operation for higher hydrocarbons at low steam ratios.

However, if this mobility is considered essential for the prevention and oxidation of non-equilibrium carbon, it introduces certain not unimportant limitations:

(i) the mobility is associated with a small but inevitable loss of alkali from the catalyst structure (8, 140). The carry-over of the volatilized potassium compound by the gas stream also causes some operational problems such as blockage in the shift converter as manifested by an increased back-pressure (32), and corrosion stress in reformer tubes by the action of potassium hydroxide on austenitic steel (12, 140).

(ii) the mobile potassium, while moving across the surface of the crystal structure, may come into contact with the metallic nickel and reduce its activity or even cause a complete deactivation for steam-methane reaction, and sufficient experimental evidence is given by Andrew (8) to substantiate this. In fact, experiments with methane as feedstock at 450 psi and 750° C, with a steam ratio of 3 and using the same nickel catalyst, have shown that the throughput to give a 10 degrees C approach to the steam-methane equilibrium had to be reduced from 2.9 kg feed/(hr) (litre of catalyst) for potassium-free catalyst to 0.6 kg feed/(hr) (litre of catalyst) for the catalyst containing 7% K_2O.

(iii) the possible migration of potassium into the alumina lattice may leave some uncovered acidic sites on the surface giving rise to the formation of carbonaceous products (116).

The reason for the volatilization of potassium from the crystal lattice is believed to be the decomposition of K_2CO_3 in the presence of high pressure steam to give KOH. In fact, the boiling point of KOH is 1327° C (95), whereas K_2CO_3 melts at 891° C and decomposes

at higher temperatures without exhibiting a definite boiling point. The dissociation pressure of K_2CO_3 is given in the literature (122) as :

Temperature (^oC)	Pressure of CO_2 (atm abs.)
730	0.0000
810	0.0013
890	0.004
970	0.012
1000	0.016
1090	0.022

Accordingly, it cannot be expected that K_2CO_3 volatilizes as such at the reformer conditions. Noting that the vapour pressure of KOH is 1 mm Hg at 718° C (95), it is most likely that the potassium carry-over takes place in the form of KOH. This would exclude the suggestion made by Nicklin et al. (116) that the alkali on the catalyst is present during the reforming as the carbonate. No access could be obtained to data on the dissociation pressures of the reactions :

$$2\ KOH \rightleftarrows K_2O + H_2O$$

$$K_2O \rightleftarrows 2K + \tfrac{1}{2}\ O_2$$

but Parkyns (119) states that, in the case of K_2O, dissociation occurs before volatilization, and the free energy of formation of K_2O even at 800° C is - 46,000 cal/mole, so that the amount of potassium vapour in equilibrium is very small. The vapour pressure of the unstable K_2O at 1000° K is given as 10^{-16} atm (95).

The depletion of mobile alkali concentration on the crystal lattice is compensated in commercial catalyst by incorporating in the catalyst structure a non-volatile potassium compound (Kalsilite, $KAlSi\ O_4$) (8,31),which by a slow hydrolysis reaction with steam and/or carbon dioxide liberates mobile alkali at a rate equal to the rate of

volatilization. The possible adverse effect of the introduced silica seem to be completely counter-balanced by the potassium.

To obviate the undesirable consequences of volatilized alkali Nicklin et al. (116) suggested the use of uranium instead of potassium as the main component for neutralization of acidic sites, and obtained satisfactory results with nickel-urania- α- alumina catalysts containing only non-volatile alkaline compounds instead of the potassium and thereby also avoided the penetration of potassium ions into the crystal lattice.

This brief summary is by no means intended to reflect all aspects of the very complicated task of developing an entirely satisfactory catalyst formulation with respect to the chemical composition, crystallographic structure, kinetic behaviour, physical strength and catalytic performance. However, it does indicate why it has proved to be more rational, and in fact necessary, to classify the catalysts used in reforming technology according to the requirements they have to fulfil. In recent years, developments have even considered zoned catalyst systems, in which two different catalyst types are charged into the reformer tube in order to perform separate required functions not attainable in a single catalyst formulation (8, 31).

Thus, the formulation and manufacture of reforming catalysts are grouped as follows:

(i) primary reforming catalysts for methane as feedstock at temperatures up to 850^{o} C

(ii) primary reforming catalysts for naphtha as feedstock within the temperature range 400 - 850^{o} C

(iii) secondary reforming catalysts at temperatures up to 1300^{o} C.

The catalyst used in the present work was one from the second group developed by Imperial Chemical Industries, Ltd. referred to as

I.C.I. 46 - 1 naphtha reforming catalyst.

6.2.2 The Chemical Composition of the Catalyst Used.

The chemical analysis of the catalyst 46 - 1 on ignition-loss-free basis is given in the Catalyst Handbook (31) as:

	%
NiO	21
CaO	11
SiO_2	16
Al_2O_3	32
MgO	13
K_2O	7

The active component is nickel, present in the manufactured form of the catalyst as oxide (NiO), which has to be reduced to metallic form in situe immediately before use. MgO and CaO are combined in the crystal structure with Al_2O_3 and SiO_2, so that any danger of their hydration is prevented. SiO_2 in its combined state with basic MgO and CaO incorporated does not offer a potential source for silica evolution. It is claimed that the inclusion of CaO is for the formation of refractory calcium-aluminates to act as hydraulic binder in the catalyst support and maintain the high physical strength without any loss of stability due to sintering. Like other reforming catalysts, it is very susceptible to sulphur poisoning and the maximum limit of sulphur which can be tolerated without affecting the catalyst activity is given as 0.5 ppm w/w. (31, 179). The poisoning effect of sulphur is believed to be reversible and a poisoned catalyst can recover its full activity by passing hydrogen and steam over the catalyst at 800° C (26) or when operated with feedstock containing sulphur in concentrations below a given level. In general, the sensitivity of the catalyst to poisoning is increased with:

(i) the increase of the activity of catalyst (31)

(ii) the decrease of operating temperature (8, 31).

More details of the catalyst's physical properties and chemical behaviour are available in the Catalyst Handbook (31), but the above mentioned features are the significant ones in the present context.

6.3 THE SPECIFIC SURFACE OF THE CATALYST.

6.3.1 Introduction.

Brunauer, Emmett and Teller (B.E.T.) (29) proposed a theory for multi-layer adsorption from which a value for the size of the monomolecular layer could be calculated. From the B.E.T. theory, the physical adsorption of a gas on a solid adsorbent may be represented by:

$$V = \frac{V_m \, c \, \frac{p}{p_o}}{1 - \frac{p}{p_o}} \left[\frac{1 - (n+1)\left(\frac{p}{p_o}\right)^n + n\left(\frac{p}{p_o}\right)^{n+1}}{1 + (c-1)\left(\frac{p}{p_o}\right)^{n+1}} \right] \qquad (6.1)$$

where:

V = total volume of the gas adsorbed at an equilibrium pressure p, cm^3

V_m = volume of the gas adsorbed in a monomolecular layer, cm^3

p = equilibrium pressure of the adsorbate, mm Hg

p_o = saturation pressure of the adsorbate, mm Hg

$\frac{p}{p_o}$ = relative pressure

n = number of layers, the thickness of each layer corresponding to the diameter of the adsorbate molecule, and

c = a constant related exponentially to the heat of condensation and the heat of adsorption.

For n = 1, Equation (6.1) can be re-arranged to give the idealized Langmuir equation for chemisorption:

$$\theta = \frac{V}{V_m} = \frac{K_A \, p}{1 + K_A p} \qquad (6.2)$$

where:

θ = fraction of adsorbent surface which is covered by a monomolecular

layer of adsorbate molecules, and

$K_A = \frac{c}{p_o}$, is the equilibrium constant for adsorption.

In applying the B.E.T. derivation, which is based on the phenomenon of physical adsorption, to the simplified form of Langmuir equation, it should be borne in mind that the following assumptions have to be made:

(i) the catalyst has a uniform activity for adsorption, i.e. all the active centres have the same activity for adsorption and the rest of the surface has none,

(ii) there is no interaction between adsorbed molecules,

(iii) all the adsorption occurs by the same mechanism, and each adsorbed complex has the same structure.

For $n = \infty$ Equation (6.1) reduces to

$$\frac{p}{V(p_o - p)} = \frac{1}{V_m c} + \frac{(c - 1)p}{V_m c p_o} \qquad (6.3)$$

called the B.E.T. equation.

A plot of $\frac{p}{V(p_o - p)}$ versus $\frac{p}{p_o}$ is usually linear over the range of relative pressures 0.05 to 0.35 and can be extrapolated to $\frac{p}{p_o} = 0$ to evaluate the intercept $\frac{1}{V_m c} = 1$. Since the slope of the straight line is $\frac{c - 1}{V_m c} = s$, the volume of the gas adsorped as a monomolecular layer, V_m, is calculated on elimination of c from:

$$V_m = \frac{1}{I + s} \quad cm^3 \qquad (6.4)$$

The specific surface may be calculated from the following relationship:

$$S_g = \frac{V_m}{w} \quad K \quad cm^2/g \qquad (6.5)$$

where w is the weight of the catalyst sample and K is a constant for for each adsorbate. The latter is associated with the area occupied by one adsorbed molecule, usually in the liquid state and can be calculated from the relationship:

$$K = \frac{N_o A}{V_{mol}} \qquad (6.6)$$

in which:

N_o = Avogadro's number, (6.02) (10^{23}) molecules/mole

A = area covered by one molecule, cm^2, and

V_{mol} = the volume per mole of adsorbate at the conditions of V_m.

Since V_m is recorded at standard temperature and pressure, V_{mol} = 22,400 cm^3/mole.

The value of A has been the subject of considerable investigations. Some differences have been observed between the projected area of a molecule on the surface when arranged in close two-dimensional packing and the area obtained by assuming the molecules perfectly spherical (153). The proposed equation to calculate the area is:

$$A_A = 1.09 \left(\frac{M_A}{N_o \rho_A} \right)^{2/3} \qquad (6.7)$$

where M_A is the molecular weight of adsorbate, and ρ_A is its density in pure liquid form at the temperature of the adsorption experiment. Alternatively, the value of K is usually given in tabulated form. For nitrogen as adsorbate at liquid nitrogen temperature, K = 4.38 for specific surface expressed in m^2/g. (57)

Although the B.E.T. method has certain limitations with respect to the assumed geometric configuration of the molecules forming the multilayer, it has proved a useful tool in the determination of the total area of an adsorbent covered with a monolayer. In addition to the highly improved volumetric techniques, gravimetric and dynamic methods have been developed. In the dynamic method a mixture of helium and the gas to be adsorbed is passed continuously over the sample of adsorbent. Details of the specific techniques are given in the pertinent literature(57, 74, 88, 103, 153, .155).

A volumetric type apparatus was available and was therefore used in the present work. All specific area and isotherm measurements were performed at liquid nitrogen temperatures with high purity nitrogen as adsorbate. Helium used for dead space determinations was 99.9% pure and obtained from Air Products, Ltd.

Preliminary determinations indicated the approximate specific surface of the catalyst samples. Since the pore areas to be measured were not in the low magnitude range of 1 - 5 m^2/g, the use of Krypton gas as adsorbate was not considered necessary.

6.3.2 The B.E.T. Apparatus.

The apparatus used is shown in Fig. 6.1 and consisted of a system of five interconnected units:

(i) the sample tube, burettes, manometer, mercury reservoirs, and the Mc Leod gauge

(ii) the gas purification unit and the gas storage reservoirs

(iii) the nitrogen thermometer and its manometer

(iv) a high vacuum source consisting of an oil backing pump, a mercury diffusion pump, and cold traps

(v) vacuum and pressure sources for levelling the mercury in the burettes during operation.

The apparatus was mounted on a frame by clamps. The individual pieces of the apparatus in Fig. 6.1 are lettered, and the stopcocks are numbered. All the stopcocks used were for high vacuum operation. The burettes provided with water jackets, manometers, cold traps and reservoirs were made to specification. The individual and cumulative bulb volumes of the gas burettes, B and B', are tabulated in Appendix (Table A - 6.1). The temperature of the gas burettes was controlled with a thermometer inserted in the water-jacket of burette B. An

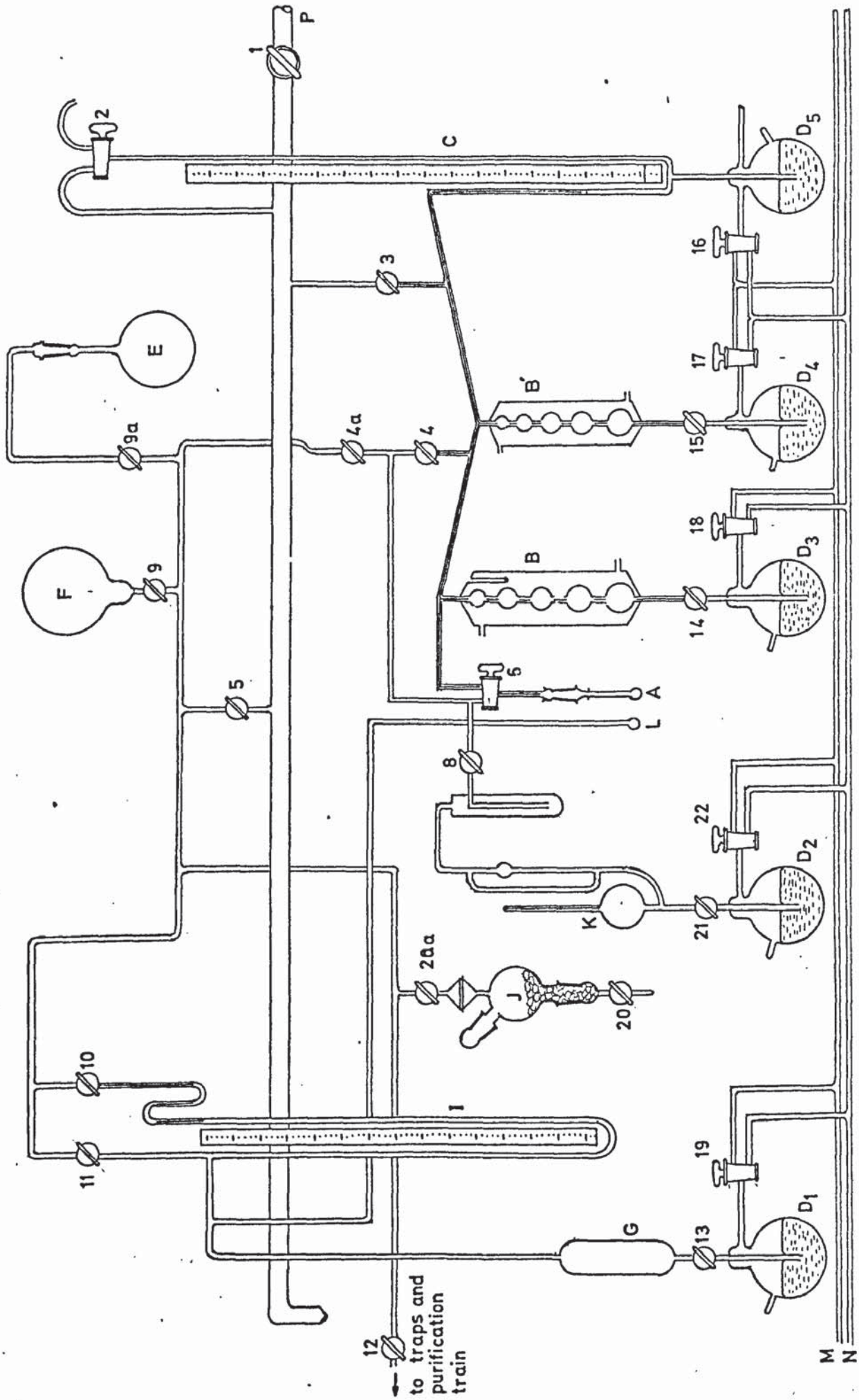

Fig.6.1 The B.E.T. Apparatus

A	Sample tube
B, B'	Gas burettes, calibrated, for measuring the working volumes of gas
C	Manometer to measure the gas pressure over the sample and in the gas burettes
D_1 to D_5	Mercury reservoirs for the manometers, burettes, and Mc Leod gauge
E	Gas reservoir for helium
F	Gas reservoir for nitrogen
G	Uncalibrated gas holder, used to compress nitrogen sufficient to produce liquid-vapour equilibrium in the nitrogen thermometer bulb at liquid nitrogen temperature
I	Manometer for nitrogen thermometer system
J	Drying tube filled with anhydrous calcium sulphate
K	Mc Leod gauge
L	Nitrogen thermometer bulb
M	Line connecting the system to mechanical oil pump
N	Line connecting the system to pressure source
O	To purifying traps
P	To high vacuum source

An S-shaped capillary tube was placed at the top of the right leg of the manometer of the nitrogen thermometer. This device was used to set the vacuum leg of the manometer and eliminated the necessity of constant pumping.

Nitrogen and helium gases used for measurements were passed through a simple purifying trap, filled with 3/16 in. glass beads and cooled to liquid nitrogen temperature to remove water vapour and other condensable gases. Before each reservoir was charged with the respective gas, it was connected through stopcocks 9 and 11 to manometer I and evacuated through 5 and 1. Then, with stopcock 5 closed, the gas was introduced from the pressure cylinders through the purifier and stopcock 12. When a pressure of about 800 mm was obtained on manometer I, stopcocks 9 and 12 were closed and the system evacuated.

A dewar flask was used for the liquid nitrogen bath and was covered with a lid to prevent condensation of atmospheric oxygen in the dewar and to maintain a relatively stable bath temperature.

The heating unit, employed for degassing the samples, was a small sand bath. A mercury-in-glass thermometer (0 - 300° C) placed in the heater near the sample tube was used to control the baking-out temperature.

6.3.3. The Procedure.

Before any measurements were attempted with the apparatus, it was vacuum tested. For this purpose the system was pumped off under high vacuum using a mercury diffusion pump and a mechanical backing pump with cold traps. After six hours of pumping and flame brushing of the connecting lines with a gas flame, all stopcocks were closed and the apparatus was allowed to equilibrate for two hours. The vacuum in the equipment was controlled with the Mc Leod gauge. A change in vacuum from $(4.02)\ (10^{-6})$ mm Hg to $(1.21)\ (10^{-5})$ mm Hg over a period of four hours

was considered acceptable. A high-frequency vacuum tester was used to check the system for imperfections in the sealed glassware.

6.3.3.1 Calibration of the Zero-Bulb-Volume.

The section of capillary, connecting stopcock 6 to the burettes B and B' and to the zero-line level of the mercury in the left leg of manometer C, was the zero-bulb-volume. Since it was a part of the working system, its volume was calibrated using the pressure-volume relationship. For this purpose, stopcocks 1, 3, 4, 4a, 5, 6 and 8 were closed, the vacuum in the system being approximately 10^{-5} mm Hg. The mercury in each burette was set at the top etched line. The mercury level in manometer C was raised to about 200 mm above the fixed zero-line. Helium was then introduced slowly through stopcocks 9a, 4a, and 4 until manometer C registered a pressure of approximately 350 mm Hg. Stopcocks 9a, 4a, and 4 were closed, the mercury level in the left leg of the manometer was adjusted to the zero-line using stopcock 16, and the pressure (p_1) of helium entrapped in the zero-bulb-volume was recorded. The mercury level in burette B was then lowered by means of stopcock 14 to the second etched line so that the volume occupied by helium became (zero-bulb + B 1), the manometer C zeroed again, and the pressure (p_2) corresponding to the new volume recorded. The zero-bulb-volume (Z.B.V) was calculated from the following relationship:

$$\text{Z.B.V.} = \frac{P_2 V_{B1}}{P_1 - P_2} \quad \text{cm}^3 \qquad (6.8)$$

and was taken as an average from ten determinations carried out with combinations of different bulb volumes of the burettes B and B'. The results obtained from one set of determinations are given in Table 6.2 in the Appendix. To facilitate computations of volumes of gases at standard conditions, Table A-6.3 of bulb conversion factors for both burettes was prepared for each bulb setting and for each combination of bulbs. The volume of gas measured under one set of conditions was

converted to its volume of standard conditions by the use of Equation (6.9):

$$V_2 = \frac{P_1 V_1}{T_1} \quad \frac{273.16}{760} \quad cm^3 \qquad (6.9)$$

where the subscripts 1 and 2 denote the operating and standard conditions, respectively. The bulb conversion factor, defined as F_V, is

$$F_V = (V_1) \quad \frac{273.16}{760} \quad \frac{d_t}{d_o} \qquad (6.10)$$

where:

V_1 = the cumulative volume of the bulbs, cm^3

d_o = the density of mercury at 0^o C, g/cm^3

d_t = the density of mercury at the operating temperature of the bulbs, g/cm^3.

6.3.3.2 Degassing the Sample.

For the specific surface determinations the weights of the samples were approximately 0.6 g. After connecting the sample tube, A, to the apparatus and opening stopcock 6, the sample was heated under continuous evacuation at 220 $\pm$ 5 ^oC for three hours to remove adsorbed gases from its surface. The end of degassing was checked with the Mc Leod gauge by controlling the vacuum inside the whole system at intervals of one hour. After the completion of degassing, stopcock 6 was closed and the sample was allowed to cool.

6.3.3.3 Determination of the Dead-Space-Factor.

The volume of the free space in the sample tube and in the connecting line to stopcock 6 was determined before every measurement of specific surface at the adsorption temperature. Helium was used to determine this volume, because it is chemically inert, i.e. no chemisorption can take place, and it is not physically adsorbed even

at liquid nitrogen temperature.

With the sample attached to the apparatus, degassed and cooled, the sample tube was isolated from the burette system by stopcock 6. Stopcocks 1, 3, 4, 4a, 5, 6, and 8 were closed, and the mercury level in manometer C was set to about 250 mm above the zero-line using stopcock 16. Approximately 28 cm^3 (STP) of helium was then admitted to the burette system with B 5 as the operating volume, through stopcocks 9a, 4a, and 4. After closing these stopcocks, the mercury level of manometer C was zeroed and the pressure of the helium recorded. The volume of the gas taken was determined by Equation (6.9), after noting the pressure in the burettes at six different bulb settings. The liquid nitrogen bath was then placed around the sample tube, stopcock 6 opened, and the helium was allowed to expand into the sample tube. When thermal equilibrium was established, the level of mercury in manometer C was zeroed using stopcock 16, the pressure was recorded, and the volume ofhelium at standard temperature and pressure remaining in the burette system, was calculated. The volume of helium present in the sample tube was the difference between the total helium admitted and the quantity remaining in the burette system at the equilibrium pressure. The ratio of the volumeof helium in the sample tube to the pressure at thermal equilibrium had to be constant. The constancy of this ratio,called the dead-space-factor (133), was checked by changing the volumes in the burettes and obtaining different equilibrium pressures. The magnitude of the dead-space-factor is given by Faeth (57) as of the order 0.001 to 0.01 cm^2/mm Hg; it varied depending on the volume of the dead space surrounding the sample.

After the determination of the dead-space-factor, the helium gas was removed from the adsorption system by connecting the apparatus to the high vacuum source through stopcock 1.

A sample calculation for the dead-space-factor is given in the

Appendix (Table A - 6.4).

6.3.3.4 The Nitrogen Isotherm.

A few millilitres of mercury were run into the gas holder H through stopcock 13. The nitrogen thermometer system was then connected to the vacuum source by opening stopcocks 10, 11 and 5. When the burette system, the sample tube and the nitrogen thermometer system were evacuated to 10^{-6} mm Hg, stopcocks 1, 3, 5, 6, 8, 10 and 11 were closed, and an appropriate volume of nitrogen (approx. 25 cm^3 at STP) was admitted through stopcocks, 9, 4a, and 4 into the burette system from the nitrogen gas reservoir as described already for helium. The mercury level in manometer C was then adjusted to zero, and the pressure recorded. The burette temperature was also noted. Check determinations of the volume of nitrogen were made by changing the burette volumes and recording the corresponding pressures. The initial volume of nitrogen was then calculated using Equation (6.9). At this stage the gas thermometer was filled with nitrogen through stopcocks 11 and 9, until a pressure difference of 550 mm Hg was reached in manometer I, while keeping stopcocks 10, 5, 4a and 4 closed. Stopcock 9 was then closed but stopcock 11 was left open. The liquid nitrogen bath was placed around the sample tube A and the nitrogen thermometer bulb (L) ; special care was taken to immerse both bulbs in the liquid nitrogen to the same depth. To determine the vapour pressure of liquid nitrogen (p_o), the gas holder H was filled with mercury through stopcock 13 until nitrogen started to condense in bulb L. Condensation took place between 765 and 780 mm Hg, depending on the temperature of the liquid nitrogen bath. p_o was then recorded as the difference in heights of the mercury in manometer I. Stopcock 6 was then opened slowly and the pressure indicated on manometer C decreased as the nitrogen expanded into the evacuated sample tube and adsorption progressed. The mercury

in the burettes was adjusted at this stage of measurement to produce a pressure near 100 mm Hg, and the system was allowed to equilibrate. When equilibrium was reached, the mercury level in manometer C was adjusted to zero, and the pressure (p) of the burette system, the combination of the bulbs used, the burette temperature (T_B), and the vapour pressure of liquid nitrogen (p_o) at the liquid nitrogen bath temperature were recorded. The volume in the burettes was then reduced by changing the mercury levels through stopcocks 14 and 15, to obtain a bulb combination which caused the pressure in the system to increase. When equilibrium was again established, another set of data was recorded, and the above procedure was repeated until 8 - 10 sets of data in the desired range (0.025 - 0.25) of the relative pressure, p/p_o were obtained. For the determination of the complete isotherm, data were taken at intervals until values of p/p_o approached unity. The evaluation of recorded data is illustrated in tabulated form in Appendix (Table A - 6.5) for only one determination. The plots of $p/V_a\ (p_o - p)$ against p/p_o necessary for the calculation of the total specific surface (B.E.T. area) are shown in Fig. 6.2.

6.3.4 The Results and Their Discussion.

Three sets of determinations were carried out, each set consisting of two samples of different weights prepared from the same catalyst pellet. The differences in the results obtained for every set were within 3%. Fig. 6.2 represents the plots corresponding to the second measurements. The values of the total B.E.T. areas for the catalyst 46 - 1 at different stages of the reforming experiments are given in Table 6.1.

The B.E.T. measurements gave the total pore areas of the catalyst samples. The catalytically active area, effective for the reforming reaction, is the area occupied by the metallic nickel on the pore surface, which may be measured by any of the B.E.T. methods

Fig:6.2 Total Specific Surface (B.E.T. area) of the Catalyst Samples.

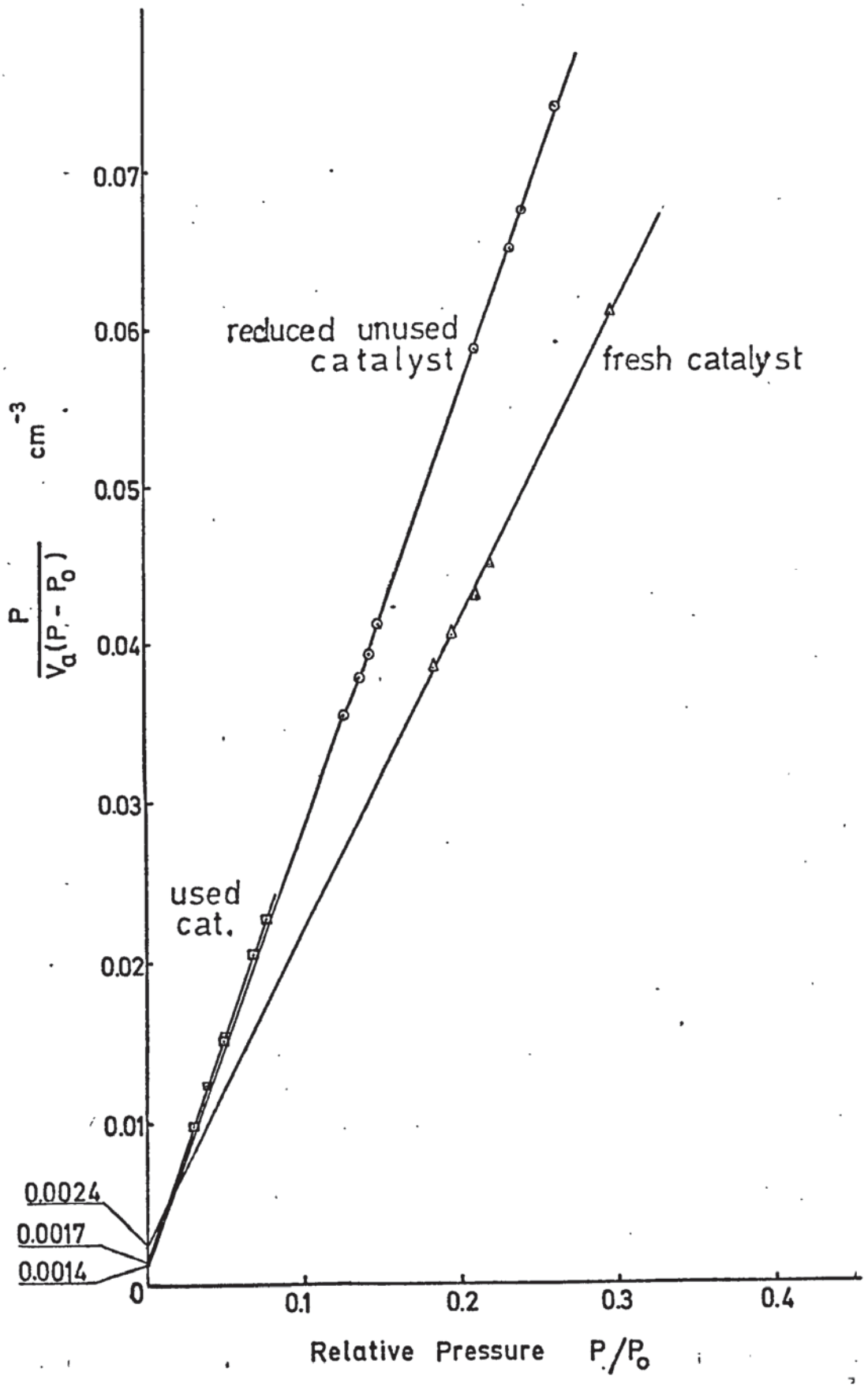

using hydrogen (124,153), or carbon monoxide gases as adsorbate, or by line broadening of the X-ray diffraction patterns (1, 31). Whereas the carbon monoxide adsorption measurements and X-ray diffraction analyses give fair agreement for most catalysts, it is claimed that the CO adsorption method always gives very much lower values for alkalized catalysts. In fact, typical nickel surface areas obtained by the line broadening technique (1), were 1 - 2 m^2/g of catalyst after running at about 500° C, whereas the values for the same catalyst obtained from carbon monoxide measurements were only 0.2 - 0.4 m^2g. At higher operating temperatures, these values were reduced to 0.2 and 0.04 m^2g, respectively.

TABLE 6.1

Specific Surface of the Catalyst Samples

Catalyst Samples	B.E.T. Area m^2/g	B.E.T. Area m^2/g	B.E.T. Area (average) m^2/g
1. Fresh catalyst, unreduced.	32.84	32.05	32.45
2. Catalyst after reduction at 650° C for 16 h.	28.88	29.80	29.34
3. Catalyst, reduced at 650° C and used in reforming experiments at 540° C, barometric pressure, with a steam : methane ratio of 3.0	25.86	25.29	25.58

No attempts were made in the present work to determine the active nickel area of the catalyst used.

The difference between the B.E.T. areas of the unreduced and reduced catalyst is generally attributed to a change in crystallite size and structure of the catalyst. In the present investigation, this difference was found to be 32.05 - 29.80 = 2.25 g/cm^2 for an

activation period of 16 hours at 650° C. The effects of the reduction period and temperature on the change of the B.E.T. area of reforming catalysts are not yet established in quantitative terms. For the present work it has to be stated that, in spite of every care, contact of the activated catalyst pellet with air was inevitable during dismantling of the reactor, transferring the catalyst pellet into a hydrogen filled glass bottle, preparing the sample by crushing the pellet, weighing and transferring it into the sample tube of the B.E.T. apparatus. It is not inconceivable that a strong chemisorption of oxygen by the highly activated nickel, even at temperatures as low as 20° C, might have contributed to the change of the surface structure of the nickel atoms to result in a decrease of the B.E.T. area. The extent of this probable chemisorption and the effectiveness of the degassing procedure before each specific surface measurement to eliminate the effects of any chemisorbed species were not determined as part of this research.

The decrease in B.E.T. areas for used reforming catalysts seems to be more characteristic than the absolute value of the fresh catalyst, and a common observation. In this investigation with methane as the feedstock, the B.E.T. area of the catalyst, activated at 650° C for 16 hours and operated at 540° C, 1 atm abs. pressure for a period of 14 hours, was found to have decreased from 32.15 to 25.29 m^2/g. It is fairly well-established that the extent of the decrease is a function of temperature and duration of the reforming operation. In fact, it has been stated that after several months of operation at 500° C, B.E.T. values of 10 - 12 m^2/g were typical for the same catalyst as used in this work, whereas at about 770° C, values of 1.5 - 2.5 m^2g were obtained (1). The main reasons for such a substantial decrease of specific surface with increasing temperature are the growth of the crystallites, and consequently, the partial

destruction of the crystal structure due to sintering.

According to Dowden (54), the onset of a rapid decrease in the specific area of a normal crystalline solid can be empirically associated with a temperature somewhere between surface Tammann temperature (0.3 x melting point, ^{o}K), and the Tammann temperature of the bulk (0.5 x melting point, ^{o}K). In this case the catalyst, being a multicomponent mixture of NiO - Al_2O_3 - SiO_2 - Cao - MgO - K_2O does not exhibit a definite melting point. It is, therefore, not possible to assign a definite temperature level for the beginning of sintering. Although the effects of composition on high temperature behaviour (i.e. eutectic formation, distinct melting points) of some constituents of the catalyst have been exhaustively investigated as individual three-component systems (23), it is not possible to apply these results to the complex nature of the catalyst, and to the knowledge of the author, a precise treatment of this subject is not available in the literature.

The possibility that the formation of radicals (CH_2, CH) or of non-equilibrium carbon during course of the reforming reactions may promote a decrease in the specific surface should be borne in mind. A permanent carbon deposit would result in plugging of pores and may also contribute in an indirect manner to the formation of nickel carbide (159) which might accelerate the crystal growth, or cause distortions in the existing crystallite structure.

6.4 DETERMINATION OF THE DENSITIES AND POROSITY.

Determinations of the apparent and true densities of the catalyst pellets were carried out only for unreduced samples. The bulk density of the ground, unreduced catalyst was also determined for different particle sizes and these values are tabulated in Appendix A - 4.4.

6.4.1 The Apparent Density (ρ_p).

The apparent density was determined with pellets which were machined to different sizes. Since the samples were in cylindrical form measurable accurate to 0.1 mm, it was not considered necessary to apply the mercury displacement method to determine the volume. The average figure for the apparent density was found to be 2.371 g/cm^3.

6.4.2 The True Density (ρ_t).

The helium displacement technique was used to determine the true density of the catalyst pellet. Helium gas has several properties which make it ideal for density measurement :

(i) it is chemically inert

(ii) it is not adsorbed on the catalyst surface

(iii) it can penetrate pores not accessible to other displacing fluids.

(iv) it is virtually ideal in its behaviour as a gas.

The same B.E.T. apparatus was used for the determination as employed for the isotherm measurements. A volumetric flask of 25 ml capacity fitted with a standard ground joint was used as the sample tube. The apparatus was prepared in an identical manner to that described in Section 6.3.3. After a check determination of the zero-bulb-volume, the volume of the empty sample flask was determined. For this purpose, the system was evacuated with the mercury diffusion pump and the empty sample flask degassed at 200 $\pm$ 5° C. Afterwards a 600 ml beaker, filled with water at room temperature was placed around the sample flask. Then stopcock 6 was closed, Helium was introduced into the burette system, with bulb volume B 4, through stopcocks 9a, 4a, and 4 until a pressure difference of 390 mm Hg was obtained on manometer C. The mercury level in the manometer was zeroed and the pressure, p_1, and the temperatures of the burette system and water bath around the sample recorded. The volume of helium introduced was checked with other bulb combinations of

the burette system.

Stopcock 6 was then opened, and five minutes were allowed for equilibrium to be established. Manometer C was again adjusted to zero, and the new pressure, p_2, was recorded. The volume of the sample flask was then calculated from Equation (6.11), which is similar to Equation (6.8):

$$V_c = V_1 \left[\frac{p_1 - p_2}{p_2} \right] \qquad (6.11)$$

where:

V_c = the volume of the empty sample flask, cm^3

V_1 = the calibrated working volume of the burette system up to stopcock 6, cm^3

p_1 = the pressure of helium before connecting the burette system to the sample flask (stopcock 6 closed), mm Hg

p_2 = the pressure of helium after connecting the burette system to the sample flask (stopcock 6 open), mm Hg.

This procedure was repeated six times and an average value taken. The result of a calibration run are given in Table A - 6.6 (Appendix).

Stopcock 6 was then closed, the sample flask removed from the system, and a sample of about 30 g with 1 - 3 mm particle size transferred into the sample flask. It was then fitted onto the equipment, and the sample degassed at 200 $\pm$ 5° C applying a vacuum of 10^{-6} mm Hg. Then the sand bath was removed, the sample allowed to cool, and immersed in the water bath.

The procedure for the determination of the true density was similar to that used in the calibration. First stopcock 6 was closed and helium was introduced into the burette system through stopcocks 9a, 4a, and 4 until a pressure of about 125 mm Hg was reached on manometer C at B 4 bulb level. The system was equilibrated thermally, the manometer zeroed and the pressure, p_1, recorded. Stopcock 6 was

then opened, the system again permitted to attain equilibrium, and the new pressure recorded. For the case of constant temperature and the same bulb levels in the burette system before and after opening stopcock 6, the following relationship served to calculate the volume of solid present in the sample flask :

$$p_1 V_1 = p_3 [V_1 + (V_c - V_d)] \qquad (6.12)$$

where:

p_1 = the pressure of helium indicated on manometer C before opening stopcock 6, mm Hg

p_3 = the pressure of helium indicated on manometer C after opening stopcock 6, mm Hg

V_1 = the working volume of the burette system, cm^3

V_c = the volume of empty sample flask, cm^3

V_d = the volume occupied by the solid in the sample flask, cm^3

Solving for V_d :

$$V_d = (V_1 + V_c) - V_1 \frac{p_1}{p_3} \qquad (6.13)$$

and the true density of the catalyst is:

$$\rho_t = \frac{\text{weight of the sample}}{V_d} \qquad (6.14)$$

The procedure was repeated five times at various bulb volumes and the average value was calculated. The results are given in Table 6.2.

The true density of the unreduced catalyst was found to be 3.026 g/cm^3.

6.4.3 The Porosity.

The porosity (void fraction) of the catalyst pellets defined as :

$$\theta = \frac{\text{void (pore) volume of the pellet per gram}}{\text{total volume of the pellet per gram}}$$

TABLE 6.2

DETERMINATION OF THE TRUE DENSITY OF THE CATALYST

Stopcock 6	Burette and bulb used	Volume $(V_1 + V_c)cm^3$	Temperature of burette system	Temperature of the sample flask	Pressure observed p_1 (mm Hg)	Pressure observed p_3 (mm Hg)	$V_1(\frac{p_1}{p_3})$	$V_d = [V_1+V_c] - V_1\frac{p_1}{p_3}$	$\rho_t = \frac{W}{V_d}$ g/cm^3
Closed	B4 + B'0	72.180	20°	20.2°	122.4				
"	B3 + B'0	54.837	20°	20.0°	194.4				
"	B2 + B'0	45.748	20°	20.0°	284.8				
"	B4 + B'4	82.223	20.6°	20.6°	100.9				
"	B4 + B'2	76.103	20.9°	20.8°	113.0				
Open	B4 + B'2	76.103	20.9°	20.9°		84.8	67.651	8.452	3.248
"	B4 + B'4	82.223	20.2°	20.0°		77.8	73.779	8.444	3.251
"	B2 + B'0	45.748	20.0°	20.0°		153.8	37.269	8.479	3.237
"	B3 + B'0	54.837	20.0°	20.0°		123.6	46.401	8.436	3.254
"	B4 + B'0	72.180	20.0°	20.0°		90.0	63.709	8.471	3.240
									Average ρ_t: 3.246
Weight of the sample: 27.4493						Volume of sample flask V_c = 25.335 ml			

was calculated from the apparent and true densities as follows:

from the relationships

$$\theta = \frac{V_g}{V_g + \frac{1}{\rho_t}} \tag{6.15}$$

and

$$\theta = \frac{V_g}{\frac{1}{\rho_p}} \tag{6.16}$$

V_g can be eliminated to give:

$$1 - \theta = \frac{\rho_p}{\rho_t}$$

where:

V_g = total pore volume per gram of catalyst pellet, cm^3

$\frac{1}{\rho_t}$ = volume of solid per gram of catalyst, cm^3/g

$\frac{1}{\rho_p}$ = volume of the pellet per gram of catalyst, cm^3/g

Hence, for $\rho_p = 2.371$ g/cm^3 and $\rho_t = 3.026$ g/cm^3, an average value for the catalyst porosity (void fraction) was computed as 0.2165 (21.65 %).

Additional determinations were carried out by boiling dry pellets of known weights in distilled water for 20 minutes, to displace the air in the pores, replacing the hot water with cold water, drying the pellets superficially with a slightly moistened cloth and reweighing the pellets. This procedure, repeated for six samples, gave results varying over a rather wide range (18.13 - 23.14 %). This was apparently due to the extraction of soluble compounds to different extent (K^+) from the pellet.

Although it was an approximate check, the value of porosity obtained from apparent and true densities was compared with the void volume determined by isotherm measurements. Neglecting the contribution of the external surface of particles to the total pore area, i.e.

assuming that the nitrogen adsorbed represents only the pore volume, and assuming furthermore, that at the highest relative pressure ($\frac{p}{p_o} = 0.986$), which was obtained in the B.E.T. apparatus, all the pores were filled with liquid nitrogen, the total pore volum was calculated to be

$$V_g = (50.82)\ (0.001547) = 0.0786\ cm^3/g$$

where 50.82 cm^3/g was the nitrogen adsorbed at S.T.P., and 0.001547 the conversion factor for cm^3 liq. N_2 (34.65 cm^2/mole): cm^3 gas. N_2(22400 cm^3/mole)(STP). From Equation (6.15), the porosity was calculated to be 19.21 %.

The difference between the two porosity values, i.e. 21.65 % and 19.21 %, may be decreased by considering the extrapolation of the adsorption - desorption isotherm to a relative pressure of 1.00. Thus the volume of nitrogen adsorbed was read as 58.0 cm^3/g. Hence,

$$V_g = (58.00)\ (0.001547) = 0.08974\ cm^3/g$$

From Equation (6.15) :

$$\theta = \frac{V_g}{V_g + \frac{1}{\rho_t}}\ (100) = 21.36\ \%$$

and from Equation (6.16) :

$$\theta = V_g \cdot \rho_p (100) = 21.28\ \%$$

These estimates compare favourable with 21.65 % obtained from the density measurements, and the differences were considered to be within experimental error.

6.5 THE PORE VOLUME DISTRIBUTION.

6.5.1 Introduction.

Methods for the calculation of the pore volume distribution of porous solids from nitrogen isotherms have been described by several investigators (4, 14, 39, 126, 150, 175). They are all based on the fact that at the experimental conditions of the

isotherm measurement, the quantity of gas adsorbed by the porous solid is essentially the sum of the gas held by the forces of physical adsorption on the geometric pore surface of the solid particle and that of the gas present as condensate within the pores of the adsorbent due to capillary condensation. Wheeler (175) proposed a theory which combined the B.E.T. multilayer adsorption and capillary condensation viewpoints. It can be summarized by the equation:

$$V_s - V = \pi \int_{r_{P_n}}^{\infty} (r - t)^2 L(r)\, dr \qquad (6.17)$$

where:

V_s = the volume of gas adsorbed at saturation pressure (p_o), cm^3

V = the volume of gas adsorbed at pressure (p), cm^3

$L(r)\, dr$ = the total length of pores whose radii fall between r and (r + dr), cm

r_{P_n} = the critical radius, which is the radius of the largest pore still completely filled with liquid adsorbate at any particular pressure (p), cm

t = the multilayer thickness which is normally built up at pressure (p), cm.

Wheeler considered the radius of the pore to be equal to the sum of the multilayer thickness as calculated from the B.E.T. theory and the radius of the capillary which can be calculated from the Kelvin equation. He also suggested that the pore size distribution L(p) can be approximated by a simple distribution function.

Shull (150) pointed out that the B.E.T. thicknesses become much larger than experimentally observed thicknesses for flat surfaces in the high pressure region, and developed a simplified computational method for fitting the experimental data to Maxwellian or Gaussian distribution functions.

Barrett, Joyner and Halenda (14) developed a computational method on the basis of a simplified pore model with the following fundamental assumptions:

(i) the solid is composed of open-ended, cylindrical pores, such that all pores of equal radius can be regarded as responding in the same manner to changes of relative pressure ($\frac{p}{p_o}$) of the adsorbate, and

(ii) the cylindrical capillary, which causes the condensation of adsorbate, is concentric with the pore.

They also considered that the equilibrium during the desorption between the gas phase and the adsorbed phase within the pores is governed by only two mechanisms:

(i) physical adsorption on the pore walls, which would occur to the same extent whether the area involved constituted walls of pores or a flat surface impenetrable to nitrogen, and

(ii) capillary condensation in the inner capillary volume.

With an analytical treatment of the desorption process based on the assumption that the relative pressure differed infinitesimally from unity so that substantially all pores were filled with liquid adsorbate nitrogen, Barrett and co-workers (14) derived the following equation for the computation of pore volume distribution with respect to pore radii :

$$V_{p_n} = R_n \Delta V_n - R_n \Delta t_n \sum_{j=1}^{n-1} c_j A_j \qquad (6.18)$$

where the subscript n indicates the stage of desorption induced by lowering the relative pressure. Also :

$$R = \frac{\bar{r}_p^{\,2}}{(\bar{r}_k + \Delta t)^2}$$

where $\bar{r}_p$ is the average radius of the pores emptied of their condensate

during a decrement of the relative pressure, $\bar{r}_k$ is the average radius of the inner capillary from which evaporation occurs as the relative pressure is lowered, and Δt is the reduction in thickness of the physically adsorbed layer of molecules on the pore walls. V_{p_n} is the volume of all the pores with radii equal to or smaller than r_{p_n}, which were filled with capillary condensate up to the (n - 1)th stage of the desorption process. It corresponds to the experimental volumes of nitrogen, adsorbed by the solid at the relative pressure $(\frac{p}{p_o})_n$, and can be evaluated from the desorption isotherm. ΔV_n is the observed volume of nitrogen desorbed between the (n - 1) and (n)th stages of desorption. The summation $\sum_{j=1}^{n-1} c_j A_j$ is simply the sum of the average area in emptied pores down to, but not including, the pore that was emptied of capillary condensate during the nth desorption. c_j in this summation term stands for $\left[\frac{\bar{r}_p - t_{\bar{r}}}{\bar{r}_p}\right]$, where $t_{\bar{r}}$ is the thickness of the physically adsorbed layer at the corresponding value of relative pressure.

In combination with the functional relationship between thickness of the physically adsorbed layer (t) and relative pressure $\frac{p}{p_o}$, and with the Kelvin equation which relates the radius of the concave surface of the liquid in a capillary to its vapour pressure, Equation (6.18) was used by Barrett et al. in evaluation of the pore volume distribution.

The Kelvin equation in its classical form is :

$$\ln \frac{p}{p_o} = \frac{-2\sigma V \cos\theta}{R_g T (r)} \qquad (6.19)$$

where:

p = the measured vapour pressure of the liquid in the capillary

p_o = the saturation pressure of the liquid at T ^oK

σ = the surface tension of the liquid in the capillary, dyne/cm

V = the molal volume of the liquid, cm^3/mole

θ = the contact angle, deg.

r = the radius of curvature of the meniscus, cm

R_g = the gas constant, (8.3143) (10^7) ergs/(mole) (^oK)

T = the absolute temperature, ^oK.

and defines the vapour pressure lowering over a concave meniscus ($\theta < 90^o$) formed at the solid-liquid boundary, when adhesive rather than cohesive forces predominate. Since at liquid nitrogen temperature the surface of the capillaries is already completely covered by the physically adsorbed nitrogen, the capillary condensate wets the surface so that the contact angle is zero, and accordingly, the radius of the meniscus becomes the radius of the capillary, r_k, which is the difference between the radius of the pore, r_p, and the thickness of the layer formed by the physical adsorption, t_r. Hence, the Kelvin equation takes the form :

$$\ln \left(\frac{p}{p_o}\right) = \frac{-2\sigma V}{R_g T (r_k)} \qquad (6.20)$$

where:

r_k = $(r_p - t_r)$

$\frac{p}{p_o}$ = the relative pressure

σ = the surface tension of liquid nitrogen at the temperature of the bath

V = the molal volume of liquid nitrogen

The functional relationship between the thickness of the physically adsorbed layer, t_r, and the relative pressure has been the subject of considerable investigations (110,126). In general a correlation of the following type has proved to be satisfactory (153):

$$t_r = A \left(\log \frac{p_o}{p}\right)^{-\left(\frac{1}{n}\right)} \quad \text{Å} \qquad (6.21)$$

where A and n depend on the nature of the catalyst surface. For nitrogen as adsorbate at - 195.8° C, Wheeler has proposed (153) :

$$t_r = (7.34)\ (\ln \frac{p_o}{p})^{-1/3} \qquad (6.22)$$

The correction term, $R_n\ \Delta t_n \sum_{j=1}^{n-1} c_j\ A_j$, in Equation (6.18) was introduced by Barrett et al. (14) to allow for the changes in the capillary surfaces, from which evaporation takes place at successive stages of desorption. An analysis by the authors showed that assigning a constant average value to c_j depending on the range of pore radii, caused only minor deviations, but greatly simplified the computational work. The satisfactory average values of c_j for a range of pore radii maxima are given in Table 6.3.

TABLE 6.3

THE AVERAGE VALUES OF c FOR A RANGE OF PORE RADII MAXIMA (14)

$c = \frac{\bar{r}_p - t_{\bar{r}}}{\bar{r}_p}$	Range of Pore Radii (Å)
0.75	0-40
0.80	40-80
0.85	60-100
0.90	80-200

The effect of the correction term on the overall calculation has also been discussed, and it has been found, whatever the value of c, $R_n\ \Delta t_n\ c \sum_{j=1}^{n-1} A_j$ is negligibly small for all pores above 165 Å radius. On the other hand, it has been observed that the value of the correction term can be as much as 50% of the term $(R_n\ \Delta V_n)$ for pores of radii about 18-22 Å .

Although Equation (6.18) is theoretically applicable up to relative pressures infinitesimally close to unit and provides a useful

method of computation of pore volume distribution, it has certain limitations. Firstly, the logarithmic relationship between the pore radius and the relative pressure:

$$r_p = r_k + t_r = \frac{-2\sigma V}{RT \ln \frac{p}{p_o}} + \frac{7.34}{(\ln \frac{p}{p_o})^{1/3}} \qquad (6.23)$$

results in increasingly larger increments of radius as saturation is approached. Secondly, the vapour pressure of capillary condensates is not affected significantly by radii of curvature greater than about 300 Å (153). The applicability of the method is, therefore, restricted to a pore radius of approximately 300 Å as an upper limit.

It is also recognized by the authors that the Kelvin relationship for capillary condensates becomes doubtful as the capillary radius approaches the diameter of the adsorbate molecules, due to changes in density and surface tension. Thus, the lower limit for pore radii to be considered in pore volume distribution correlations obtained with nitrogen isotherms is set at 20 Å.

The contribution of the pores with radius larger than 300 Å to the overall pore volume depends largely on the micro and macro-pore structure of the catalyst. For some mono-disperse pore systems which give pore volume maxima within a range 50 - 100 Å, the volume of condensate contained in the pores larger than 300 Å is estimated to be about 10% of the total condensate volume. Since the number of these large pores is generally small compared with the number of smaller pores, their area is claimed to be less than 1% of the total area of the porous solid (14).

However, although pore radii within the range 100 - 300 Å cover a part of the inter-particle macro-pore region, for a solid composed entirely of macro-pores with radii between 100 and 500 Å, this method loses its accuracy and validity. Nevertheless, the use of this procedure to calculate the pore volume distribution with

respect to pore radii may justify itself, if the computed cumulative pore area results in reasonable agreement with the B.E.T. area, obtained from the low pressure part of the isotherm.

In the present investigation the analysis of nitrogen desorption isotherms to establish pore volume distributions with regard to pore radii is based on the procedure detailed above.

6.5.2 Calculation Procedure.

As described in the previous Section, the calculation of pore volume distribution, based on an analysis of the desorption process with the assumption that all the pores are filled with liquid nitrogen ($\frac{p}{p} \approx 1.00$), required data from a complete isotherm. The data was obtained by the use of the B.E.T. adsorption apparatus. The technique was the same as that used to determine the monomolecular layer from nitrogen isotherms at the low relative pressure range. The complete isotherms were represented by plotting the volume of nitrogen adsorbed per gram of sample against the relative pressure.

Three isotherm measurements were performed with the following samples:

(i) Unused catalyst, not activated, prepared by grinding the pellets to 125 - 150 μ particle size

(ii) Unused catalyst, not activated, prepared by crushing the pellet to 2.5 - 3.5 mm particle size

(iii) Catalyst pellets reduced at 650° C and used in reforming experiments at 540° C, barometric pressure, with a steam : methane mole ratio of 3 and afterwards crushed to 1.0 - 3.5 mm particle size.

The recorded data and its evaluation for one isotherm are illustrated in Table A - 6.5 in the Appendix. The isotherms obtained are shown in Fig. 6.3.

Fig: 6.3 Nitrogen Isotherms

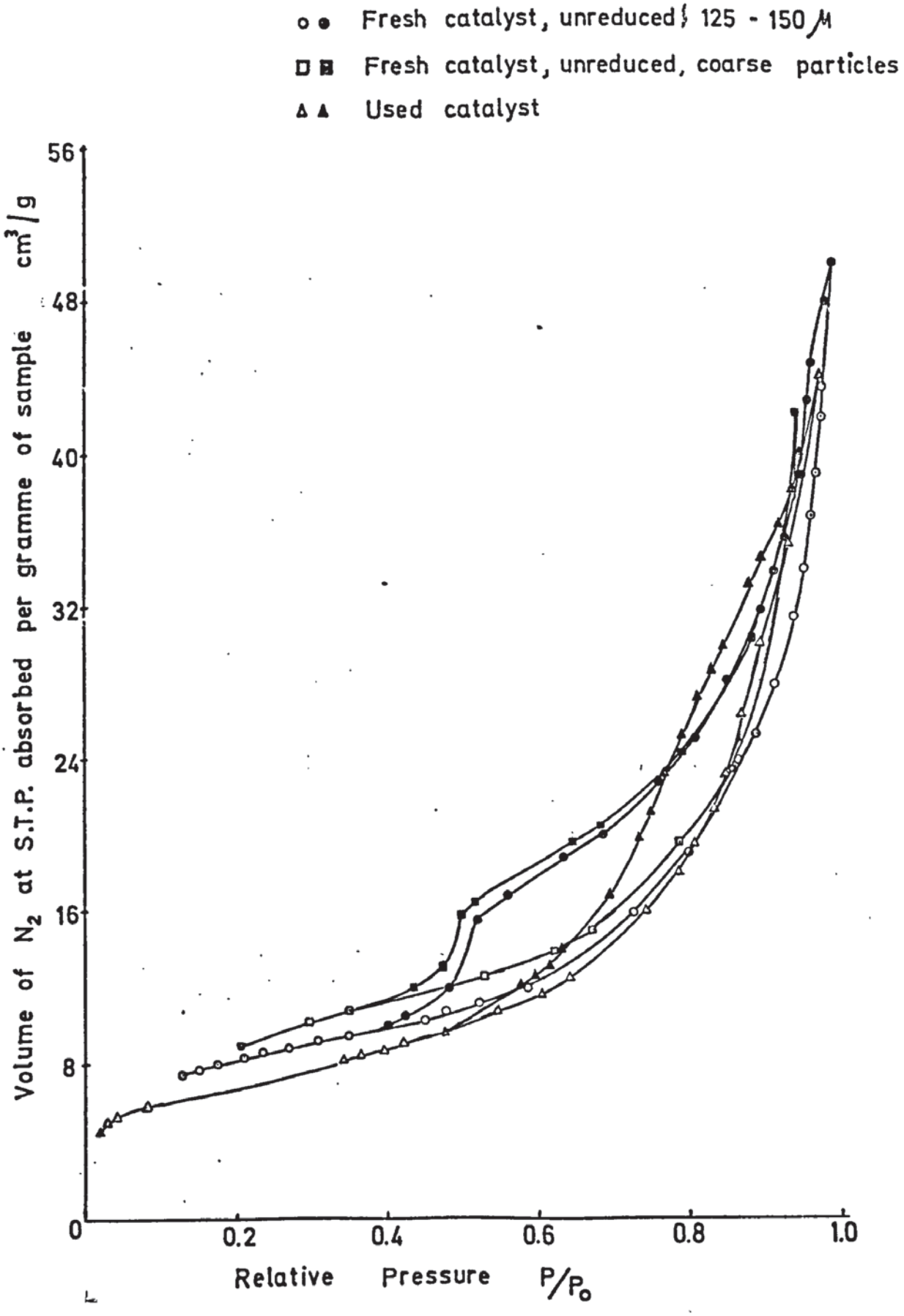

For the calculation of the pore volume distribution a master work sheet was prepared giving computed values of pore radii for given values of relative pressure (Table 6.4). The radius of the capillary, r_k (Column 3, Table 6.4) was computed from the Kelvin equation rearranged as:

$$r_k = \frac{2\,\sigma\,V}{(2.303)(RT)(\log \frac{p_o}{p})} \quad . \qquad (6.24)$$

The value of T was found by interpolation from a plot of vapour pressure of liquid nitrogen versus temperature. Necessary data for such a plot (Fig. A - 6.2 in Appendix) were taken from International Critical Tables (86) and Landolt-Börnstein, Zahlenwerte and Funktionen (95). It can be seen from Fig. A - 6.2 that the temperature of liquid nitrogen in the sample flask has changed within the limits of 77.3 and 77.5° K for all B.E.T. and isotherm measurements. An average value of 77.4° K was used for the computations.

The numerical value of the surface tension of liquid nitrogen, σ, was obtained from a plot of surface tension versus temperature (Fig. A -6.3 in Appendix), which was prepared using the data given in the literature (86). Within the range of liquid nitrogen temperature, the surface tension varied between 8.82 and 8.86 dynes/cm, and an average value of 8.84 was accepted for the calculations.

The molal volume of liquid nitrogen, V at 77.3° K is given in the literature as 34.65 cm^3/mole (14). The gas constant, R_g, in consistent units, was taken as (8.3143) (10^7) ergs/(mole) (°K).

Thus, the group $\left[\frac{2\,\sigma\,V}{(2.303)(R_g T)}\right]$ has the value 4.134 Å, in agreement with the value 4.14 used by B.J.H. (14).

Hence:
$$r_k = \frac{4.134}{\log \frac{p_o}{p}} \qquad (6.25)$$

The thickness of the physically adsorbed layer, t_r (Column 4),

TABLE 6.4

Computed Values of Pore Radii for Given Values of Relative Pressure

	1	2	3		4	5	6	7
	$\frac{p}{p_o}$	$\log \frac{p_o}{p}$	r_k	$\sqrt[3]{\log \frac{p}{p_o}}$	t_r	r_p	$\bar{r}_p$	$\bar{t}$
1	0.973	1.0277	347.4	0.2283	24.33	371.73		
2							330.35	23.31
3	0.965	1.0362	266.7	0.2493	22.28	288.98		
4							268.60	21.71
5	0.959	1.0427	227.1	0.2629	21.13	248.23		
6							227.09	20.44
7	0.950	1.0526	186.2	0.2812	19.75	205.95		
8							195.49	19.39
9	0.944	1.0593	166.0	0.2920	19.02	185.02		
10							171.08	18.48
11	0.934	1.0707	139.2	0.3097	17.94	157.14		
12							152.13	17.73
13	0.929	1.0764	129.6	0.3171	17.52	147.12		
14							120.27	16.17
15	0.886	1.1286	78.6	0.3748	14.82	93.42		
16							84.18	14.24
17	0.856	1.1682	61.3	0.4070	13.65	74.95		
18							68.09	13.15
19	0.822	1.2165	48.6	0.4396	12.64	61.24		
20							55.27	12.13
21	0.777	1.2870	37.7	0.4787	11.61	49.31		
22							42.47	10.89
23	0.688	1.4534	25.45	0.5456	10.18	35.63		
24							33.11	9.87
25	0.636	1.5723	21.04	0.5814	9.56	30.60		
26							29.65	9.44
27	0.613	1.6313	19.44	0.5968	9.31	28.71		
28							26.96	9.06
29	0.560	1.7857	16.42	0.6315	8.80	25.22		
30							24.16	8.68
31	0.520	1.9231	14.55	0.6574	8.55	23.10		
32							22.56	8.42
33	0.500	2.000	13.73	0.6703	8.29	22.02		
34							21.76	8.20
35	0.488	2.0492	13.27	0.6779	8.10	21.50		
36							21.08	8.08
37	0.470	2.1276	12.61	0.6894	8.06	20.67		
38							19.68	7.88
39	0.421	2.3753	11.00	0.7214	7.69	18.69		
40							18.58	7.67
41	0.415	2.4096	10.82	0.7255	7.65	18.47		
42							18.36	7.63
43	0.409	2.4450	10.65	0.7296	7.61	18.26		
44							18.06	7.58
45	0.398	2.5125	10.33	0.7368	7.54	17.87		
46							17.33	7.43
47	0.366	2.7322	9.47	0.7586	7.32	16.79		

TABLE 6.4 (cont.)

	1	8	9		10	
	$\frac{p}{p_o}$	$\bar{r}_k$	Δt	$\bar{r}_p^2$	$(r_k+\Delta t)^2$	R
1	0.973					
2		307.05	2.05	109131	95543	1.142
3	0.965					
4		246.90	1.15	72146	61529	1.172
5	0.959					
6		206.65	1.38	51569	43277	1.191
7	0.950					
8		176.05	0.73	38216	31251	1.222
9	0.944					
10		152.60	1.08	29268	23618	1.239
11	0.934					
12		134.40	0.42	23144	18176	1.273
13	0.929					
14		104.10	2.70	14465	11406	1.268
15	0.886					
16		69.95	1.17	7086	5058	1.401
17	0.856					
18		54.95	1.01	4636	3132	1.480
19	0.822					
20		43.15	1.03	3055	1952	1.565
21	0.777					
22		31.57	1.43	1804	1089	1.656
23	0.688					
24		23.24	0.62	1096	569	1.926
25	0.636					
26		20.22	0.25	879	419	2.097
27	0.613					
28		17.93	0.51	727	340	2.138
29	0.560					
30		15.49	0.25	583	248	2.350
31	0.520					
32		14.14	0.26	509	208	2.447
33	0.500					
34		13.56	0.19	473	189	2.502
35	0.488					
36		13.00	0.24	444	175	2.537
37	0.470					
38		11.81	0.37	387	148	2.615
39	0.421					
40		10.91	0.04	345	120	2.875
41	0.415					
42		10.74	0.04	337	116	2.896
43	0.409					
44		10.49	0.07	326	112	2.911
45	0.398					
46		9.90	0.22	300	102	2.941
47	0.366					

at the corresponding relative pressure was computed from the relationship (153) :

$$t_r = (7.34)\ (\ln \frac{p}{p_o})^{-1/3} \quad \text{Å} \qquad (6.22)$$

The pore radius, r_p (Column 5), is the sum of the Kelvin radius, r_k, and the thickness of the adsorbate layer, t_r. Columns 6, 7, and 8 are self-explanatory and are the arithmetic averages $\bar{r}_p$, $\bar{t}_r$, and $\bar{r}_k$, of r_p, t_r, and r_k, respectively. $\bar{r}_p$ and $\bar{r}_k$ represent the average of the radii of the largest and smallest pore emptied by a decrement of $\frac{p}{p_o}$ between two successive steps of desorption.

Column 8, Δt, is the difference between two $\bar{t}_r$ values, used to calculate:

$$R = \frac{\bar{r}_p^2}{(\bar{r}_k + \Delta t)^2} \qquad (6.26)$$

which is the term relating the pore volume to the capillary volume according to the assumed cylindrical pore model (Column 9).

The evaluation of the data recorded in successive steps of desorption, i.e. the volumes of nitrogen desorbed per gram of catalyst at the corresponding decrements of relative pressure, is illustrated in Table 6.5. Details of the computation are as follows:

Column 1 : The relative pressure, $\frac{p}{p_o}$, at any stage of desorption.

Column 2 : The values of pore radii, r_p and $\bar{r}_p$, taken from Columns 5 and 6 of Table 6.4, respectively, Å.

Column 3 : The variation in thickness of the physically adsorbed layer between two steps of desorption, taken from Column 9 of Table 6.4, Å.

Column 4 : The experimental volumes of nitrogen, $V_{ad.}$ cm^3 at S.T.P, remaining adsorbed at the relative pressures of Column 1 in pores with radii smaller than the radius of pores corresponding to the value of $\frac{p}{p_o}$.

Column 5 : The liquid volume of adsorbed nitrogen, $V_{liq.}$, cm^3,

calculated by multiplying the figures of Column 4 by the conversion factor 0.01547.

Column 6 : The volume of liquid nitrogen desorbed between two consecutive relative pressures of Column 1, ΔV cm^3/g. This column represents the distribution uncorrected for physically adsorbed nitrogen.

Column 7 : R, taken from Table 6.4

Column 8 : Column 6 multiplied by the appropriate value of R.

Column 9 : The coefficient, C, of the correction term (C) $(\sum A_{p_{n-1}})$, obtained as a product of (R)(Δt)(c). The value of c in the calculations is taken as 0.80 corresponding to an average pore radius 40 - 80 Å,(Table 6.3).

Column 10: The correction term $R_n \Delta t_n c \sum_{j=1}^{n-1} A_{p_j}$ to allow for the thickness of the physically adsorbed layer, calculated by multiplying (R) (Δt)(c) by the value of ΣA_p of Column 14 of the preceding step of desorption. Before subtracting the values $C_n \sum A_{p_{n-1}}$ from those of Column 8, it is multiplied by 10^{-4} to convert Å unit (Δt) and m^2/g ($\sum$Ap) to cm^3 liq.N_2.

Column 11: The corrected volume of liquid nitrogen, ΔV_p, desorbed from pores between the radius limits indicated in Column 2. The values of this column are identical to those of Column 8 at $\bar{r}_p$ values for which the correction term is negligible.

Column 12: The cumulative pore volume, $\sum \Delta Vp$, obtained by progressive summing of Column 11.

Column 13: The area of pores having average pore radius as indicated in Column 2, calculated from the Wheeler relationship

$$A_p = \frac{2\,(\Delta V_p)}{\bar{r}_p} \times 10^4 \quad m^2/g \qquad (6.27)$$

Column 14: The cumulative pore area, A_p, obtained by successive summing of A_p values of Column 13. The values of this

column are used to calculate the next correction term in Column 10.

Tables 6.4 and 6.5 illustrate the computations for only one sample (unused catalyst) but the pore volume distribution was determined for both unused (powdered) and used catalyst. The third isotherm in Fig. 6.3 obtained from the crushed pellet has not been evaluated, since the desorption pattern was almost identical to that obtained from the powdered sample.

The results of the calculations are shown in Fig. 6.4 and 6.5. Fig. 6.4 represents the pore volumes of the catalyst in terms of penetration (Curve 1 and 2) and total pore volume in pores of radius equal to or larger than $\bar{r}_p$ (Curve 1a, and 2a) at any average pore radius $\bar{r}_p$. The derivative of the penetration curve, $\frac{dV_p}{d \log \bar{r}_p}$, is the distribution function of pore volume with respect to pore radius describing the contribution of the various pore sizes to the total pore volume. Since the correlations involved the log of relative pressures, log scales were used for pore radii to be more consistent with the experimental data. The values of $\frac{dV_p}{d \log \bar{r}_p}$ were calculated by numerical differentiation using the actual experimental data, and not from the values obtained from the smoothened penetration curve. The plots $\frac{dV_p}{d \log \bar{r}_p}$ against $\bar{r}_p$ are shown in Fig. 6.5.

TABLE 6.5

Evaluation of the Desorption Process
for the Calculation of Pore Volume Distribution

	1	2	3	4	5	6	7	8
	$\frac{p}{p_o}$	r_p	Δt	V_{ad}	V_{liq}	ΔV	R	$R\Delta V$
1	0.973	371.73		47.982	0.0742			
2			2.05			0.0047	1.142	0.0054
3	0.965	288.98		44.948	0.0695			
4			1.15			0.0033	1.172	0.0038
5	0.959	248.23		42.796	0.0662			
6			1.38			0.0047	1.191	0.0056
7	0.950	205.95		39.899	0.0617			
8			0.73			0.0029	1.222	0.0035
9	0.944	185.02		37.996	0.0588			
10			1.08			0.0039	1.239	0.0048
11	0.934	157.14		35.463	0.0549			
12			0.42			0.0001	1.273	0.00012
13	0.929	147.12		35.440	0.0548			
14			2.70			0.0082	1.268	0.0104
15	0.886	93.42		30.126	0.0466			
16			1.17			0.0029	1.401	0.0040
17	0.856	74.95		28.265	0.0437			
18			1.01			0.0035	1.408	0.0049
19	0.822	61.24		26.000	0.0402			
20			1.03			0.0037	1.565	0.0058
21	0.777	49.31		23.579	0.0365			
22			1.43			0.0052	1.656	0.0086
23	0.688	35.63		20.216	0.0313			
24			0.62			0.0016	1.926	0.0030
25	0.636	30.60		19.193	0.0297			
26			0.25			0.0008	2.097	0.0016
27	0.613	28.71		18.840	0.0291			
28			0.51			0.0030	2.138	0.0064
29	0.560	25.22		16.839	0.0261			
30			0.25			0.0020	2.350	0.0047
31	0.520	23.10		15.620	0.0241			
32			0.26			0.0031	2.447	0.0076
33	0.500	22.02		13.600	0.0210			
34			0.19			0.0018	2.502	0.0045
35	0.488	21.50		12.400	0.0192			
36			0.24			0.0012	2.537	0.0030
37	0.470	20.67		11.600	0.0180			
38			0.37			0.0017	2.615	0.0040
39	0.421	18.69		10.543	0.0163			
40			0.04			0.0003	2.875	0.0008
41	0.415	18.47		10.349	0.0160			
42			0.04			0.0003	2.896	0.0008
43	0.409	18.26		10.167	0.0157			
44			0.07			0.0002	2.911	0.0006
45	0.398	17.87		9.991	0.0155			
46			0.22				2.941	
47	0.366	16.79						

TABLE 6.5 (cont.)

	9	10	11	12	13	14
	$C=R\Delta t_c$	$C\Sigma A_{p_{n-1}}$	$\frac{\Delta V_p}{(R\Delta V - C\Sigma A_p)}$	$\Sigma\Delta V_p$	$A_p = \frac{2\Delta V_p}{\bar{r}_p}$	ΣA_p
1		$(x10^{-4})$				
2			0.0054	0.0054	0.326	0.326
3						
4	1.011	(0.00003)	0.0038	0.0092	0.282	0.608
5						
6	1.315	0.0008	0.0048	0.0140	0.422	1.030
7						
8	0.714	0.0007	0.0028	0.0168	0.286	1.316
9						
10	1.071	0.0014	0.0034	0.0202	0.397	1.713
11						
12	0.428	(0.00007)	(0.00005)	0.0203	0.006	1.719
13						
14	2.739	0.0005	0.0049	0.0302	1.646	3.365
15						
16	1.311	0.0004	0.0036	0.0338	0.855	4.220
17						
18	1.138	0.0005	0.0044	0.0382	1.292	5.512
19						
20	1.290	0.007	0.0051	0.0433	1.845	7.357
21						
22	1.895	0.0014	0.0072	0.0505	3.390	10.747
23						
24	0.955	0.0011	0.0019	0.0524	1.147	11.894
25						
26	0.419	0.0005	0.0011	0.0535	0.741	12.635
27						
28	0.872	0.0011	0.0053	0.0588	3.931	16.566
29						
30	0.470	0.0008	0.0039	0.0627	3.228	19.794
31						
32	0.509	0.0010	0.0066	0.0693	5.851	25.645
33						
34	0.380	0.0010	0.0035	0.0728	3.216	28.861
35						
36	0.487	0.0014	0.0016	0.0744	1.518	30.379
37						
38	0.774	0.0024	0.0020	0.0764	2.032	32.411
39						
40	0.092	0.0003	0.0005	0.0769	0.538	32.949
41						
42	0.093	0.0003	0.0005	0.0774	0.544	33.493
43						
44	0.163	0.0005	0.0001	0.0775	0.553	34.026
45						
46						

6.5.3 THE RESULTS AND THEIR DISCUSSION.

An immediate check of the consistency of the results obtained with the B.J.H. method for computing the pore volume distribution can be made by comparing the value for the cumulative pore area (Column 14 of Table 6.5) with the value of specific surface from B.E.T. determination. The differences observed between these values are given in Table 6.6.

TABLE 6.6

Pore Area Differences of Catalyst Samples

Sample	B.E.T. Area (m^2/g)	Pore area computed by B.J.H. method.		% Deviation from B.E.T. area
		$\sum A_p$ (m^2/g)	Smallest pore radius Å	
Unused Catalyst (125 - 150 μ)	32.05	30.38	20.7	- 5.21
		34.03	17.87	+ 6.17
Used catalyst	25.29	23.60	26.3	- 6.68
		27.12	21.5	+ 7.23

In both measurements, the cumulative pore areas calculated by the B.J.H. method exceeded the specific surfaces obtained from B.E.T. measurements by 6.17 and 7.23 %, respectively. It has also to be pointed out that in both cases, the surface of the pores with radii smaller than 21.5 and 17.9 Å are not included in these figures. As can be seen from the isotherm plots (Fig. 6.3), at relative pressures below 0.488 (r_p = 21.50 Å) and 0.398 (r_p = 17.87 Å), the amount of nitrogen remaining adsorbed is 0.0158 and 0.0155 g/cm^3, respectively. These quantities correspond to nitrogen adsorbed on the external

surfaces and fissures within the particles which are both relatively very small and negligible, and also to nitrogen in the pores with smaller radii than stated above. The B.J.H. procedure in combination with Equations (6.22) and (6.25) to evaluate the volume and area of these pores by a forward calculation gives inconsistent results. The discrepancy was eliminated by Barrett and co-workers (14) by performing this calculation simultaneously in the forward and backward directions. They claimed that, by assigning the remaining volume to the smallest pore, $\bar{r}_p$ = 12.5 Å, and equalising the computed $\sum \Delta V_p$ to the measured quantity of nitrogen adsorbed at a relative pressure of 0.967 $\bar{r}_p$ = 300 Å, the value for $\sum A_p$ should check the B.E.T. area within 5%.

In the present investigation, the deviation of the B.J.H. values, $\sum \Delta V_p$ and $\sum A_p$, from the measured volume of nitrogen adsorbed and B.E.T. area, respectively, may have originated from the following sources:

(i) Experimental :

The magnitude of the relevant pressure decrements to be obtained during the desorption process depended on the limited number of combinations of the burette bulbs of the volumetric B.E.T. apparatus. It was not possible to change the values of relative pressures by 0.001 or even by 0.01, as recommended by B.J.H. The stepwise progress of the calculation requires very small decrements of relative pressures in order to obtain a higher accuracy.

(ii) Computational :

Experimentally measured volumes of adsorbed nitrogen were used in the calculations. Only a limited number of points were taken from the complete isotherm curves, and these were confined to the ranges of $\frac{p}{p_o}$, where small changes of relative pressure

could not be achieved due to the experimental restrictions. An experimental error (reading the mercury levels) at any stage of desorption affected the uncorrected and corrected volumes of desorbed nitrogen and the pore area corresponding to the range of pore radii, and remained in the subsequent steps of calculation. This fact is also the reason for the small fluctuations of the points forming the penetration and pore curves (Fig. 6.4). Since the distribution curves of pore volumes with respect to pore radii (Fig. 6.5) were plotted from the actual values of penetration curves, this effect is also reflected in the curves of Fig. 6.5. In addition, the calculations were subject to rounding-off errors.

(iii) Theoretical :

The author believes that the value of the thickness of the adsorbed nitrogen layer, t_r, affects the results of the B.J.H. technique of computation more than anything else, since the change in thickness of this layer contributes significantly to the total nitrogen adsorption, i.e. capillary condensation plus multi-layer adsorption, especially in the range of low relative pressures, thus affecting the numerical values of the correction factors.

Considerable differences between the values used by B.J.H. and calculated by the author from Equation (6.22) which is given in the literature (153) resulted. Pierce (126) who modified the B.J.H. method while retaining the basic assumption with respect to the pore model and other essential features, calculated the thickness of the layers from the following relationship :

$$t = (3.6)\, n \qquad (6.27)$$

where n is the number of statistical layers in the adsorbate film remaining at each relative pressure, and 3.6 is the thickness of an adsorbed layer of nitrogen obtained on dividing the molecular volume by the area of an adsorbed nitrogen molecule (16.2 Å). He used

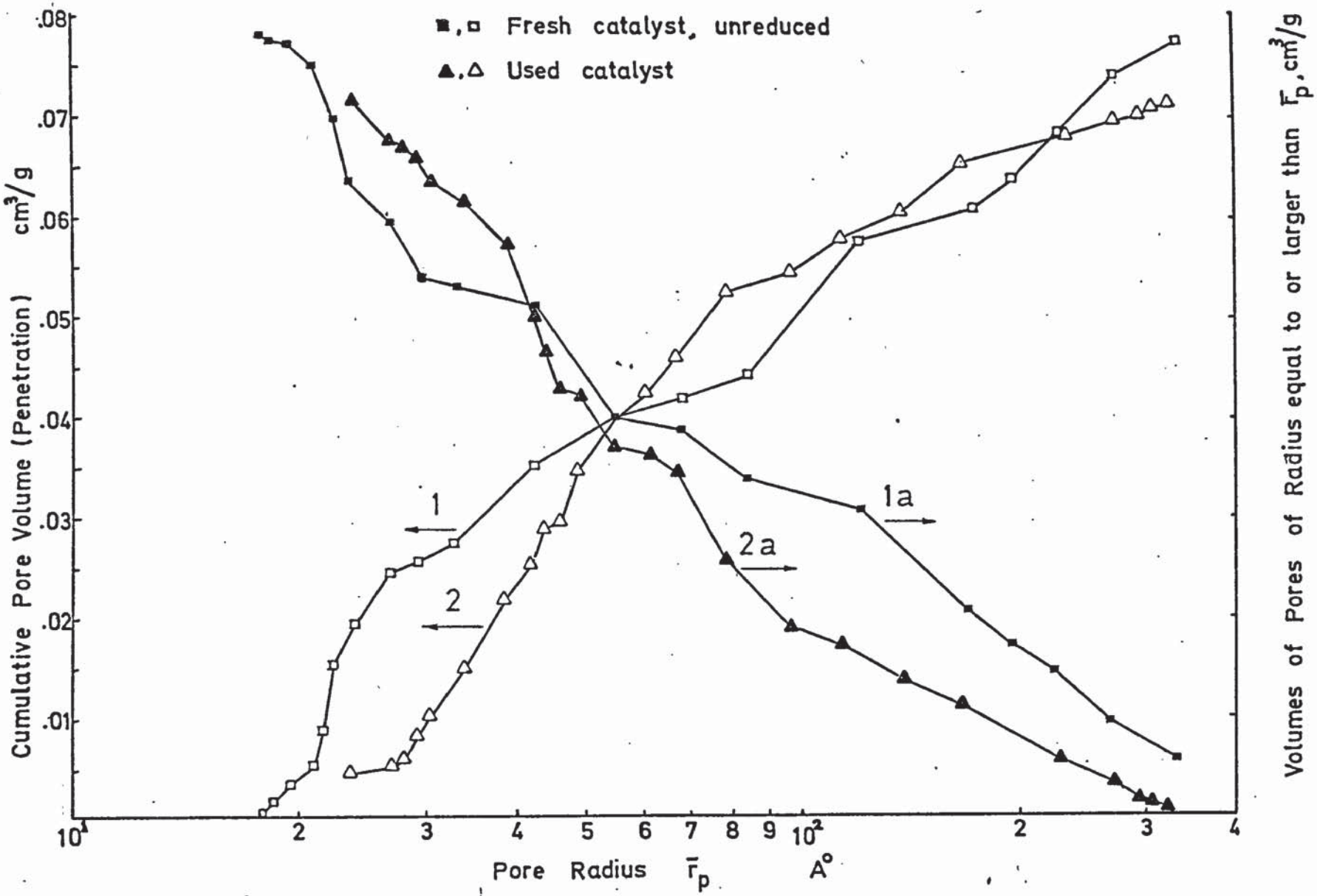

Fig:6.4. Pore volumes of used and unused catalyst.

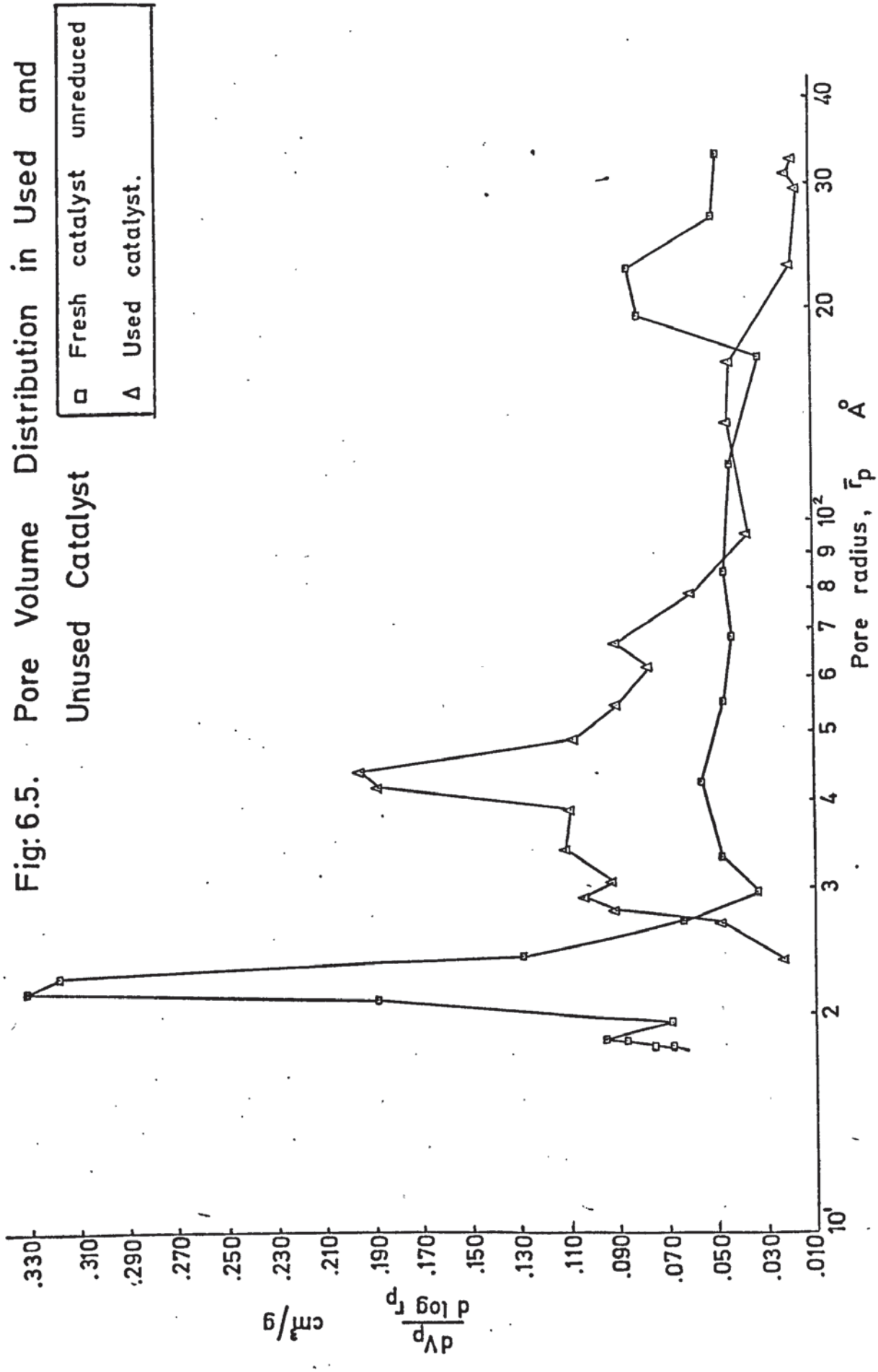

Fig: 6.5. Pore Volume Distribution in Used and Unused Catalyst

published values for n in his calculations, but reported that at relative pressures above 0.8, the selection of the values presented some difficulties. This fact has also been stated by Shull (150). Pierce (126) has used for relative pressures above 0.80, n values which caused the curve of $R = \frac{(r_p)^2}{(r_k)^2}$ against $\frac{p}{p_o}$ to "extrapolate smoothly to a value of $R = 1.00$ at $\frac{p}{p_o} = 1.0$", but offered no theoretical justification for this procedure. Furthermore, the values of n, which should be integers since they indicate the number of adsorbed layers are in fact given as non-integer figures for relative pressures less than 0.95. Mingle and Smith (110) stated that the thickness depends upon the type of catalyst material, the mean pore radius, and the heat of adsorption. They also observed that the results using Equation (6.22) did not agree with the data at low values of relative pressures (0.20 - 0.50) and derived the following equation which gave satisfactory results for Vycor glass:

$$t = 5.15 \, (\bar{r}_p)^{-0.085} \left[\frac{\log \, (1 - \sqrt{c})/(1 - c)}{\log \frac{p}{p_o}} \right]^{\frac{1}{1.42(1 + 0.00212c)}} \qquad (6.28)$$

where:

c = B.E.T. constant

V_g = the total pore volume

S_g = the B.E.T. area.

In spite of the differences in the values of t_r used by B.J.H. (14), Pierce (126), and the author, (Table 6.7), the results obtained from the computations performed in the present work provided adequate information for comparisons between the pore volume distribution of both used and unused catalysts to be made.

The differences (6.17 % and 7.23 %) between B.E.T. areas and computed pore areas ($\sum$Ap) were considered to be within experimental limits.

TABLE 6.7

Some Values for Pore Radii, Kelvin Radii and Thickness of Adsorbed Nitrogen Layers

	Relative Pressure $\frac{p}{p_o}$	Kelvin Radius r_k Å	Thickness of Multi-layer t Å	Pore Radius r_p Å	Value of R
B.J.H.	0.950	181.48	18.52	200	1.215
PIERCE	"	195.0	32.0	227	1.24
This Work	"	186.2	19.75	205.95	1.2221
B.J.H.	0.488	13.03	6.92	20	1.980
PIERCE	0.500	13.80	6.4	20.2	2.15
This Work	0.488	13.3	8.20	21.5	2.5283

Fig. 6.5 illustrates the contribution of the pores of various radii to the total pore volume and pore area. It can be seen from these plots that a substantial portion of the pore area of the unused (not activated) catalyst is within pore radii of 18 - 30 Å. Retaining the assumption of the cylindrical pore model, this area was calculated from :

$$A_p = \frac{2\,V_p}{\bar{r}_p} \times 10^4 \qquad (6.29)$$

where:

$\bar{r}_p$ = 24 Å, taken as the arithmetic average radius of pores falling within the range 18 - 30 Å

V_p = the cumulative pore volume of pores within this range, cm^3/g

A_p = the cumulative pore area within the same range, m^2/g

Thus, the value of A_p, which represented the micro-pore area

was found to be 20.8 m^2/g corresponding to two thirds of the total B.E.T. area. The remaining one third seemed to be distributed among the pores with larger radii. The second peak traced by the distribution curve within the macro-pore range (170 - 330 Å) was found insufficiently significant to consider the catalyst to be a bi-disperse pore system.

The distribution plot obtained from the used catalyst sample indicated that the pore radii responsible for the main portion of area was spread over a wider range, 28 - 61 Å . The area corresponding to an average pore radius of 45.5 Å has been calculated to give 15.94 m^2/g which is 63% of the total B.E.T. surface. The main reason for such a shift, i.e. the formation of larger pores at the expense of smaller ones, was definitely the effects of sintering which caused the change of the crystallite size and structure on the pore surfaces.

The distribution plots also indicated that the area of the pores of the unused catalyst with pore radius > 170 Å diminished considerably. In fact, the pore area of the unused catalyst corresponding to the region 170 - 330 Å ($\bar{r}_p$ = 251 Å) was calculated to be 1.34 m^2/g, whereas the pore area of the used catalyst for the same region ($\bar{r}_p$ = 245 Å) was found to be 0.48 m^2/g. This reduction might be attributed to surface sintering, as well as to a deposition of non-equilibrium carbon formed during the course of reforming reactions which would have caused a shift of pore volume to the region of pores with smaller radii. Since the pores with large radii provided an easy access to the reactant molecules for intrapellet diffusion and reaction, it was considered not unlikely that the carbon, formed as a reaction intermediate and not reacted by any of the carbon removal reactions, would have reduced the pore volume, although there was no

substantial quantitative evidence to support this possibility. However, Andrew (8), from the results of experiments with naphtha as feedstock and at steam ratios well above the thermodynamic minimum, has concluded that the presence of both the voidage and the nickel as the active constituent of the heterogeneous surface, were prerequisites for non-equilibrium carbon formation. This fact has also been observed in the present investigation. The conversions achieved in reforming experiments with powdered catalyst of different particle sizes were considerably lower than those obtained with catalysts in pellet form at identical operating conditions. The decrease in the rate of conversion coupled with an increase of back-pressure were sufficient indications of a deactivation of the catalyst particles by encapsulation with carbon, which might have caused the blocking of the catalyst bed and channelling of the reactant gas stream. There seems to be no reason why the conclusions drawn from these experimental observations and considered to be valid for void spaces of several thousands Å magnitude, should not be extended to pores with 400 - 500 Å diameter.

A comparative examination of the isotherms (Fig. 6.3) substantiated the marked changes in the pore structure of the catalyst. The hysteresis characteristics of the isotherms obtained from used and unused catalyst samples were completely different, whereas the adsorption-desorption paths of unused catalyst in powdered (125 - 150 μ) or granular form were almost identical. The desorption isotherms of unused catalyst samples exhibited a rather flat region ending in a sharp and reproducible break (point B) at a relative pressure of 0.52, and then joined the adsorption branch at relative pressures of 0.35 - 0.39 (point A), whilst the desorption isotherm of used catalyst did not trace a similar pattern.

Although there exists at present no well-established theory

to account for hysteresis phenomena, it is known that hysteresis effects are related to the pore structure of the adsorbent. Considering the notable differences of the hysteresis loops of used and unused catalyst samples, it was concluded that the reduction process and the reforming conditions even for a very short period of time, caused substantial changes in the pore structure. Partial physical collapse of the fine pore structure might account for this difference. However, it is known that the hysteresis is not intimately associated with specific surfaces, because adsorbents of the same nature with widely differing areas may have very similar hysteresis effects (133). Therefore, it was considered unlikely that a reduction in B.E.T. area was the only cause of the considerable change in hysteresis. From the very similar hysteresis characteristics of finely ground and crushed samples, it was evident that the grinding process had not affected the pore structure responsible for the hysteresis effects.

A systematic investigation of the time-temperature effects on the change of hysteresis shapes cf reforming catalysts in combination with examinations of the crystallite structure would enable elucidation not only of the structural transformations on the surface, but also might point the way to finding a specific relation between adsorption-desorption processes and surface structure of the catalyst.

6.6 THE ACTIVITY OF THE CATALYST.

The catalyst as supplied contained its active component, nickel, in oxide form which is stable under atmospheric conditions. The activation involving the reduction to metallic nickel was performed in situ at 650° C in a stream of hydrogen and steam.

Qualitative analyses with lead acetate solution, of the reactor exit gases during the activation process indicated the presence of some sulphur compounds in the fresh catalyst which produced hydrogen

sulphide on reduction.

Each series of reforming experiments was run with a new catalyst charge, and therefore, activation was carried out prior to every set of runs. The conditions of the activation process with respect to the length and temperature of the reduction were established by Woodcock (179) as a result of a systematic study. Therefore, it was not considered necessary to investigate the conditions required to obtain a stabilised catalyst activity.

The activation schedule practiced during the present research consisted of:

(i) increase of the reactor temperature to 300° C under a steady flow of dry hydrogen at a rate of $(40)(10^{-3})$ moles/min

(ii) at 300° C addition of steam at a rate of $(6)\ (10^{-3})$ moles/min to the hydrogen stream

(iii) increase of the reactor temperature to 600° C at a rate of 80 - 100 deg C/h keeping the flowrates of hydrogen and steam at the same level

(iv) adjustment of the hydrogen : steam molar ratio in the feed to 9, and finally

(v) increase of the catalyst bed temperature to $650 \pm 2^{\circ}$ C.

The catalyst was exposed to the steady flow of the reducing medium at this temperature level for a period of 16 hours. The sum of two overnight intervals, during which the temperature of the reactor was lowered to 450° C and the catalyst was kept under a static hydrogen atmosphere, was approximately 24 hours.

The limits for the hydrogen : steam molar ratios to provide a reducing atmosphere calculated on the basis of the reactions:

$$NiO + H_2 \rightleftarrows Ni + H_2O$$

are given in the literature (31, 179). From the plot of $p_{H_2O} : p_{H_2}$ versus temperature, $p_{H_2O} : p_{H_2}$ ratios below 13 were found to be sufficient to ensure a reducing atmosphere. While steam was undesirable thermodynamically, its presence prevented fast reduction and structural re-arrangement of the crystal lattice (179).

Although activation temperatures above 700° C were recommended (31) to completely remove the sulphur, if present, from the catalyst structure, no hydrogen sulphide was detected in the exit gas after 8 - 10 hours of reduction.

The existence of constant activity was also checked in order to set a time limit for the length of reforming experiments. This was considered necessary, since a decline of activity of the catalyst has been reported by a number of investigators who studied the kinetics of reforming or methane synthesis reactions (3, 16,17, 22, 47 124), whereas other workers claimed not to have observed any decrease of activity within the duration of the experimentation (2). This change in catalyst activity has to be attributed not only to the operating conditions involved (i.e. temperature, pressure, type of hydrocarbon, and steam : carbon molar ratio in the feed), but also to the constituents and to the mode of preparation of the catalyst, as well as to its particle size and activation conditions used for reforming experiments. In fact, the rates of decline in catalyst activity, as reported by the researchers, differed greatly from each other. According to published literature, the time required to reach a constant level of activity might change between 2 - 3 hours (16, 17, 124) to 30 - 40 hours (22).

The actual reasons for an initial decrease of catalyst activity and termination at a stabilised level, thus forming a threshold, are not yet known. It is very unlikely that a change of the specific

surface during this period could have produced this effect, since the decrease is restricted. The other possibility is the formation of kinetic carbon or carbon radicals as a result of a reaction mechanism which involves a network of parallel and consecutive, reversible reactions leading to a probable existence of intermediate products at equilibrium. In fact, according to Bhatta and Dixon (16) the decline in activity was found to be independent of the partial pressure of hydrocarbon (butane), but decreased linearly with increasing partial pressure of steam which presumably has either reacted with carbon deposited or prevented the latter's formation by reacting with the intermediates.

In order to assess the effect of time under actual reforming conditions on the catalyst activity, reforming experiments were carried out at 540° C and barometric pressure with a steam : methane ratio 3 : 1 and constant total feedrate (methane flowrate $(2.20)(10^{-3})$ moles/min, steam $(6.84)(10^{-3})$ moles/min). These experiments were extended to 8 consecutive hours and continued the next day for another 4 hours at the same conditions, while the catalyst was kept overnight under a static hydrogen atmosphere at 450° C. Since 2 - 3 hours were required to attain thermal equilibrium after replacing the hydrogen atmosphere by methane, no samples were taken during the initial period. The samples of product gas were analysed every two hours. The conversions calculated from analytical results (26.2 ± 0.6 %) indicated no progressive loss of activity. Since each series of experimental runs lasted no more than 14 hours(excluding an overnight interval), the activity of the catalyst was assumed to remain constant, and it was decided to maintain the described procedure of activation and conditions of keeping the catalyst overnight for the subsequent reforming experiments.

CHAPTER 7

MASS AND HEAT-TRANSFER EFFECTS

7.1 INTRODUCTION.

If activated chemisorption and formation of transition complexes are responsible for steam-methane catalysis, then the heterogeneous character of the system and the presence of phase boundaries introduce the need to consider the physical transport processes of heat and mass between the bulk gas phase and catalytic sites.

It is well-established that even in isothermal conditions the observed rate of a catalytic reaction as well as the nature of the products formed are extensively affected by the rate of transfer of reactant molecules to the catalytic sites and product molecules back into the main body of ambient phase. In cases of non-isothermal operation, which in fact is inevitably encountered in large scale work, the effects of physical transport on the rates of conversion become more pronounced.

In a kinetic study conditions must be established such that the rate of diffusional rate processes may be considered as very fast in comparison with the chemical processes taking place in contact with the catalyst. This is imperative for two reasons:

(i) The kinetic, adsorption, and driving force terms of the intrinsic rate expression involve the temperatures and and concentrations of the reacting species at the gas-catalyst interface, which not being measurable quantities, must be separately evaluated.

(ii) Significant concentration and temperature gradients may lead to a falsification of the true kinetics of the system, since the observed concentrations and temperatures, as well as the calculated values for reaction rates used for interpretations are those of the bulk gas phase. The observed course of the reaction, being the sum of the events occurring on the catalyst as a result of the conditions

actually existing at each point of the external and internal surface, may follow a completely different path if such gradients were absent.

Although general quantitative treatments of the consequences of mass and energy transfer resistances are extensively discussed in numerous textbooks (9, 28, 36, 83, 99, 123, 141, 153), a summary of the basic principles involved in the interpretation and evaluation of the mass transport effects on the overall (observed) rate follows, since it has formed the major objective of this work.

7.2 GENERAL ASPECTS OF MASS TRANSFER EFFECTS.

Because of the radical differences in the mechanisms of the physical mass transport and chemical surface phenomena involved in heterogeneous catalysis, the stages through which the conversion process of reactants into products proceeds, are conventionally classified in the following groups:

(i) the mass transfer of reactants and products to and from the bulk gas phase and the exterior surface of the catalyst particle;

(ii) the diffusional transfer of reactants and products into and out of the pore structure of the catalyst particle;

(iii) the activated adsorption of reactants and activated desorption of products at the catalytic sites;

(iv) the surface reaction of chemisorbed reactants to form chemisorbed products via some transition complexes or reaction intermediates (radicals).

This classification does not imply, however, that the chemical transformation will take place in a definite sequence of steps as listed above. In fact, the bulk gas phase mass transfer (i) and surface phenomena (iii and iv) are in a series-relationship with each other, and therefore, can be related separately, whereas the pore diffusion (ii) occurs simultaneously with chemical reaction and can never be treated independently. Thus, it is not possible to eliminate the interaction between (i and ii) and surface kinetics (iii and iv), which often makes the overall phenomenon difficult to analyse and evaluate kinetically. The individual rates of these processes are affected by factors of a widely dissimilar nature, with the exception of concentration gradients (driving force) of the reacting species involved at the transition boundaries of each stage, which influence all four rates, although

to different extents.

The bulk gas phase mass transport is determined by the flow characteristics of the system and the transport properties of the gas. The rates of pore diffusion are affected by the pore dimensions and pore volume distribution, by the size of the catalyst particles, by the diffusional characteristics of the system, and by the rate at which the surface processes (iii and iv) proceed at the catalytic sites. The rates of the activated adsorption-desorption processes are defined by the character and magnitude of the catalytic surface, and by the activation energies of adsorption and desorption of every species involved in the reaction. Thus they are highly temperature sensitive. Provided that the reaction does not entail a chain mechanism, the rate of the chemical reaction of chemisorbed reactants to form chemisorbed products is a function of the intrinsic activity and extent of catalytic sites available on the internal and external surface of the catalyst particle, and of the activation energy of the reaction or series of probable consecutive reactions.

The relative importance of these different rate processes determines the mechanism with which the reaction proceeds, and influences the distribution of concentrations in the system. One or theother may govern the rate of any particular reaction for any given set of conditions, and in the limiting case and at steady-state, the slowest step will determine the observed rate of the reaction. If the overall rate of the reaction is limited by a slow mass transfer process, then the potential of the kinetically favoured reaction can be greatly reduced, and of greater importance, the selectivity of the catalyst may be altered. The effects of mass transfer resistances are greatest in the case of very active catalysts, or if the kinetic potential is enhanced by increasing the temperature.

A characteristic feature of the effect of mass transfer

resistances on the kinetics of heterogeneous catalytic reactions at particular flow conditions, and catalyst properties is the change of the apparent activation energy for the overall reaction, which may be followed on an Arrhenius-type diagram. This fact, first pointed out by Wicke (176) and worked out by others (28, 141, 153, 171,173), serves to separate the heterogeneous catalytic reactions into three distinct regimes. (Fig. 7.1).

If the surface phenomenon of adsorption and desorption do not have a pronounced effect on the kinetic mechanism of an irreversible reaction, then the observed rate of conversion can be expressed by the simple correlation:

$$r_{obs.} = A_a \, e^{-\frac{E_a}{RgT}} \left[C_A^a \quad .... \right]$$

where:

$r_{obs.}$ = the observed rate of the reaction, mole of A converted per min. per cm^3 reactor volume

C_A = the concentration of the reactant A in the bulk phase, mole per cm^3 reactor volume

E_a = the apparent activation energy for the reaction, cal per mole

R_g = the gas constant, cal/ (mole)(^oK)

T = the absolute temperature, ^oK

A_a = the apparent frequency factor.

Thus, for heterogeneous reactions without complex kinetics, the apparent activation energy can be calculated from the slope of the straight line obtained from a plot illustrated in Fig. 7.1. If such a plot gives a curve (dotted) with changing slope, it can be concluded that the system is under conditions of mass transfer limitations. Region A on the diagram represents a low temperature region, in which the rate of reaction is very low, the potential for the diffusion flux is insignificant, and intrinsic kinetics

Fig: 7.1 The Reaction Regimes and Apparent Activation Energies of Simple Heterogeneous Catalytic Reactions.

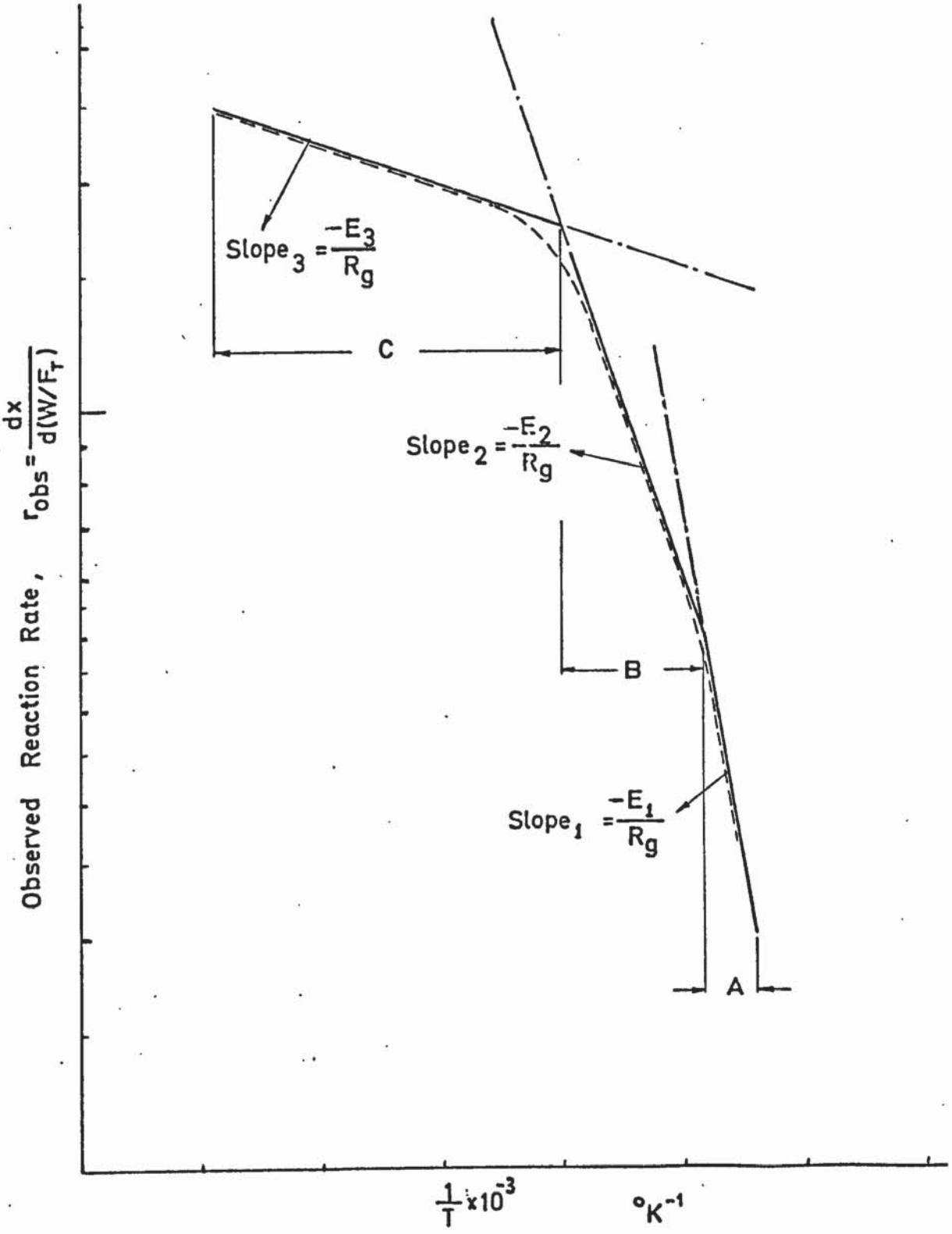

will govern the overall rate of conversion. The activation energy calculated from the slope within this region will correspond to the true activation energy of reaction. The increase of reaction temperature, all other conditions remaining the same, would increase not only the rate of diffusion flux for a given concentration difference between the bulk phase and the catalyst surface structure, but also the potential of the intrinsic reaction rate. However, the temperature effects on the diffusional mass flow are not significant compared with the exponential increase of the reaction rate constant $A\, e^{-\frac{E_a}{RgT}}$. Thus the products of the reaction become localised on the gas-solid interface and the stagnant gas in the catalyst pores, which constitutes the major catalytic surface, then presents the main resistance. Hence, concentration gradients within the catalyst pores become more effective than those in the ambient fluid. This second regime (region B) in which pore diffusion resistances begin to be appreciable is usually called the "pore-diffusion limited region". With further increase of the temperature, the concentration difference between the bulk gas phase and the external surface of the catalyst particle becomes more significant, since in this temperature range the intrinsic activity of the catalyst is promoted to such an extent that the concentration of the reactant at the outside surface of the catalyst pellet approaches zero. The rate limiting process in this third regime, called the "film-diffusion limited region", is the mass transfer from the ambient gas phase to the catalyst surface and shows the same characteristics as bulk diffusion, (ordinary molecular diffusion). Since in gas phase reactions, the effect of temperature on diffusion rates is equivalent to an activation energy of the order of 1000 - 3000 cal/mole, the apparent activation energy of the overall reaction will be found to have this magnitude. In this regime, all reactions

will appear also to be first order regardless of their intrinsic kinetics, since mass transfer is a first order process.

The apparent activation energies of processes proceeding in the second regime, as computed from an Arrhenius-type plot, are found to be the arithmetic average of the activation energies for the intrinsic reaction rate (Regime A), and for the bulk diffusion (Regime C), provided that the reaction is not of a complex nature. Also the apparent order of the reaction will gradually shift towards first order.

Although these considerations in differentiating three distinct reaction regimes form a useful tool in characterising the controlling factors in a gas-solid catalytic reaction, it should be noted that they are subject to some restrictions in addition to the basic assumption that the intrinsic mechanism does not involve complex rate expressions as derived by a Langmuir-Hinshelwood treatment of the kinetics. It is also assumed that the temperatures of the gas and catalyst at any point of the system are the same, which is questionable, since considerable temperature gradients may develop between interior and exterior surfaces of the catalyst, as well as between the exterior surface and the bulk gas phase, particularly in the case of reactions with significant heat effects. Furthermore, a substantial reduction in the apparent activation energy by an increase of temperature of the reacting system is not sufficient evidence that mass transfer limitation is present, because such a change may also originate solelyfrom, or as a resultant of combined effects of simultaneous change in the mode of adsorption, or in the kinetic mechanism of the chemical reaction, or even by a concurrent reaction in both the heterogeneous and homogeneous phases. Nevertheless, in spite of these limitations and not very distinct indications, the transition behaviour of heterogeneous catalytic systems with respect

to reaction regimes is used for diagnostic characterisation of the interaction between mass transport and intrinsic kinetics. The relative location and extent of the three regimes to be observed on the Arrhenius diagram depends on several factors.

(i) In the pore diffusion regime (B), the rate but not the apparent activation energy will be promoted by reducing the size of the catalyst particles or by altering the pore structure (increase of pore diameters). With smaller catalyst particles the straight line of regime B will shift upward, whilst its slope will remain the same. In the case of two extreme cases (catalysts with exceedingly large pore diameters, or with non-porous catalysts), the regime B can be eliminated, and the transition will occur directly from the intrinsic to the film-diffusion region.

(ii) In the film-diffusion regime C, the rate of conversion is strongly dependent on the superficial mass flow rate of the ambient gas, whereas in regime B, the rate of pore diffusion will not be affected by change in the bulk mass flow.

Hence, the experimental approach to determine the regime corresponding to a given set of operating conditions is to observe the effects of temperature, particle size and superficial mass velocity, on the rate of conversion.

The techniques applied in general for the qualitative diagnosis and quantitative treatment of mass transport effects are outlined in the next sections. The results obtained in the present investigation to minimise the mass transport effects on the rate of reaction are discussed in the context of the above techniques in Chapter 8.

7.3 EXTERNAL MASS AND HEAT TRANSFER.

7.3.1 External Mass Transfer.

According to classical boundary layer theory, there will be a region near the solid surface where the velocity of the flowing gas, even in the case of fully developed turbulent flow, is extremely low. For this reason the transport of heat and mass between the gas and catalyst surface is primarily by molecular diffusion, and the rate of mass transfer normal to the surface is described by the molecular diffusion coefficient $D_{i,\,m}$, where the subscript i denotes the diffusing component, and m the surrounding mixture through which the diffusion proceeds. However, the transport of species in the bulk stream towards this boundary layer takes place by a convective mechanism, and the rate is essentially independent of the diffusion coefficient. The thickness of the film through which the molecular diffusion proceeds is a function of the velocity of the bulk gas phase. Because of the continuous and unpredictable change of the flow pattern and the velocity distribution, the mass transfer rates for the combined transport process in the bulk phase and in the boundary layer, are described by semi-empirical correlations in which the specific transport property for every individual component is substituted by an overall mass transfer coefficient. These correlations are developed on the basis of the assumption that the external surface of the catalyst is uniformly accessible to the reactants, i.e. the thickness of the boundary layer is uniform over the entire catalyst surface, and the conditions in the bulk gas phase giving rise to the transport of mass to each element of external surface, are identicalover the entire surface. This assumption reduces the behaviour of the system, in the absence of chemical reaction, to one-dimensional, and the point value of an average mass transfer coefficient will define any

solid-gas system at the same conditions in the bed, independently of the surface properties of the catalyst. Some experimental data show that variations exist (153), and analytical treatments for predicting local variations of transfer coefficients are discussed by Petersen (123). However, the error introduced by the use of a point value for mass transfer coefficient is found to be negligible, and calculated overall reaction rates based on these methods were in agreement with the observed values of rates within the accuracy of experimental data (153). The mass transfer coefficient and the mass flux between the bulk gas phase and catalyst surface, are correlated in terms of dimensionless groups which characterize the flow conditions of the diffusing phase:

$$j_D = \frac{k_c}{G}\left(\frac{\mu}{\rho D_{i,m}}\right)^{2/3} = f\left[\frac{d_p G}{\mu}\right] \qquad (7.1)$$

$$j_D = \frac{k_G P_f}{G_m}\left(\frac{\mu}{\rho D_{i,m}}\right)^{2/3} = f\left[\frac{d_p G}{\mu}\right] \qquad (7.2)$$

where:

j_D = mass transfer factor, dimensionless

k_c = mass transfer coefficient, based on concentration of diffusing species, cm/sec

k_G = mass transfer coefficient, based on partial pressure of diffusing species, mole/(cm^2) (sec) (atm); $k_G = k_c \cdot \frac{1}{R_g T}$

ρ = density of the bulk gas phase, g/cm^3

G = superficial mass velocity of the bulk gas phase, based on total or superficial bed cross section normal to the direction of mean flow, g/(sec)(cm^2)

G_m = molal superficial mass velocity, mole/(sec)(cm^2)

P_f = pressure film factor, atm (

μ = viscosity of the bulk gas, g/(sec)(cm)

$D_{i,m}$ = coefficient of molecular diffusion of species i in the multicomponent mixture m, cm^2/sec

$\left[\frac{\mu}{\rho D_{i,m}}\right]$ = N_{Sc} (Schmidt number)

d_p = equivalent diameter (diameter of a sphere having the same surface area as the particle), cm

$\left[\frac{d_p G}{\mu}\right]$ = N_{Re} (Reynolds number).

A great number of studies are available in the literature correlating the dimensionless groups $\left[\frac{k_g P_f}{G_m}\right] (N_{Sc})^{2/3}$ to j_D, to $(\varepsilon)(j_D)$, or to N_{Re}. Some of these correlations are reported in the form of graphs of j_D or $(\varepsilon)(j_D)$ versus N_{Re}, where ε represents the void fraction of the catalyst bed (44, 153), and others are given in analytical form (141,182, 184):

$$\varepsilon j_D = (0.357) (N_{Re})^{-0.359} \qquad (7.3)$$

Equation 7.3 is claimed to allow for axial mixing effects which become increasingly significant at relatively low Reynolds numbers ($3 < N_{Re} < 2000$). The equations given by Yoshida and co-workers (184) are:

$$\text{for } 0.01 < N_{Re} < 50 \qquad j_D = (0.84) (N_{Re})^{-0.51} \qquad (7.4)$$

$$\text{for } 50 < N_{Re} < 1000 \qquad j_D = (0.57) (N_{Re})^{-0.41} \qquad (7.5)$$

Provided that the chemical reaction is restricted entirely to the surface of catalyst, i.e. there exists a strict series-relationship between bulk phase mass transport and chemical reaction, that no free-radical chain reactions take place homogeneously, and that the reaction is limited to the external surface of the catalyst particles, a quantitative evaluation of the effects of mass transfer resistances can be performed by calculating the concentration of reaction components at the gas-solid interface, and comparing them with the measured bulk concentrations. Since the mass transport is a first order process:

$$r_{obs,m} = k_c S_x (c_{i,b} - c_{i,s}) \qquad (7.6)$$

where:

$r_{obs,m}$ = observed rate of the reaction, moles/(sec) (g of catalyst)

k_c = mass transfer coefficient, based on concentration, cm/sec

S_x = external area per unit mass of the catalyst, cm^2/g

$c_{i,b}$ = bulk phase concentration of the component i, $moles/cm^3$

$c_{i,s}$ = surface concentration of the component i, $moles/cm^3$

The rate of mass transfer is equal to the observed rate of reaction under steady-state conditions. Replacing k_c in Equation (7.6) by $j_D \left(\frac{G}{\rho}\right) (N_{Sc})^{-2/3}$ and solving the resulting equation for $c_{i,s}$ will give the value of surface concentration of the i th component. Although this procedure gives quantitative indication of the extent of mass transfer resistances in terms of differences between bulk and surface concentrations at various levels of feedrates and conversions, the method applies only to non-porous catalysts, and suffers from the accuracy of correlations for mass transfer coefficient.

However, by systematic experimentation it is possible to obtain qualitative results. The interpretation of the results obtained is based on the fact that the film thickness representing the magnitude of the external diffusional resistances is a strong function of the velocity of the bulk gas. Although these systematic procedures do not lead to quantitative conclusions concerning the surface concentrations, they do establish the operational limits beyond which the film diffusion starts to become a rate controlling factor.

One method is to perform a series of runs at different gas velocities (total feedrates) but at identical feed composition with the amount of catalyst adjusted to maintain a constant value of W/F_T. The conversions obtained are then plotted versus gas velocity (122), or against feedrates (99). The range of gas velocities (feedrates) for which the conversion level remains constant will indicate the region where film diffusion resistance does not influence the rate of reaction. The limit of feedrate below which the gas film resistance starts to affect the overall rate is then the point where the conversion begins to drop.

A second procedure consists of a series of runs at varying values of W/F_T and with changing weights of catalyst charges in each series. The values of conversion are then plotted versus W/F_T. If the curves thus obtained, or portions of them, coincide for a given range of W/F_T, then it can be concluded that the film diffusion resistance within this region of W/F_T is eliminated, whilst differences in conversion levels for a W/F_T value is evidence for gas phase resistance, causing a reduction in reaction rates (99, 122, 162).

In both of these procedures it should be remembered that plug flow conditions must prevail throughout, and any effect of back-mixing or axial dispersion should be negligible.

Finally, the change of the apparent activation energy of the overall reaction with respect to temperature may also be used as a diagnostic test for the presence or absence of external mass transfer resistance. (Section 7.2). In view of the restricting assumptions discussed earlier, this method is not considered dependable.

The procedure applied in the present work to establish the operational limits for a minimized film diffusion resistance, and

the analytical evaluation of the results obtained are discussed in the next chapter. However, it is worth noting here that for qualitative testing of gas film resistance, the first and the second procedures are devised for use in differential or integral reactors with catalyst charges of small particle size. The plots of conversion versus gas velocity (or total feedrate) or conversion versus W/F_T gave inconsistent results with a single-pellet integral reactor used in this work. The procedure for evaluation of the results was, therefore, modified and the reasons for and the details of this modification are given in Section 8.3.

7.3.2. External Heat Transfer.

The above considerations with respect to the effects of external mass transfer resistances are based on isothermal conditions within the reactor. Although not directly interconnected, appreciable temperature differences may be produced because of heat transfer resistances between the catalyst surface and the gas phase.

In general, thermal resistances, in combination with mass transfer effects, may cause marked differences between the intrinsic and observed reaction rates. For exothermic reactions, diffusive and thermal resistances have opposite effects such that the rate of reaction, as interpreted, corresponding to the conditions prevailing in the bulk gas phase may be higher or lower than the rate on the catalytic surface according to the impedances in heat and mass transport processes and exothermicity of the reaction. The rate of the reaction at the surface will be increased because of temperature rise, but decreased due to the reduction in concentration of reactants. For endothermic reactions both resistances supplement each other so that the rate at the catalyst surface will be progressively less than the rate evaluated on the basis of the bulk gas temperatures and concentrations. Frequently thermal resistances are much more severe than the effects of diffusive impedances.

Since heat and mass transport between bulk gas and solid take place by similar mechanisms, data on heat transfer in fixed beds are correlated in the same manner as data on mass transfer. Thus :

$$j_H = \left[\frac{h}{c_p G}\right]\left[\frac{c_p \mu}{\lambda}\right]^{2/3} = f\left[\frac{d_p G}{\mu}\right] \qquad (7.7)$$

where:

j_H = heat transfer factor, dimensionless

h = heat transfer coefficient, cal/(cm^2) (sec) (^oC)

c_p = heat capacity of the reacting mixture, cal/(g) (^oC)

G = superficial mass velocity of the bulk gas phase, g/(sec)(cm^2)

μ = viscosity of the reacting mixture, g/(cm)(sec)

λ = thermal conductivity of the reacting mixture, cal/(sec)(cm)(^oC)

$\left[\frac{c_p \mu}{\lambda}\right] = N_{Pr}$, Prandtl Number

$\left[\frac{d_p G}{\mu}\right] = N_{Re}$, Reynolds Number.

The heat transferred between solid and gaseous media is given by equation

$$Q_t = h\, S_x (T_b - T_s) \qquad (7.8)$$

where:

Q_t = rate of heat transfer (the heat flux), cal/(sec)(g of catalyst)

S_x = external area of the catalyst, cm^2/g of catalyst

T_s = surface temperature of the catalyst, ^oK

T_b = bulk gas phase temperature, ^oK.

It has to be noted here that this correlation does not include any heat flux by radiation which cannot be neglected in high temperature reactions.

The functional relationships between j_H and N_{Re}, or the numerical value of the ration j_H/j_D are reported extensively in the literature (44, 141, 148, 153, 182,184). On the basis of these relationships it is possible to estimate at steady-state conditions the temperature difference between bulk phase and catalyst surface,

and also the extent of mass and heat transfer interaction during the course of the reaction. For a first-order or film-diffusion controlled reaction the energy balance on the gas-solid interface will give the correlation between temperature and concentration differences in quantitative terms:

$$k_c S_x (c_b - c_s) (-\Delta H) = h S_x (T_s - T_b) \qquad (7.9)$$

where ΔH is the heat of reaction per mole. Substituting the expressions for k_c and h from Equations 7.1 and 7.7, respectively, will yield :

$$T_s - T_b = (-\Delta H) \frac{1}{c_p} \left(\frac{N_{Pr}}{N_{Sc}}\right)^{2/3} \left[\frac{j_D}{j_H}\right] (c_b - c_s) \qquad (7.10)$$

This equation indicates the fact that in spite of possibly unimportant mass transfer limitations, if the heat effects of reactions are considerable, substantial temperature differences between the catalytic surface and gas phase may be generated which can cause a transition from one reaction regime to another or some instability effects (60, 123, 153).

Bulk gas phase temperatures were not measured in the present work. The temperature differences obtained from the thermowells situated on the reactor outside wall and in the catalyst pellet varied within the range 5 - 8° C. (Section 4.5.3). In addition, as a result of operating temperatures (540 - 700° C), substantial amounts of heat transfer occurred by radiation. Consequently it was concluded that, although the catalyst charge used in each series of experimental runs was new and very active, radial temperature gradients within the bulk gas-catalyst interface were unlikely to be present to affect the kinetic regime within the catalyst bed.

7.4 INTERNAL MASS AND HEAT TRANSFER.

7.4.1 Internal Mass Transfer.

Since the predominant portion of the catalytic surface is in the interior of the catalyst, the resistances to mass and heat transport within the pores have substantial effects on the rate of the reaction and may cause erroneous conclusions to be reached concerning the intrinsic mechanism. As the surface reactions in the porous structure proceed simultaneously with the transfer of reactants into the pores, concentration gradients will be established along the length of each pore so that the chemical potential decreases in the direction of diffusion, and under isothermal conditions, the average reaction rate throughout the interior of the catalyst particle will always be less than it would be if there were no internal diffusion limitations. The magnitude of these gradients depends on the dimensions and geometry of each pore as well as on the position of the catalyst particle within the bed, and on the transport properties of the species in the reaction mixture. If the rate of surface reactions (i.e. activated chemisorption, chemical reaction, and activated desorption) is fast compared with the diffusional processes in the pores (high temperature, very active catalyst), the reaction will occur on the outer periphery of the pellet, and part of the interior surface will not be utilized.

The extent of the pore diffusion limitation is characterised by the 'effectiveness factor', η , defined as the ratio of the observed rate of reaction to that which would occur if all of the surface throughout the interior of the catalyst particle were exposed to the reacting mixture of the same concentration and temperature as that prevailing at the external surface of the pellet. The reaction rate for isothermal conditions may then be given as:

$$r_{obs} = \eta\, k_s\, S_v\, f\,(c_A \ldots\ldots)_s \qquad (7.11)$$

where:

where:

r_{obs} = observed reaction rate per unit volume of the pellet

η = effectiveness factor, dimensionless

k_s = intrinsic reaction rate constant based on total surface of catalyst

S_v = $\rho_p S_g$, total surface area of the catalyst per unit volume of the pellet, cm^2/cm^3

ρ_p = apparent density of the catalyst pellet, g/cm^3

S_g = total surface of the catalyst as measured by the B.E.T. method, cm^2/g

$f(c_A...)_s$ = the concentration dependent term to be evaluated at the concentrations prevailing on the external surface.

A given catalyst pellet is relatively less effective for gaseous reactions which proceed at high rate with an increase in volume, creating at steady-state conditions an intrapellet total pressure gradient and thereby retarding the diffusion of reactants towards the catalytic sites in the pores. Unlike film diffusion the rate of internal mass transfer is not affected by changes in the bulk mass flow. Therefore, even with sufficiently high bulk mass velocities to keep the film diffusion resistances at a minimum, it is still unlikely that the catalyst can be used to its fullest potential.

Analogous to the interaction of external mass and heat transport resistances, the effect of the temperature gradients within the pores is to increase the rate for an exothermic reaction whereas for endothermic reactions, concentration and temperature gradients both reduce the rate and consequently the effectiveness factor,

The analytical treatment of mass and heat transport phenomena combined with chemical reaction within the porous structure, and the prediction of the effectiveness factor of a catalyst have to

be based on certain fundamental assumptions which may be summarised as follows:

(i) Pore model:

The pores are irregularly shaped, vary in cross-section along their lengths with probable interconnections between each other, and may be open at both ends or sealed at one end. Thus it is not possible to define the direction and the effective length of the diffusion path for the actual porous structure. The random and irregular arrangement of the pores has to be converted therefore, into an explicit model of well defined geometry.

The parallel-path pore model, first proposed by Wheeler (175), and the random-pore model suggested by Wakao and Smith (166) are being applied extensively for this purpose. According to the former, the pore structure is visualized as an array of parallel cylindrical tubes having an experimentally found pore-radii distribution. An adjustable parameter, "tortuosity factor, τ ", is introduced to account for the increased length of the tortuous diffusion path in real pores, for the skin effects and for the constrictions and enlargements along the channels of irregular shapes through which diffusion occurs. This factor is specific for every porous solid and may normally change within the limits 0.6 - 8.0. It is reported that an average value of 4 is representative for most commercial catalysts and does not induce significant error (141). However, when the size of diffusing molecules begins to approach the mean diameter of the pores, the collisions with the pore walls would have a retarding effect on the flux. Consequently, the tortuosity factor of a given catalyst established experimentally using one type of gas cannot be applied to any gas if there is a substantial difference in molecule diameters.

In view of the geometric configuration, the ratio of the total cross sectional area of the pores at any plane to the total area of the porous mass in this plane would be identical to the void fraction (i.e. porosity of the catalyst). Thus the effective transport property of a diffusing component in a given porous solid can be written as:

$$D_{eff} = D \frac{\theta}{\tau} \qquad (7.12)$$

where:

D_{eff} = effective diffusion coefficient of a gas diffusing in a porous solid, based on total cross-section of the mass normal to the direction of diffusion, cm^2/sec

D = diffusion coefficient of the gas (for molecular mode or Knudsen flow mode diffusion), cm^2/sec

θ = porosity of the catalyst, cm^3/cm^3

τ = tortuosity factor, dimensionless.

This geometric model is claimed to give satisfactory agreement with experimental data if the distribution of the pore radii is limited to a relatively narrow range (141).

The random-pore model is more appropriate for catalyst structures having a bimodal pore size distribution (bidisperse structure). The pellet is considered as an assembly of small particles surrounded by short and irregular void regions (macro-pores). The pores within the particles are supposed to have relatively small radii (micro-pores). Like in the parallel-path pore model, both macro and micro-pores are visualized as having straight cylindrical geometry with average pore radii $\bar{r}_{macro}$ and $\bar{r}_{micro}$, respectively. The mass transport within the pellet structure is assumed to be the sum of the diffusion through the macro-pore region, micro-pore region and a series contribution involving both regions. The effective diffusion coefficient

for this model is given by

$$D_{eff} = D_M \varepsilon_M^2 + \frac{\varepsilon_m^2 (1 + 3\varepsilon_M)}{1 - \varepsilon_M} D_M \quad . \tag{7.13}$$

where

D_M = diffusion coefficient for molecular or Knudsen diffusion in macro-pore region, cm^2/sec

D_m = diffusion coefficient for molecular or Knudsen diffusion in micro-pore region, cm^2/sec

ε_M = void fraction of macro-pore region, cm^3/cm^3

ε_m = void fraction of micro-pore region, cm^3/cm^3.

It is worth noting that the developed expression does not involve an adjustable parameter like tortuosity factor; however, the distinction between macro-and micro-pores to evaluate the respective diffusion coefficients and porosities introduces some uncertainties.

(ii) Surface diffusion:

There is sufficient experimental evidence to confirm that molecules adsorbed on solid surfaces possess some mobility which under certain conditions may make a significant contribution to the diffusive flux. The surface migration at relatively high temperature levels is considered to occur if the diffusing species are held on the solid surface by an activated process forming a monolayer. Thus it depends on surface characteristics of the solid as well as on physico-chemical properties of the adsorbed species. The suggested correlations involve, therefore, the adsorption equilibrium constant and are analogous to Fick's first law, but cover only a limited range of application, in which the adsorption process is assumed to be at equilibrium, and the concentration of the adsorbate in the monolayer is low corresponding to low surface coverage (linear portion of the Langmuir isotherm) (141,153). The usefulness of such a relationship is to establish the temperature dependency of the surface diffusity which has to be determined separately for each specific

gas-catalyst system. As a result, the effective diffusivity which reflects the combined molecular, Knudsen and surface diffusion properties of the system, cannot be predicted accurately. However, if adsorbed molecules are held so strongly as to be essentially immobile, surface diffusion is considered to be insignificant (141). Although the relative contribution of surface diffusion would increase with the increase of surface or decrease of mean pore radius (137,153), available data indicates that the contribution of the surface diffusion is not significant in the overall mass transfer at elevated temperature (141,142).

(iii) The variation of the effective diffusion coefficient:

The analytical treatment of simultaneous mass transport and surface reaction at steady state conditions is based on the assumption that the mass flux is represented by Fick's first law with a constant effective diffusion coefficient. The assumed pore model, if it is sufficiently appropriate and valid, accounts for the changes of direction of diffusion as well as for the variation of the pore area through which mass transport takes place. But the validity of the model may become dubious if the catalyst structure and pore radii distribution alter during the course of the reaction which would cause, even at isothermal conditions, a shift between the modes of the diffusion processess (molecular diffusion - Knudsen flow). If the contribution of surface diffusion in the overall mass flow is small and neglected, then the effective diffusion coefficient of component A diffusing in a "binary gas mixture (AB) - catalyst" system with constant molar density (no volume change on reaction) is given by:

$$\frac{1}{D_{eff}} = \frac{1 - \alpha y_A}{(D_{AB})_{eff}} + \frac{1}{(D_{A,K})_{eff}} \qquad (7.14)$$

where:

D_{eff} = effective diffusion coefficient of component A, cm^2/sec

$(D_{AB})_{eff}$ = effective diffusion coefficient of component A for molecular mode diffusion, cm^2/sec

$(D_{A,K})_{eff}$ = effective diffusion coefficient of component A for Knudsen flow type diffusion, cm^2/sec

y_A = mole fraction of component A in the binary mixture, mole/mole

α = $1 + \frac{N_B}{N_A}$, N_B and N_A are the molal fluxes of B and A, respectively. In case of non-equimolal counter-diffusion, the ratio N_B/N_A is related to the respective molecular weights by $N_B/N_A = -(M_A/M_B)^{\frac{1}{2}}$ (153)

According to Equation (7.14), the effective diffusion coefficient is subject to change not only with respect to the mode of diffusion, but also to the mole fraction of diffusing species, and is dependent on the nature of the reaction(change in volume)and position on the external surface of the pellet. It is suggested,however, that because of other uncertainties,the error introduced by such a change in the effective diffusion coefficient is negligible (153). If the range of the pore radii distribution of the catalyst pellet remains such that the mass flow proceeds solely by Knudsen flow throughout the course of the reaction, then the effective diffusion coefficient, D_{eff} in Equation (7.14), will be equal to $(D_{A,K})_{eff}$ and thus affected only by the change of mean pore radius. The effect of such a variation on D_{eff} is usually neglected, unless the mean pore diameter is not decreased to an extent that it approaches the diameter of diffusing molecules; this would cause an increase of the tortuosity factor.

(iv) Isotropic catalyst structure and constant intrinsic activity:

Further important assumptions made in the quantitative treatment to predict the effectiveness factor of a catalyst for given operating conditions are the isotropy of the catalyst structure and the invariancy of intrinsic activity. It is reported in the literature that the values of local effective diffusion coefficients

of a given gas in a given catalyst may change appreciably with the longitudinal distance along the pellet (30), or with the parallel or perpendicular direction to the extrusion axis of the pellet (171). These variations are explained by an unusual scattered macro-pore size distribution with position in the pellet, and by the presence of fine fissures with different permeability (skin effects), caused primarily by uneven inter-particle frictions and stresses during the manufacture of the catalyst (141). Therefore, the effective diffusion coefficient may change even for the same pellet according to its location in the bed. The presence of such anisotropies in the catalyst structure may also lead to physical instabilities during the course of the reaction, and can result in a radical change of the pore structure and hence in the mode of diffusion. Another important aspect of structural anisotropy is the non-uniform distribution of the catalytic sites on the pore surfaces, or a change in the intrinsic activity during the course of reaction, in spite of a uniform distribution of the catalytic centres (poisoning effects, even or uneven carbon lay-down in pores). Some quantitative treatment of this effect is given by Wheeler (175) for isothermal first-order reaction in a cylindrical pore (38).

(v) Forced flow:

The contribution of the forced flow to the overall mass transport in the pores is usually neglected. The diffusion coefficient for forced flow is related to the pore radius r_p, total pressure difference Δp and viscosity μ of the diffusing gas by (38):

$$D_{poi} = \frac{r_p^2 \Delta p}{8\mu}$$

which gives an approximate value of 0.1 $cm^2/sec.$ for D_{poi} at 1 atm pressure, and pore radius of 10^{-4} cm. Noting that the molecular diffusion coefficients are of similar magnitude, this type of mass transfer can compete with molecular type diffusion, if the catalyst

structure has very large pores (10,000Å), and the operating pressure is relatively high (>150 atm). Since the combination of these conditions is rather exceptional, intraparticle mass transport due to large total-pressure gradients is not expected to occur.

7.4.2 INTERNAL HEAT TRANSFER.

Significant temperature gradients may occur in the structure of the catalyst pellet depending primarily on the magnitude of the enthalpy change of the reaction and on the thermal conductivity of the gas-catalyst system. The effect of temperature gradients on the overall rate of reaction may be more severe than those of the concentration gradients for highly exothermic reactions in low thermal conductivity gas-catalyst systems, resulting in sintering. Simultaneous mass and heat balance equations around the boundary surface of the catalyst particle provide the necessary relationship between temperature and concentration at steady-state conditions. The mass flux of the reactants across this boundary surface equals the total rate of reaction within and beyond this surface; the corresponding heat of reaction must then be transferred across the same boundary.

For a single reactant, mth order irreversible reaction and spherical catalyst pellet of radius R, and neglecting the effects of temperature and concentration changes on the effective diffusion coefficient and effective thermal conductivity, these equations can be written as:

$$(D_{eff}) \left[\frac{d^2c}{dr^2} + \frac{2}{r} \frac{dc}{dr} \right] - k_v c^m = 0 \qquad (7.15)$$

and

$$(\lambda_{eff}) \left[\frac{d^2T}{dr^2} + \frac{2}{r} \frac{dT}{dr} \right] - k_v c^m (-\Delta H) = 0 \qquad (7.16)$$

with boundary conditions:

$\frac{dc}{dr} = 0$ at $r = 0$, $c = c_s$ at $r = R$ and

$\frac{dT}{dr} = 0$ at $r = 0$, $T = T_s$ at $r = R$

where:

k_v = intrinsic reaction rate constant based on volume of the catalyst particle, (cm^3 of reacting mixture)^m/(cm^3 of catalyst volume) (mole)$^{m-1}$(sec)

c = concentration of the reactant in the boundary, mole/cm^3

D_{eff} = effective diffusion coefficient, based on total cross section normal to the direction of diffusion, cm^2/sec

T = temperature of the gas and catalyst structure in the boundary, ^oK

λ_{eff} = effective thermal conductivity of the combined gas-catalyst system considered as a continuous medium, cal/(sec)(cm)(^oK)

$-\Delta H$ = enthalpy change of the reaction (assumed to be independent of temperature changes), cal/mole

c_s = concentration at the external surface of the spherical catalyst pellet, mole/cm^3

T_s = temperature of the gas and catalyst at the external surface, ^oK.

Eliminating the rate term between equations (7.15) and (7.16) yields:

$$D_{eff}\left[\frac{d^2c}{dr^2} + \frac{2}{r}\frac{dc}{dr}\right] = \frac{1}{(-\Delta H)}\lambda_{eff}\left[\frac{d^2T}{dr^2} + \frac{2}{r}\frac{dT}{dr}\right] \qquad (7.17)$$

$$D_{eff}\frac{d}{dr}\left(r^2\frac{dc}{dr}\right) = \frac{1}{(-\Delta H)}\lambda_{eff}\frac{d}{dr}\left(r^2\frac{dT}{dr}\right) \qquad (7.18)$$

Integration of Equation (7.18) for the limits

$\frac{dc}{dr} = 0$ and $\frac{dT}{dr} = 0$ at $r = 0$, and $\frac{dc}{dr}$ and $\frac{dT}{dr}$, respectively, will give:

$$(D_{eff})\frac{dc}{dr} = \frac{1}{(-\Delta H)}\lambda_{eff}\frac{dT}{dr} \qquad (7.19)$$

Thus the magnitude of the temperature gradient

$$\frac{dT}{dr} = (-\Delta H)\frac{D_{eff}}{\lambda_{eff}}\frac{dc}{dr} \qquad (7.20)$$

is a function of the heat effect of the reaction, of the prevailing

concentration gradient and of the transport properties of the system. Integrating Equation (7.20) for the boundary conditions $c = c_s$ and $T = T_s$ at $r = R$ yields:

$$T - T_s = (-\Delta H) \frac{D_{eff}}{\lambda_{eff}} (c_s - c) \qquad (7.21)$$

This relation, first derived by Damköhler, is valid for all kinetics and particle geometry (141,153). Hence, temperature and concentration profiles in the catalyst pellet for non-isothermal conditions at steady-state can only be established if the temperature term of the reaction rate constant, $k = A.e^{-\frac{E}{R_g T}}$, and the differential equations for simultaneous mass and heat transfer, Equations (7.15) and (7.16), are solved. Equation (7.21) serves also to calculate the maximum temperature difference between the exterior surface and the interior of the catalyst pellet, and will occur if the concentration of the reactant decreases to zero within the pellet at some distance from the surface. Thus it is an indication of the possible magnitude of the temperature gradients which may develop in the particle. In fact, Weisz and Hicks (172) introduced in their method of graphical evaluation of non-isothermal effectiveness factor, for a given catalyst geometry and reaction type, the two independent parameters:

Heat generation function parameter:

$$\beta = (-\Delta H) \left(\frac{D_{eff}}{\lambda_{eff}}\right) \left(\frac{1}{T_s}\right) c_s \qquad (7.22)$$

and Arrhenuis parameter:

$$\gamma = \frac{E}{R_g T_s} \qquad (7.23)$$

The parameter β represents the ratio of the maximum temperature difference which can occur between the interior of the catalyst pellet to the temperature at the particle surface. Its value is positive for exothermic, and negative for endothermic reactions; $\beta = 0$ represents the isothermal case where η becomes independent of the Arrhenius parameter. The parameter γ is a criterion for

the effect of temperature on the exponential term of the Arrhenius-type expression.

7.4.3 QUANTITATIVE TREATMENT.

The mathematical treatment of simultaneous mass and heat transfer with chemical reaction in the porous structure of the catalyst pellet and the quantitative description of the factors which determine the effectiveness of the catalyst have been the subject of innumerable studies following the classical papers of Damköhler (42), Zel'dovich (185), and Thiele (161). The equations derived describe the concentration profile within the catalyst structure and correlate the effectiveness factor η to a dimensionless quantity (Thiele modulus, $\emptyset$) which includes, even for reactions of a simple kinetic nature, important parameters of the system such as the intrinsic reation rate constant, the effective diffusion coefficient, the reactant concentration of the external surface of the pellet, and a characteristic length parameter at the pellet. The exact functional relationship between the effectiveness factor and Thiele modulus depends on the following factors:

(i) isothermal or non-isothermal conditions

(ii) particle model geometry

  (a) single pore visualized as a straight cylindrical capillary

  (b) spherical shape

  (c) semi-infinite slab

  (d) cylindrical (solid or hollow) shape

(iii) kinetic nature of the reaction

  (a) irreversible or reversible

  (b) single-reactant or multi-reactants

  (c) integer power order kinetics.

  (d) no volume change or volume change

  (e) Langmuir-Hinshelwood type expressions

  (f) consecutive reactions

(iv) absence or presence of radial dispersions in the pores affecting the mass and heat flux for pores with extremely large diameters.

For the simple case of single reactant-irreversible reaction with integer power kinetics and spherical catalyst geometry, the Thiele modulus is given by:

$$\phi_s = R\sqrt{\frac{k_v \cdot c_s^{m-1}}{D_{eff}}} \qquad (7.24)$$

where:

ϕ_s = Thiele modulus for spherical geometry, dimensionless

R = radius of the spherical pellet, cm

k_v = intrinsic rate constant, based on volume of the catalyst

c_s = concentration of the reactant of the external surface of the pellet, mol/cm^3

m = order of the reaction.

If the reaction is first-order, then for isothermal conditions and no volume change on reaction, without radial dispersion effects in the pores, the effectiveness factor is related to the modulus by:

$$\eta_s = \frac{3}{\phi_s}\left[\frac{1}{\tanh \phi_s} - \frac{1}{\phi_s}\right] \qquad (7.25)$$

For the single pore model or semi-infinite flat plate geometry, however, the relationship as given by Equation 7.25 takes the forms:

$$\eta_{sp} = \frac{\tanh \phi_{sp}}{\phi_{sp}} \quad \text{(single pore model)} \qquad (7.26)$$

$$\eta_L = \frac{\tanh \phi_L}{\phi_L} \quad \text{(flat plate)} \qquad (7.27)$$

respectively, where:

$\phi_{sp} = \bar{L}\sqrt{\frac{2\,k_s}{\bar{r}_p\, D_{eff}}}$, modulus for single pore model

$\bar{L}$ = mean length of the pore, cm

k_s = intrinsic rate constant for first-order reaction, based on surface of the pore

$\bar{r}_p$ = mean pore radius, cm

$\phi_L = L\sqrt{\frac{k_v}{D_{eff}}}$, modulus for flat plate geometry

L = thickness of the plate, cm

k_v = intrinsic rate constant for first-order reaction, based on volume of the plate.

Aris (10) has shown that if a unifying parameter may be specified in the modulus as the ratio of pellet volume V_c to pellet external surface area S_c, it is possible to render the functional relationship $\eta = f(\phi)$ virtually independent of particle geometry, and the function $\eta = f(\phi)$ as derived for one pellet geometry can be used for any other pellet shape with little error. Thus, the Thiele modulus as given by Equation (7.24) has the generalized form

$$\phi = L\sqrt{\frac{k_v . c_s^{m-1}}{D_{eff}}} \qquad (7.28)$$

where L is the length parameter $\frac{V_c}{S_c}$ and equals $\frac{R}{3}$ for spherical geometry.

The dependence of effectiveness factor on the Thiele modulus is represented in the literature in the form of graphs obtained by elaborate numerical techniques, since analytical solution of the differential equations describing the simultaneous mass flow and reaction is frequently not possible. Methods for asymptotic solution have been presented by Petersen (123). The possible effects of non-isothermal conditions, or the complexities caused by the kinetic nature of the reaction (Langmuir-Hinshelwood kinetics) are incorporated in the plots as additional parameters (Arrhenius and heat generation function parameter in the case of the non-isothermal conditions mentioned in Section 7.4). The major advantage of these generalized graphs is their use for a quantitative prediction of the effectiveness factor of the catalyst, if the intrinsic kinetics of the reaction in question are identical to those as represented by the graphs, and if the intrinsic rate constant, the effective diffusion coefficient and the surface concentrations are known so that the modulus can be

evaluated. The difficulty of knowing a priori an accurate value of the intrinsic constant rate for use in the calculation of the modulus is circumvented by Wheeler (175) and Weisz and co-workers (171,172, 173) by modifying the Thiele modulus to give another dimensionless quantity:

$$\Phi = \frac{L^2}{D_{eff}} \quad \frac{1}{c_s} \quad (r_{obs}) \tag{7.29}$$

where:

$L = \frac{V_c}{S_c}$, length parameter of the pellet, cm.

r_{obs} = observed reaction rate as determined from the experiments, based on pellet volume.

All the terms in Equation (7.29) may be either calculated or observed. For single reactant mth order irreversible reactions the relationship between the Thiele modulus and Φ can be derived, if the observed reaction rate is written as:

$$r_{obs} = \eta \, k_v \, c_s^{\,m} \tag{7.30}$$

and the term $k_v \, c_s^{\,m-1}$ in the Thiele modulus (Equation 7.28) is replaced by $\frac{1}{c_s} \left[\frac{r_{obs}}{\eta}\right]$ to give:

$$\phi^2 = \frac{L^2}{D_{eff}} \frac{1}{c_s} \left[\frac{r_{obs}}{\eta}\right] \tag{7.31}$$

which yields:

$$\phi^2 \eta = \frac{L^2}{D_{eff}} \frac{1}{c_s} \quad (r_{obs}) = \Phi \tag{7.32}$$

This relationship becomes more complex if the reaction involves Langmuir-Hinshelwood type kinetic expressions as developed by Hougen and Chou and Roberts and Satterfield (33, 138, 139).

In the case of volume change on reaction, Thiele (161), Weckmann and co-workers (169,170) modified the Thiele modulus for single reactant integer order reactions, by incorporating the stoichiometric coefficient ν of the reaction in terms of a volume change modulus

$\gamma' = y_A (\nu_A - 1)$, where y_A is the mole fraction of the reactant A. For first-order reactions Hawthorn (141) has developed the following correlation for the modified Thiele modulus:

$$\phi' = \phi \left[\frac{\gamma'}{\ln (1 + \gamma')} \right]^{0.7} \qquad (7.33)$$

On the basis of the plots $\eta = f (\Phi)$ attempts have also been made by Wèisz and co-workers (171,172, 173) to develop for practical applications a general criterion to characterize any conditions which may secure a catalyst performance without any diffusion resistance effects (i.e. $\eta > 0.95$). Their derivation was limited to zero, first, and second order, single reactant irreversible conditions. Bischoff (19), however, extended this criterion to include any type of kinetic expression for isothermal and non-isothermal conditions, but valid only for values of $\eta < 1$ in the case of exothermic reactions.

An excellent review of the studies in this field up to 1969 is given by Satterfield (141).

7.4.4 QUALITATIVE TREATMENT.

The functional relationship between the effectiveness factor and Thiele modulus for any particle geometry and intrinsic kinetics of the reaction and the plots $\eta = f (\phi)$ or $\eta = f (\Phi)$ imply that, for a given kinetic nature and under isothermal conditions, the extent to which concentration gradients that can develop within the pellet are significant, is governed predominantly by the magnitude of the modulus. For a single reactant, integral order, irreversible reaction with simple kinetics, the effectiveness factor approaches unity as an asymptote as the length parameter of the particle (radius of the sphere or cylinder, thickness of the slab), or the intrinsic rate constant (activity of the catalyst, operating temperature) are

made small, and the effective diffusion coefficient is made large. Noting that the observed rate of reaction per unit volume of the pellet is given by the expression

$$r_{obs} = \eta \; k_v \; f\,(c_A \ldots\ldots)_s \,, \qquad (7.34)$$

at sufficiently large values of the modulus ($\phi > 10$ for first-order reactions), the effectiveness factor becomes inversely proportional to ϕ, and the relationship between them takes the asymptotic form

$$\eta = \frac{1}{\phi} \quad \text{or} \quad \frac{1}{\Phi} \qquad (7.35)$$

Consequently r_{obs} will also become inversely proportional to the length parameter of the pellet. Since this quantity is defined by the ratio of volume of pellet to its external surface area, the observed rate per unit volume of catalyst will be directly proportional to the surface area of the pellet exposed to the reacting gas, if all other conditions remain the same. An equivalent statement is that an increase in observed reaction rate per unit volume with increase of the external surface is sufficient evidence for significant diffusional impedances in the porous structure, and indicates qualitatively a low value for η. This fact will be discussed in the next chapter.

The usual procedure to minimize the effect of intrapellet diffusional gradients in kinetic studies and to attain effectiveness factors approaching unity is to perform experimental runs under identical operating conditions (structure and activity of the catalyst, temperature, concentration and effective diffusion coefficient of reacting species), with progressively smaller particle sizes, and to compare the observed reaction rates. No increase in the values of observed reaction rates with decrease of particle size indicates that the catalyst performance has reached almost full effectiveness ($\eta \approx 1$). Since by definition, the observed reaction rate per unit volume is $r_{obs} = \eta \; k_v \; f\,(c_A)$, the ratio of the observed rate for the

larger size pellet to that for the finer at identical experimental conditions is equal to the ratio of effectiveness factors:

$$\frac{(r_{obs})_1}{(r_{obs})_2} = \frac{\eta_1}{\eta_2} \qquad (7.36)$$

If a value for η_2 is known, or if it is very close to unity for very small particle sizes, then η_1 can easily be calculated.

Although limited to simple specific cases, methods of experimental evaluation of effectiveness factor are given elsewhere (141, 153, 173).

CHAPTER 8

RESULTS AND DISCUSSION

8.1 INTRODUCTION.

The defining equation for the rate of reaction in a tubular flow system at steady-state conditions is based on the mass balance around an infinitesimal element dV_R of reactor volumeand is given by:

$$r = \frac{(F_T)\, dx}{dV_R} = \frac{dx}{d(V_R/F_T)} \qquad (8.1)$$

where x is the fractional conversion measured as mass of a particular reactant converted for total mass of feed F_T. For gas-solid catalytic reactions, assuming that the catalyst is fully effective ($\eta = 1.0$) and its activity remains constant throughout, the rate is referred to the mass of catalyst W by:

$$r_m = \frac{dx}{d(W/F_T)} \qquad (8.2)$$

It should be remembered, however, that these relationships are valid only, if the conditions in the dynamic system fully satisfy the plug flow assumption which represents an idealized state of flow such that :

(i) over any cross-section normal to the fluid motion, the mass flow rate and the properties (pressure, temperature, and composition) of the gas are uniform, and

(ii) there is no mass flux relative to the bulk flow due to diffusion in the direction of flow.

In the present work the analysis, evaluation and interpretation of the experimental results are based on the relationship given by Equation (8.2). It is,therefore, considered relevant to discuss briefly the conditions which may invalidate the plug flow assumption, and the precautions taken in the experiments to minimize the occurrence of these conditions.

8.2 DEVIATIONS FROM PLUG FLOW CONDITIONS.

The deviations from the uniformity of flow and fluid properties

over a cross-section of the catalyst bed normal to the direction of flow may occur for the following reasons:

(i) entry and exit effects

(ii) channelling and velocity gradients

(iii) radial temperature gradients

(iv) radial and axial concentration gradients.

The methods generally used in practice for determining the degree of deviation from plug flow involve the step input signal or delta function pulse injection of a tracer at the inlet followed by the measurement of tracer concentration with time at the outlet. For approaching plug flow the downstream signal of the tracer gives a steep increase (F - curve) or rises to a sharp peak (C - curve) on the concentration-time curve plotted in terms of dimensionless co-ordinates, i.e. reduced concentration and reduced time.

Theoretical treatment and quantitative consequences of non-ideal flow are given elsewhere (9, 46, 99).

8.2.1 Entry and Exit Effects.

Entry and exit effects occur as a result of contraction and expansion of the flow cross-section which cause a disturbance of the flow profile of the bulk gas and may give rise to the formation of some non-flow but eddying regions in the bed. To minimize the entry and exit effects the catalyst pellets to be tested were sandwiched in the reactor between stainless steel pellets of the same diameter as the catalyst. The heights of columns formed by the stainless steel pellets were each twice the height of the catalyst pellet. Moreover, a stainless steel cone located underneath the bottom pellet gave a gradual change of the flow cross-section.

In the case of the experiments with ground catalyst (250 - 300 μ particle diameter), the bed was sandwiched between two layers of pumice which is reported to be inactive towards the reforming

reaction (155). Since the particle sizes of pumice and catalyst were identical, the distribution of the free macro-volume was assumed to be the same in both beds. However, two successive experiments carried out with 250 - 300 μ particle diameter resulted in massive carbon deposition, and blocking of the catalyst bed. This behaviour was attributed firstly to the presence of pumice which could have catalyzed the pyrolysis of methane and inhibited the carbon-steam reaction. Therefore, other runs with ground catalyst were performed without pumice layers. The result, discussed in Section 8.7, showed that the carbon laydown was primarily a function of the particle size of the catalyst, and presence or absence of pumice layers had no influence on the extent of carbon formation.

8.2.2 Channelling and Velocity Gradients.

Channelling, frequently encountered in fluid-solid contacting, is the uneven distribution of the flowing bulk fluid along the cross-section and stems from a non-homogeneous voidage. The fluid stream takes the path of least resistance, resulting in some regions of the solid surface not coming into contact with the fluid. The non-uniform arrangement of the packing in the bed, which causes the variation of voidage, originates from:

(i) packing density

(ii) size distribution of the particles

(iii) ratio of particle diameter (d_p) to reactor tube diameter (D_R)

According to the catalyst configuration in Reactor No. 1 channelling as such could not occur in the experiments with cylindrical catalyst pellets. In the case of the runs with ground catalyst in Reactor No. 2, care was taken to obtain a catalyst charge with uniform bulk density and voidage in the reactor tube by continuously tapping the tube at the catalyst bed height during loading.

The variations of the void fraction in the bed with radial position have been discussed by Tierney and co-workers (163). They showed that an unevenly packed bed of particles with a wide size range results in zones of loosely agglomerated particles enclosing large void volumes. It is reported that even in fully developed turbulent flow of non-reacting systems, at one pellet diameter away from the wall, the void fraction is changed so that at high values of the ratio $d_p : D_R$, the linear velocity of the bulk can greatly exceed that prevailing at the centre. It is claimed, however, that when the ratio $d_p/D_R \leqslant \frac{1}{30}$, the divergence of the velocity profile from the assumption of uniform velocity is less than 10% (147,153).

In experiments with ground catalyst the value of the ratio d_p/D_R varied according to the particle diameter, the inside diameter of the reactor tube being constant at 5.6 ± 0.1 mm. Six sets of runs with four different ranges of particle size were carried out:

Sieve fraction B.S. Mesh No.	Particle Diameter corresponding to Nominal Aperture Size, d_p (μ)	$\frac{d_p}{D_R}$
100 - 85	150 - 180	1 : 34
60 - 52	250 - 300	1 : 20
44 - 36	355 - 425	1 : 15
30 - 25	500 - 600	1 : 10

It is interesting to note here that the blocking of the catalyst bed with deposited carbon and the rate of decrease of conversion at identical operating conditions (temperature, pressure, steam : methane ratio, flowrate) were increased with the decrease of catalyst particle size. The carbon build-up was extremely fast, when the catalyst bed was least susceptible to channelling, i.e $d_p/D_R = \frac{1}{34}$. Coarse particles gave higher conversion and blocking of the bed took relatively longer periods of time.

8.2.3 Radial Temperature Gradients.

Radial temperature gradients developed across the reactor

cross-section are by far the most important factor which gives rise to deviations from plug flow, whereas axial temperature gradients do not violate the conditions necessary for the plug flow assumption. Radial gradients occur primarily if the reaction has significant heat effects or if the reacting fluid-catalyst system, considered as a continuous medium, has a low thermal conductivity, or if the reactor tube has inadequate wall heat transfer properties. They become more pronounced if radial velocity gradients in the bulk gas phase prevail across the cross-section. The conditions effecting the qualitative character and magnitude of radial temperature gradients are described in length by Denbigh and Turner (46) and others (9, 99).

It should be remembered, however, that the absence of temperature gradients in the bulk gas phase does not imply that there will be no temperature differences between the gas and the catalyst surface. The effects of these differences which produce substantial disagreement between observed and intrinsic reaction rates are summarized in Section (7.3.2).

In the course of the research, temperatures measured by thermowells located on the reactor outside wall and inside the catalyst pellet along the catalyst bed were minimized to a range of 5 - 8 degrees C (Section 4.5.3). It was concluded, therefore, that radial temperature differences were most unlikely to cause a deviation from plug flow.

8.2.4 Radial and Axial Concentration Gradients.

These gradients are caused by the combined effect of ordinary (molecular) diffusion, eddy (turbulent) diffusion created by turbulent flow, convective movement due to radial and axial temperature inequalities, and of the influence of packing in causing a displacement of bulk gas (dispersion). In general, the effect of diffusion in the radial direction is to reduce the transverse concentration

gradients so that a closer approach to the idealized plug flow is achieved. Axial diffusion has its effects in the opposite sense. For flow through packed beds dispersion in the radial and axial directions is characterized by the Peclet number (N_{Pe}) defined as:

$$N_{Pe} = \frac{(u)(d_p)}{D_d} \tag{8.3}$$

where:

u = average velocity of the bulk gas, cm/sec

d_p = equivalent particle diameter, cm

D_d = radial ($D_{d,rad}$) or axial ($D_{d,ax}$) eddy diffusion (dispersion) coefficient, cm^2/sec.

Since the mechanism of dispersion is different in the axial and radial directions for Reynolds number above unity, the value of the dispersion coefficient, and consequently the Peclet number, will differ in the two directions. According to the correlations between axial and radial Peclet numbers and Reynolds number given by Wilhelm (177) and adapted by Aris (9), the value of N_{e} for radial dispersion changes within the limits 5 - 10 for $1 < N_{Re} < 10$ and reaches an asymptotic value of 12 at $N_{Re} > 100$. N_{Pe} for axial dispersion changes between 1 and 2 within the same range of N_{Re} and attains an asymptotic value of about 2 at $N_{Re} > 10$. It is reported that at axial $N_{Pe} = 2$, each fluid regionat any cross-section within the bed behaves like a well-mixed stage, and a packed bed whose depth exceeds 20 to 30 particle diameters will give in this flow region essentially a plug flow profile (46,141). In the present investigation the Reynolds number of the flow varied within the limits 2 - 20 for the runs made to determine the limits of the film- and pore-diffusion resistances. It is evident that the assumption of plug flow conditions within this low range of N_{Re} becomes doubtful, and that velocity gradients may exist over the cross-section normal to the flow. As a matter of fact, the hydrodynamics of flow takes

up a complex nature because of the non-uniform volume change on reaction during the passage of the reacting gas along the catalyst bed. It is not inconceivable that the velocity gradients along the flow profile may be compensated by this volume change. Since the temperature distribution along the catalyst bed varied only within a range of 2 - 4 degrees C (Section 4.5.3), velocity gradients caused by extreme temperature differences were unlikely to occur. Denbigh (46) considers the radial diffusion to be important if the radial temperature gradients are of considerable magnitude. The effects of axial diffusion is found to be usually less significant (46).

Hence, it has been assumed that a plug flow profile existed throughout the experiments in spite of low N_{Re}.

8.3 FILM-DIFFUSION LIMITATIONS.

The effects of diffusive resistances in the bulk gas phase on the apparent mechanism and on the rate expression of a reaction are discussed in Section (7.3.1). The experimental procedures and criteria generally applied for a qualitative estimation of bulk phase mass transfer limitations are outlined in the same section.

8.3.1 Experimental Procedure.

In the present investigation, the operational limits for a minimized film diffusion resistance were established by performing series of runs with varying weights of catalyst (W) at different total feedrates (F_T), and conversions were compared at given values of W/F_T on plots of x_{CH_4} versus W/F_T where x_{CH_4} is the moles of methane converted per mole of total feed. In analytical terms, the integration of Equation (8.1) yields

$$\frac{W}{F_T} = \int_0^{x_{CH_4}} \frac{dx_{CH_4}}{r_m}$$

where the integral, which is a function of x_{CH_4}, should remain constant for various values of F_T, provided that the ratio W/F_T remains constant. A decrease in conversion is evidence for an increased film resistance causing a change in the reaction rate (r_m).

The experiments were conducted at the following operating conditions:

Temperature, ^oC	: 539 ± 1
Pressure	: barometric
H_2O : CH_4 molar ratio	: 3.0 ± 0.1
Catalyst mass, g	: 5.3815
	: 5.1632
	: 3.8964
	: 5.2133
	: 3.4689
	: 0.7772
	: 2.7050

The results obtained are shown in the form of plots conversion x_{CH_4} versus W/F_T in Fig. 8.1.

8.3.2 Results and Discussion.

As will be seen from Fig. 8.1, the family of curves exhibits certain irregularities compared with those expected from the analytical approach. These deviations have been attributed to the fact that, because of the catalyst pellet geometry in Reactor No. 1, a change in mass of catalyst pellets was associated either :

(i) with a variation of the inner diameter, and hence cross-sectional area, of the annulus between the reactor inner wall and catalyst outer diameter, or

(ii) with a change of the external surface area of the catalyst exposed to the reacting gas.

The former gave a change in linear velocities of the gas for a

Fig. 8.1 The Conversion X_{CH_4} as a Function of the Ratio W/F_T

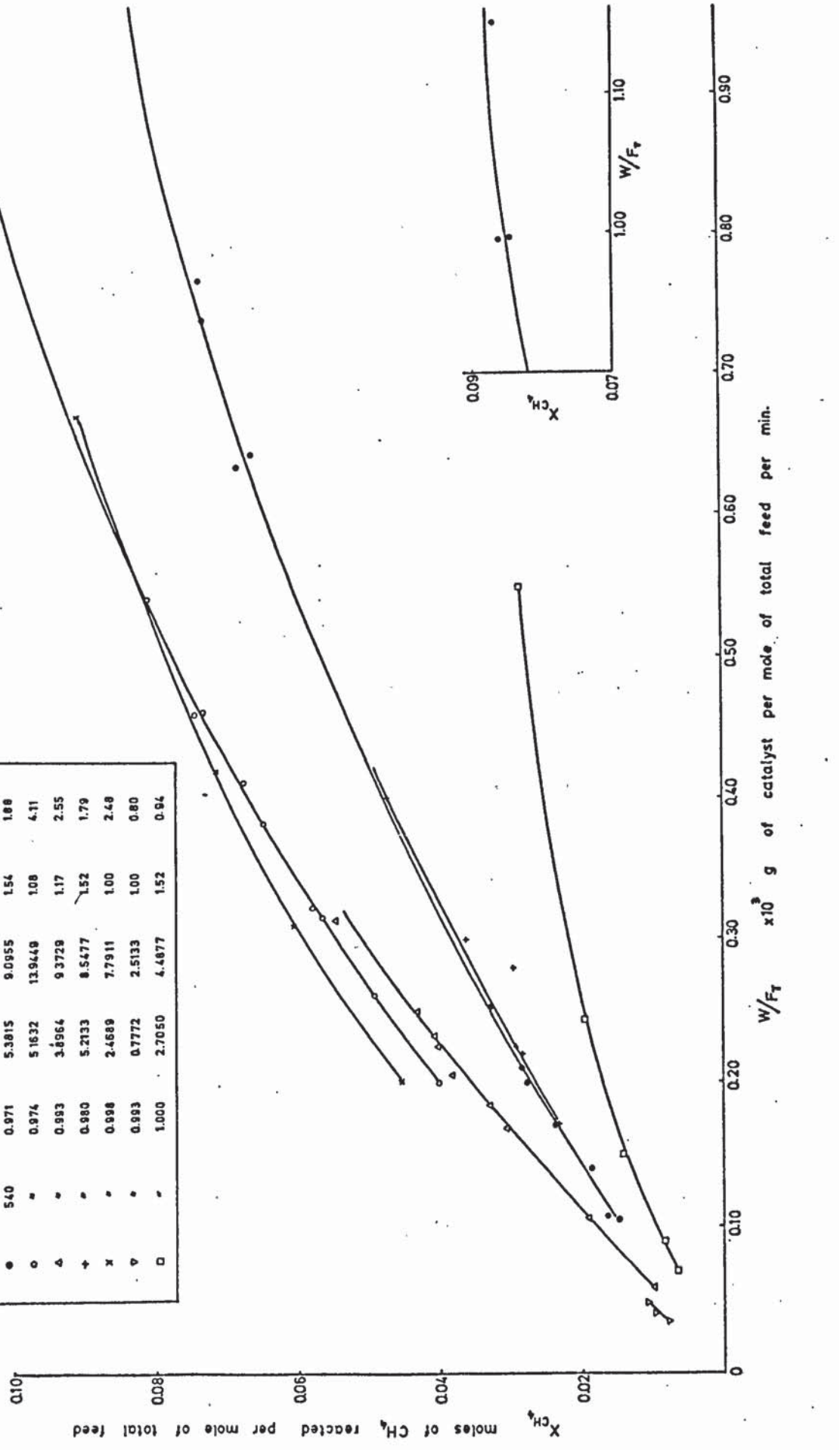

given feedrate whereas the latter resulted in a variation of gas-catalyst contact area. The extent of both effects resulting in deviations from that expected has been examined as follows:

(i) The linear velocities of reacting gas, calculated from arithmetic-mean-volumetric flow rates between the inlet and exit conditions of the catalyst bed, were plotted versus W/F_T for each set of runs (Fig. 8.2). The gas velocity for any given catalyst dimension could thus readily be obtained from this graph as a function of W/F_T.

(ii) A second graph has been prepared illustrating the variation of conversion x_{CH_4} as a function of the linear velocity for each series of runs (Fig. 8.3)

For any given value of W/F_T, the linear gas velocity v for every run was obtained as ordinates of Fig. 8.2. These values of v were then transferred to Fig. 8.3 and the corresponding values of conversion x_{CH_4} were marked on their respective curves. A horizontal path of conversion level within a range of gas velocities for given values of W/F_T as parameter would have indicated the limits of feedrates and catalyst weights below which the gas film resistance started to affect the observed reaction rate. This path is traced on Fig. 8.3 with dashed lines for various W/F_T values.

From the irregular shapes of these traces, it was evident that the variation of cross-sectional area of the annulus affecting the linear gas velocities was not the unique cause of the deviations. Since the Reynolds number is more appropriate to characterize the hydrodynamics of flow, it is normally used as the basic co-ordinate in correlating external mass and heat transfer resistances (Section 7.3), and hence Figures 8.2 and 8.3 were replotted with N_{Re} as abscissa. The Reynolds number adopted in the present study was defined as:

Fig. 8.2 The Linear Velocity V of the Reacting Gas Plotted as a Function of the Ratio $\frac{W}{F_T}$

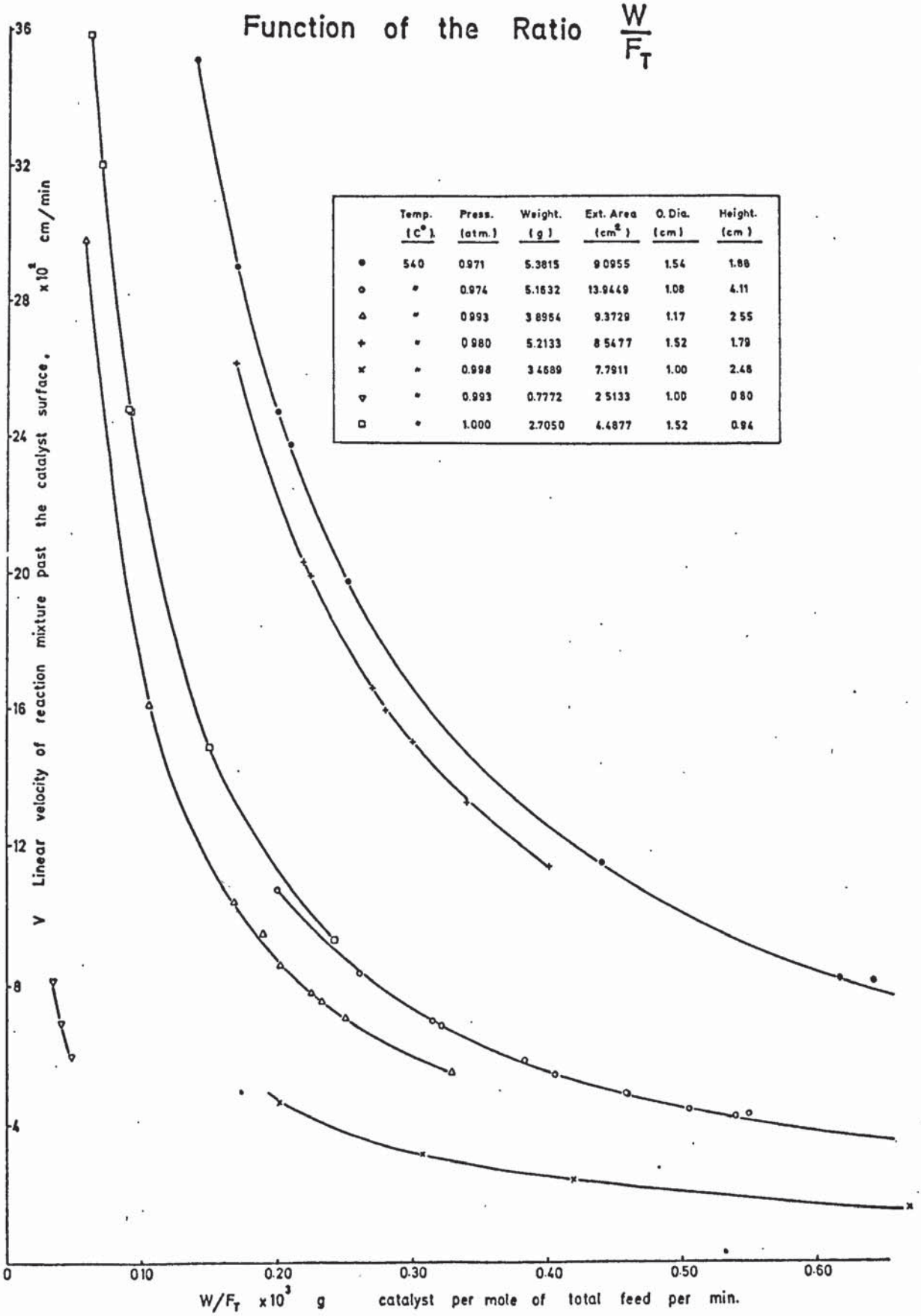

	Temp. (C°)	Press. (atm.)	Weight. (g)	Ext. Area (cm²)	O. Dia. (cm)	Height. (cm)
●	540	0.971	5.3815	9.0955	1.54	1.86
○	"	0.974	5.1632	13.9449	1.08	4.11
△	"	0.993	3.8954	9.3729	1.17	2.55
+	"	0.980	5.2133	8.5477	1.52	1.79
×	"	0.998	3.4589	7.7911	1.00	2.48
▽	"	0.993	0.7772	2.5133	1.00	0.80
□	"	1.000	2.7050	4.4877	1.52	0.94

Fig. 8.3 The Conversion X_{CH_4} Plotted as a Function of Linear Velocity

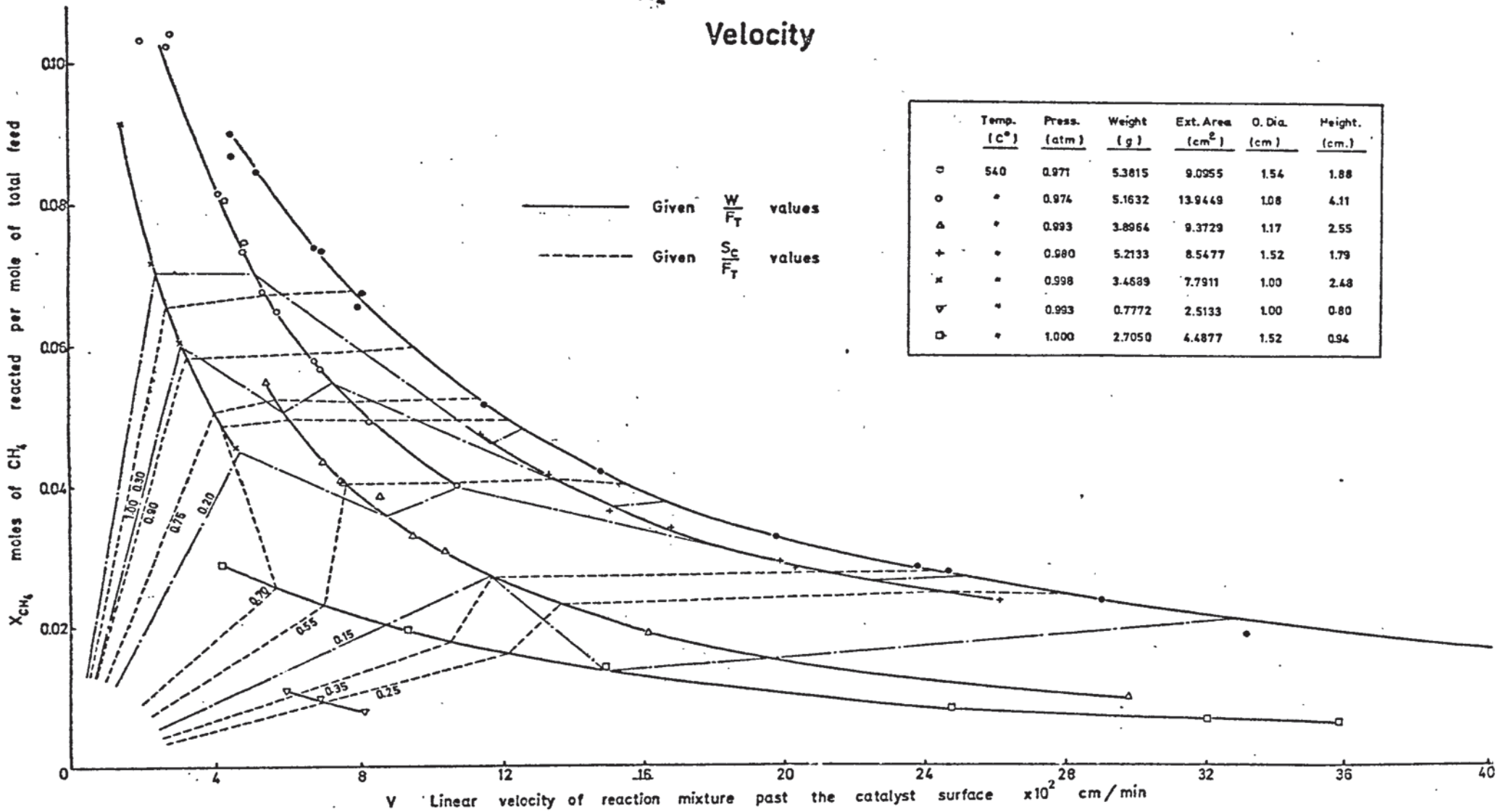

	Temp. (C°)	Press. (atm)	Weight (g)	Ext. Area (cm^2)	O. Dia. (cm)	Height. (cm.)
□	540	0.971	5.3815	9.0955	1.54	1.88
○	"	0.974	5.1632	13.9449	1.08	4.11
△	"	0.993	3.8964	9.3729	1.17	2.55
+	"	0.980	5.2133	8.5477	1.52	1.79
×	"	0.998	3.4589	7.7911	1.00	2.48
▽	"	0.993	0.7772	2.5133	1.00	0.80
◇	"	1.000	2.7050	4.4877	1.52	0.94

$$N_{Re} = \frac{(D_R - D_c)\ G}{\mu_m} \tag{8.4}$$

where:

D_R = inside diameter of the reactor tube, cm

D_c = outside diameter of the catalyst pellet, cm

G = superficial mass flowrate, g/(cm^2)(sec)

μ_m = viscosity of the reaction mixture, g/(cm)(sec)

Since there was no change of mass of the reacting gas during the reaction (no carbon formation), G was calculated on the basis of initial feeds of methane and steam. The viscosity of the reaction mixture, μ_m was computed from the viscosities of the individual components, μ_i and μ_j, using the modified equation obtained from the kinetic theory developed by Chapman and Enskog (129) :

$$\mu_m = \sum_{i=1}^{n} \frac{\mu_i}{\left[1 + \sum_{\substack{j=1 \\ j \neq i}}^{n} \phi_{ij} \frac{y_j}{y_i}\right]} \tag{8.5}$$

where:

ϕ_{ij}, collision function of the species i and j, was evaluated by the estimation method of Wilke (129):

$$\phi_{ij} = \frac{\left[1 + \left[\frac{\mu_i}{\mu_j}\right]^{\frac{1}{2}} \left[\frac{M_j}{M_i}\right]^{\frac{1}{4}}\right]^2}{\left[1 + \frac{M_i}{M_j}\right]^{\frac{1}{2}} \sqrt{8}} \tag{8.6}$$

where M_i and M_j are the molecular weights of the species i and j, respectively. ϕ_{ji} was found by interchanging the subscripts to yield:

$$\phi_{ji} = \phi_{ij} \left(\frac{\mu_j}{\mu_i}\right)\left(\frac{M_i}{M_j}\right) \tag{8.7}$$

The viscosities of individual components were computed using the simplified equation derived from the Chapman-Ensk og treatment and reported to be valid for the temperature and pressure range relevant to the present investigation:

$$\mu_i = 0.00002669 \frac{(M_i\ T)^{\frac{1}{2}}}{\sigma_i^2\ \Omega_v} \qquad (8.8)$$

where:

σ_i = diameter of the molecule based on the assumption of a rigid, non-interacting, spherical model, Å

Ω_v = collision integral for viscosity, evaluated by the Lennard-Jones intermolecular potential function for non-polar species (CH_4, H_2, CO_2, CO) and by the Stockmayer potential function for the polar component (H_2O).

Although the Reynolds number, as defined was independent of the velocity and density variations resulting from the increase of volume on reaction, the paths of conversion with changing Reynolds number at constant W/F_T values retained their irregular shapes (Figs. 8.4 and 8.5). This fact led to the conclusion that the change of the external area of the pellet (S_c) exposed to the reacting gas had a pronounced effect on the extent of conversion.

To establish the contribution made by the external surface area, conversions were plotted against the ratio S_c/F_T (Fig. 8.6) and it was evident that the conversion curves showed a marked tendency to converge below a certain value of S_c/F_T ($< (0.8)\ (10^3)$ cm^2 of catalyst external surface per mole of total feed per min). The experimental points exhibited, in general, only small deviations from the curves representing the conversion x_{CH_4} as a function of S_c/F_T for the low values of S_c/F_T (high feedrates), whereas at high values of S_c/F_T ($> 2.5 \times 10^3$ corresponding to 3 - 4 ml/h water feedrates), they were rather scattered. This scattering stemmed essentially from the mode of operation of the water feed pump and the non-uniformity of evaporation rates of water at these very low ranges of feed, which induced an irregular variation of

Fig. 8.4 Reynolds Number N_{Re} of the Reacting Gas as a Function of the Ratio $\frac{W}{F_T}$

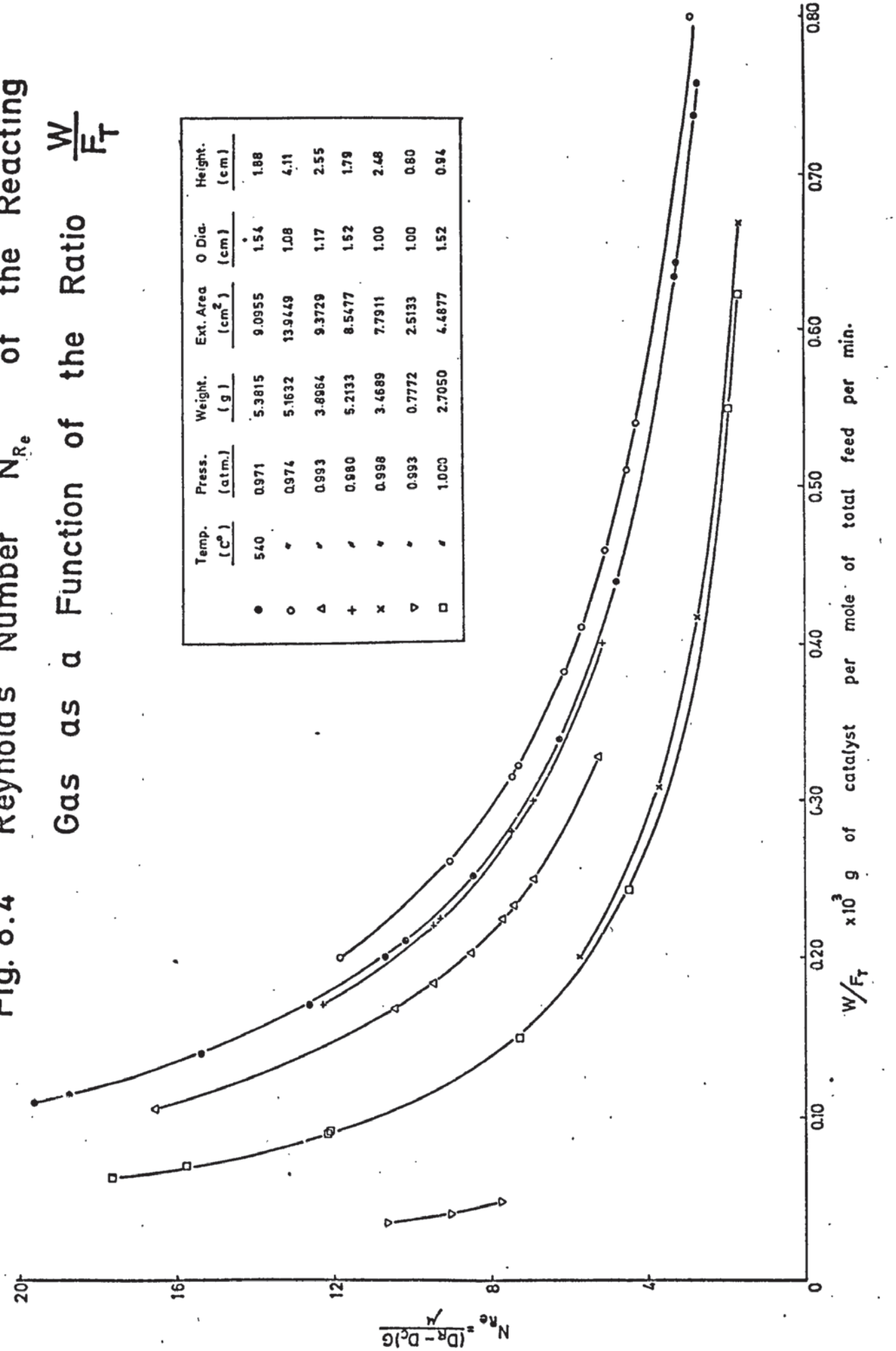

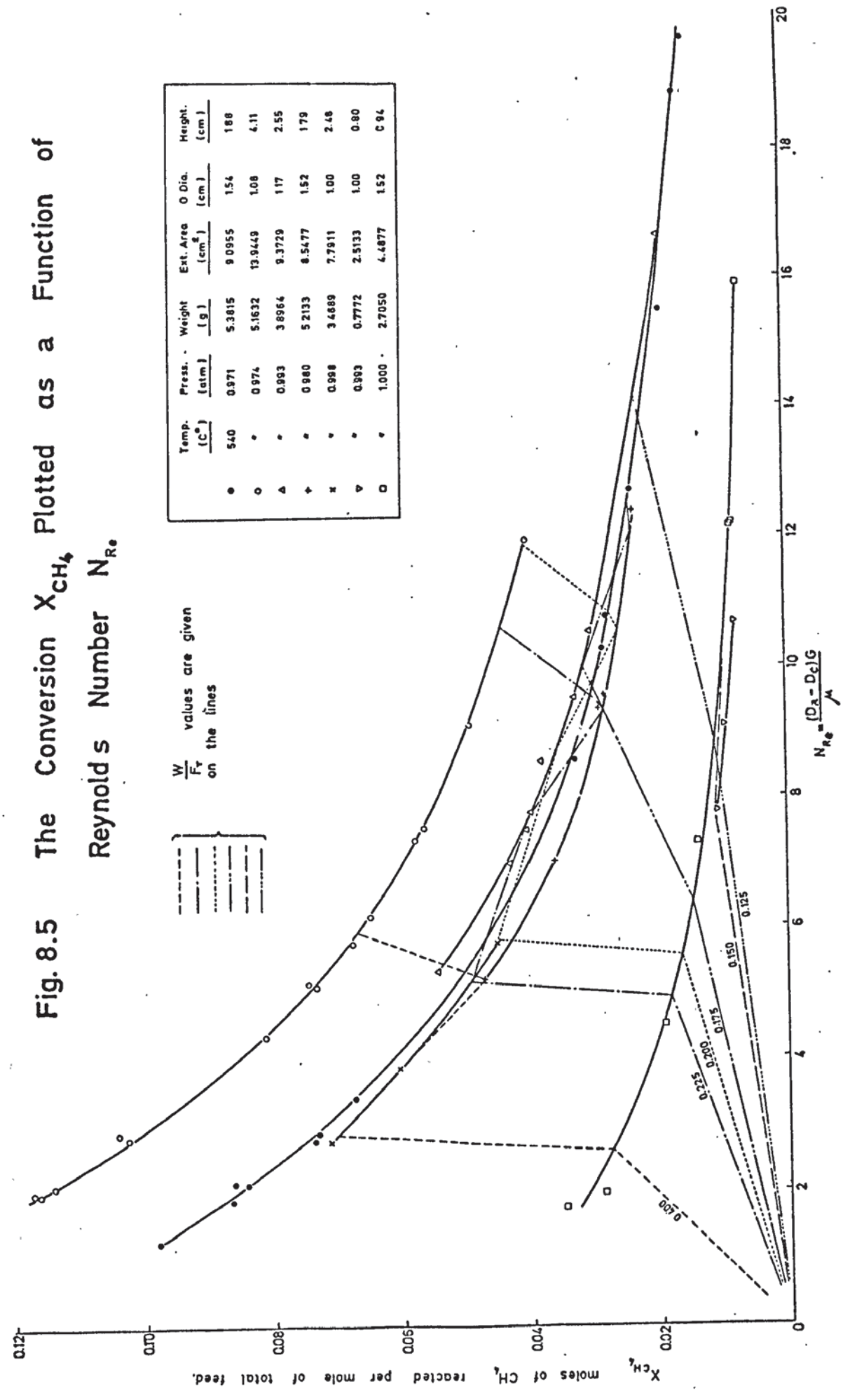

Fig. 8.5 The Conversion X_{CH_4} Plotted as a Function of Reynold s Number N_{Re}

Fig. 8.6 The Conversion X_{CH_4} as a Function of the Ratio S_c/F_T

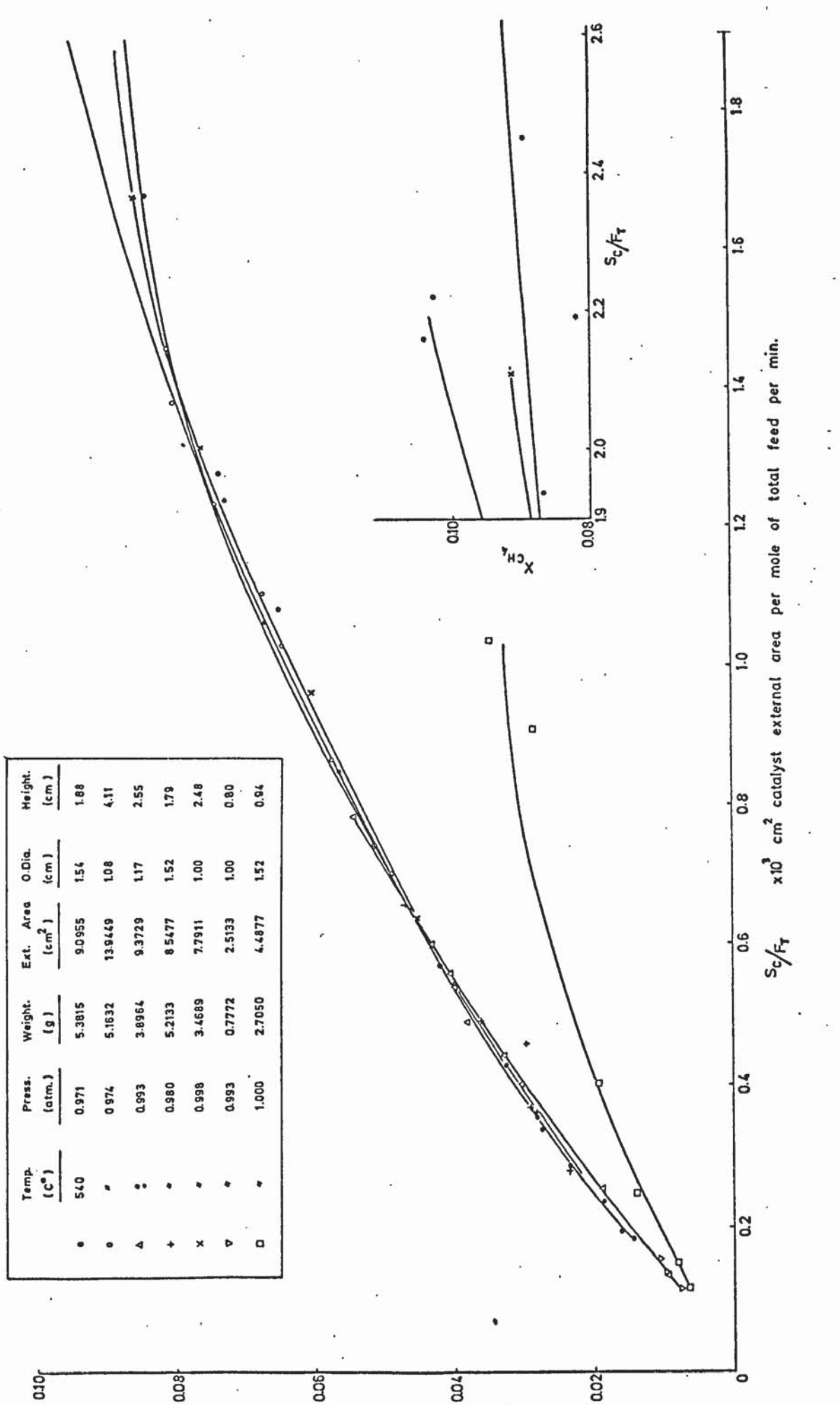

steam : methane ratio in the feed. The experimental points for $S_c/F_T > (2.5)\ (10^3)$, therefore, are not included in the graph Fig. 8.6, since they represented very small feedrates, and consequently, they were immaterial with regard to the boundary for the onset of external mass transfer resistances.

A more distinct picture for the effect of superficial mass velocity on the observed rate of reaction was obtained by replotting Figs. 8.2 to 8.5 on the basis of S_c/F_T values (Figs. 8.7, 8.8, and 8.9). The paths of conversion levels for increasing linear gas velocities, but at constant values of S_c/F_T obtained from Fig. 8.7, were traced on Fig. 8.3 (dotted lines). Although the irregularities in conversion paths observed in the case of W/F_T values(dashed lines) were smoothed out to a large extent by considering the external surface of the catalyst pellets, they still indicated some inconsistencies caused by the change of the physical properties of the reacting gas during the course of the reaction. The incompatibility was eliminated by replacing the linear gas velocity by the Reynolds number as co-ordinate (Figs. 8.8 and 8.9). In fact, using Fig. 8.9, which represents a parametric plot of x_{CH_4} versus N_{Re} for constant values of S_c/F_T, the limiting values of N_{Re} for definite S_c/F_T ratios were established for minimized external mass transfer resistances. It was, therefore, concluded that the pattern of the variation of conversion with respect to linear velocity or the constancy of conversion level with increased gas velocity (122) does not provide a conclusive criterion to define qualitatively the limits for film-diffusion impedances.

The following calculation of pellet height, which constitutes a numerical indication rather than a quantitative evaluation of film resistances, was carried out assuming that the operation was totally

Fig. 8.7 The Linear Velocity V of the Reacting Gas Plotted as a Function of the Ratio $\frac{S_c}{F_T}$

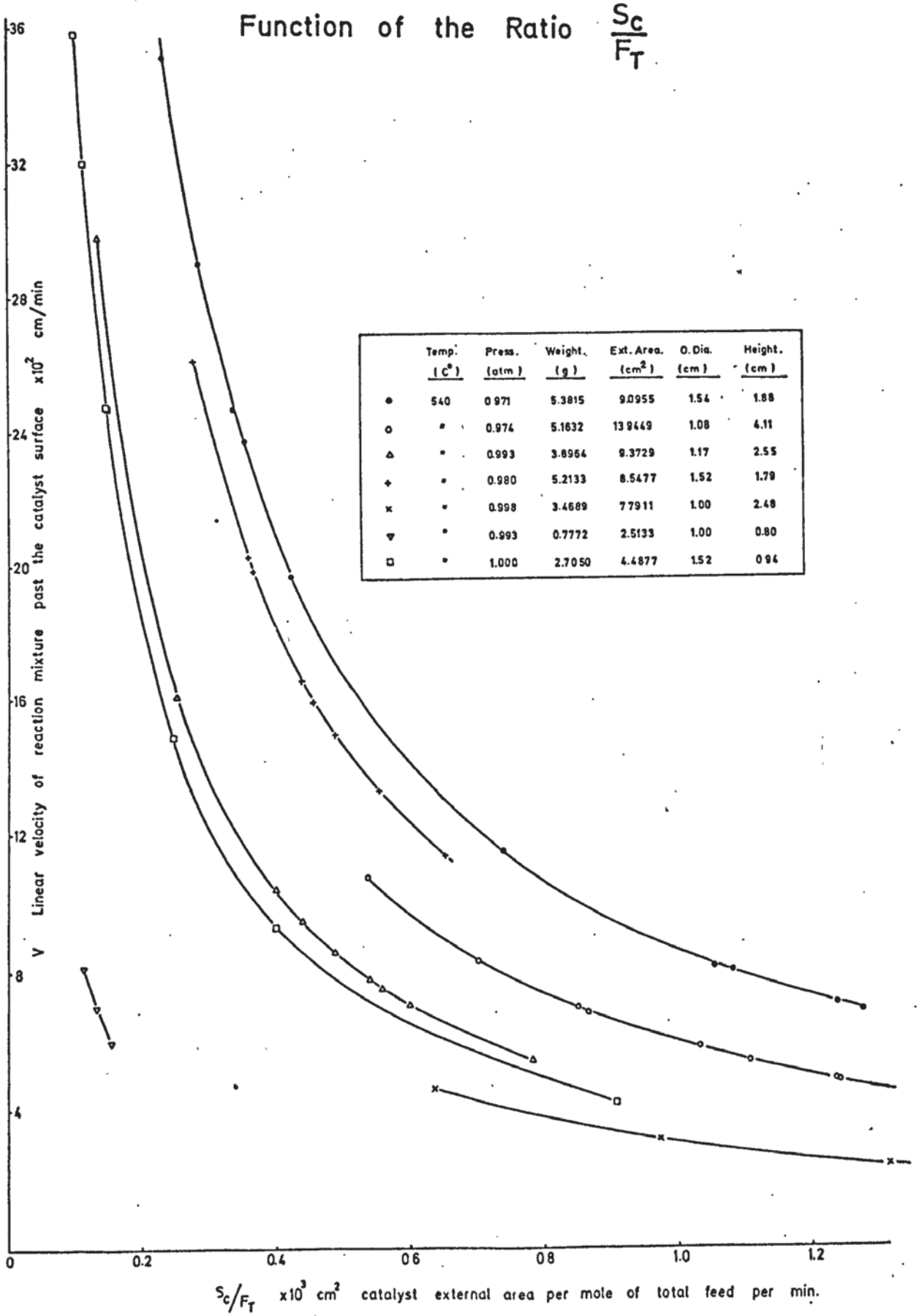

	Temp. (C°)	Press. (atm)	Weight. (g)	Ext. Area. (cm²)	O. Dia. (cm)	Height. (cm)
●	540	0.971	5.3815	9.0955	1.54	1.88
○	"	0.974	5.1632	13.9449	1.08	4.11
△	"	0.993	3.8964	9.3729	1.17	2.55
+	"	0.980	5.2133	8.5477	1.52	1.79
×	"	0.998	3.4689	7.7911	1.00	2.48
▽	"	0.993	0.7772	2.5133	1.00	0.80
□	"	1.000	2.7050	4.4877	1.52	0.94

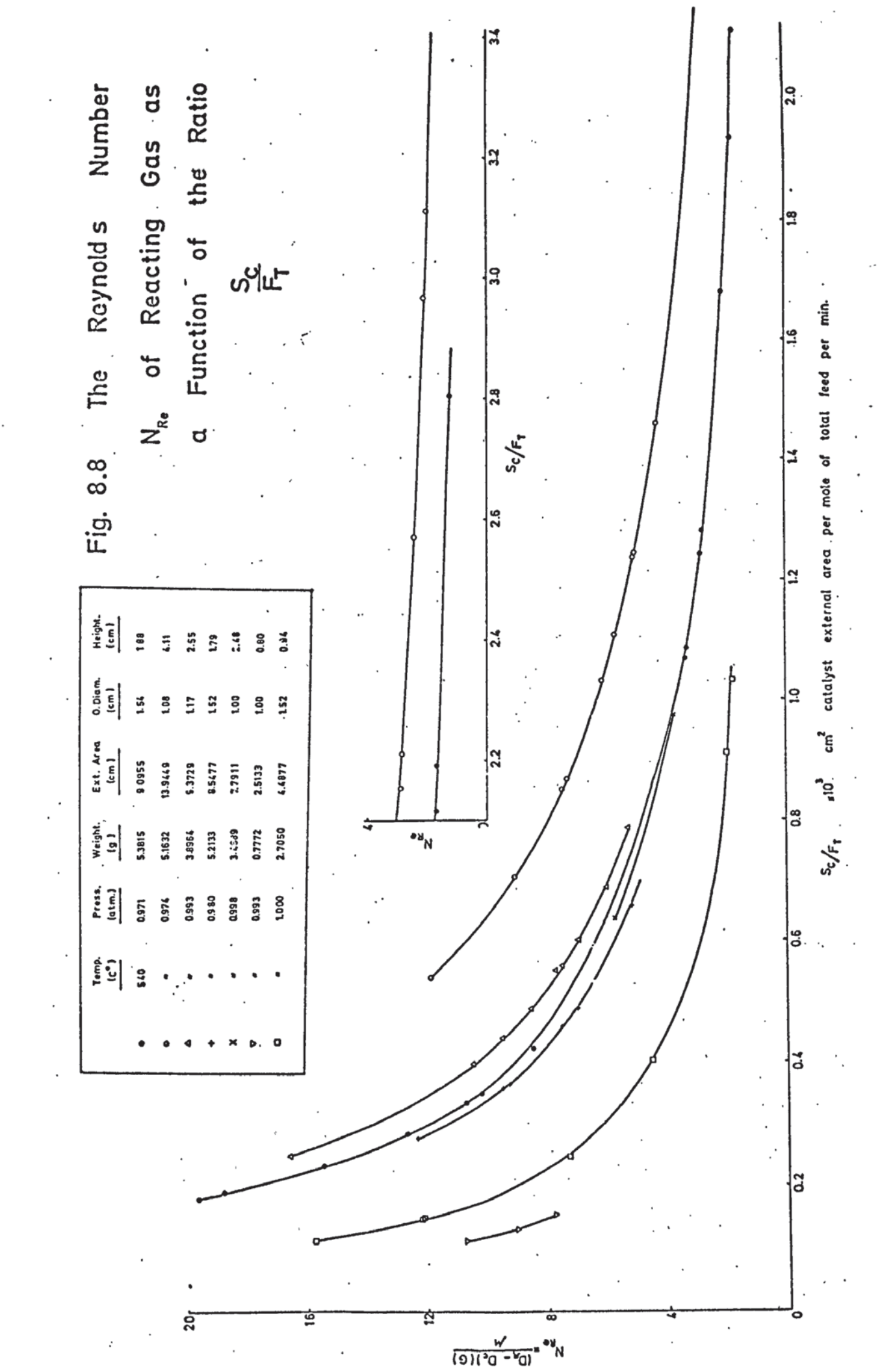

Fig. 8.8 The Reynolds Number N_{Re} of Reacting Gas as a Function of the Ratio $\frac{S_c}{F_T}$

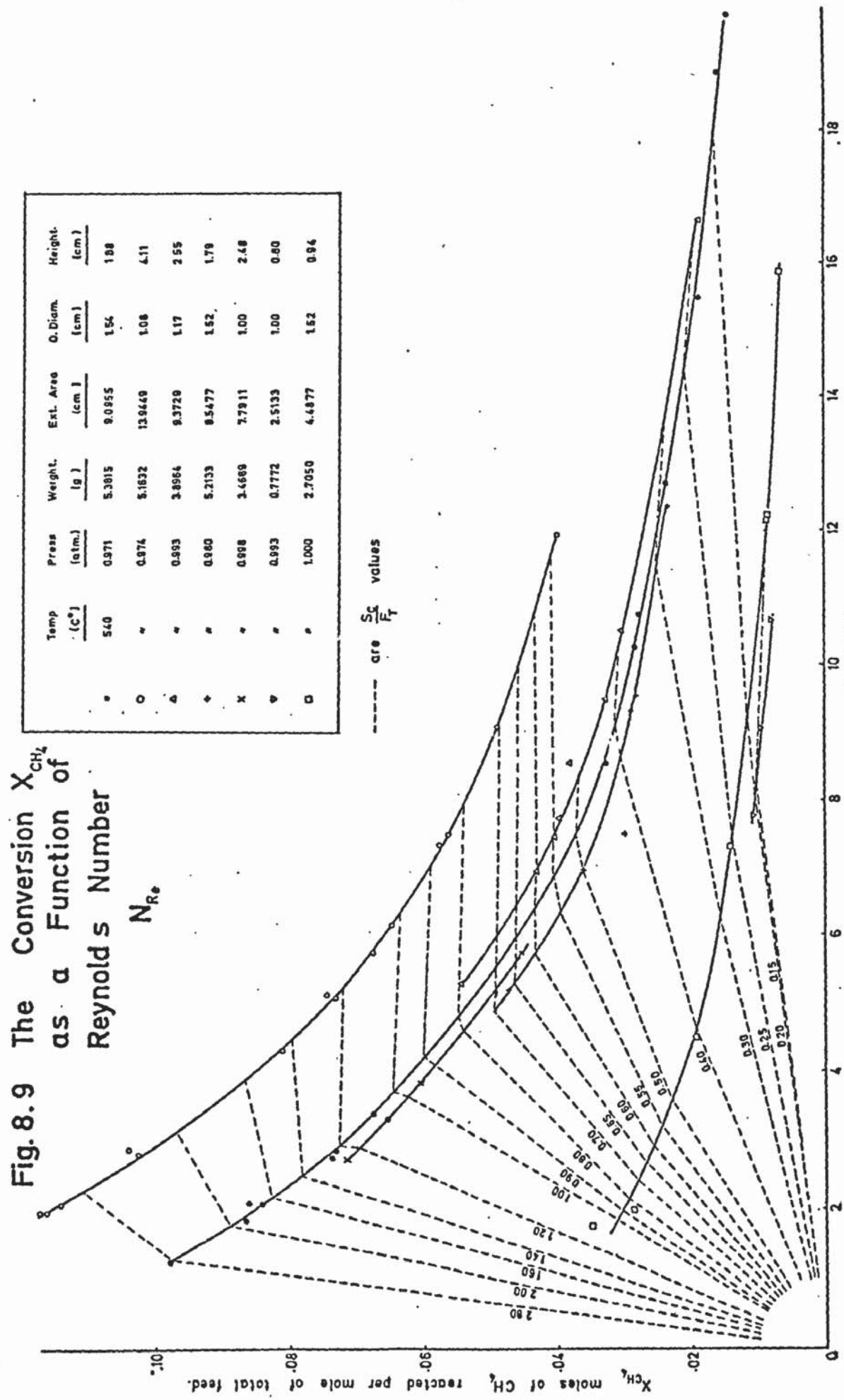

Fig. 8.9 The Conversion X_{CH_4} as a Function of Reynolds Number N_{Re}

under gas film diffusion control. It was further assumed that:

(i) the mass transfer coefficient, k_G, remained constant along the catalyst bed,

(ii) the catalyst surface and ambient gas stream were under isothermal conditions, and

(iii) plug flow conditions prevailed throughout.

Then, the observed reaction rate, $r_{obs,s}$, based on external surface of the pellet at steady-state condition can be written as :

$$r_{obs,s}\ \pi\ D_c\ dh = -\ F_T\ dy_{CH_4,\ b} \tag{8.9}$$

where h is the height of the external surface of the catalyst pellet exposed to the reacting gas, D_c is the pellet diameter, and $y_{CH_4,b}$ is the mole fraction of methane in the reaction mixture. The rate of mass transfer in the bulk gas phase is given by:

$$r_D = k_G\ (p_{CH_4,b} - p_{CH_4,s}) \tag{8.10}$$

If the operating conditions correspond totally to a film-diffusion controlled regime, then the observed rate of reaction, $r_{obs,\ s}$, is equal to the mass transfer rate, r_D, of methane to the unit external surface of the pellet, and $p_{CH_4,s} = 0$. Hence

$$r_{obs} = k_G\ p_{CH_4,b} = k_G\ y_{CH_4,\ b}\ P_T \tag{8.11}$$

where p_T is the total operating pressure.

Combining Equations (8.9) and (8.11) and rearranging:

$$k_G\ P_T\ \pi\ D_c\ dh = F_T \left[\frac{dy_{CH_4,b}}{y_{CH_4,\ b}}\right] \tag{8.12}$$

The mass transfer coefficient, k_G can be substituted from the correlation :

$$j_D = k_G \frac{P_f'}{G_M} (N_{Sc})^{2/3} = \frac{1}{\varepsilon}\ (0.357)\ (N_{Re})^{-\ 0.359}$$

With the reactor diameter D_R, and since $\varepsilon = 1.0$ in the

present case:

$$k_G = (0.357)\left[\frac{F_T}{\frac{\pi}{4}(D_R^2 - D_c^2)}\right]\frac{1}{P_{f,CH_4}}(N_{Sc})^{-2/3}(N_{Re})^{-0.359} \quad (8.13)$$

Substituting this expression for k_G in Equation (8.12) and assuming $G_M = F_T$ (the difference is negligible because of low conversion and excess of steam) yields:

$$\left[\frac{(4)(0.357)}{\pi}\right]\frac{F_T}{(D_R^2 - D_c^2)}\left(\frac{P_T}{P_{f,CH_4}}\right)\pi D_c\,(N_{Sc})^{-2/3}(N_{Re})^{-0.359}\,dh = F_T\left(\frac{dy_{CH_4,b}}{y_{CH_4,b}}\right)$$

Rearranging and integrating this expression between $y_{CH_4,i}$ and $y_{CH_4,f}$, the initial and final mole fractions of methane, respectively, gives:

$$h = \frac{(D_R^2 - D_c^2)}{1.428\,D_c}\left(\frac{P_{f,CH_4}}{P_T}\right)(N_{Sc})^{2/3}(N_{Re})^{0.359}\int_{y_{CH_4,f}}^{y_{CH_4,i}}\frac{dy_{CH_4,b}}{y_{CH_4,b}} \quad (8.14)$$

The height of the catalyst pellet was then evaluated for the following set of operating conditions :

D_R = 1.83 cm

D_c = 1.54 cm

P_T = 0.971 atm abs. (barometric pressure operation)

P_{f,CH_4} = the pressure film factor for methane, evaluated according to Yoshida et al. (184) :

$$aA + bB \rightarrow rR + sS$$

$$P_{f,A} = P_T - \left[P_{A,b}\,\frac{(a + b - r - s)}{a}\right]$$

where P_T and $P_{A,b}$ are the total operating pressure and the partial pressure of A in the bulk gas phase, respectively.

It should be noted here that the accurate expression for the pressure film factor in gaseous diffusion processes is given as the

logarithmic mean value of

$$p_T - p_A \quad \left(\frac{a + b - r - s}{a}\right)$$

over the boundary limits of the gas film (83) :

$$p_{f,A} = \frac{(p_T - p_{A,b}\,\delta_A) - (p_T - p_{A,s}\,\delta_A)}{\ln\left[\dfrac{p_T - p_{A,b}\,\delta_A}{p_T - p_{A,s}\,\delta_A}\right]} \qquad (8.15)$$

where $\delta_A = \left(\frac{a + b - r - s}{a}\right)$.

Furthermore, the partial pressure of methane is subject to change along the catalyst bed because of the reaction. The evaluation of the pressure film factor according to Equation (8.15) would, therefore, involve a trial-and-error calculation, and the term p_{f,CH_4} should be included in the integral given in Equation (8.14). However, since the variation of partial pressure of methane, $p_{CH_4,b} = p_A$, is not large for small conversion levels, the calculation of p_{f,CH_4} using the arithmetic average of the terminal values of methane partial pressure at h = 0 and h = h and assuming it constant along the height of the gas-catalyst interface is justifiable in the context of the other assumptions made. Thus, for 0.971 atm abs. total operating pressure, 11.13 % conversion, and H_2O : CH_4 molar ratio 3.0 in the feed :

$p_{CH_4,i} = (0.25)\ (0.971) = 0.243$ atm

$p_{CH_4,f} = 0.2044$ atm

$$p_{f,CH_4} = 0.971 - \left(\frac{0.243 + 0.2044}{2}\right)\ \left(\frac{1 + 2 - 1 - 4}{1}\right) = 1.42 \text{ atm}$$

N_{Sc} for gases varies within the limits 0.5 - 2.0 (184) ; $(N_{Sc})^{2/3}$ would correspond accordingly to 0.63 - 1.587 and the arithmetic average of these values (viz. 1.11) is considered to be representative. N_{Re} for this run is 10.74 and so $(N_{Re})^{0.359} = 2.345$. The initial and the final mole fractions of methane were 0.25 and 0.2105, respectively.

Hence from Equation (8.14) :

$$h = \left[\frac{1.83^2 - 1.54^2}{1.428 \times 1.54}\right]\left[\frac{1.42}{0.97}\right](1.11)\,(2.345)\,\ln\left(\frac{y_{CH_4,i}}{y_{CH_4,f}}\right)$$

$$h = 1.67 \ln \frac{0.25}{0.2105} = 0.287 \text{ cm}$$

This result indicates that a pellet height of approximately 0.29 cm is sufficient to obtain a conversion of 11%, if the reaction were controlled by the mass transfer from the ambient stream to the pellet surface. Since the height of the catalyst in this run was 1.88 cm, it can be inferred that the reaction rate was affected primarily by other controlling factors. A calculation, carried out for the same flow condition and conversion, but with respect to the other reactant (H_2O) as the limiting component, resulted in an estimated pellet height of 0.25 cm.

A further calculation for another run with the same catalyst pellet, but at N_{Re} = 1.26 and 39.70 % conversion, methane being the limiting component, resulted in a pellet height of 0.51 cm which indicated the onset of the influence of external mass transfer resistances.

For the range of operating conditions used in the present research, estimations of the corresponding range of gas film partial pressure difference ($p_{CH_4,b} - p_{CH_4,s}$), were made using the correlation presented by Yoshida et al. (184). The correlation uses the hydraulic radius for the definition of N_{Re}, and hence the present N_{Re} values in terms of hydraulic diameter have been divided by 4 to enable the film driving force, Δy_{CH_4}, to be read from the correlation. The ranges of the individual parameters needed for this analysis are:

(i) N_{Sc} 0.5 - 2.0 is relevant for gaseous systems,

(ii) The mole fraction film factor y_{f,CH_4} is taken as 1.5 as the extreme value,

(iii) $R = \frac{r_{m,CH_4}}{a_m \cdot \emptyset \, G_M}$ is based on a range of values of r_{m,CH_4} = 0.000142 (α = 2 and highest N_{Re}) and r_{m,CH_4} = 0.000045 (α = 7 and lowest N_{Re}), on a fixed value of a_m = 1.60 cm^2 for the external catalyst surface per gram of catalyst, and for the evaluation of G_M, on an annulus area of 0.62 - 2.63 cm^2 combined with a total feedrate F_T = (40 - 400) (10^{-4}) moles/min. Hence, the range of values of R was 0.02 to 0.0015.

From these extreme values, the ranges of $\Delta p_{CH_4} = \Delta y_{CH_4}$ (for operation at barometric pressure), read from the correlation, were found to be 0.009 to 0.02 atm. Δp_{CH_4} = 0.009 implied negligible film-diffusion resistances, whereas Δp_{CH_4} = 0.02(resulting from the lowest Reynolds numbers) indicated 8% difference between the surface partial pressure and bulk phase partial pressure of methane.

8.3.3 . Conclusion.

The graphical analysis of the experimental results led to the following conclusions :

(i) The irregularities observed in plots of 'conversion versus W/F_T ratio' were caused predominantly by the variations of the pellet external surface in contact with the reacting gas. The changes of the annulus cross-section, and consequently the changes of the linear gas velocity for the same reactant feedrates at different catalyst diameters, but at almost the same catalyst mass, did not have pronounced effects on the extent of conversion.

(ii) The clear dependence of the extent of conversion on the external surface of the catalyst pellets was a significant indication that the observed rate of reaction was markedly influenced by pore-diffusion limitations.

(iii) The inconsistencies of the parametric plots of conversion

against linear gas velocities for constant values of S_c/F_T ratio implied that the linear gas velocity or the gas flowrate was not the appropriate co-ordinate for the estimation of the onset of film-diffusion resistances. In fact, the irregularities were eliminated by substituting for velocity the Reynolds number and an ever-increasing value of conversion but approaching an asymptotic value was then obtained.

A further advantage of the Reynolds number as the basic co-ordinate appeared in evaluating the effect of pressure on the extent of conversion (Section 8.4).

(iv) It was possible to infer from Fig. 8.9 the limiting value of N_{Re} at which the external mass transfer resistance at any S_c/F_T value influences the reaction rate. As a matter of fact, the locus of the points, at which conversions attained a constant level, would have indicated the Reynolds number boundary below which the film-diffusion started to affect the observed reaction rate. However, no attempt has been made to draw such a locus, since the number of points defining that specific part of the curves was considered insufficient, especially for $N_{Re} < 3$. Nevertheless, for the case of single pellet experiments, it was concluded that flowrates corresponding to $N_{Re} > 4$ definitely ensured operation free of gas film-diffusion limitations at 540° C.

(v) Finally, based on the above, the author wishes to point out a possible limitation in the comments of Chambers and Boudart given in a communication (32) indicating that the conversion versus velocity diagnostic test may fail because of its lack of sensitivity under flow conditions corresponding to very low values of N_{Re}, since "the dependence of the coefficients

of heat and mass transfer on flowrate may be so weak as to render a test of conversion versus flowrate quite insensitive". Their conclusions are drawn on the basis of the discrepancies observed in correlations between flowrate, gas velocity, N_{Re} and W/F_T ratios, and of the experimental data obtained from the dehydrogenation reaction of cyclohexane on a platinum-alumina catalyst. The details of the experimental conditions and the characteristics of the catalyst with respect to the size, pore volume distribution and activity are not stated. There is no indication whether or not the effect of external surface for the same catalyst mass was taken into account. However, the uncertainties of the correlations might have been eliminated by replacement of W/F_T by S_c/F_T.

8.4 EFFECT OF PRESSURE.

It is appropriate to analyse and discuss the effects of pressure on the course and outcome of the reaction between steam and methane from several different points of view.

In industrial practice the use of reforming pressures higher than atmospheric has the advantage of allowing a smaller size of equipment to be used, increasing thereby the specific throughput of the reactor and simplifying the very important problem of heat transfer. Moreover, the application of higher pressures in a process such as steam reforming, which involves a marked increase of volume, will result in a considerable saving in the cost of energy for compression of product gases, if these are to be used for high-pressure synthesis or submitted to purification or distributed under pressure.

From the thermodynamic standpoint, on the other hand, high pressure operation exerts unfavourable effects on the overall yield and equilibrium gas composition, which may be partially compensated,

however, by increase of the reforming temperature. These aspects have been discussed in Chapter 2.

In investigating the kinetic mechanism of a gas-solid catalytic reaction by the Langmuir-Hinshelwood approach, special emphasis is placed on the evaluation of that experimental data which reflects the effects of total pressure variations on the initial reaction rate. Details of the interpretation technique of the results thus obtained are given elsewhere (37, 153,182).

With regard to the effects of pressure on the observed rate of reaction, Woodcock (179) observed an increase of conversion with increase of total pressure from barometric to 250 psig for given steam : methane and W/F_T ratios. Phillips and co-workers (124), who studied the kinetics of the heptane-steam reaction, conducted experiments to determine the effect of total pressure on the reaction rate at constant W/F_T and steam : heptane molar ratios. According to their results which were confined to high conversions (65 - 76%), an increase of total pressure from 94 psia to 303 psia caused increase of conversion of only 3 - 4 %. Soonawala (155) reported a rise of conversion of avtur ($C_{11}H_{22}$) with increase of total pressure, and attributed this fact to the reduction of volumetric flowrate of the reaction mixture which, in turn, extended the apparent residence time of the gas in the catalyst bed.

8.4.1 Experimental Procedure.

In the present investigation the effects of total pressure changes on the observed rate of reaction were studied at the following operating conditions:

Temperature, ^{o}C	:	600 ± 1
		650 ± 1
		700 ± 1

Catalyst mass, g	:	5.3720
		5.7294
		5.4516
Total feedrates, (10^{-3}) moles/min	:	41.5 ± 0.2
		44.5 ± 0.2
		46.0 ± 0.2
H_2O : CH_4 molar ratio	:	3.0 ± 0.1
Total pressures, atm abs.	:	barometric
		3.97 ± 0.01
		6.97 ± 0.01
		12.96

All the runs were performed with cylindrical catalyst pellets and the total feedrates were adjusted to such levels that the film-diffusion limitations could be assumed to be absent.

8.4.2 Results and Discussion.

The results obtained from the runs are presented as a plot of conversion against total pressure at two temperatures (Fig.8.10). The data corresponding to 600° C are not shown in Fig. 8.10, since the feedrates and W/F_T or S_c/F_T ratios were not identical in all the runs. However they are included in Table 8.1, which summarizes the experimental conditions and the results obtained.

It is evident from Fig. 8.10 that the increase of the operating pressure did not effect an increase of conversion. This is not unexpected since it has been established in the previous section that the Reynolds number, which is independent of pressure, within a range of 1 - 15 atm, is the primary factor affecting the extent of conversion, provided that the temperature and steam: methane molar ratio in the feed remained the same, and the rate expression was not influenced by the variation of total pressure.

Two further plots (Figs. 8.11 and 8.12) were prepared to

TABLE 8.1

SUMMARY OF THE RESULTS INDICATING THE EFFECTS OF TOTAL PRESSURE.

Temperature, ^{o}C	600	600	600
Pressure, atm abs.	0.989	0.989	0.989
Weight of pellet W, g	5.729	5.724	5.279
External area S_c, cm^2	8.988	8.988	8.988
H_2O : CH_4 molar ratio	3.01	2.98	2.97
Total feedrate (10^{-3}) moles/min	41.67	41.66	41.68
W/F_T ratio (10^3)	0.138	0.138	0.137
S_c/F_T ratio (10^3)	0.216	0.216	0.216
Reynolds number, N_{Re}	15.67	15.68	15.70
Conversion, x_{CH_4}	0.0255	0.0251	0.0234
Conversion, %	10.21	10.01	9.30
Gas composition (dry basis)			
H_2, %	28.49	28.11	27.39
CO, %	0.89	0.88	0.82
CH_4, %	64.20	64.68	65.86
CO_2, %	6.41	6.32	5.94

TABLE 8.1 (cont'd)

Temperature, ^{o}C	600	600	600	600
Pressure, atm abs.	12.96	12.96	12.96	12.96
Weight of pellet W, g	5.372	5.372	5.372	5.372
External area S_c, cm^2	8.882	8.882	8.882	8.882
H_2O : CH_4 molar ratio	2.98	3.00	3.01	3.01
Total feedrate, (10^{-3}) moles/min	44.219	44.781	44.874	44.874
W/F_T ratio (10^3)	0.121	0.120	0.120	0.120
S_c/F_T ratio (10^3)	0.201	0.198	0.198	0.198
Reynolds number, N_{Re}	16.70	16.93	16.96	16.96
Conversion, x_{CH_4} (moles of CH_4 converted per mole of total feed)	0.0237	0.0219	0.0223	0.0218
Conversion, %	9.45	8.77	8.95	8.73
Gas composition (dry basis)				
H_2, %	26.79	25.55	26.77	25.40
CO, %	0.90	0.76	0.82	0.76
CH_4, %	66.29	67.91	66.67	68.10
CO_2, %	6.02	5.76	5.74	5.75

TABLE 8.1 (cont'd)

Temperature, ^{o}C	650	650	650
Pressure, atm abs.	0.989	0.989	0.989
Weight of pellet W, g	5,729	5.729	5.729
External area S_c, cm^2	8.988	8.988	8.988
H_2O : CH_4 molar ratio	3.00	2.99	3.06
Total feedrate, (10^{-3}) mole/min	41.576	41.681	41.413
W/F_T Ratio (10^3)	0.138	0.137	0.138
S_c/F_T Ratio (10^3)	0.216	0.216	0.217
Reynolds number, N_{Re}	14.84	14.88	14.77
Conversion, x_{CH_4} (moles of CH_4 converted per mole of total feed)	0.0309	0.0301	0.0311
Conversion, %	12.34	12.02	12.62
Gas composition (dry basis)			
H_2, %	32.37	32.03	32.84
CO, %	1.32	1.25	1.35
CH_4, %	59.30	59.80	58.69
CO_2, %	7.03	6.92	7.13

TABLE 8.1 (cont'd)

Temperature, ^{o}C	650	650	650	650
Pressure, atm abs.	3.98	3.98	3.98	3.97
Weight of pellet W, g	5.729	5.729	5.729	5.729
External area S_c, cm^2	8.988	8.988	8.988	8.988
H_2O : CH_4 molar ratio	2.96	3.03	2.99	3.00
Total feedrate (10^{-3}) moles/min	41.630	41.363	41.530	41.019
W/F_T ratio (10^3)	0.138	0.139	0.138	0.140
S_c/F_T ratio (10^3)	0.216	0.217	0.216	0.219
Reynolds number, N_{Re}	14.86	14.75	14.82	14.63
Conversion, x_{CH_4} (moles of CH_4 converted per mole of total feed)	0.0306	0.0328	0.0305	0.0319
Conversion, %	12.22	13.21	12.20	12.75
Gas composition (dry basis)				
H_2, %	31.62	33.74	31.34	32.93
CO, %	1.29	1.37	1.27	1.27
CH_4, %	60.10	57.49	60.28	58.52
CO_2, %	6.99	7.39	7.10	7.28

TABLE 8.1 (cont'd)

Temperature, ^{o}C	650	650
Pressure, atm abs.	6.968	6.968
Weight of pellet W, g	5.729	5.729
External area S_c, cm^2	8.988	8.988
H_2O : CH_4 molar ratio	3.01	2.98
Total feedrate (10^{-3}) moles/min	40.913	41.069
W/F_T ratio (10^3)	0.140	0.140
S_c/F_T ratio (10^3)	0.220	0.219
Reynolds number, N_{Re}	14.59	14.66
Conversion, x_{CH_4} (moles of CH_4 converted per mole of total feed)	0.0325	0.0313
Conversion, %	13.02	12.47
Gas composition (dry basis)		
H_2, %	32.78	32.51
CO, %	1.48	1.47
CH_4, %	58.46	59.08
CO_2 %	7.27	6.94

TABLE 8.1 (cont'd)

Temperature, ^{o}C	650	650	650	650
Pressure, atm abs.	12.956	12.956	12.956	12.956
Weight of pellet W, g	5.729	5.729	5.729	5.729
External area S_c, cm^2	8.988	8.988	8.988	8.988
H_2O : CH_4 molar ratio	3.00	2.99	3.00	3.02
Total feedrate (10^{-3}) moles/min.	41.576	41.520	41.576	41.363
W/F_T ratio (10^3)	0.138	0.138	0.138	0.139
S_c/F_T ratio (10^3)	0.216	0.216	0.216	0.217
Reynolds number, N_{Re}	14.83	14.81	14.83	14.75
Conversion, x_{CH_4} (moles of CH_4 converted per mole of total feed)	0.0318	0.0316	0.0316	0.0328
Conversion, %	12.72	12.64	12.63	13.21
Gas composition (dry basis)				
H_2 , %	32.81	32.72	32.56	33.65
CO , %	1.34	1.33	1.31	1.36
CH_4, %	58.64	58.77	58.91	57.59
CO_2, %	7.20	7.17	7.20	7.40

TABLE 8.1 (cont'd)

Temperature, ^{o}C	700	700
Pressure, atm abs.	0.980	0.980
Weight of pellet W, g	5.451	5.451
External area S_c, cm^2	8.988	8.988
H_2O : CH_4 molar ratio	2.99	2.98
Total feedrate (10^{-3}) moles/min	37.523	36.675
W/F_T ratio (10^3)	0.145	0.149
S_c/F_T ratio (10^3)	0.240	0.245
Reynolds number, N_{Re}	12.72	12.43
Conversion, x_{CH_4} (moles of CH_4 converted per mole of total feed)	0.0451	0.0464
Conversion, %	17.99	18.49
Gas composition (dry basis)		
H_2, %	40.53	41.33
CO, %	2.23	2.32
CH_4, %	48.77	47.82
CO_2, %	8.46	8.53

TABLE 8.1 (cont'd)

Temperature, ^{o}C	700	700	700
Pressure, atm abs.	3.98	3.98	3.98
Weight of pellet W, g	5.729	5.729	5.729
External area S_c, cm^2	8.988	8.988	8.988
H_2O : CH_4 molar ratio	2.99	2.98	3.01
Total feedrate (10^{-3}) moles/min	39.305	39.553	39.311
W/F_T ratio (10^3)	0.146	0.145	0.146
S_c/F_T ratio (10^3)	0.229	0.227	0.229
Reynolds number, N_{Re}	13.34	13.42	13.34
Conversion, x_{CH_4} (moles of CH_4 converted per mole of total feed)	0.0429	0.0429	0.0432
Conversion, %	17.12	17.06	17.32
Gas composition (dry basis)			
H_2, %	39.39	39.27	39.62
CO, %	2.16	2.18	2.22
CH_4, %	50.24	50.38	49.93
CO_2, %	8.22	8.18	8.25

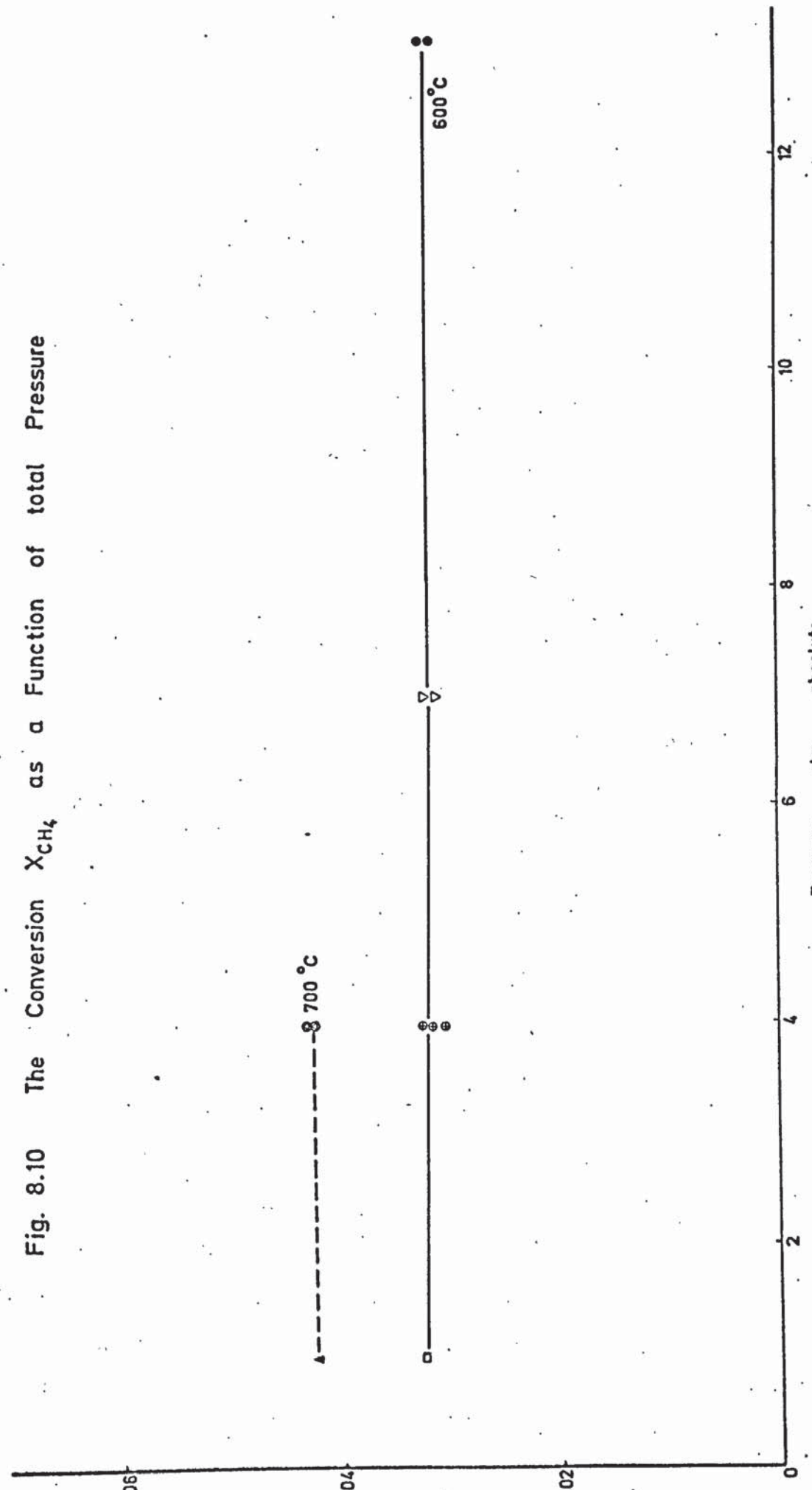

Fig. 8.10 The Conversion X_{CH_4} as a Function of total Pressure

Fig.8.11 The Reynolds Number N_{Re} of the Reacting Gas as a Function of the Ratio S_c/F_T (at different temperature and total pressure levels : $\alpha = 3.0$)

	Temp. (C°)	Press. (atm)	Weight (g)	Ext. Area. (cm^2)	O. Dia. (cm)	Height. (cm)
+	540	0.971	5.3815	9.0955	1.54	1.88
+	600	0.992	5.5047	8.9884	1.53	1.87
□	650	0.987	5.4516	8.9884	1.53	1.87
▲	700	0.980	5.4516	8.9884	1.53	1.87
○	600	12.96	5.3720	8.8819	1.52	1.86
●	650	3.947	5.7294	8.9884	1.53	1.87
▽	650	6.968	5.7294	8.9884	1.53	1.87
●	650	12.960	5.7294	8.9884	1.53	1.87
●	700	3.98	5.7294	8.9884	1.53	1.87

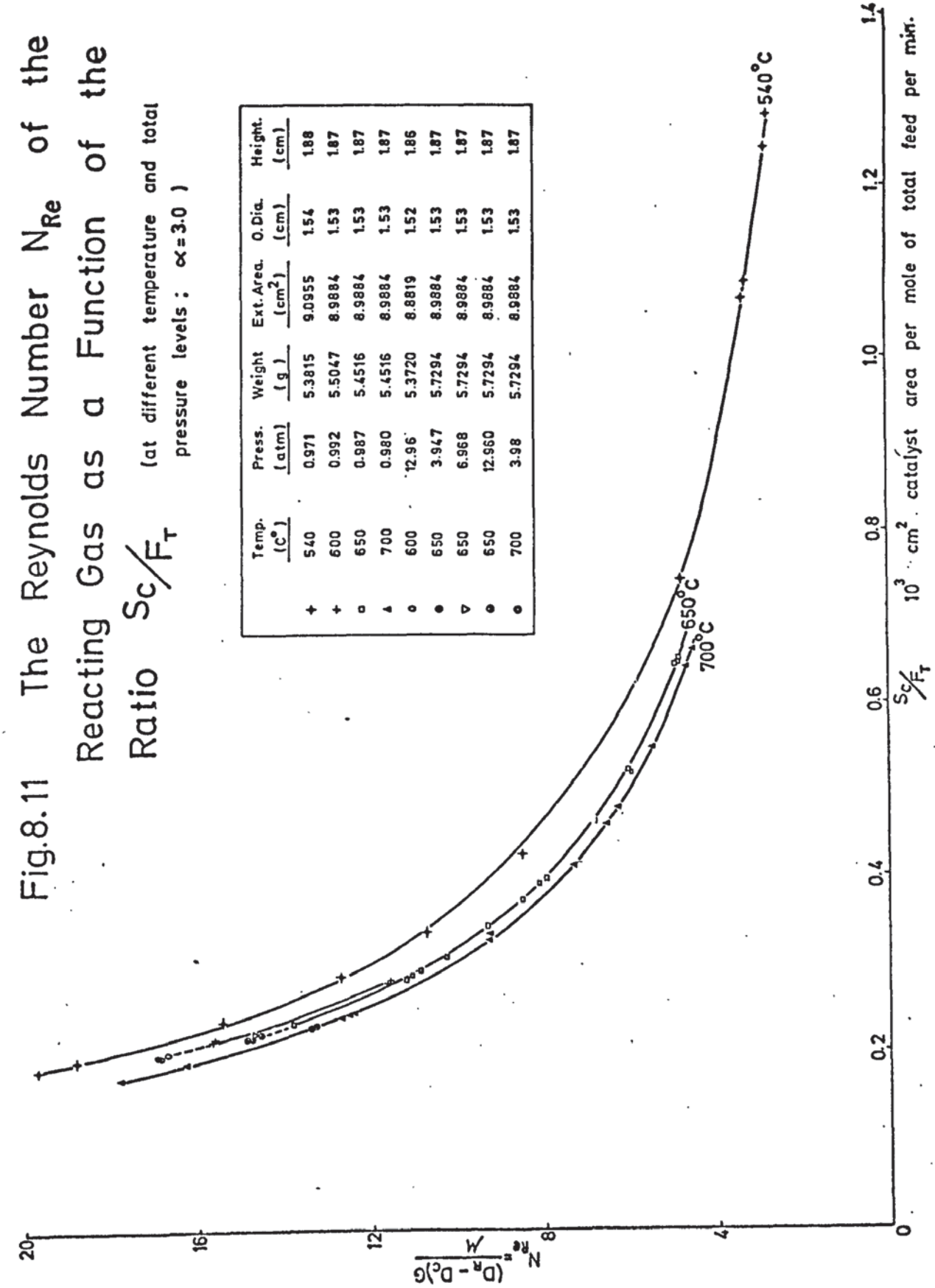

Fig. 8.12 The Conversion X_{CH_4} as a Function of Reynolds Number N_{Re}

(at different temperature and total pressure levels ; $\alpha = 3.0$)

	Temp. (C°)	Press. (atm)	Weight (g)	Ext. Area. (cm^2)	O.Dia. (cm)	Height. (cm)
+	540	0.971	5.3815	9.0955	1.54	1.88
+	600	0.992	5.5047	8.9884	1.53	1.87
□	650	0.987	5.4516	8.9884	1.53	1.87
▲	700	0.980	5.4516	8.9884	1.53	1.87
○	600	12.960	5.3720	8.8819	1.52	1.86
●	650	3.947	5.7294	8.9884	1.53	1.87
▽	650	6.968	5.7294	8.9884	1.53	1.87
●	650	12.960	5.7294	8.9884	1.53	1.87
⊙	700	3.980	5.7294	8.9884	1.53	1.87

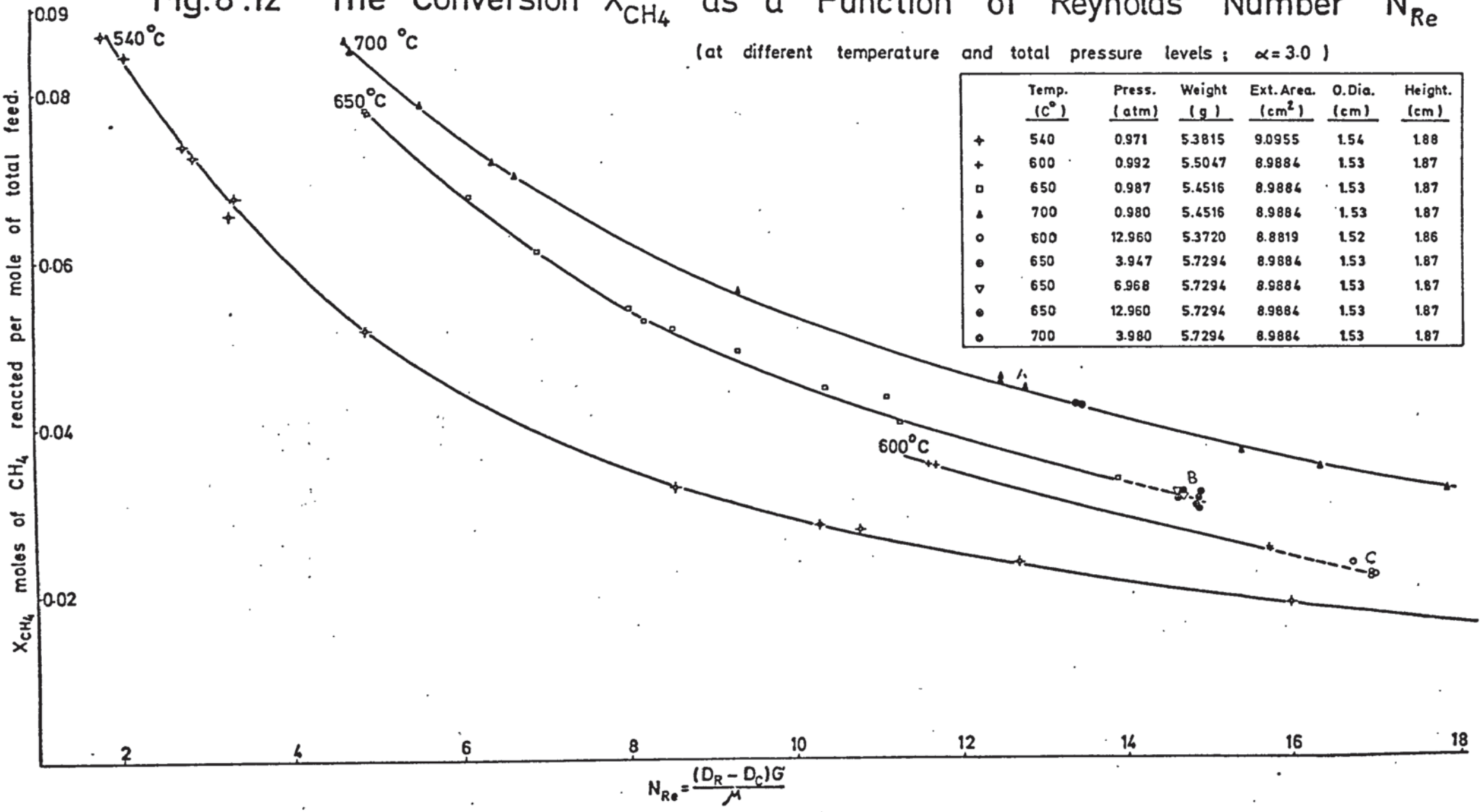

examine the results of the pressure variation experiments. Fig. 8.11 is a plot of N_{Re} versus S_c/F_T ratio and indicates the Reynolds numbers of each run at different total pressures and S_c/F_T ratios with temperature levels as parameter. In the other plot, Fig. 8.12, conversion is plotted against N_{Re} for results obtained at four different temperatures, and each temperature line embraces the results of all pressures. The negligible effect of pressure is seen from a cluster of points such as those in regions A, B, and C, which include results at the full range of test pressures. Since for a given W/F_T ratio, the conversion can never increase with decreasing gas velocity, it is not correct to attribute an increase of conversion to an increase in contact time arising from a reduction in gas velocity. An increase in conversion with pressure must result from a dependence of the rate expression itself on total pressure.

Based upon the distribution of pore radii (70% of the pores were in the range of 18 - 30 Å) the mass transport within the pores would be expected to occur by Knudsen flow; it was, therefore, not likely that the mass transfer characteristics within the pores would be influenced by a change of total pressure, since, unlike molecular diffusion, the effective diffusivity for the Knudsen regime is independent of total pressure.

From the point of view of the probable kinetic mechanisms involved, no change in the extent of conversion with the increase of the reactant concentrations in the ambient stream by increasing the total pressure at constant H_2O : CH_4 molar ratio in the feed implies that the catalytic surface, functioning by a dual-site mechanism is already saturated with the reactants at 1 atm abs. pressure so that further increase of pressure does not increase the coverage. Consequently the adsorption of reactants cannot be considered a controlling factor for the overall reaction ;

either chemical reaction or desorption of one or more of the product components, or simultaneously both chemical reaction and desorption must be controlling steps.

Since no variation in the extent of conversion with pressure was observed at certain values of W/F_T and S_c/F_T, no further investigation of pressure effects at other W/F_T ratios was undertaken.

8.4.3. Conclusion.

No effect of pressure on conversion has been found within the pressure range 1 - 13 atm abs. for given values of (W/F_T) and (S_c/F_T) at temperatures 600, 650, and 700° C.

8.5 EFFECT OF TEMPERATURE.

The effect of temperature on conversion or on the observed rate of reaction is not conclusive in selecting and discussing plausible kinetic mechanisms for gas-solid catalytic reactions. It is, however, of major importance in determining the kinetic and thermodynamic parameters such as the apparent and true activation energies of the reaction, the enthalpy and entropy of formation of the activated adsorption compounds formed between the catalyst and reactants and products.

Some aspects of the Arrhenius-type plot of the observed reaction rate against temperature to differentiate between various reaction regimes, and to evaluate the apparent activation energy of the reaction have been discussed in Section (7.2).

8.5.1 Experimental Procedure.

The effect of temperature on conversion was investigated at three temperature levels, 540°, 650° and 700° C. All the runs were carried out with cylindrical catalyst pellets and the experimental conditions are summarized below:

Pressure	: barometric
Catalyst mass, g	: 5.3815 5.5047 5.4516

Total flowrate,	:	(4.7 - 48.9)	(540° C)
(10^{-3}) moles per min		(13.9 - 38.8)	(650° C)
		(16.4 - 52.3)	(700° C)
H_2O : CH_4 molar ratio	:	3.0 ± 0.1	
Temperatures, °C	:	540 ± 1	
		650 ± 1	
		700 ± 1	

The feedrates of the reactants were adjusted to cover a wide range of Reynolds numbers (1 - 20). In addition to the above experiments, some supplementary runs were carried out at 600°, 710°, 740°, and 750° C, but at given W/F_T and S_c/F_T ratios as a common basis for comparison of the results.

8.5.2 Results and Discussion.

The results obtained from the runs are presented as a plot of conversion x_{CH_4} against temperature at the flow conditions indicated in Fig. 8.13. The equilibrium conversion of methane for the same conditions of total pressure (1 atm abs.), steam : methane molar ratio (3.0), and temperature is also shown on the same graph. It is apparent from Fig. 8.13 that the incremental increase of observed values of conversion with increase of temperature was less than the corresponding incremental increase of equilibrium conversion. This might be attributed to the low values of W/F_T applied in these runs. In fact, this plot corresponds to the right half of a graph which illustrates the locus of conversion ver sus reaction temperature for reversible reactions occurring at isothermal conditions in any kind of reactor with different values of reactor holding time $\tau = \frac{V_R}{F_{A_o}} C_{Ao}$, as given by Levenspiel (99). However, it has to be mentioned that a probable change of the intrinsic kinetics of the reaction within the temperature range studied might also have influenced the extent of conversions observed.

Two identical graphs have been prepared showing the dependence of x_{CH_4} on W/F_T and S_c/F_T ratios at different temperatures (Figs. 8.14 and (8.15). The derivatives of these curves at given W/F_T or S_c/F_T

Fig. 8.13 The Experimental and Equilibrium Conversions X_{CH_4} as a Function of Temperature

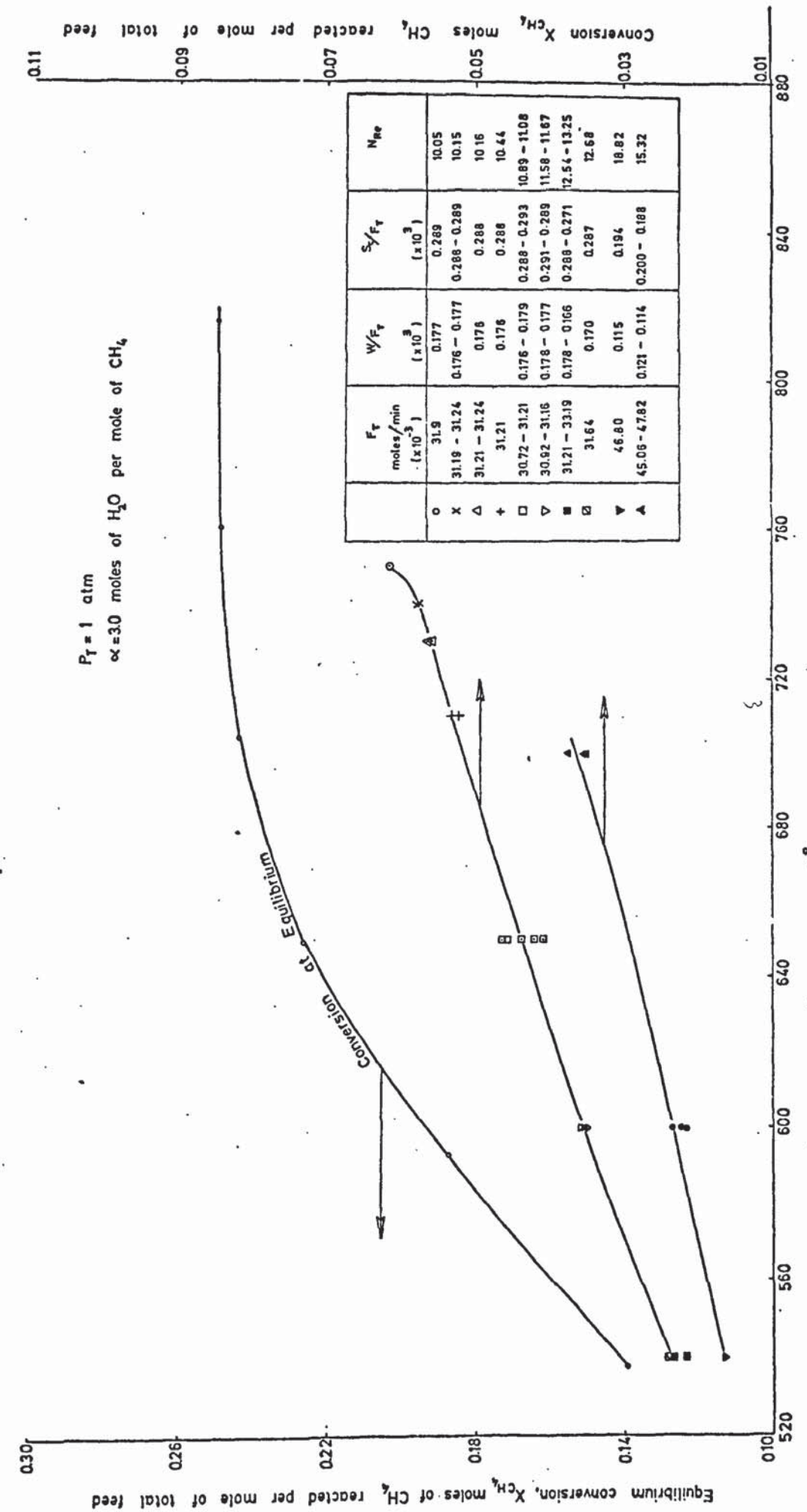

	F_T moles/min ($\times 10^{-3}$)	W/F_T ($\times 10^3$)	S_V/F_T ($\times 10^3$)	N_{Re}
o	31.9	0.177	0.289	10.05
x	31.19 - 31.24	0.176 - 0.177	0.288 - 0.289	10.15
Δ	31.21 - 31.24	0.176	0.288	10.16
+	31.21	0.176	0.288	10.44
□	30.72 - 31.21	0.176 - 0.179	0.288 - 0.293	10.89 - 11.08
▽	30.92 - 31.16	0.178 - 0.177	0.291 - 0.289	11.58 - 11.67
■	31.21 - 33.19	0.178 - 0.166	0.288 - 0.271	12.54 - 13.25
⊠	31.64	0.170	0.287	12.68
▼	46.80	0.115	0.194	18.82
▲	45.06 - 47.82	0.121 - 0.114	0.200 - 0.188	15.32

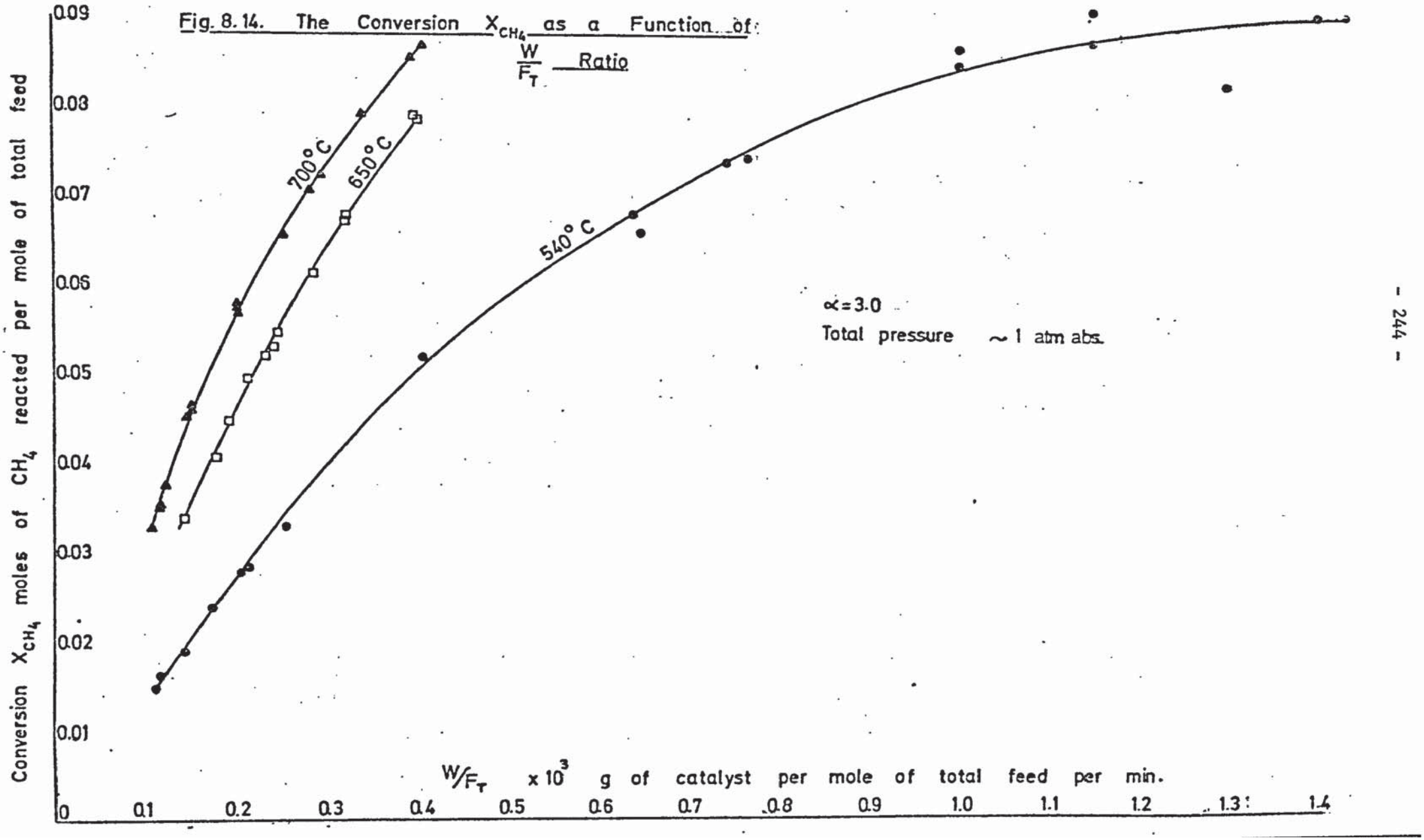
Fig. 8.14. The Conversion X_{CH_4} as a Function of $\frac{W}{F_T}$ Ratio
Conversion X_{CH_4} moles of CH_4 reacted per mole of total feed
0.09
0.08
0.07
0.06
0.05
0.04
0.03
0.02
0.01
0
700° C
650° C
540° C
∝=3.0
Total pressure ~ 1 atm abs.
W/F_T x 10^3 g of catalyst per mole of total feed per min.
0.1
0.2
0.3
0.4
0.5
0.6
0.7
0.8
0.9
1.0
1.1
1.2
1.3
1.4

Fig. 8.15. The Conversion X_{CH_4} as a Function of $\frac{S_c}{F_T}$ Ratio

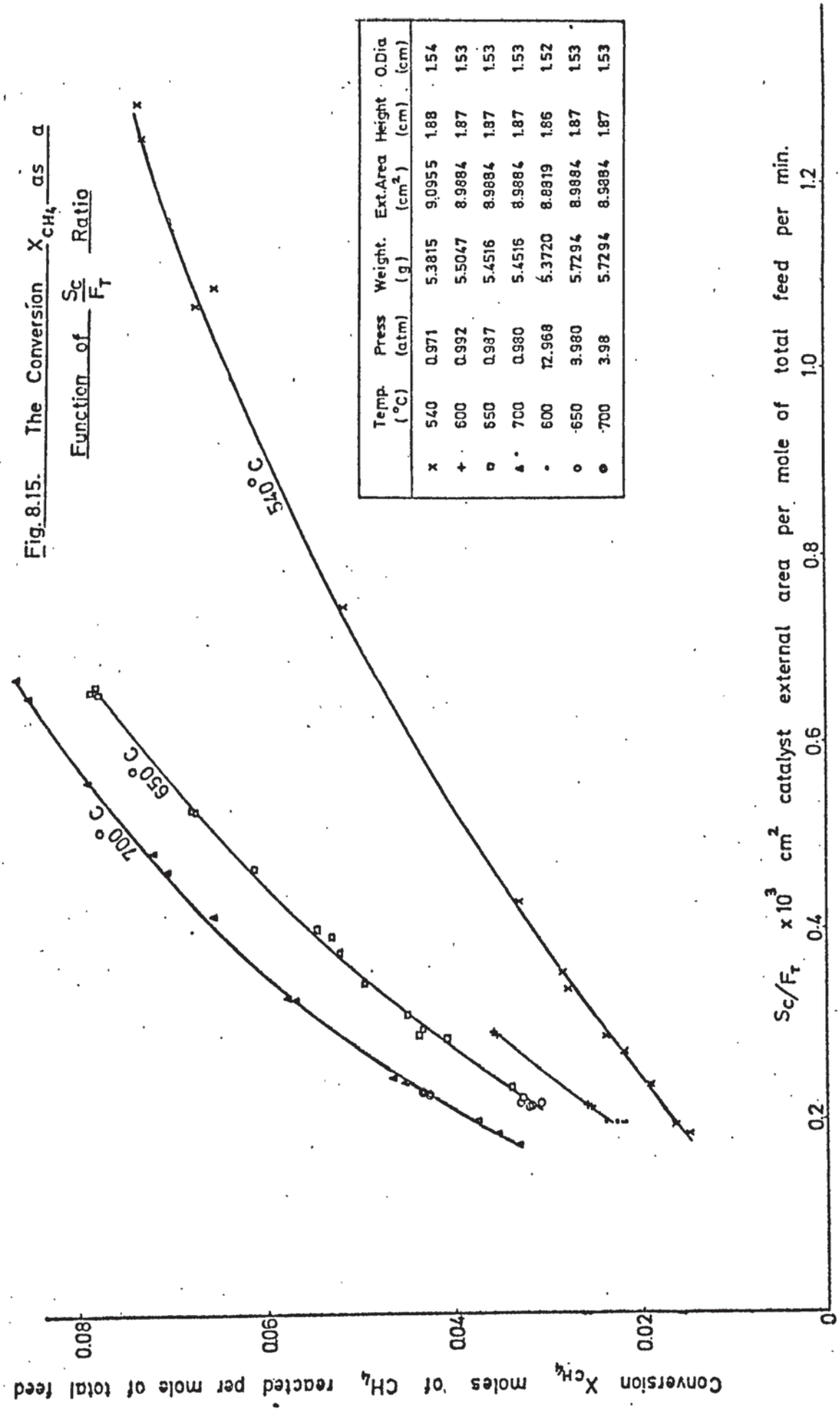

	Temp. (°C)	Press (atm)	Weight. (g)	Ext.Area (cm^2)	Height (cm)	O.Dia (cm)
x	540	0.971	5.3815	9.0955	1.88	1.54
+	600	0.992	5.5047	8.9884	1.87	1.53
□	650	0.987	5.4516	8.9884	1.87	1.53
▲	700	0.980	5.4516	8.9884	1.87	1.53
•	600	12.968	5.3720	8.8819	1.86	1.52
○	650	3.980	5.7294	8.9884	1.87	1.53
●	700	3.98	5.7294	8.9884	1.87	1.53

values represent the observed reaction rates based on the mass or on the external surface area of the pellet and the values of $\left[\frac{dx_{CH_4}}{d(W/F_T)}\right]$ and $\left[\frac{dx_{CH_4}}{d(S_c/F_T)}\right]$ were calculated by numerical differentiation. The results obtained for certain ranges of Reynolds numbers are given in Table 8.2. The logarithms of the observed reaction rates are also plotted versus $\frac{1}{T}$ to give the Arrhenius-type diagram (Fig. 8.16). Since it was established that the external surface of the pellet was a controlling parameter for the extent of conversion, the observed reaction rates on this plot are expressed on this basis, although the catalyst dimensions of the experiments were practically identical. (Table 8.2). The Reynolds number of every run at each of the three temperatures differed from each other. Therefore, average values of two or three consecutive runs had to be used in the plot so that the points could correspond to approximately the same N_{Re}. The other reason for employing average values was the rather large fluctuation of the derivatives since they were calculated by the computer from experimental points and did not form a smoothed curve representing the relationship between conversion and S_c/F_T ratio.

For N_{Re} = 11.23 - 11.48, the Arrhenius diagram of the reacting system exhibits a straight line relationship. Decreasing the N_{Re} to a range 5.93 - 6.56 resulted in a less definite pattern of lower slope. This uncertainty stemmed from the greater degree of scatter of the experimental points at low total feedrates (large S_c/F_T values) and were attributed to the mode of operation of the apparatus. However, they do give an indication of the onset of film diffusion resistances at temperatures higher than 540° C, which appeared to be negligible at this temperature level (Section 8.3).

8.5.3 Conclusion.

From an Arrhenius-type diagram based on average values of

TABLE 8.2

Effect of Temperature on the Observed Rate of Reaction

Temperature, ^{o}C	540		
Pressure, atm abs.	0.971		
Weight of the catalyst, W, g	5.3815		
External area of the pellet, S_c, cm^2	9.0955		
Outside diameter, cm	1.54		
Height of the pellet, cm	1.88		
Volume of the pellet, V_c, cm^3	2.410		
S_c/V_c, cm^2/cm^3	3.774		
$S_x = S_c/W$, cm^2/g	1.690		
			Mean
Total feedrate, F_T, x 10^{-3} moles per min	31.64	25.64	
W/F_T ratio, x 10^3	0.170	0.210	
S_c/F_T ratio, x 10^3	0.288	0.355	
H_2O : CH_4 molar ratio	3.01	3.01	
Conversion, %	9.54	11.33	
x_{CH_4}, moles of CH_4 converted per mole of total feed	0.0236	0.0282	
N_{Re}	12.68	10.26	11.47
Mean linear velocity, cm/min	2900	2376	
Observed reaction rates:			
$dx_{CH_4}/d(W/F_T) = r_{obs,m}$, x 10^{-4}	1.34	1.31	
$dx_{CH_4}/d(S_c/F_T) = r_{obs,s}$, x 10^{-4}	0.890	0.682	
log $r_{obs,s}$	-4.050	-4.166	- 4.105

TABLE 8.2 (cont'd)

Temperature, ^{o}C	540
Pressure, atm abs.	0.971
Weight of the catalyst, W, g	5.3815
External area of the pellet, S_c, cm^2	9.0955
Outside diameter, cm	1.54
Height of the pellet, cm	1.88
Volume of the pellet, V_c cm^3	2.410
S_c/V_c, cm^2/cm^3	3.774
$S_x = S_c/W$, cm^2/g	1.690

				Mean
Total feedrate, F_T, x 10^{-3} moles per min	21.36	15.87	12.24	
W/F_T ratio, x 10^3	0.252	0.339	0.440	
S_c/F_T ratio, x 10^3	0.426	0.573	0.743	
H_2O : CH_4 molar ratio	3.00	3.02	3.00	
Conversion, %	13.18	16.99	20.71	
x_{CH_4} moles of CH_4 converted per mole of total feed	0.0330	0.0423	0.0518	
N_{Re}	8.52	6.31	4.84	6.56
Mean linear velocity, cm/min	1974	1478	1152	
Observed reaction rates:				
$dx_{CH_4}/d\,(W/F_T)$ = $r_{obs,m}$, x 10^{-4}	1.12	1.01	0.896	
$dx_{CH_4}/d(S_c/F_T)$ = $r_{obs,s}$, x 10^{-4}	0.662	0.601	0.532	
log $r_{obs,s}$	-4.179	-4.221	-4.274	-4.223

TABLE 8.2 (cont'd)

Temperature, ^{o}C	650^{o}C
Pressure, atm abs.	0.987
Weight of the catalyst, W,g	5.4516
External area of the pellet, S_c, cm^2	8.9884
Outside diameter, cm	1.53
Height of the pellet, cm	1.87
Volume of the pellet, V_c, cm^3	2.326
S_c/V_c, cm^2/cm^3	3.864
$S_x = S_c/W$, cm^2/g	1.649

					Mean
Total feedrate, F_T, x 10^{-3} moles per min	31.58	19.42	17.18	13.94	
W/F_T ratio, x 10^3	0.176	0.281	0.317	0.391	
S_c/F_T ratio, x 10^3	0.288	0.463	0.524	0.646	
H_2O : CH_4 molar ratio	3.00	3.01	2.99	2.98	
Conversion, %	16.22	24.54	27.12	31.03	
x_{CH_4}, moles of CH_4 converted per mole of total feed	0.0410	0.0613	0.0679	0.0779	
N_{Re}	11.23	6.85	6.05	4.89	5.93
Mean linear velocity, cm/min	3183	1995	1776	1455	
Observed reaction rates:					
$dx_{CH_4}/d(W/F_T) = r_{obs,m}$, x 10^{-4}	3.19	1.62	1.59	0.78	
$dx_{CH_4}/d(S_c/F_T) = r_{obs,s}$, x 10^{-4}	1.64	0.976	0.937	0.516	
log $r_{obs,s}$	-3.785	-4.011	-4.028	-4.287	-4.145

TABLE 8.2 (cont'd)

Temperature, ^{o}C			700	
Pressure, atm abs.			0.980	
Weight of the catalyst, W, g			5.4516	
External area of the pellet, S_c, cm^2			8.9884	
Outside diameter, cm			1.53	
Height of the pellet, cm			1.87	
Volume of the pellet, V_c, cm^3			2.326	
S_c/V_c, cm^2/cm^3			3.864	
$S_x = S_c/W$, cm^2/g			1.649	
Total feedrate, F_T x 10^{-3} moles per min	37.52	36.67	27.51	Mean
W/F_T ratio, x 10^3	0.145	0.149	0.198	
S_c/F_T ratio, x 10^3	0.240	0.245	0.327	
H_2O : CH_4 molar ratio	2.99	2.98	3.00	
Conversion, %	17.99	18.49	22.96	
x_{CH_4}, moles of CH_4 converted per mole of total feed	0.0451	0.0464	0.0569	
N_{Re}	12.72	12.43	9.29	11.48
Mean linear velocity, cm/min	4031	3948	2290	
Observed reaction rates:				
$dx_{CH_4}/d(W/F_T)$ = $r_{obs,m}$, x 10^{-4}	3.24	3.17	2.10	
$dx_{CH_4}/d(S_c/F_T)$ = $r_{obs,s}$, x 10^{-4}	2.53	2.52	2.10	
log $r_{obs,s}$	-3.597	-3.598	-3.896	-3.676

TABLE 8.2 (cont'd)

Temperature, ^{o}C	700
Pressure, atm abs.	0.980
Weight of the catalyst, W, g	5.4516
External area of the pellet, S_c, cm^2	8.9884
Outside diameter, cm	1.53
Height of the pellet, cm	1.87
Volume of the pellet, V_c, cm^3	2.326
S_c/V_c, cm^2/cm^3	3.864
$S_x = S_c/W$, cm^2/g	1.649

			Mean
Total feedrate, F_T x 10^{-3} moles per min	19.56	16.35	
W/F_T ratio, x 10^3	0.279	0.333	
S_c/F_T ratio, x 10^3	0.460	0.551	
H_2O : CH_4 molar ratio	2.99	2.99	
Conversion, %	28.16	31.50	
x_{CH_4}, moles of CH_4 converted per mole of total feed	0.0709	0.0790	
N_{Re}	6.58	5.48	6.03
Mean linear velocity, cm/min	2154	1812	
Observed reaction rates:			
$dx_{CH_4}/d(W/F_T) = r_{obs,m}$ x 10^{-4}	1.264		
$dx_{CH_4}/d(S_c/F_T) = r_{obs,s}$, x 10^{-4}	0.757	0.789	
log $r_{obs,\ s}$	-4.121	-4.103	-4.112

Fig. 8.16. The Arrhenius Plot of $H_2O - CH_4$ System ($H_2O : CH_4 = 3.0$)

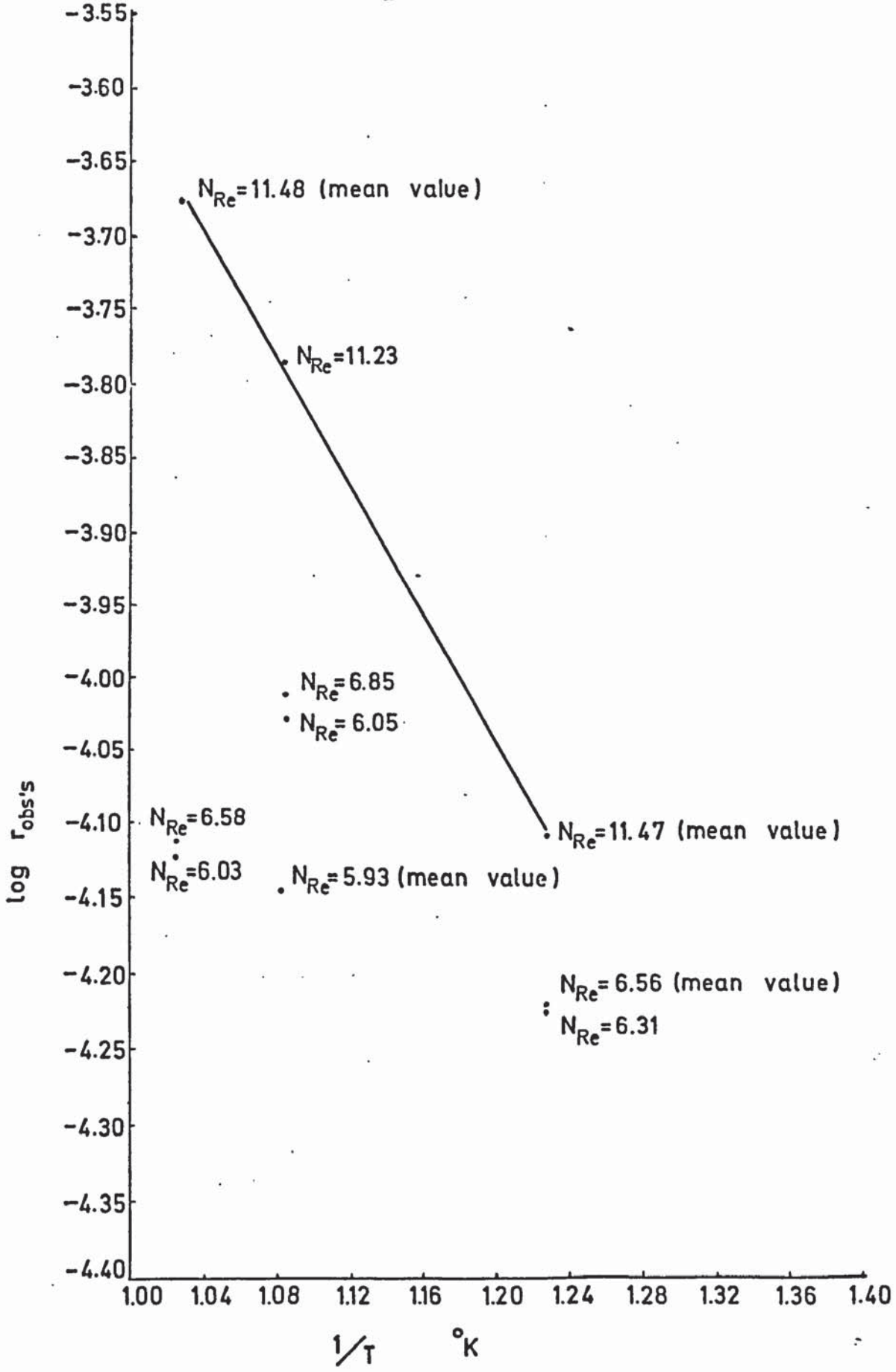

experimental observations, it was evident that for a given range of the Reynolds number, it was possible to ensure operating conditions at which film diffusion control was minimized. It is worth noting that the straight line relationship of this plot was obtained for very similar N_{Re}, whereas the corresponding values of total feedrate, W/F_T, and S_c/F_T ratios were all different.

8.6 EFFECT OF INITIAL REACTANT CONCENTRATIONS.

An analysis of the dependence of the observed rate of reaction on the feed composition may make two major contributions in establishing the intrinsic mechanism of a gas-solid catalytic system:

(i) on the assumption that the rate of the intrinsic reaction is controlled uniquely by one step, it may indicate the probable kinetic mechanism, i.e. distinction between either adsorption of any one of the reactants, or one of the probable chemical reactions taking place in a definite sequence, or desorption of any one of the products may be made.

(ii) it enables a determination of the order of the reaction with respect to each of the reactants.

8.6.1 Experimental Procedure.

The effect of the initial concentrations of the reactants on the extent of conversion was studied by conducting five series of runs each at six different values of steam to methane molar ratio in the feed. All the runs were carried out with cylindrical catalyst pellets and the experimental conditions are summarized below:

Temperature, ^{o}C	:	540 ± 1
Pressure, atm abs.	:	0.987 - 0.992
Catalyst mass,g	:	5.6724 5.7294 5.8183 5.7142 5.7313

Total feedrates, (10^{-3}) moles per min	:	56.74 - 61.65 28.34 - 31.21 19.38 - 21.17 14.29 - 15.46 9.70 - 9.72
W/F_T ratio, (10^3)	:	0.100 - 0.092 0.202 - 0.184 0.300 - 0.275 0.400 - 0.369 0.590 - 0.560
S_c / F_T ratio, (10^3)	:	0.135 - 0.124 0.270 - 0.245 0.397 - 0.363 0.538 - 0.497 0.791 - 0.751
H_2O : CH_4 molar ratio in the feed	:	2.0 ± 0.1 3.0 ± 0.1 4.0 ± 0.1 5.0 ± 0.1 6.0 ± 0.1 7.0 ± 0.1
Reynolds number	:	22.88 - 23.10 11.52 - 11.59 7.75 - 7.77 5.68 - 5.70 3.84 - 3.85

With the exception of the lowest one the selected feedrates were in the range in which the resistances induced by the bulk phase diffusion process were a minimum. Even the lowest steam : methane molar ratio in this series of runs was kept well above the thermodynamic minimum of 1.25 for the prevailing temperature and pressure conditions. This was considered desirable for two reasons:

(i) The mode of operation of the water feed pump at very low discharge rates, caused non-uniformities in the evaporation of water, and consequently, instantaneous fluctuations in the initial concentrations of the reactants, which could have falsified the results.

(ii) The presence of steam in the reacting mixture at higher partial pressures than the thermodynamic minimum easily prevented the possible accumulation on the active sites of any carbonaceous products or of kinetic carbon formed during the sequence of

reactions. Such accumulation would have reduced the activity of the catalyst.

8.6.2 Results and Discussion.

The results obtained are presented in Table 8.3 and as plots of conversion x_{CH_4} versus W/F_T and S_c/F_T values (Figs. 8.17 and 8.18) with CH_4 : H_2O molar ratio as a parameter. It is evident from Figs. 8.17 and 8.18 that an increase of methane partial pressure in the feed caused an increase of conversion if other operating conditions remained the same. This fact is also illustrated in Fig. 8.19 where the conversion is plotted against initial partial pressure of methane.

The derivatives of the curves given in Figs. 8.17 and 8.18 at different W/F_T and S_c/F_T ratios represent the values of the observed reaction rates based on the mass and external surface of the catalyst pellet, respectively. These values, calculated by numerical differentiation, are plotted versus W/F_T and S_c/F_T (Figs. 8.20 and 8.21), and are extrapolated graphically to $W/F_T = S_c/F_T = 0$ to obtain the initial reaction rates as indicated on the ordinates of respective plots. The variation of the initial reaction rates with the initial partial pressure of methane is shown in Figs. 8.22 and 8.23. Since the runs were carried out at barometric pressure, the partial pressure of the reacting components were equal to their mole fractions.

For the two reason given the functional relationship between the initial reaction rate and mole fraction of methane in the feed could not be studied over the whole range $0 < y_{CH_4,i} < 1.0$:

(i) in the region of very low water feedrates (i.e. high $y_{CH_4,i}$) operational restrictions of the water pumping system affected the uniformity of the feed composition ;

(ii) at the operating conditions relevant to the experimental runs, the upper limit for $y_{CH_4,i}$ from the thermodynamic point of view was calculated to be 0.44, beyond which a continuous deposition

TABLE 8.3

The Effect of Initial Reactant Concentrations on Conversion

	H_2O : CH_4 molar ratio					
	2.0	3.0	4.0	5.0	6.0	7.0
W/F_T $(x10^3)$	0.100	0.100	0.100	0.098	0.096	0.092
S_c/F_T $(x10^3)$	0.135	0.135	0.135	0.132	0.130	0.124
Conversion, %	4.40	5.03	5.31	5.47	5.53	5.52
x_{CH_4}	0.0146	0.0126	0.0106	0.0091	0.0079	0.0069
$r_{obs,m}=dx_{CH_4}/d(W/F_T)$ $x10^{-4}$	1.412	1.23	1.045	0.90	0.794	0.728
$r_{obs,s}=dx_{CH_4}/d(S_c/F_T)$ $x10^{-4}$	1.056	0.910	0.773	0.667	0.589	0.547
W/F_T $(x10^3)$	0.202	0.200	0.199	0.198	0.194	0.184
S_c/F_T $(x10^3)$	0.270	0.267	0.265	0.264	0.258	0.245
Conversion, %	8.58	9.84	10.39	10.68	10.78	10.71
x_{CH_4}	0.0285	0.0246	0.0208	0.0178	0.0154	0.0134
$r_{obs,m}=dx_{CH_4}/d(W/F_T)$ $x10^{-4}$	1.346	1.150	0.981	0.840	0.743	0.683
$r_{obs,s}=dx_{CH_4}/d(S_c/F_T)$ $x10^{-4}$	1.014	0.858	0.745	0.588	0.569	0.518
W/F_T $(x10^3)$	0.299	0.300	0.300	0.298	0.291	0.275
S_c/F_T $(x10^3)$	0.396	0.397	0.397	0.394	0.385	0.363
Conversion, %	12.41	14.23	15.10	15.54	15.68	15.52
x_{CH_4}	0.0414	0.0356	0.0302	0.0259	0.0224	0.0194
$r_{obs,m}=dx_{CH_4}/d(W/F_T)$ $x10^{-4}$	1.265	1.055	0.894	0.786	0.688	0.628
$r_{obs,s}=dx_{CH_4}/d(W/F_T)$ $x10^{-4}$	0.940	0.792	0.679	0.588	0.526	0.476

TABLE 8.3 (cont.)

	H_2O : CH_4 molar ratio					
	2.0	3.0	4.0	5.0	6.0	7.0
W/F_T $(x10^3)$	0.400	0.399	0.399	0.395	0.389	0.369
S_c/F_T $(x10^3)$	0.538	0.537	0.537	0.532	0.524	0.497
Conversion, %	16.05	18.25	19.39	19.96	20.16	20.04
x_{CH_4}	0.0535	0.0456	0.0382	0.0333	0.0288	0.0250
$r_{obs,m}=dx_{CH_4}/d(W/F_T)$ $x10^{-4}$	1.146	0.969	0.826	0.731	0.630	0.580
$r_{obs,s}=dx_{CH_4}/d(S_c/F_T)$ $x10^{-4}$	0.847	0.721	0.608	0.531	0.463	0.438
W/F_T $(x10^3)$	0.591	0.590	0.590	0.590	0.590	0.560
S_c/F_T $(x10^3)$	0.793	0.791	0.792	0.792	0.791	0.751
Conversion, %	22.09	25.04	26.66	27.74	28.35	28.42
x_{CH_4}	0.0735	0.0626	0.0533	0.0463	0.0405	0.0355
$r_{obs,m}=dx_{CH_4}/d(W/F_T)$ $x10^{-4}$	0.906	0.741	0.648	0.566	0.511	0.4592
$r_{obs,s}=dx_{CH_4}/d(S_c/F_T)$ $x10^{-4}$	0.668	0.556	0.477	0.418	0.371	0.338

Fig: 8.17 The Effect of Initial Reactant Concentrations on Conversion

($\alpha = H_2O : CH_4$ molar ratio in the feed)

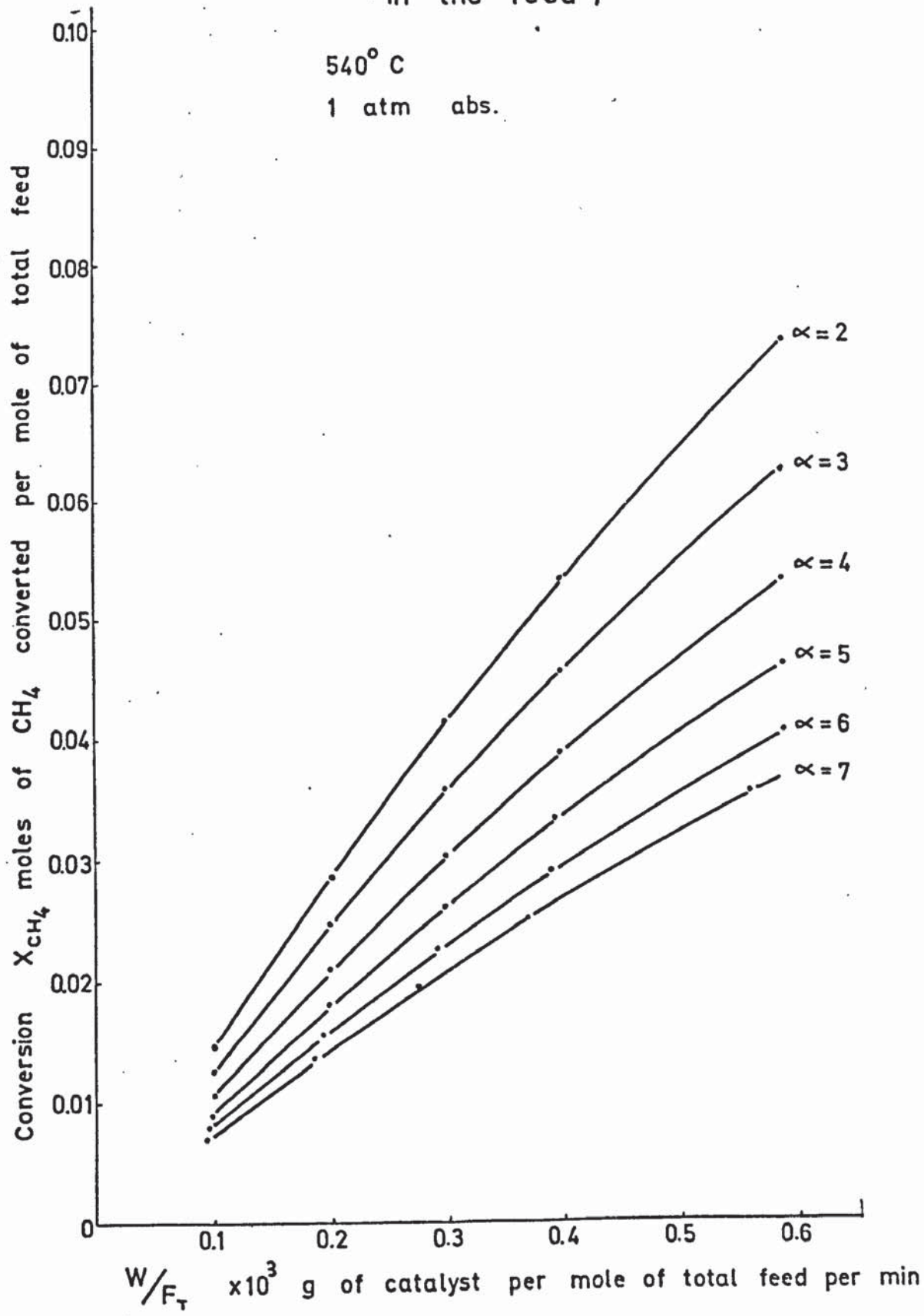

Fig: 8.18 The Effect of Initial Reactant Concentrations on Conversion.

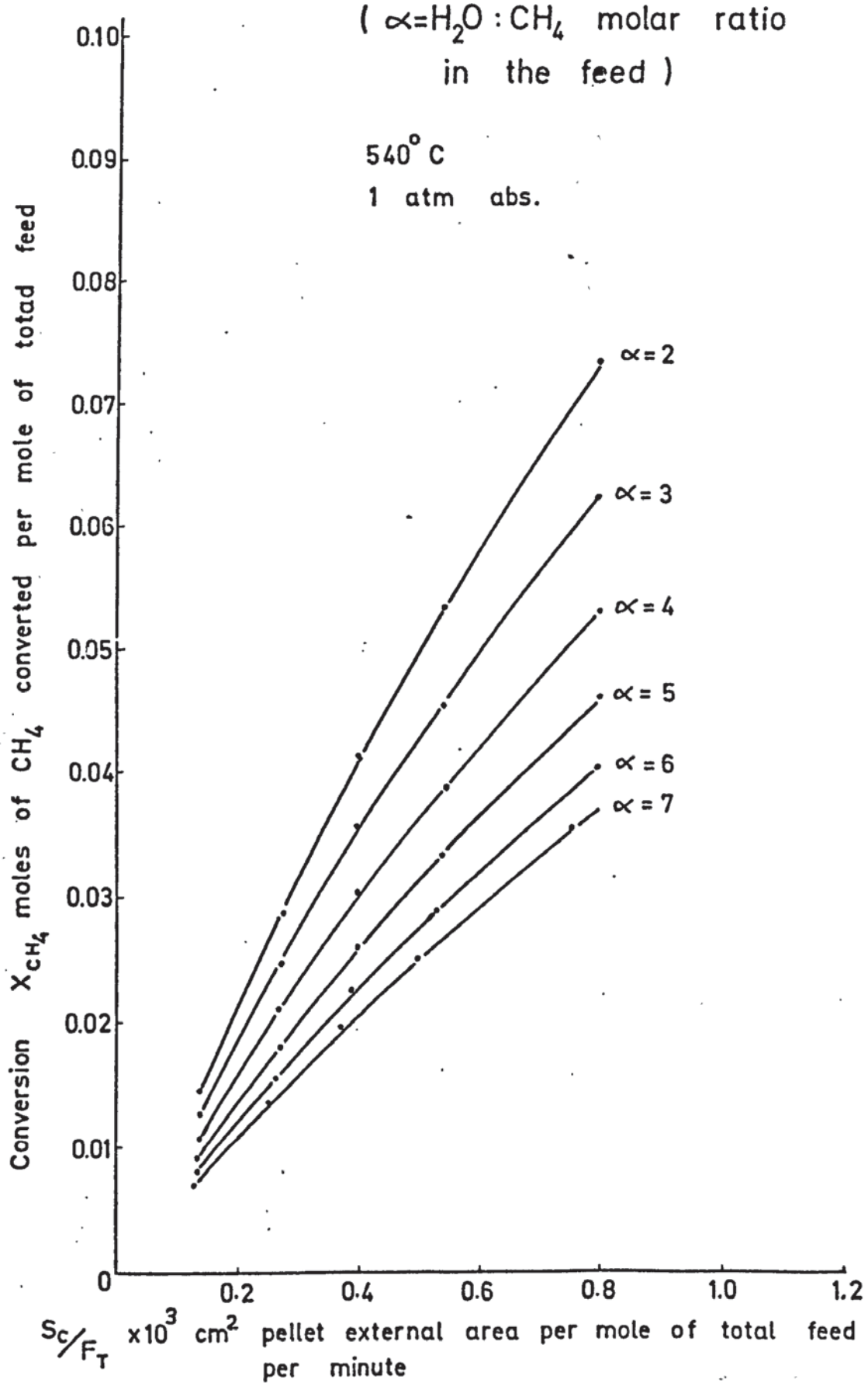

Fig: 8.19 The Conversion X_{CH_4} as a Function of Initial Partial Pressure of Methane

$(p_{CH_4,i} = y_{CH_4,i})$

Curves	1	2	3	4	5
$W/F_T \times 10^3$	0.092 - 0.10	0.184 - 0.202	0.275 - 0.300	0.369 - 0.400	0.560 - 0.591
$S_c/F_T \times 10^3$	0.124 - 0.135	0.245 - 0.270	0.363 - 0.397	0.497 - 0.538	0.751 - 0.793

540° C

1 atm abs.

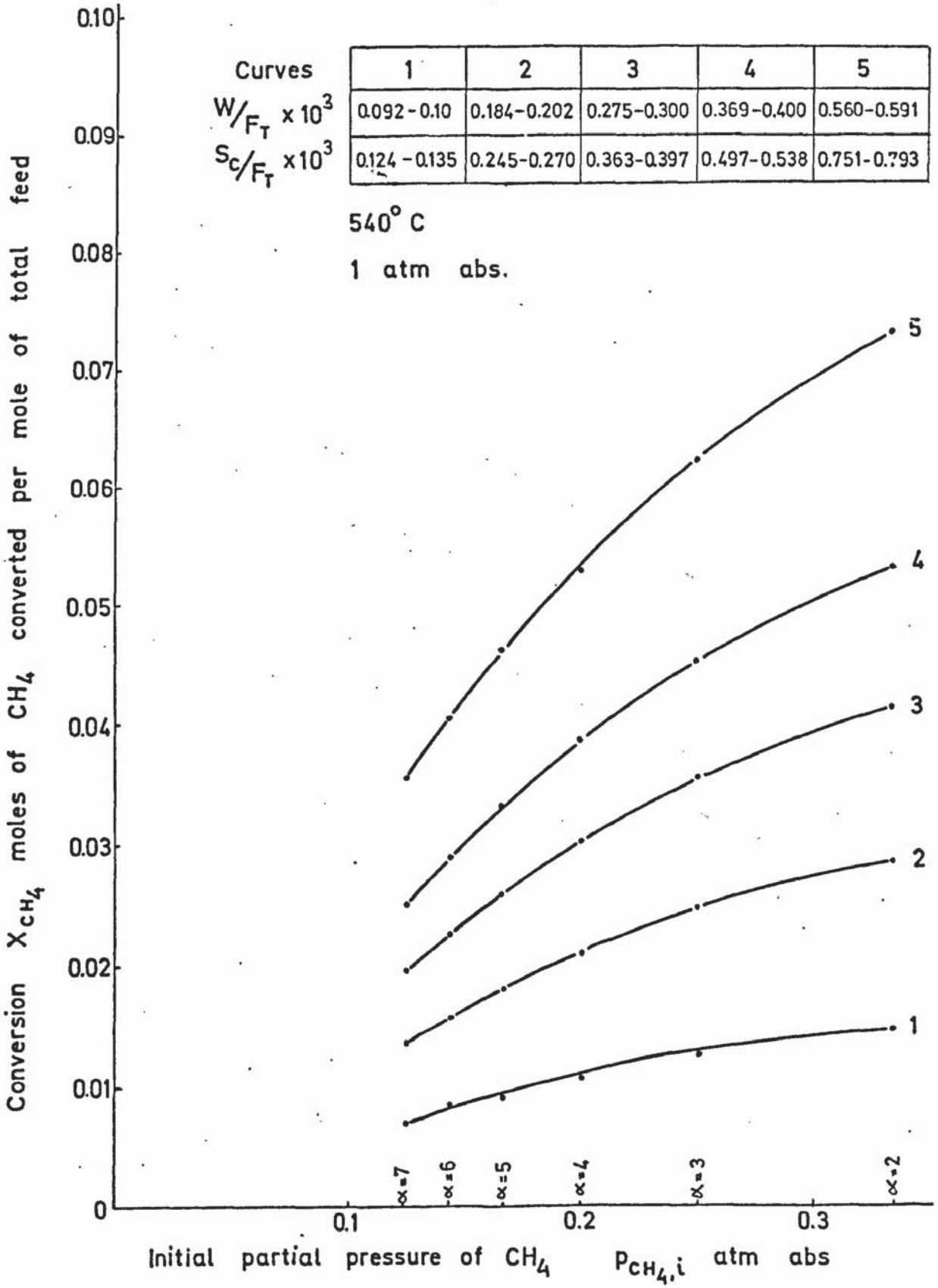

Fig: 8.20 The Observed Reaction Rate $r_{obs,m}$ as a Function of $\frac{W}{F_T}$ Ratio

($\alpha = H_2O : CH_4$ molar ratio in the feed)

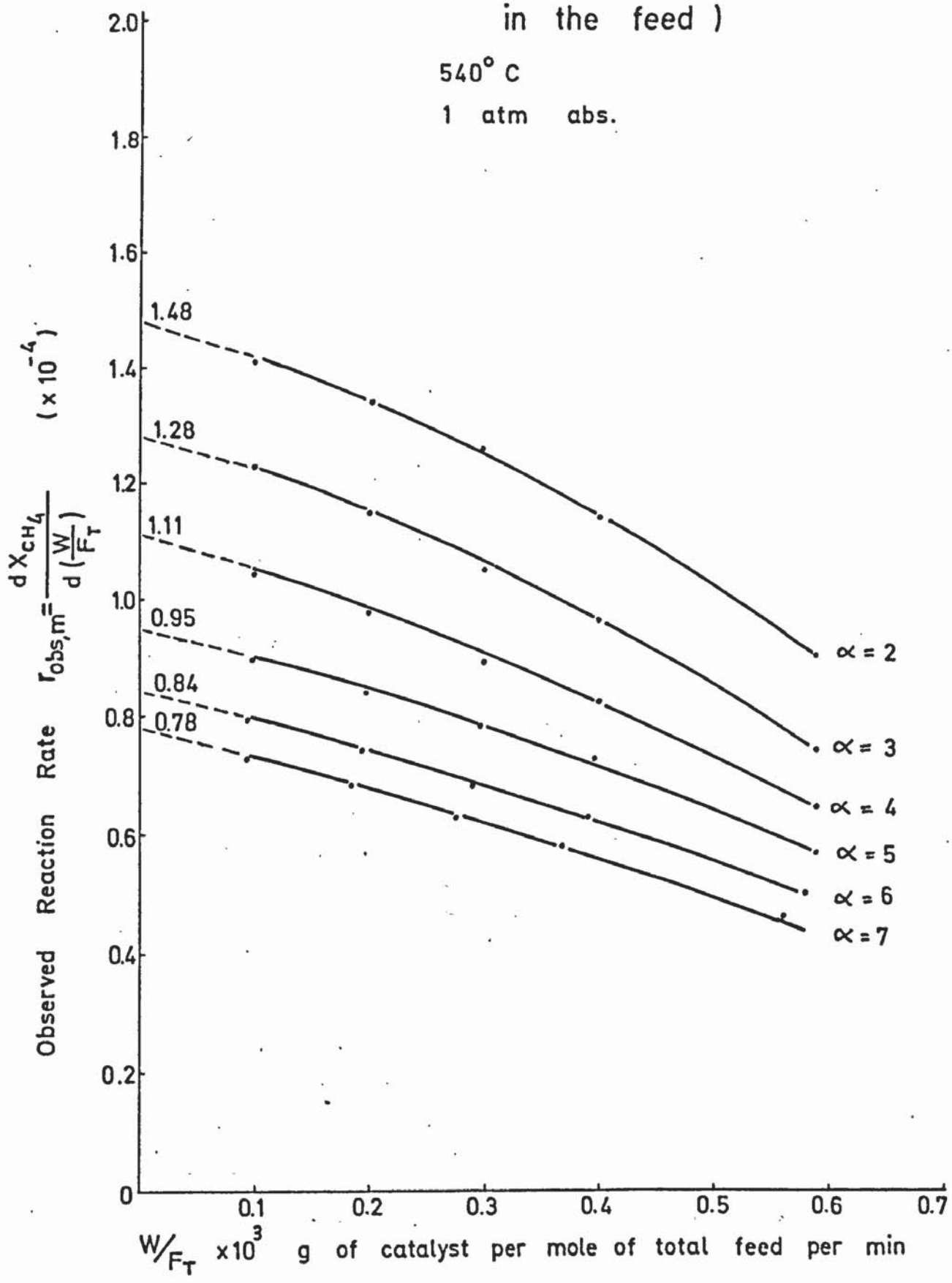

Fig: 8.21 The Observed Reaction Rate $r_{obs,s}$ as a Function of $\frac{S_c}{F_T}$ Ratio.

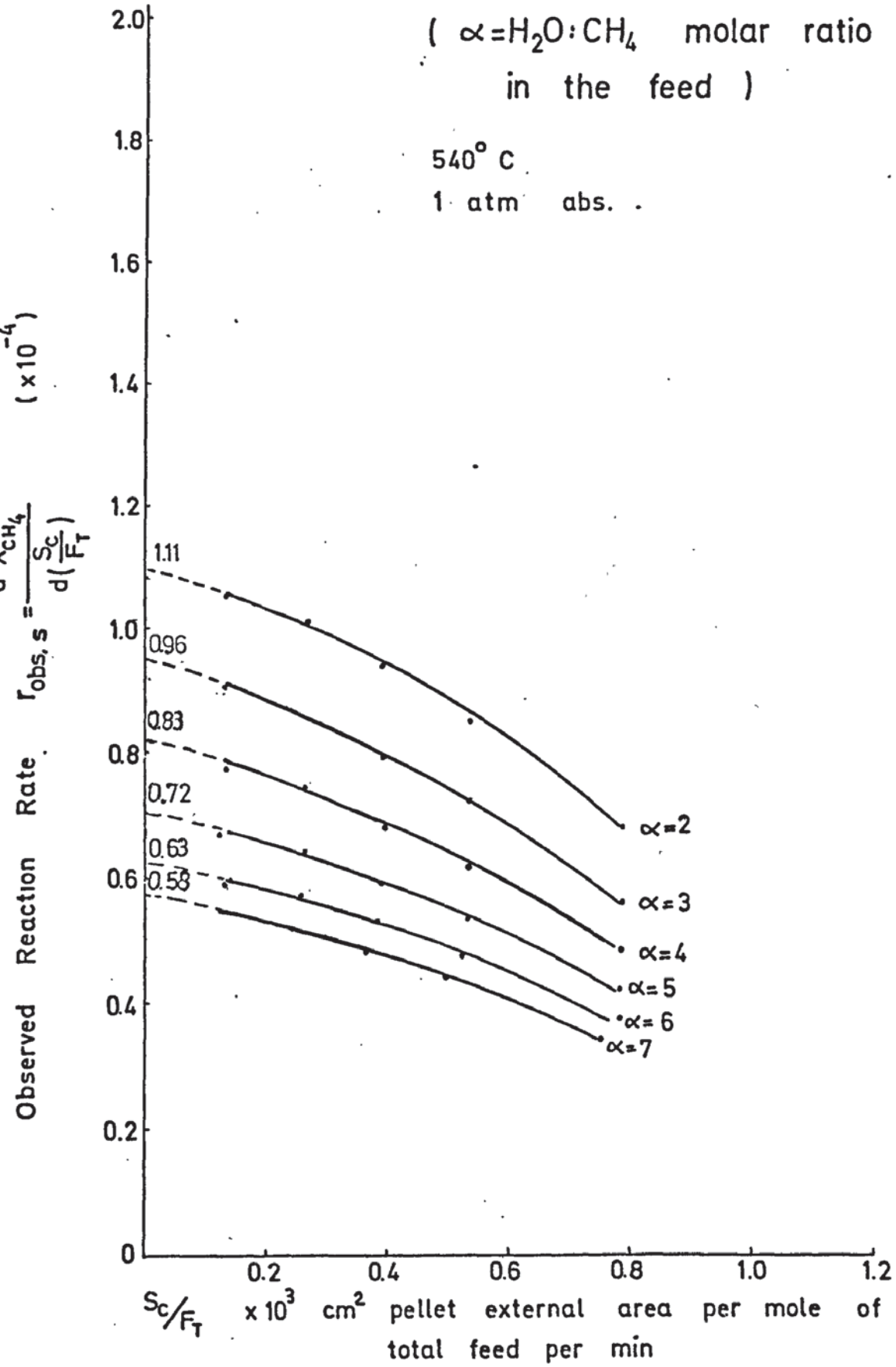

Fig: 8.22. The Initial Reaction Rate $r_{obs,m,i}$ as a Function of Initial Mole Fraction of CH_4 $y_{CH_4,i}$

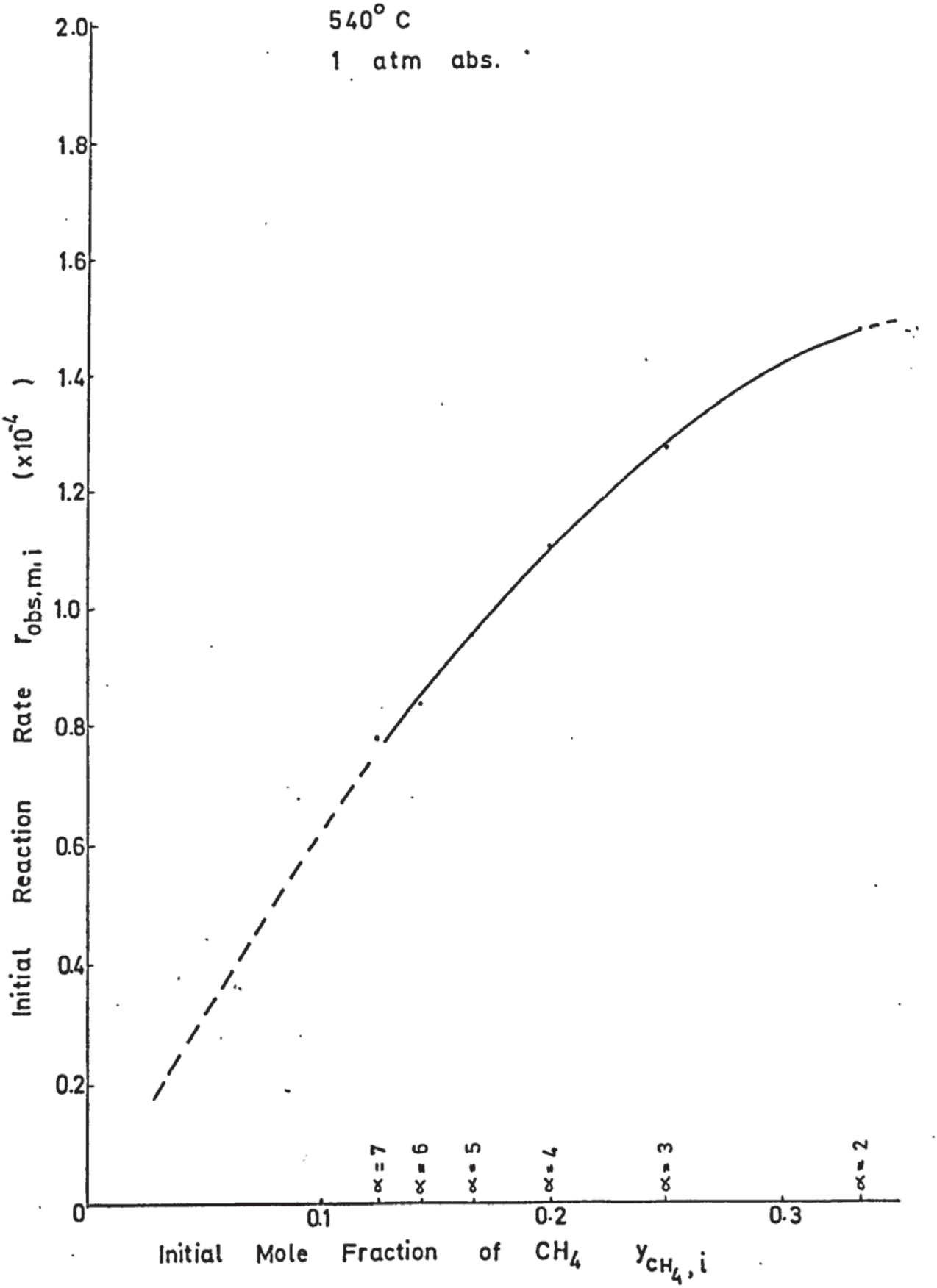

Fig: 8.23. The Initial Reaction Rate $r_{obs,s,i}$ as a Function of Initial Mole Fraction of CH_4 $y_{CH_4,i}$

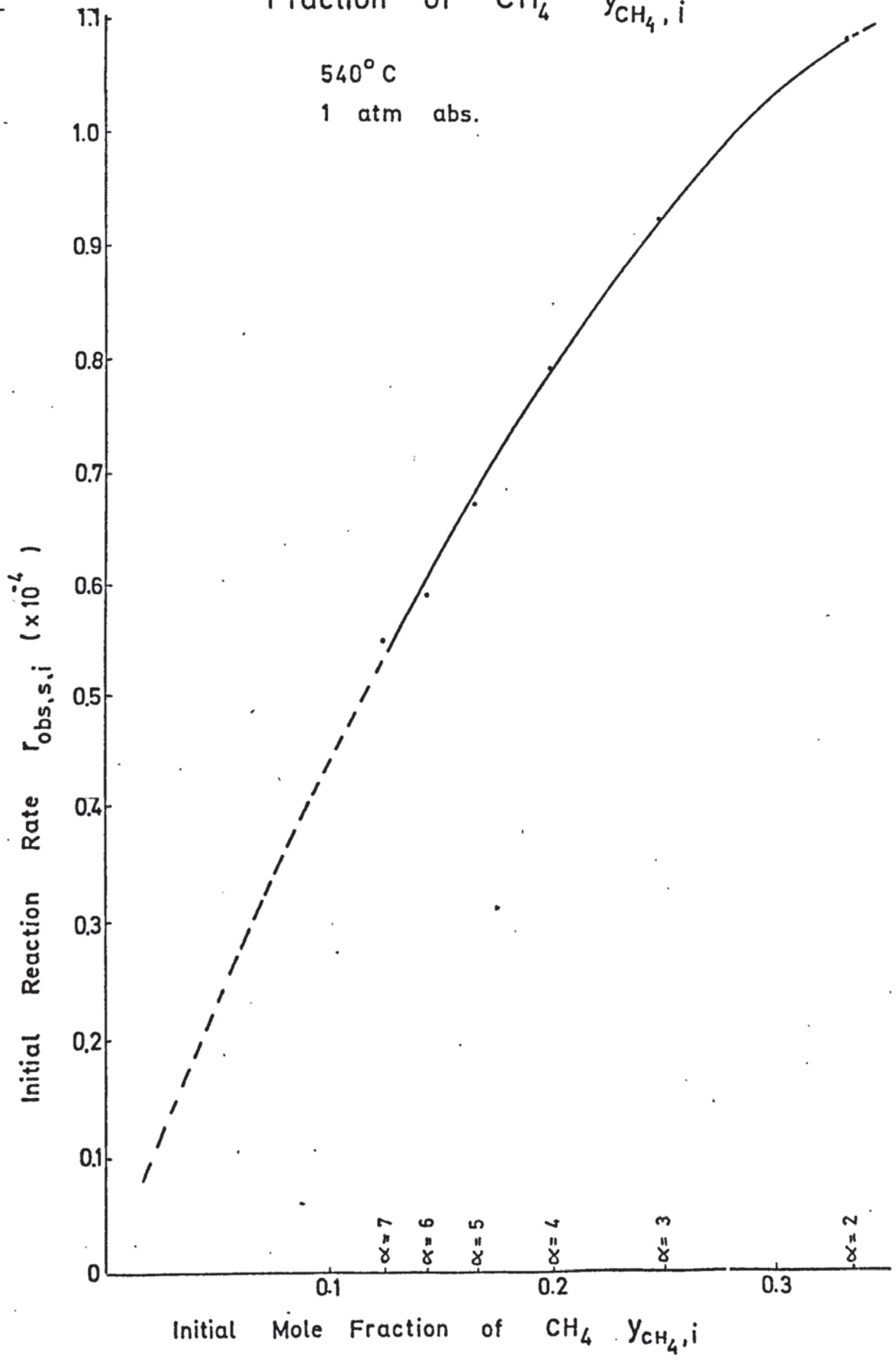

of equilibrium carbon would take place, provided that the reacting system had attained thermodynamic equilibrium. Although the catalyst mass in the reactor and the flow conditions were not adequate to enable a close approach to equilibrium, an increase of methane mole fraction to this limiting value would definitely have promoted the formation and probable build-up of kinetic carbon.

Thus it was practically impossible to cover the whole range of variation of $y_{CH_4,i}$ between 0 and 1.0. In the present work the initial mole fraction of methane was increased up to 0.333.

In spite of the termination of the curve at $y_{CH_4,i} = 0.333$, the plot "initial reaction rate $r_{obs,s,i}$ against methane mole fraction" tends to give a maximum most likely between 0.33 and 0.50, which would correspond to the stoichiometric feed composition according to the reactions:

$$CH_4 + H_2O \rightarrow CO + 3\ H_3 \text{ and}$$
$$CH_4 + 2\ H_2O \rightarrow CO_2 + 4\ H_2,$$

provided that the reaction is controlled over the whole range of $y_{CH_4,i}$ by a single rate-limiting step.

However, discussion is worthwhile of other possibilities for the shape of the curve within and outside the range investigated:

(i) the curvature in the region $0.20 < y_{CH_4,i} < 0.33$ may be due to experimental erros and incorrect extrapolation in obtaining the intial rates, so that the functional relationship between $r_{obs,i}$ and $y_{CH_4,i}$ is essentially linear, indicating that the overall rate is controlled by the adsorption process of methane or steam, or

(ii) the curve may continue asymptotically in the horizontal direction

beyond $y_{CH_4,i} = 0.33$, suggesting a desorption controlled reaction mechanism within this region.

The first argument is unlikely to be valid, since the experimental data was sufficiently consistent and the error in graphical extrapolation was within $\pm$ 2%, whilst an error of approximately 20% would have been necessary at the point $y_{CH_4,i} = 0.33$, if the relationship between $r_{obs,i}$ and $y_{CH_4,i}$ were linear.

An asymptotic behaviour of the curve in Fig. 8.22 within the range $0.33 < y_{CH_4,i} < 1.0$ would have indicated that the reaction is controlled either by the adsorption of methane or by the chemical reaction in the region of low $y_{CH_4,i}$, and governed by the desorption of any of the reaction products in the region of higher $y_{CH_4,i}$.

Since the extent of conversion was not affected by an increase of total pressure (Section 8.4), it was previously concluded that the adsorption of the reactants did not have a controlling influence on the course of the overall reaction. This is now supported by the non-linear relationship between $r_{obs,i}$ and $y_{CH_4,i}$ (Figs. 8.22 and 8.23) at least for operating pressures $\geqslant$ 1 atm abs. and for $y_{CH_4,i} \geqslant 0.1$.

If it is assumed that the overall reaction is controlled by a single rate-limiting step, then the only remaining alternative is that the overall reaction is controlled by the chemical reaction stage.

It has been explained why the path of the curve beyond $y_{CH_4,i} = 0.44$ cannot be defined on an experimental basis. However, assuming that the pattern traced by the curve exhibits a maximum, it becomes evident that it will terminate at $r_{obs,i} = 0$, $y_{CH_4,i} = 1.0$, since in this extreme case of the absence of steam, there will be no reaction. According to Yang and Hougen (184), the inverse parabolic pattern of the plot of " observed reaction rate against mole fraction of limiting component A", intercepting the abcissa at $y_A = 0$ and $y_A = 1.0$ may also

be evidence of a desorption controlled reaction mechanism; however, it is stated that this is confined only to reactions of the type $A + B \leftrightarrows R$.

It is also of interest to consider the effects of the extent of conversion on the magnitude of the observed reaction rates. The experimental results obtained from this particular series of runs are cross-plotted as observed reaction rate $r_{obs,m}$ against conversion x_{CH_4} at different values of W/F_T ratio, the steam : methane molar ratio being the parameter (Fig. 8.24). The curves exhibit a consistent behaviour which is not affected by the change of feed composition.

Yang and Hougen (182) have briefly referred to the effects of conversion on the observed reaction rate with regard to the selection of a plausible mechanism and rate-controlling step and indicated that, in general, when adsorption is controlling the rate against conversion curve is concave downwards, and when surface reaction is rate-controlling it is concave upwards. This statement implied that if the chemical reaction is the rate-controlling mechanism, the plot conversion versus W/F_T ratio should show in general a steep increase in the region of very low W/F_T ratios, levelling off almost immediately in the horizontal direction at increasing W/F_T values, whereas in an adsorption controlled reaction regime a rather smooth increase and levelling off of this curve is expected.

The findings of the present investigation seem to contradict this argument. Indeed, although it has been established from different points of view that the adsorption of reactants was not of a controlling character on the overall rate of reaction, the curves in Fig. 8.24 are concave downwards, indicating according to Yang and Hougen an adsorption controlled mechanism. The reasons for the contradiction are twofold :

(i) the data in this series of runs were confined to extremely low

Fig: 8.24. Effect of the Extent of Conversion X_{CH_4} on the Observed Reaction Rate $r_{obs,m}$

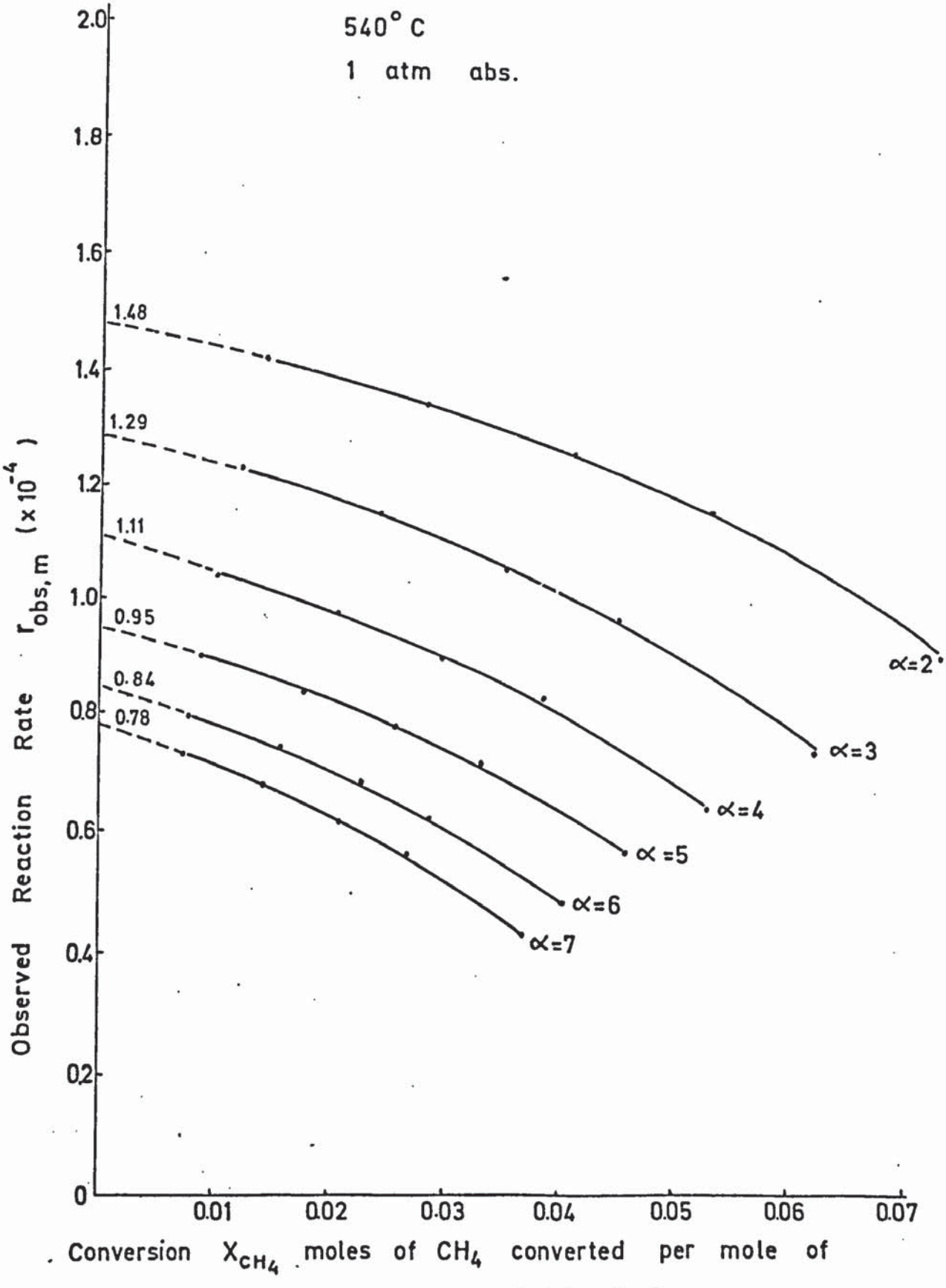

W/F_T values, so that at higher values of W/F_T a concave trend of the curves could be obtained. In fact, a fairly rapid levelling off of the plots of conversion versus W/F_T ratio has been observed at high values of W/F_T. (Fig. 8.1)

(ii) The reaction mechanism of the steam-methane catalytic system involves a sequence of degradation reactions of methane to form methyl, methylene and/or CH - radicals and is followed by the water gas shift reaction as an additional catalytic process which comprises identical controlling effects of surface phenomena. It is not inconceivable, therefore, that the complex nature of the system and the integral effect of the interactions in the intermediate steps (in spite of the steady-state assumption) are the principal causes for the contradiction.

As a matter of fact, the shape of this curve within a fairly narrow range of conversion cannot be a reliable and conclusive criterion in selection of the kinetic mechanism and the rate-controlling step of a catalytic system over a wide range of operating conditions, since experimental errors of even a very small magnitude would affect the numerical value of the derivatives of the curves of conversion versus W/F_T which give the values of observed reaction rate.

8.6.3 Conclusion.

From the discussion above, it is definitely concluded that within the range of operating parameters considered in the experimentation, the initial reaction rate is controlled by a chemical reaction step involved in the sequence of surface reactions. At higher concentrations of methane in the initial feed, it is conceivable that desorption of one of the products may also become rate controlling, provided that the plot "initial reaction rate against mole fraction of methane" becomes asymptotic at higher $y_{CH_4,i}$ values.

8.7 PORE-DIFFUSION LIMITATIONS.

The effects of pore diffusion resistances on the apparent mechanism and on the rate equation of a gas-solid catalytic reaction are discussed in Section (7.4.1). The experimental procedures and criteria generally practiced for a qualitative estimation of mass transfer resistances in the pores and for the calculation of the effectiveness factor of a catalyst are outlined in Sections (7.4.3) and (7.4.4). From the relationship between the effectiveness factor and the Thiele modulus $\emptyset$, it is evident that the pore diffusion resistances of a catalyst with given pore size distribution and activity characteristics are minimized, and the effectiveness factor approaches unity as an asymptote

(i) if the length parameter of the catalyst particle is small, or

(ii) if the intrinsic rate constant is small, or

(iii) if the effective diffusion coefficient is large.

Since the reactants, their concentrations in the reactor input stream, and specific pore properties were the same within the scheme of the experiments, it is assumed that the effective diffusivity of the reacting species remained unchanged. Hence, in the kinetic part of the study, in order to reduce the extent of diffusional gradients inside the pellet, a low reaction temperature 540° C, has been chosen, diminishing the intrinsic rate constant of the surface phenomena so that the potential required to provide the diffusion flux becomes insignificant, and intrinsic kinetics could be observed. In view of the temperature levels usually applied in large scale reforming processes of methane (750 - 800° C), the temperature of the experiments was therefore rather low. Since there was no information available on the particle size of catalyst having an effectiveness factor η approaching unity, it was not possible to calculate η of the pellets used in the present investigation from

the rate per unit mass or volume of catalyst tested in the experiments to that given for the finer size having $\eta \approx 1$. Therefore, it was decided to perform a series of runs with finely divided catalyst until no increase in rate per unit quantity of catalyst occurred on sub-division. The particle sizes tested and the results obtained are detailed in the next section.

8.7.1 Experimental Procedure.

The catalyst pellets were first crushed in a glass pestle and mortar and then ground in a cylindrical porcelain ball mill. In order to minimize the possible contamination of the catalyst material with the silica which might come from simultaneous grinding of the porcelain balls, large size pellets were used as the grinding medium. The ground material was separated on B.S. sieves to the following mesh sizes :

B.S. Sieves No.	Nominal Aperture μ
30 - 25	500 - 600
44 - 36	355 - 425
60 - 52	250 - 300
85 - 100	150 - 180

The particles were assumed to have a mean diameter, d_p, corresponding to the average of the nominal apertures of the sieve fractions. The deviation from spherical geometry was allowed for by multiplying d_p by a shape factor ϕ_s. This factor (sphericity) was estimated according to the method of Rittenhouse (136) based on the visual comparison of the particles photographed under the microscope with those in a standard table.

The reactor used in these experiments is described in Section 4.3.1 and the following operating conditions were applied :

Temperature, ^{o}C : 540 ± 1

Pressure, : barometric

H_2O : CH_4 molar ratio : 3.0 ± 0.1

W/F_T ratio (10^3)	:	0.1 - 1.0
Catalyst mass, g	:	0.8735 (251 - 295 μ) 0.8887 (251 - 295 μ) 0.8854 (251 - 295 μ) 0.9037 (425 - 699 μ) 0.9250 (353 - 725 μ) 2.8548 (353 - 600 μ) 1.3360 (500 - 600 μ)

The procedures for catalyst activation and adjustment of the flowrates of methane and steam were identical to those applied in the runs carried out with cylindrical pellets.

8.7.2 Results and Discussion.

All the runs with ground catalyst resulted in massive carbon deposition independent of the feedrate of the reactant or W/F_T ratio. The formation of carbon started apparently as soon as the steam-hydrogen mixture of the activation stage was replaced by the steam - methane mixture, since even the first sample taken from the reactor exit gas stream gave a very low conversion compared to that obtained with cylindrical pellets at similar catalyst mass and W/F_T ratio. (Table 8.4). It is mentioned in Section 4.6.2 that a period of 2 - 3 hours was allowed to attain steady-state temperature and activity conditions in the catalyst bed. The following observations were the evidence suggesting that carbon formation was taking place:

(i) the mass balance checks showed large discrepancies in favour of hydrogen concentration in the exit stream,

(ii) an increase of the feedrate to give a W/F_T ratio of approximately (0.1) (10^3) resulted in the build-up of a back-pressure in the reactor up to 10 psig which led to the conclusion that the catalyst bed was choked with agglomerated particles.

Prolonged operation at low flowrates also caused a significant change in the extent of conversion. At higher feedrates the conversion dropped to lower levels than the increased flow could account for, and this was attributed to channelling effects. The results obtained were

TABLE 8.4

Effect of Particle Size on Conversion

Particle size (μ)	Catalyst Mass (g)	W/F_T (10^3)	F_T (10^{-3})	Conversion %	Difference in H_2-mass balance	W/F_T (10^3)	F_T (10^{-3})	Conversion %	Difference in H_2-mass balance
353 < <425	0.925	0.235	3.93	6.40	-	0.161	9.53	2.86	2.81
N_{Re}			0.75				1.83		
353< <600	2.8548	0.310	9.20	13.70	0.61	0.178	15.97	6.53	-
N_{Re}			1.87				3.10		
500< 600	1.3360	0.361	3.71	4.78	0.10	0.169	7.89	1.82	0.23
N_{Re}			0.98				2.10		
Pellet (cm) ø=1.54 h=1.88	5.3815	0.252	21.36	13.18	0.09	0.170	31.64	9.54	0.22
N_{Re}			8.52				12.68		
ø=1.08 h=4.11	5.1632	0.315	16.40	22.68	0.09	0.200	25.86	16.03	-0.01
N_{Re}			7.50				11.91		
ø=1.17 h=2.55	3.8964	0.327	11.93	21.96	-0.38	0.167	23.38	12.33	-0.51
N_{Re}			5.30				10.49		
ø=1.52 h=1.79	5.2133	0.300	17.38	14.59	0.05	0.170	30.61	9.37	0.23
N_{Re}			6.97				12.35		

rather inconsistent because of the extent and progress of carbon deposition and plugging of the catalyst bed. This severe carbon deposition and blocking of the bed was firstly attributed to the presence of pumice layers, between which the catalyst bed was sandwiched. It was thought that the carbon, formed primarily on pumice particles by the pyrolysis of methane, caused agglomeration within the layers which led to channelling of the gas and decreased the contact time. The entrainment of nascent carbon by the gas stream into the catalyst bed could also have been a reason for the deactivation. Therefore other runs were performed without pumice layers ; the results obtained, however, showed that the presence or absence of pumice layers had no influence on the onset of carbon formation.

The catalyst charge in each run was not sufficient to make a sieve analysis to determine the degree of agglomeration of particles. A visual examination of the grains under the microscope indicated that a size enlargement had occurred.

It is worthwhile recording that a gradual increase of steam : methane molar ratio in the feed from 3.0 to 7.0 without interrupting the operation did not restore the activity of the catalyst nor did it prevent blocking of the bed.

Similar observations are reported by Schnell (146) who conducted experiments for steam-reforming of butane and propane with nickel supported on α - Al_2O_3 catalyst, which was prepared by impregnation of α - Al_2O_3 pellets with nickel nitrate solution followed by drying, calcination at 500° C, and grinding. (Ni = 4.1 %, surface area 8.0 m^2/g). The particle size used in the runs corresponded to the sieve fraction 18 - 25 B.S.S. (600 - 855 μ). He found that, in reforming of propane at 600° C and barometric pressure, it was necessary to operate at a steam : carbon ratio of 10, because at lower steam ratios the catalyst

bed rapidly became choked with carbon deposits. It is also stated, however, that the runs performed with the alkalized catalyst 46 - 1 (which is the same as the catalyst used in the present investigation), and butane as feedstock did not cause a lay-down of kinetic carbon for the same catalyst size and temperature-pressure conditions even at a steam : carbon ratio as low as 3.0. The reason for this different behaviour is not discussed by Schnell (146); nevertheless according to other investigations in this field, it may be attributed to the presence of potassium in the 46 - 1 catalyst, which acted as a promoter for the carbon-steam reaction and prevented the build-up of non-equilibrium carbon (8, 31).

From the results of a series of experiments obtained in a laboratory pressure reformer and with naphtha as feedstock, Andrew (8) concluded that at steam-reforming temperatures cracking of hydrocarbon can occur not only by catalytic action, but also at a substantial rate homogeneously in the gas phase. In fact, the minimum steam ratio used in these experiments had to be increased with the dilution of the catalyst(nickel on china clay), with low specific surface and inactive Al_2O_3 in varying proportions. By diluting the bed, the heterogeneous catalytic surface was diminished in proportion, but the voidage of the bed remained virtually unchanged. Substituting the catalyst completely with inactive α - Al_2O_3 did not result in massive carbon formation even at low steam ratios, as would have occurred if only a small amount of nickel catalyst had been introduced into the reactor. It thus appeared that the presence of both the voidage and the nickel as the active constituent of the heterogeneous surface were prerequisites for massive carbon formation.

On the basis of this conclusion the increase of the susceptibility of the catalyst for the irreversible formation of non-equilibrium carbon with decrease in particle size, as it was observed in the present work, can be explained in qualitative terms. The reduction of particle

diameter brought about two changes in the physical characteristics of the catalyst bed:

(i) the external surface area of the catalyst per unit volume of the bed was increased, consequently a greater degree of active surface was made easily accessible to the reacting gas and more catalytic area was brought into contact with void volume.

(ii) the slight decrease of the bulk density of the bed with decreasing particle size indicated an increase of the bed voidage.

This should not have occurred actually if the grains were perfectly spherical and if the packing of the bed at each diameter fraction were orderly. However, since the particles were not spherical as determined from the magnified photographs of the grains by a microscope, and the bed was randomly packed, the variation of the bulk density was not unexpected. The decrease of bulk density has virtually an opposite effect to the increase of external area of particles exposed to gas flow since an increase of void volumewould mean less catalyst material per unit volume. The data available was not sufficient to draw definite conclusions as to which of the two factors responsible for the massive carbon deposition was governing the overall phenomenon.

It is interesting to note that the carbon formation took place in spite of the presence of potassium incorporated in the catalyst structure as a promoter of the carbon removal reactions. This is in contradiction with Schnell's observations, although the hydrocarbon feed was not the same in both cases. No entirely satisfactory explanation for this difference is offered, but it may be attributable to the following:

(i) In Schnell's apparatus the bed dimensions were very small

(2 mm diameter, 3 - 4 mm bed height), whereas in the present work the reactor diameter was ¼ inch O.D. and the bed height varied between 10 - 30 mm.

(ii) The feedrates used by Schnell were very high so that conversions were obtained at extremely short contact times (10^{-3} - 10^{-5} sec), whilst in this investigation the feedrate corresponded to contact times of the magnitude of 10^{-1} - (2) (10^{-3}) sec.

In conclusion, it was impossible to assess the extent of the pore diffusion resistances by the experimental method of particle size reduction.

The strong dependence of the conversion on the external surface of the cylindrical pellet indicated, however, that the pore diffusion limitations were not of negligible order of magnitude. The average pore diameter and the relatively high activity of the freshly reduced catalyst supported this. In fact, in the reforming experiments performed with 46 - 1 and with butane as feedstock at 600° C and 1 atm abs. pressure, Schnell (146) observed an increase in conversion from 8.7 % with 1/8 inch (3.2 mm) cylindrical pellets to 42.0 % with granular catalyst having particle diameter 14 - 22 B.S.S. (1.18 - 0.71 mm). Thus, it was considered worthwhile to make a further attempt to evaluate the effectiveness of the catalyst based on the assumption that $\eta < \approx 0.1$. No separate runs were carried out, but the results used to establish film-diffusion resistances were used for this purpose. For this asymptotic condition, the functional relationship between and Thiele modulus ϕ takes the form

$$\eta = \frac{1}{\phi} \qquad (7.35)$$

independent of catalyst geometry and kinetic nature of the reaction, provided that isothermal conditions prevail in the catalyst particles. Consequently, $r_{obs,v}$ becomes inversely proportional to the length

parameter of the pellet which is defined by the ratio of volume of pellet to its external surface area. If $r_{obs,v,1}$ and $r_{obs,v,2}$ are the rates of reaction observed in different cylindrical pellets having outside diameters D_1 and D_2, inside diameters d_1 and d_2, and heights h_1 and h_2, then

$$r_{obs,v,1} = \frac{1}{\phi_1} \; k_{v_1} \; f\,(C_A, \cdots\cdots)_{S,1} \tag{8.16}$$

$$r_{obs,\,v,2} = \frac{1}{\phi_2} \; k_{v_2} \; f\,(C_A, \cdots\cdots)_{S,2} \tag{8.17}$$

where the observed reaction reates and the specific reate constants are based on the volume of the catalyst, respectively. The underlying assumptions for such a computation are detailed in Section 7.4.1. Since the runs were carried out at identical temperature, pressure, flow conditions, and initial feed composition, the rate constant and the concentration dependent term of the rate expression of Equations (8.16) and (8.17) were equal. Thus

$$r_{obs,v,1} : r_{obs,v,2} = \frac{\phi_2}{\phi_1} \tag{8.18}$$

Since it was assumed that the effective diffusitivies of all species were constant, and independent of the extent of conversion and of volume increase on reaction, then the ratio $\frac{\phi_2}{\phi_1}$ can be replaced by the ratio of the length parameters $\frac{L_2}{L_1}$. The assumption of constant effective diffusivity is justified for Knudsen mode diffusion which according to the pore radii distribution, was in fact predominant. The increase in volume on reaction has no influence on effective diffusivity, if the mass flux is expressed by Fick's law and the mass transfer occurs only by Knudsen diffusion, but an increase in number of moles on reaction causes a variation of the total pressure through the pellet modifying the concentration gradients, and makes it more difficult for reactants to diffuse into the pores. Hence its effect is to decrease the effectiveness factor. The reversibility of the reaction acts in the

same direction.

Since the length parameter is defined by the ratio of the volume of pellet to its external surface area :

$$\frac{L_2}{L_1} = \frac{(D_2^2 - d_2^2)}{(D_1^2 - d_1^2)} \cdot \frac{D_1}{D_2} \qquad (8.19)$$

The values of the observed rates of reaction are obtained by numerical differentiation of the curves x_{CH_4} plotted versus W/F_T as represented in Fig. 8.1. Since the reaction rate per unit volume of the catalyst pellet $r_v = \rho_p r_m$,

$$\frac{r_{obs,m,1}}{r_{obs,m,2}} = \frac{\rho_{p_2} \cdot (D_2^2 - d_2^2)}{\rho_{p_1} (D_1^2 - d_1^2)} \frac{D_1}{D_2} \qquad (8.20)$$

where ρ_p is the apparent density of the pellet. The ratio $\rho_{p_2} : \rho_{p_1}$ differed slightly from unity. The evaluation of the ratio of the observed reaction rates was made for flowrates corresponding to high and low Reynolds numbers, thus indicating the effects of film-diffusion resistances on the values of observed reaction rates.

The results of these calculations are presented in Tables 8.5 - 8.8. The ratio of the observed reaction rates are calculated for four pairs of catalyst pellets at four different values of W/F_T. It can be seen from the tables that the values of this ratio were in most cases in close agreement with the ratio of the length parameters of the pellets. The deviations may have originated from:

(i) The magnitude of the effectiveness factor of the pellet may be slightly greater than 0.1 so that the assumption of an inverse relationship between η and Thiele modulus $\emptyset$ might have caused the differences. In fact, the ratio of the observed reaction rates were, in general, greater than the ratio of length parameters indicating greater effectiveness.

(ii) The numerical differentiation of the plots x_{CH_4} versus W/F_T was

TABLE 8.5

Ratio of Observed Reaction Rates for Different Pellet Dimensions

Pellet Characteristics	Pellet No. 1	Pellet No. 2
Mass, W g	5.3815	5.1632
Ext.Area, S_c cm^2	9.0955	13.9449
Density, ρ_p g/cm^3	2.232	2.415
O.D., D cm	1.54	1.08
I.D., d cm	1.02	0.75
D^2-d^2 cm^2	1.3312	0.6039
$\rho_{p_2} \div \rho_{p_1}$	1.082	
$D_1 \div D_2$	1.426	
$(D_2^2-d_2^2) \div (D_1^2-d_1^2)$	0.454	
$\frac{\rho_{p_2}}{\rho_{p_1}} \cdot \frac{(D_2^2-d_2^2)}{(D_1^2-d_1^2)} \cdot \frac{D_1}{D_2}$	0.70	

Pellet	No.1	No.2	No.1	No.2	No.1	No.2	No.1	No.2
W/F_T (10^3)	0.201	0.200	0.300	0.300	0.400	0.400	0.500	0.500
Conversion x_{CH_4}	0.0278	0.0402	0.0382	0.0547	0.0480	0.0672	0.0577	0.0779
N_{Re}	10.8	11.9	7.1	7.9	5.3	5.9	4.2	4.7
$r_{obs,m,1}$ (10^{-6})	119.5		107.0		90.0		80.3	
$r_{obs,m,2}$ (10^{-6})		161.3		134.8		117.9		107.7
$r_{obs,m,1} \div r_{obs,m,2}$	0.74		0.79		0.76		0.75	

TABLE 8.6

Ratio of Observed Reaction Rates for Different Pellet Dimensions

Pellet Characteristics	Pellet No.1				Pellet No.3			
Mass, W g	5.3815				3.8964			
Ext. Area, S_c cm^2	9.0955				9.3729			
Density, ρ_p g/cm^3	2.232				2.369			
O.D., D cm	1.54				1.17			
I.D., d cm	1.02				0.81			
D^2-d^2 cm^2	1.3312				0.7128			
$\rho_{p_3}:\rho_{p_1}$	1.061							
$D_1:D_3$	1.316							
$(D_3^2-d_3^2):(D_1^2-d_1^2)$	0.535							
$\frac{\rho_{p_3}}{\rho_{p_1}}\cdot\frac{(D_3^2-d_3^2)}{(D_1^2-d_1^2)}\cdot\frac{D_1}{D_3}$	0.75							
Pellet	No.1	No.3	No.1	No.3	No.1	No.3	No.1	No.3
W/F_T (10^3)	0.150	0.150	0.201	0.200	0.250	0.250	0.300	0.300
Conversion x_{CH_4}	0.0210	0.0270	0.0278	0.0348	0.0330	0.0434	0.0382	0.0510
N_{Re}	14.5	11.8	10.8	8.7	8.5	6.9	7.1	5.9
$r_{obs,m,1}$ (10^{-6})	147.3		119.5		105.1		107.0	
$r_{obs,m,3}$ (10^{-6})		171.4		164.0		168.0		140.3
$r_{obs,m,1}:r_{obs,m,3}$	0.86		0.73		0.63		0.76	

TABLE 8.7

Ratio of Observed Reaction Rates For Different Pellet Dimensions

Pellet Characteristics	Pellet No.2				Pellet No.4			
Mass, W g	5.1632				5.2133			
Ext. Area, S_c cm^2	13.9449				8.5477			
Density, ρ_p g/cm^3	2.415				2.387			
O.D., D cm	1.08				1.52			
I.D., d cm	0.75				0.97			
D^2-d^2 cm^2	0.6039				1.3695			
$\rho_{p_4}:\rho_{p_2}$	0.988							
$D_2:D_4$	0.71							
$(D_4^2-d_4^2):(D_2^2-d_2^2)$	2.267							
$\frac{\rho_{p_4}}{\rho_{p_2}}\cdot\frac{(D_4^2-d_4^2)}{(D_2^2-d_2^2)}\cdot\frac{D_2}{D_4}$	1.59							
Pellet	No.2	No.4	No.2	No.4	No.2	No.4	No.2	No.4
W/F_T (10^3)	0.200	0.200	0.300	0.300	0.350	0.350		
Conversion x_{CH_4}	0.0402	0.0265	0.0547	0.0374	0.0611	0.0425		
N_{Re}	11.9	10.5	7.9	7.0	6.8	5.9		
$r_{obs,m,2}$ (10^{-6})	161.3		134.8		123.7			
$r_{obs,m,4}$ (10^{-6})		116.0		105.0		99.1		
$r_{obs,m,2}:r_{obs,m,4}$	1.39		1.28		1.25			

TABLE 8.8

Ratio of Observed Reaction Rates for Different Pellet Dimensions

Pellet Characteristics	Pellet No.4				Pellet No.5			
Mass, W g	5.2133				2.4689			
Ext.Area, S_c cm^2	8.5477				7.7911			
Density, ρ_p g/cm^3	2.387				2.419			
O.D., D cm	1.52				1.00			
I.D., d cm	0.97				0.73			
D^2-d^2 cm^2	1.3695				0.4671			
$\rho_{p_5}:\rho_{p_4}$	1.013							
$D_4:D_5$	1.52							
$(D_5^2-d_5^2):(D_4^2-d_4^2)$	0.341							
$\frac{\rho_{p_5}}{\rho_{p_4}}\cdot\frac{(D_5^2-d_5^2)}{(D_4^2-d_4^2)}\cdot\frac{D_4}{D_5}$	0.53							
Pellet	No.4	No.5	No.4	No.5	No.4	No.5	No.4	No.5
W/F_T 10^3	0.200	0.202	0.250	0.250	0.300	0.300	0.350	0.350
Conversion x_{CH_4}	0.0265	0.0453	0.0320	0.0526	0.0374	0.0592	0.0425	0.0650
N_{R_e}	10.5	5.8	8.3	4.7	7.0	3.3	5.9	3.3
$r_{obs,m,5}$ (10^{-6})	116.0		108.0		105.0		99.1	
$r_{obs,m,4}$ (10^{-6})		165.9		142.3		124.0		110.0
$r_{obs,m,4}:r_{obs,m,5}$	0.70		0.76		0.85		0.90	

performed on three consecutive readings of x_{CH_4} from the curves at given W/F_T values, so that the observed reaction rates were greatly influenced by experimental errors. Such cases are given in the first and third bottom columns of Table 8.6.

An interesting point to be mentioned is the effect of the Reynolds number on the magnitude of deviations. With the decrease of N_{Re}, there is an approach of the ratio of observed rates towards unity suggesting a shift of the reacting system into the film-diffusion controlled regime where the rates for given W/F_T values become identical and are governed only by the mass transfer rates in the bulk gas phase.

8.7.3 Conclusion.

The experimental data obtained at 540° C provided sufficient evidence to conclude that the effectiveness factor of the catalyst 46 - 1 was rather low at an approximate value 0.1 ; at higher temperatures the increased intrinsic kinetic rate would lead to even lower values.

8.8 KINETIC MECHANISM AND RATE EQUATION.

8.8.1 Kinetic Mechanism.

The comprehensive term "kinetic mechanism" as applied to gas-solid catalytic reactions covers the surface phenomena of activated adsorption of one or more of the reacting species, the chemical reaction between adjacently adsorbed components (dual-site mechanism) or between adsorbed and unadsorbed components (single-site mechanism), and the desorption of actively adsorbed product molecules. It does, however, embrace these events as successive and integral steps in the series of molecular transformation leading ultimately to the formation of products, and provides indications of the relative rate of each step. The questions why activated adsorption takes place, and what the chemical natures of the adsorbed species are, do not enter, in general,

into the framework of a study concerning the kinetic mechanism of a gas-solid catalytic system.

Nevertheless, the modes of the adsorption and desorption processes, i.e. whether dissociative or non-dissociative adsorption occurs may be dealt with by postulated rate expressions obtained following the Langmuir-Hinshelwood approach. Although the chemical reaction step is also a stage of the overall kinetic situation, it is described mostly in a simplified, overall stoichiometric form neglecting the formation of intermediates or free radicals by some complicated chain reactions or simple parallel or consecutive reactions and their interaction with active sites.

Mechanisms may be proposed which conform to the experimental observations; this would not imply, however, that the reaction proceeds strictly and necessarily via the postulated steps. Moreover, such a conclusion is based on the assumption that only one of the probable steps involved in the total sequence of surface phenomena does control the rate of the overall process. From the standpoint of theoretical kinetics, this assumption is not acceptable; however, according to Yang and Hougen (182) it is usually found justifiable as a satisfactory basis for practical purposes.

Since the adsorption and desorption steps are more clearly defined within the frame of the expression "kinetic mechanism" than the chemical reaction, the use of the term kinetic mechanism does not seem to be appropriate to characterize the whole gas-solid catalytic system. It may be suggested that the adsorption and desorption processes could be separated from the chemical reaction as "adsorption-desorption kinetics" and the aspects of the chemical interaction could be described as the "mechanism of the actual chemical conversion".

From the experimental data obtained in the present investigation, it has been concluded that the adsorption and desorption kinetics were not rate-controlling factors for the overall outcome of the steam-

methane system at 540° C and 1 atm abs. pressure. This conclusion has been reached on the assumption that the reaction was controlled solely by one of the three steps (Sections 8.4 and 8.6).

No attempts have been made to interpret the results in terms of the kinetic mechanism of the actual chemical conversion. Suggested mechanisms of this type would tend to be speculative, since they have to be based upon hypotheses rather difficult to justify unless supported by direct experimental detection of intermediates, which would only exist in very low concentrations for short times.

The data provided, however, conclusive indications as to which of the oxides of carbon is being formed first. Plotting the ratio $\%\ CO_2/(\%\ CO + \%\ CO_2)$ against conversion x_{CH_4} (Fig. 8.25) and versus S_c/F_T ratio (Fig. 8.26), for operating conditions 540° C, 1 atm abs., $\alpha = 3.0$, and different pellet dimensions, resulted in curves which, if extrapolated to zero conversion or $S_c/F_T = 0$, gave $CO_2/(CO + CO_2)$ values very close to unity. This fact furnished sufficient evidence to conclude that the primary reaction between steam and methane has the stoichiometric form :

$$CH_4 + 2\ H_2O \rightarrow CO_2 + 4\ H_2,$$

and a stoichiometry of the type

$$CH_4 + H_2O \rightarrow CO + 2\ H_2$$

is not representative of the overall reaction. Consequently, the carbon monoxide is formed by the water gas shift reaction taking place in the reverse direction, thus :

$$CO_2 + H_2 \rightarrow CO + H_2O$$

An additional graph (Fig. 8.27) illustrates the variation of the ratio $CO_2/(CO + CO_2)$ with conversion at four different operating temperatures and reactor pressures as indicated on respective curves. The curve for 540° C in Fig. 8.27 represents the results obtained with a pellet of very similar dimensions to those used for other temperature levels.

Fig. 8.25 The Ratio $\frac{CO_2}{CO + CO_2}$ as a Function of Conversion X_{CH_4} ($\alpha = 3.0$)

	Temp. (C°)	Press. (atm.)	Weight (g)	Ext. Area (cm^2)	O Dia. (cm)	Height (cm)
●	540	0.971	5.3815	9.0855	1.84	1.88
○	"	0.974	5.1632	13.9449	1.08	4.11
△	"	0.993	3.8964	9.3729	1.17	2.55
+	"	0.980	5.2133	8.5477	1.52	1.79
×	"	0.998	3.4689	7.7911	1.00	2.48
▽	"	0.993	0.7772	2.5133	1.00	0.80
□	"	1.000	2.7050	4.4877	1.52	0.94

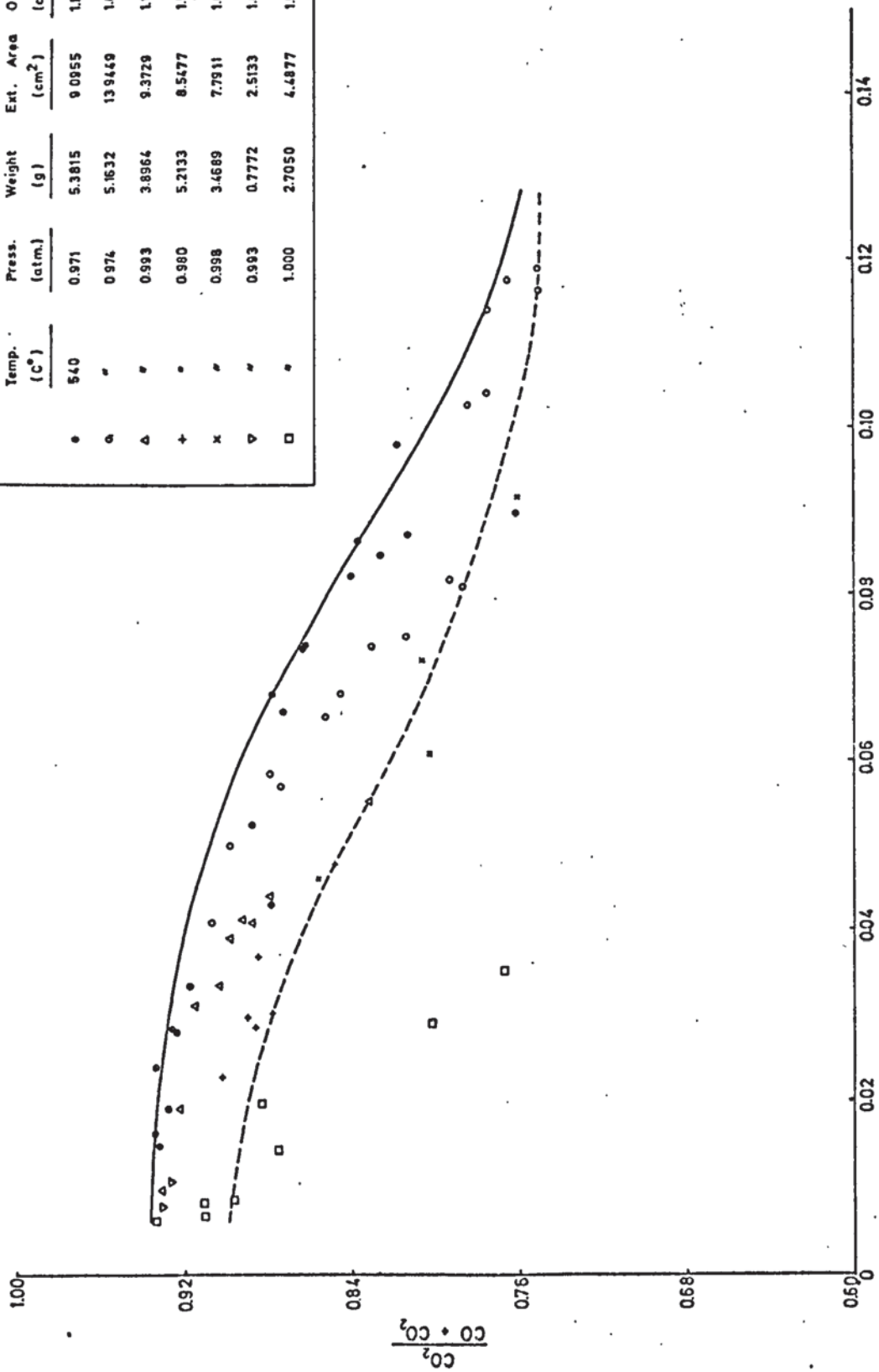

Fig. 8.26 The Ratio $\frac{CO_2}{CO + CO_2}$ as a Function of the Ratio S_c/F_T

	Temp. (C°)	Press. (atm.)	Weight (g)	Ext. Area (cm^2)	O. Dia. (cm)	Height. (cm)
●	540	0.971	5.3815	9.0955	1.54	1.68
○	"	0.974	5.1632	13.9449	1.08	4.11
△	"	0.993	3.8964	9.3729	1.17	2.55
+	"	0.980	5.2133	8.5477	1.52	1.79
×	"	0.998	3.4689	7.7911	1.00	2.48
▽	"	0.993	0.7772	2.5133	1.00	0.80
□	"	1.000	2.7050	4.4877	1.52	0.94

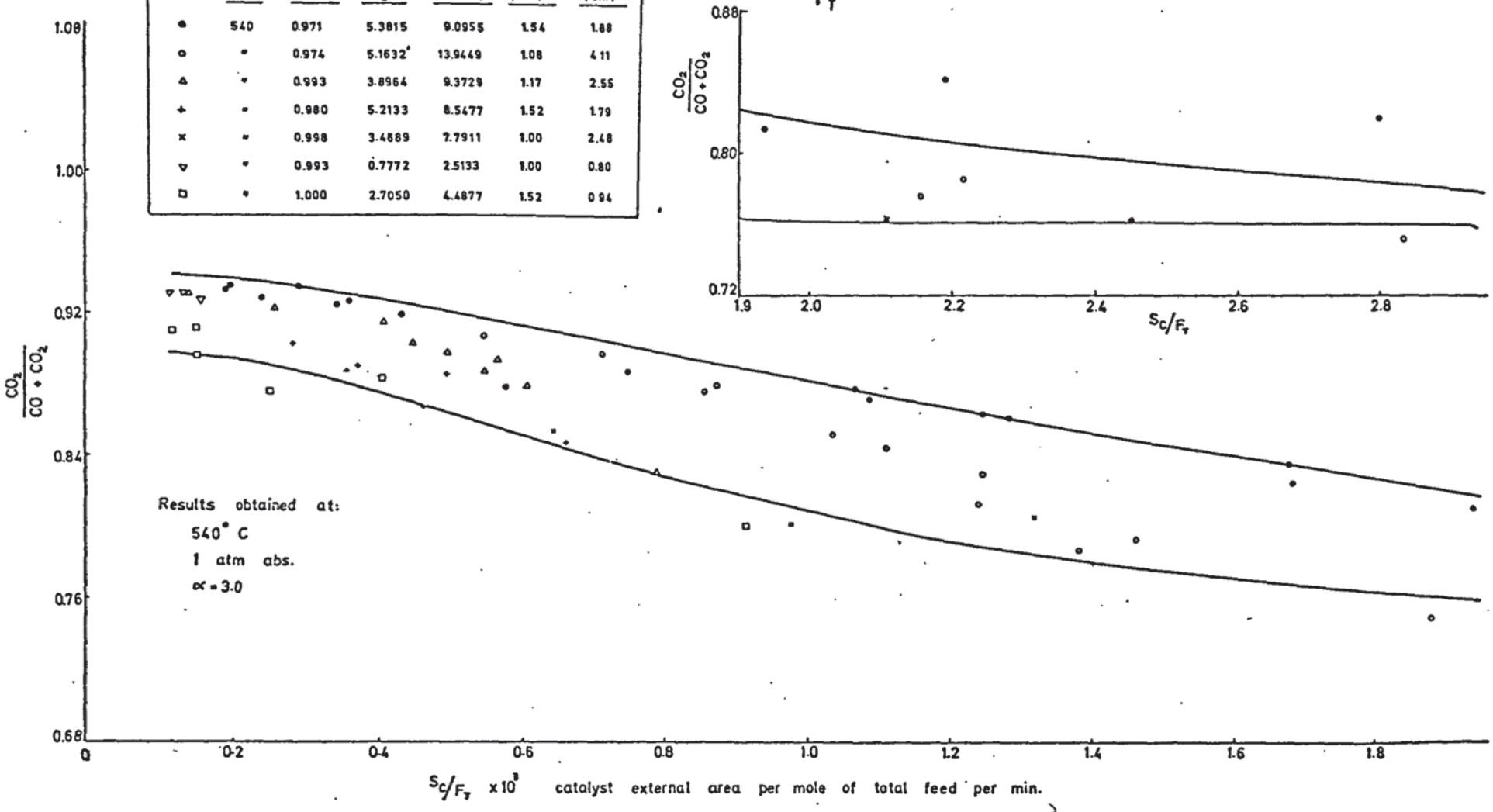

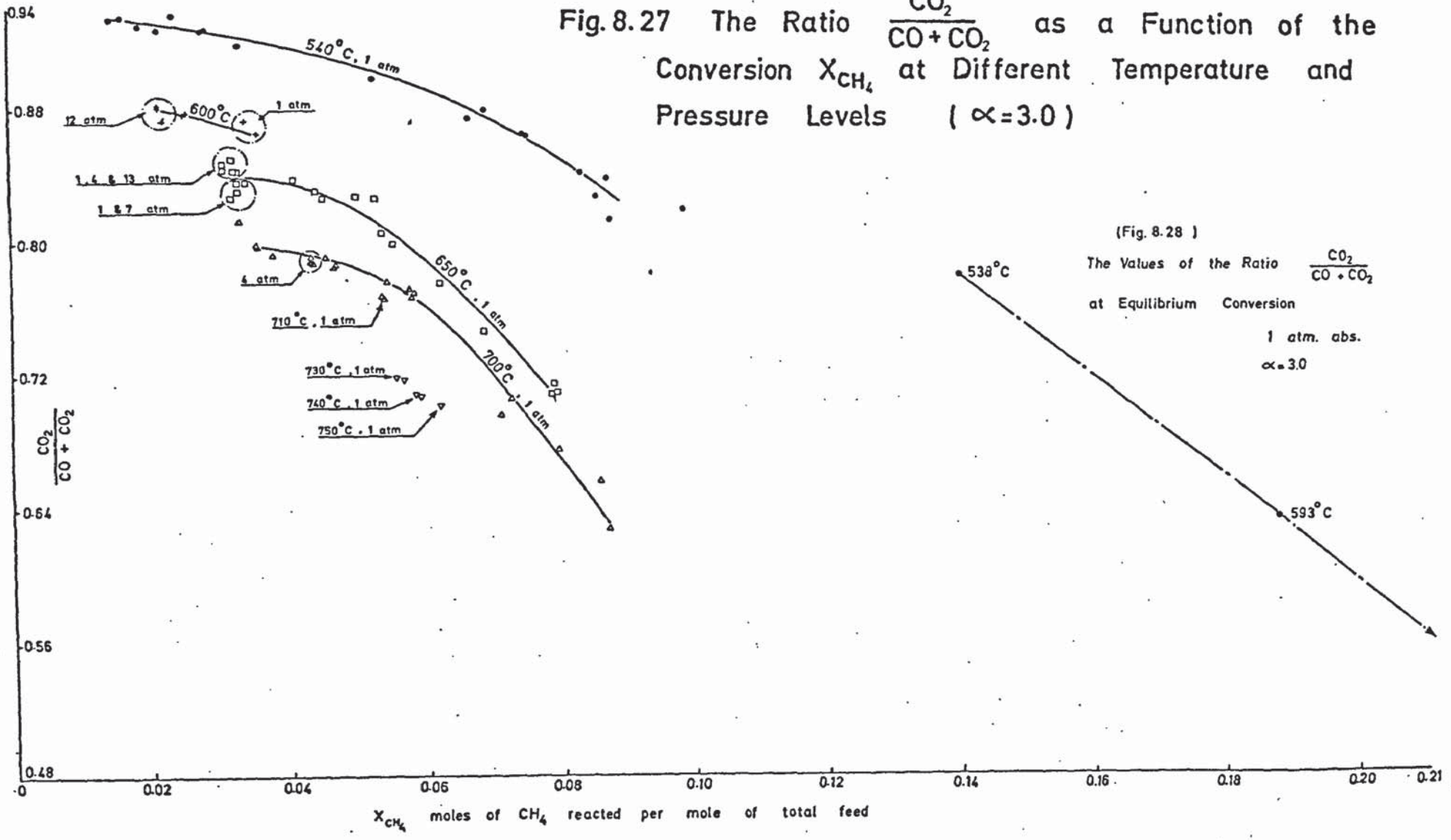

Fig. 8.27 The Ratio $\frac{CO_2}{CO + CO_2}$ as a Function of the Conversion X_{CH_4} at Different Temperature and Pressure Levels ($\alpha = 3.0$)

(Fig. 8.28)

The Values of the Ratio $\frac{CO_2}{CO + CO_2}$ at Equilibrium Conversion

1 atm. abs.

$\alpha = 3.0$

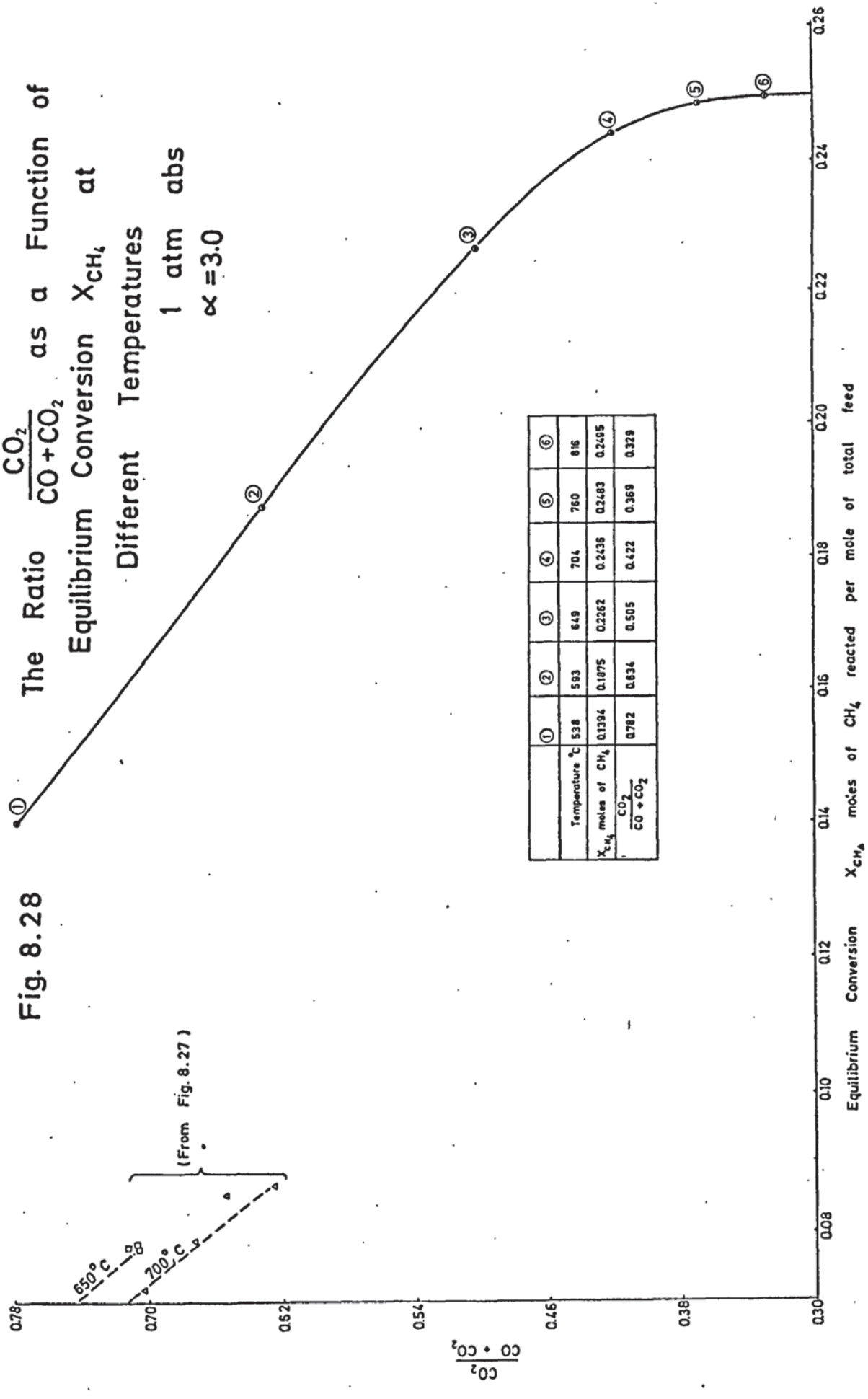

	①	②	③	④	⑤	⑥
Temperature °C	538	593	649	704	760	816
X_{CH_4} moles of CH_4	0.1394	0.1875	0.2262	0.2436	0.2483	0.2495
$\frac{CO_2}{CO + CO_2}$	0.782	0.634	0.505	0.422	0.369	0.329

The values of $CO_2/(CO + CO_2)$ at equilibrium conversions at different temperatures and 1 atm abs. reactor pressure with $\alpha = 3.0$ are shown in Fig. 8.28.

The points on the plots Figs. 8.25 and 8.26 exhibit some degree of scatter in a rather wide range of $CO_2/(CO + CO_2)$. This scatter does not originate solely from experimental errors and analytical uncertainties which would have rendered the results questionable. The reason is that for the pellets of varying dimensions used, the same conversion may result from different combinations of catalyst external areas and gas flowrates. If the catalyst's selectivity is assumed to be identical for both the steam-methane reforming and the water gas shift reaction, then it would have been expected that a plot of $CO_2/(CO + CO_2)$ against S_c/F_T ratio would result in a single curve with scattering of points within the limits of experimental error. In fact, Fig. 8.26 exhibits a narrower band than that defined by the upper and lower boundaries of $CO_2/(CO + CO_2)$ values plotted as a function of conversion in Fig. 8.25. If the water gas shift reaction, however, is catalyzed to a greater extent than the methane reforming reaction, then it is perfectly reasonable to anticipate that the $CO_2/(CO + CO_2)$ ratios corresponding to a conversion obtained with the pellet of larger external surface (points marked O on Figs. 8.25 and 8.26) will be less than the ratios for the same conversion x_{CH_4} obtained with a pellet of smaller external area (points indicated with • in the same figures). In fact, based on actual laboratory and industrial scale results, it is generally agreed that catalysts formulated from nickel supported on α- or γ-Al_2O_3 are more effective in catalyzing the water gas shift than the reforming of methane (21, 27, 164, 179).

It seems also not unlikely that the reactor inner walls may have a catalytic influence on this reaction, or the reaction may even continue homogeneously in the gas phase. These possibilities deserve

consideration as an additional plausible cause for the deviations of the points from a unique curve, because $CO_2/(CO + CO_2)$ values obtained with a pellet with small external area and small flowrate corresponding to given values of S_c/F_T were less than the values obtained for the same S_c/F_T ratio but with a larger external area and accordingly higher flowrate. Low feedrates would imply, of course, a longer residence time of the reformed gas in a section of the reactor body over a relatively high temperature range. The water gas reaction will cease when the temperature of the gas falls to a level where the rate becomes virtually zero.

Thus, the values of $CO_2/(CO + CO_2)$ for given x_{CH_4} or S_c/F_T vary with the external surface area of the pellet and the flowrates. It is, therefore, considered more appropriate to represent the relationships not in the form of single curves, but rather in the form of bands covering all the experimental points. Three characteristics of these bands in Figs. 8.25 and 8.26 deserve comment:

(i) Extrapolation of the band boundaries to zero conversion or $S_c/F_T = 0$ does not give unity for $CO_2/(CO + CO_2)$, because even at extremely low conversion or S_c/F_T values, a certain portion of the carbon-dioxide formed by the methane reforming reaction could have reacted instantaneously to give carbon monoxide.

(ii) The width of the bands narrows with increasing values of conversion or S_c/F_T indicating the approach to the limiting value of $CO_2/(CO + CO_2)$ corresponding to the equilibrium of the reactions

$$CH_4 + 2\ H_2O = CO_2 + 4\ H_2$$

$$CO_2 + H_2 = CO + H_2O$$

(iii) The degree of scatter is greatest in the middle section of the bands showing the effects of the external area and gas flowrates on the extent of the water gas shift reaction.

Fig. 8.27 illustrates the variation of $CO_2/(CO + CO_2)$ with conversion x_{CH_4} at different temperatures and operating pressures. It

can be seen from the graph that the pressure had no effect on the relative concentrations of the carbon oxides, since the values of $CO_2/(CO + CO_2)$ ratio for given x_{CH_4} were almost the same at 600°, 650° and 700° C independent of operating pressure. Furthermore, the relative location of the curves in Fig. 8.27 indicates the sensitivity of the rate of the shift reaction to temperature. In fact, for the same extent of conversion of methane, the value of $CO_2/(CO + CO_2)$ decreases rapidly, if the temperature is increased from 540 to 700° C. $CO_2/(CO + CO_2)$ values at zero conversion, which may be obtained by extrapolating the curves for 650° C and 700° C, are considerably less than unity. This is attributed to the increased rate of the water gas reaction occurring on the catalytic sites simultaneously with the reforming of methane.

In view of these facts it is possible to explain the contradiction between established opinion and the conclusions reached in this investigation with respect to the primary reforming reaction. Bodrov et al. (20, 21, 22) studied the kinetics of methane reforming on metallic nickel foil and with nickel on alumina catalysts at 800° - 900° C, barometric pressure and different steam : methane mole ratios, and found CO very much in excess over CO_2. On this basis, a kinetic mechanism was postulated for the reforming reaction with CO being formed as the primary reaction product which was assumed to be oxidized in the subsequent steps to CO_2. The rate expression developed by Bodrov and co-workers (21) gave satisfactory agreement between predicted and experimentally found conversions of methane.Akers and Camp (2) also conducted experiments for reforming of methane at different temperatures and barometric pressure. From the concentration of CO and CO_2 in the reformed gas obtained at 638° C catalyst bed temperature they concluded that both oxides of carbon were primary reaction products, but that CO_2 was being formed at an initial rate of

between two and nine times the rate of CO formation, depending on the steam : methane molar ratio in the feed.

These interpretations and conclusions of the previous investigators are not surprising, since at temperatures of 800 - 900° C, the rate of the water gas reaction was increased to such an extent that CO_2, having been formed as the initial reaction product on the active sites, had been instantaneously converted to CO, so that CO appeared virtually as the primary product. In fact, the temperature level (638° C) of the experiments conducted by Akers and Camp (2) was such that both CO_2 and CO existed in significant concentrations in the reformed gas, and led the investigators to inconclusive interpretation. Although their published data shows CO_2 and CO concentrations obtained at lower temperatures, which confirms the results of the present work as given in Fig. 8.27, they have not commented on them.

If the initial oxide of carbon were CO, corresponding to an overall reaction stoichiometry

$$CH_4 + H_2O \longrightarrow CO + 3\ H_2,$$

then the curve of $CO_2(CO + CO_2)$ against S_c/F_T such as Fig. 8.26, would have approached the value of $CO_2/(CO + CO_2)$ corresponding to the equilibrium conversion from the opposite side to that obtained in the experimental work as shown in Fig. 8.29.

In conclusion, it is the author's firm opinion that the reforming reaction of methane should be represented by the overall stoichiometry

$$CH_4 + 2\ H_2O \longrightarrow CO_2 + 4\ H_2$$

and that CO is then formed by the reaction of CO_2 according to the reverse water gas shift reaction :

$$CO_2 + H_2 \longrightarrow CO + H_2O$$

It is also believed that the high levels of CO commonly reported in the literature at high temperatures are due to the removal of some CO_2 by the relatively high rate of the shift reaction at these temperatures.

Fig: 8.29. Possible Variations of $\frac{CO_2}{CO + CO_2}$ Curve as a Function of the Ratio S_c/F_T (for CO_2 or CO as the initial reaction products)

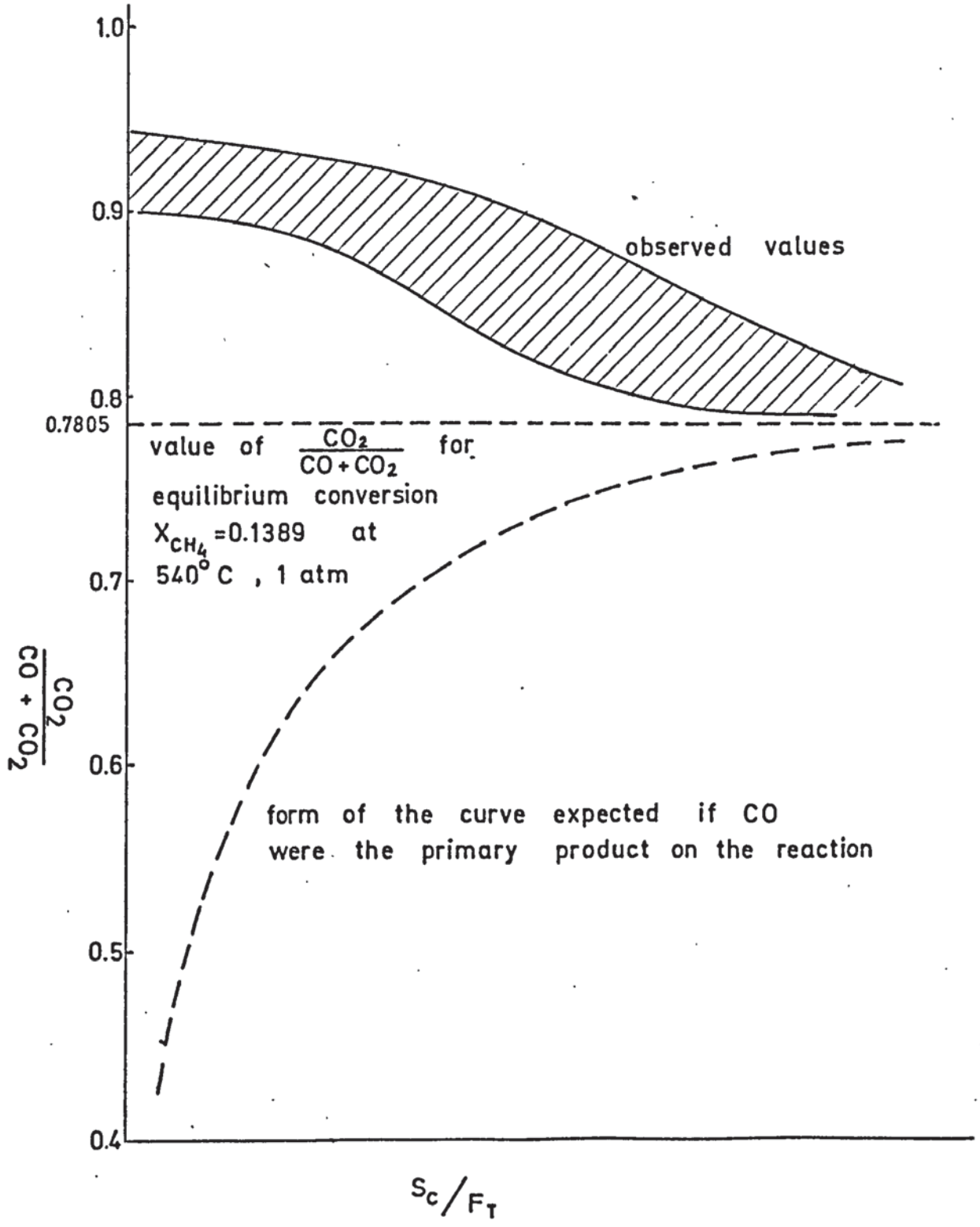

8.8.2 Rate Equation.

Although some rate equations and mechanisms for methane reforming have been proposed in former investigations, these tend to be rather conflicting. (Chapter 3). There are three fundamental reasons why this might be expected. First of all, it is well-established that the formulation and crystal structure of the catalyst have a substantial effect not only on the kinetic parameters of the steam-hydrocarbon catalytic system, but also on its thermodynamic properties in altering the equilibrium constant of the Boudouard reaction, and consequently changing the boundaries of equilibrium carbon deposition. (Chapters 2 and 6). This situation involves the formation and persistence of some stable intermediate solid compounds at a pseudo equilibrium state, which might well affect the kinetic mechanism.

Secondly, the proposed kinetic mechanisms and derived rate equations of the various authors were based on experimental observations made under operating conditions covering rather dissimilar ranges. Thus operating parameters like temperature, pressure, initial composition of the feed, catalyst weights and particle dimensions, and experimental procedures like reactor geometry, gas flowrates, extent of reaction, and sampling techniques differed quite considerably from each other in previous studies. Consequently some inconsistencies exist in the kinetic data underlying the interpretations and conclusions.

A third reason is the differences in methodology of the investigators in their approach to the development of the rate expression, i.e. whether the rate equation was purely a simplified empirical expression which fitted satisfactorily the observed data, or whether it was deduced by Langmuir-Hinshelwood type postulations.

The rate equations developed in the present work are expressions obtained by a semi-empirical approach. In view of the uncertainties about the real nature of the complex surface kinetics between

chemisorbed methane and/or steam and reaction intermediates, it was considered that a Langmuir-Hinshelwood treatment would not be warranted. Furthermore, the fundamental assumptions upon which the Langmuir treatment itself is based, are hard to justify, both theoretically and experimentally, although in practice this treatment yields rate expressions which may remain valid over a certain range of kinetic parameters. One of the basic assumptions underlying the Langmuir approach is that no interaction occurs between the adsorbed species, which implies that the catalyst is constituted of an ideal surface with constant enthalpy and activation energy of adsorption for each chemisorbed species, independent of the amount adsorbed (24). It is, however, reported that even for physical adsorption, this condition is satisfied only in extremely rare cases (174). In fact, the rate of adsorption $r_{A,\ ads.}$ of a gas A is described by the Langmuir isotherm simply as

$$r_{A,ads} = k\ p_{A,s}(1 - \theta)$$

where θ is the fractional coverage defined by

$$\theta = \frac{K_A p_{A,s}}{1 + K_A p_{A,s}}$$

K_A is the adsorption equilibrium constant of the gas A, and $p_{A,s}$ is the pressure of A at the gas-solid interface. A derivation of the adsorption rate based on statistical considerations yields, however,

$$r_{A,ads.} = \frac{\alpha\ e^{-\frac{E}{RgT}}}{(2\ \pi\ m_A\ k_B\ T\ )^{0.5}} \left[p_{A,s}\ \ (1 - \theta)\right]$$

where the term $(1 - \theta)e^{-\frac{E}{RgT}}$ is called the sticking probability of the molecules strikingthe surface, and α is the condensation coefficient (153). It is reported that this ideal expression for the rate of adsorption does not usually agree with experimental data. Observed rates decrease so rapidly with increasing coverage θ that they can be explained only if E increases with θ. It is also claimed that the

condensation coefficient α may vary with θ. According to Smith (153) these variations may be caused by surface heterogeneity, i.e. the adsorption potential of the active sites varies so that different sites exhibit different values of α and E which become functions of the fractional coverage θ. Alternately, these deviations are attributed to the interaction forces between occupied and unoccupied sites. In any event, it is considered necessary to define the rate of adsorption of A by:

$$r_{A,\ ads} = \frac{\alpha(\theta)\ e^{-\frac{E(\theta)}{RgT}}}{(2\ \pi\ m_A k_B\ T)^{0.5}} \left[p_{A,s}\ (1 - \theta)\right]$$

which is similar to the Elovich (153) isotherm:

$$r = \beta\ p\ e^{-\gamma\theta}$$

The Langmuir- Hinshelwood treatment assumes also that there is no interaction between adsorbed molecules, and that the amount of adsorbed species (reactant or highly active reaction intermediates) has no effect on the rate of adsorption. This implies that the addition of a second gas, both being adsorbed on the solid surface, will always decrease the adsorption of the first gas. Data available on chemisorption from gaseous mixtures indicates, however, that under certain conditions the adsorption of a gas from mixtures may be enhanced over that of pure gas at the same partial pressure. This behaviour is attributed to an attractive interaction between adsorbed molecules of the two constituents (174). Adsorption of this type would correspond in mathematical terms to an equation of the form

$$r_A = \frac{kp_A}{1 + K_A P_A - K_B P_B}$$

with a negative coefficient in the adsorption term indicating the increase of the adsorption rate of A in the presence of another

component B. In the usual application of the Langmuir-Hinshelwood approach, this experimental result is considered to be physically impossible, and any postulated kinetic mechanism which leads to a negative coefficient in the adsorption term is automatically discarded, since this would mean a negative adsorption-desorption equilibrium constant for species B.

The other tacit implication of no interaction between the adsorbed species effecting the rate of adsorption and desorption is the assumption that each adsorbed complex has the same structure, which cannot be justified in the case of methane reforming because of the probable formation of hydrocarbon radicals on active sites. (Chapter 3).

A further limitation of the Langmuir-Hinshelwood treatment is the necessary assumption that only one of the steps of the surface phenomena is rate-controlling for the overall kinetics and that all other kinetic rate processes are at equilibrium.

In view of these facts it is always difficult for a rate equation derived by the Langmuir theory to be accepted as the unique phenomenological model of the actual kinetic mechanism involved. It is rather a mathematical representation of one of a number of hypothetical mechanisms which fits most satifactorily the experimental observations made within a given range of kinetic parameters. It may or may not be valid at other operating conditions, and furthermore it is possible that a better fit for a wider range of operating parameters can be obtained on the basis of some other assumed mechanism. Moreover, two rate equations representing two different kinetics may result in such slight differences in fitting the experimental data, that they remain within the limits of experimental error, and yet none of them may represent the real kinetic phenomena. Such a case was observed by Woodcock (179) in his kinetic study of methane reforming at high pressure.

It is therefore, considered more appropriate in the present work

to develop rate expressions in macrokinetic terms which may be a reasonable representation of reality and which would satisfactorily fit the experimental data obtained.

The following rate expression for the initial rate of reaction is first suggested as having the simplest form and sufficient generality:

$$r_i = k\, p_{CH_4,i}^{m}\; p_{H_2O,i}^{n} \qquad (8.21)$$

The exponents m and n are the apparent orders of reaction with respect to the initial partial pressures of steam and methane; and k is the apparent rate constant valid for the range of operating conditions involved. The experiments with freshly activated catalyst at 540° C, 1 atm abs. pressure, and at varying H_2O : CH_4 ratios were correlated by regression analysis using a library statistical program issued by International Computers Ltd. The input data and the results obtained from this correlation are summarized in Table 8.9

TABLE 8.9

Comparison of Observed and Computed Initial Reaction Rates.

(moles of CH_4 reacted/g catalyst) (min)

Initial Partial Pressure of Methane $p_{CH_4,i} = y_{CH_4,i}$ (atm)	Initial Partial Pressure of Steam $p_{H_2O,i} = y_{H_2O,i}$ (atm)	Observed Initial Reaction Rate $(r_{obs,m,i})(10^{-4})$	Computed Initial Reaction Rate $(r_{comp,m,i})(10^{-4})$
0.333	0.667	1.48	1.484
0.250	0.750	1.28	1.274
0.200	0.800	1.11	1.102
0.1667	0.8333	0.96	0.965
0.1428	0.8572	0.84	0.856
0.125	0.875	0.78	0.769

From the first three columns of Table 8.9 the rate equation for

the initial reaction based on the mass of the catalyst is:

$$r_{m,i} = 0.00673 \; p_{CH_4,i}^{0.973} \; p_{H_2O,i}^{1.094} \qquad (8.22)$$

Confidence limit of the correlation: 99%

Sum of the square of the approximation errors : $(0.123)(10^{-3})$

Residual error : $(0.642)(10^{-2})$

Calculated values of rate from this correlation are given in column 4 of the table on the previous page. The agreement between the two values appear to be very satisfactory. However, it has to be pointed out that the validity and applicability of this correlation are confined to a restricted range of operating conditions. The major argument against this expression is that it implies a dependence of the initial reaction rate on total pressure. The experimental initial rate data were not sufficient to account for observed rates at higher pressures than 1 atm abs. to obtain a correlation of this type valid for a wider range of pressure. Other observations provided sufficient evidence, however, that the pressure had no effect on the extent of conversion. It was, therefore, considered useful to modify the correlation such that it could give satisfactory results even for higher pressures. The form of modification was suggested by the Langmuir-Hinshelwood rate expression for reactions which are solely controlled by the chemical reaction step:

$$r_i = \frac{k \; p_{CH_4,i}^{a} \; p_{H_2O,i}^{b}}{\left[1 + Sp^{c}_{CH_4,i} + Tp^{d}_{H_2O,i}\right]^{n}} \qquad (8.23)$$

A semi-empirical equation of this type had eight unknown parameters. The determination of these parameters by the least square approximation involved the simultaneous solution of a set of eight non-linear equations. This was not possible since only six sets of experimental data were available.

The following attempt was made to arrive at an equation which would

satisfactorily fit the observed data: some arbitrary values were assigned to the exponents a, b, c, d, and n; the number of free parameters was thus reduced to three, and the least squares approximation resulted in a system of linear equations which were solved simultaneously for the unknown parameters k, S and T. The procedure is outlined below for the case of correlating the integral rate data.

The calculation was performed by the digital computer which printed out the sum of squares, $, of residual errors:

$$\$ = \sum \left\{ \left[\frac{P_{CH_4}^{a} \; P_{H_2O,i}^{b}}{r_i} \right]^{1/n} - \left(1 + S P_{CH_4}^{c} + T P_{H_2O,i}^{d} \right) R \right\}^2$$

and the values of the initial rates computed on the basis of the adjustable parameters a, b, c, d, n, and k, S, T. ($k = 1/R^n$).

Trial values for the exponents a, b, c, d, and n were changed in the following ranges:

a = 0.973, 1.00 ;

b = 0.00 - 1.00, at 0.1 intervals ; and 2.0

c = 0.50 - 1.00, at 0.1 intervals

d = 1.00 - 2.00, at 0.2 intervals

n = 1.00 ; 2.00 - 3.00, at 0.1 intervals.

For some combinations of these parameters the sum of the squares of the residual approximation errors was minimized to a magnitude of 10^{-3}. It is interesting to compare the sum of errors for different values of adjustable parameters:

Deduced Rate Equations	Sum of the squares of approx. errors
$r_i = \dfrac{(0.00834)\, P_{CH_4,i}\, P_{H_2O,i}^{2}}{\left[1 + (0.535)\, P_{CH_4,i} + (1.278)\, P_{H_2O,i}\right]^3}$	0.0090
$r_i = \dfrac{(0.000397)\, P_{CH_4,i}\, P_{H_2O,i}^{2}}{\left[1 - (0.551)\, P_{CH_4,i} - (0.183) P_{H_2O,i}^{2}\right]^3}$	0.0084

Deduced Rate Equations

	Sum of the Squares of approx.errors
$r_i = \frac{(0.02412)\, P_{CH_4,i}\, P_{H_2O,i}^2}{\left[1 + (1.422)P_{CH_4,i}^{0.5} + (1.96)P_{H_2O,i}^{1.5}\right]^3}$	0.0077

The observed values for the initial reaction rate and computed values from the equation

$$r_i = \frac{(0.02412)\, P_{CH_4,i}\, P_{H_2O,i}^2}{\left[1 + (1.422)P_{CH_4,i}^{0.5} + (1.96)P_{H_2O,i}^{1.5}\right]^3} \qquad (8.24)$$

which gave the least deviation from the observed values are given below :

$r_{obs,m,i}$ moles/(g)(min) x 10^{-4}	$r_{comp,m,i}$ moles/(g)(min) x 10^{-4}
1.48	1.4836
1.28	1.2765
1.11	1.1101
0.96	0.9635
0.84	0.8554
0.78	0.7697

These results were considered satisfactory. However, this does not imply that the equation does represent the best fit for a correlation of the experimental observations, nor does it mean that the kinetics of methane reforming strictly correspond to a mechanism which may be interpreted by this equation.

For the correlation of overall rate data, the following form of rate expression was suggested :

$$r_m = \frac{k\, P_{CH_4}^a\, P_{H_2O}^b}{\left[1 + Sp_{CH_4}^c + Tp_{H_2O}^d + Up_{CO}^e + Vp_{CO_2}^f + Yp_{H_2}^n\right]^n} \qquad (8.25)$$

The retarding effect of the reverse reaction has not been accounted for in the driving force term of the rate equation, since the range of correlation was confined to a conversion range of 4.40 - 28.42% for which the partial pressures of products (CO, CO_2, H_2) were not sufficient to give a significant reverse driving potential. Thus for the average and highest conversion, the

partial pressure of products for the lowest steam : methane ratio (α = 2.0) corresponding to high values of reaction rates :

Conversion %	Partial Pressure, atm CO	CO_2	H_2
8.58	0.0018	0.0248	0.1047
12.41	0.0033	0.0345	0.1480
16.05	0.0052	0.0427	0.1865
22.09	0.0084	0.0548	0.2447

Furthermore, according to the stoichiometry, the hydrogen partial pressure would have to be raised to the fourth power. Although the thermodynamic equilibrium constant of the reaction

$$CH_4 + 2\ H_2O \rightleftharpoons CO_2 + 4\ H_2$$

is relatively small at 540° C (K_{eq} = 0.1884), the term $\frac{1}{K_{eq}} p_{CO_2} p_{H_2}^4$ was 0.001 for the highest conversion 22.09%. However, the products were retained in the adsorption term because their respective powers were taken as unity for non-dissociative adsorption, and they occupied active centres having significant retarding effect on the rate. In fact, Akers and White (3) studied the kinetics of the reverse reaction over a Ni-kieselguhr catalyst and concluded that the rate controlling step was the surface reaction between three non-dissociatively adsorbed hydrogen molecules and one adsorbed carbon monoxide molecule. The carbon dioxide was considered to have formed as a by-product and assumed to be appreciably adsorbed. They included, therefore, the partial pressure of carbon dioxide in the adsorption term.

The rate expression suggested by Equation (8.25) involved fourteen unknown parameters. The evaluation of these parameters for a satisfactory fit was again carried out by the least squares approximation. The number of unknowns had to be reduced by giving arbitrary trial values to the exponents, a, b, c, d, e, f, h, and n, in order to form a system of linear equations with six free parameters.

The calculation procedure is summarized below:

Equation (8.25) was rearranged to give:

$$\left[\frac{r}{p_{CH_4}^{a}\ p_{H_2O}^{b}}\right]^{1/n} = \frac{1}{\left[R + RSp_{CH_4}^{c} + RTp_{H_2O}^{d} + \text{----} + RYp_{H_2}^{h}\right]}$$

where the apparent rate constant k is replaced by $\frac{1}{R^n}$. To minimize the sum of the squares of approximation errors, , the partial derivatives of the function

$$\$ = \sum \left\{ \left[\frac{p_{CH_4}^{a}\ p_{H_2O}^{b}}{r_{obs,m}} \right]^{1/n} - \left[R + RSp_{CH_4}^{c} + \text{---+} RYp_{H_2}^{h}\right] \right\}^2$$

with respect to the free parameters R, RS, RT, RU, RV, and RY were set equal to zero, i.e. :

$$\frac{\partial \$}{\partial R} = 0 = 2 \sum_{i=1}^{n} \left\{ \left[\frac{p_{CH_4}^{a}\ p_{H_2O}^{b}}{r} \right]^{1/n} - \left[R + RSp_{CH_4}^{c} + \text{---+} RYp_{H_2}^{h}\right] \right\} \quad (-1)$$

$$\vdots$$

$$\frac{\partial \$}{\partial (RY)} = 0 = 2 \sum_{i=1}^{n} \left\{ \left[\frac{p_{CH_4}^{a}\ p_{H_2O}^{b}}{r} \right]^{1/n} - \left[R + RSp_{CH_4}^{c} + \text{---+} RYp_{H_2}^{h}\right] \right\} \left[(-1)(p_{H_2}^{h})\right]$$

Rearranging these equations yielded a system of simultaneous linear equations which were solved by the digital computer. The development of the set of linear equations for the computer programming is outlined in Appendix A-8.1. Trial values for the exponents a, b, c, d, e, f, h, and n were varied in the following ranges:

a = 0.9, 1.0 ;

b = 1.0 - 2.0 ; at 0.1 intervals

c = 1.0 and 1.1

d = 1.0 and 1.1

e = 0.9 - 1.2, at 0.1 intervals

f = 0.9 - 1.2, at 0.01 intervals

h = 1.0 - 1.2, at 0.1 intervals

n = 2 and 3.

The computer printed out the values of the apparent rate constant k, and the coefficients S, T, U, V, and Y in the adsorption

term of Equation (8.25). The numerical value of the reaction rate was also calculated and printed for each set of parameter combination on the basis of the partial pressures computed from analytical data. More than 160 combinations were tested; the sum of the squares of the residual approximation errors, corresponding to 30 sets of observed rate data, could only be diminished to the magnitude 10^{0}. It is interesting to note that the rate equation of the form of Equation (8.25) appeared to be very sensitive to even minute variations of the exponents. Some of these cases are indicated in Table 8.10, Columns 2, 3, 4, and 5. The values of parameters which gave the smallest sum of squares of approximation errors are also included in Table 8.10.

The observed values for the integral rate and the computed values from the equation of the type indicated in Table 8.10, using the exponents and coefficient of Column 2 of the table, are compared in Table 8.11. Although the rate equation deduced by this method is by no means the best fit of the experimental data, the differences between observed and computed values of reaction rates are not very significant and may be considered as within the limits of experimental erros. For comparison, the rates computed using the exponents and coefficients for the least sum of squares of approximation errors (Column 6 of Table 8.10) are included as the last column of Table 8.11. The reason why the values of Column 2 were selected for this comparison was that the exponents were all integers which would simplify the calculations for other cases. The major limitation of this rate expression is that its validity is confined to a given set of operating conditions, i.e. 540° C, 1 atm abs. pressure, steam : methane feed ratios $2.0 < \alpha < 7.0$, and conversions to 22.09 % (for $\alpha = 2.0$) and 28.42 % (for $\alpha = 7.0$). It may be considered worthwhile extending this

study to higher temperatures which would result in higher conversions, so that the rate expression given by Equation (8.25) may be improved to cover a wider range of operating conditions. Such an improvement may enable the rate equation to be extrapolated to operating conditions encountered in large scale reforming practice.

TABLE 8.10

TRIAL VALUES FOR PARAMETERS OF RATE EQUATION

$$r_m = \frac{k\, p_{CH_4}\, p_{H_2O}^{\,b}}{\left[1 + Sp_{CH_4}^{c} + Tp_{H_2O}^{d} + Up_{CO}^{e} + Vp_{CO_2}^{f} + Yp_{H_2}^{h}\right]^n}$$

and the corresponding Sum of Squares of Errors (for 30 sets of observations)

	1	2	3	4	5	6
Exponents						
a	1.0	1.0	1.0	1.0	1.0	1.0
b	1.0	2.0	2.0	2.0	2.0	2.0
c	1.0	1.0	1.0	1.0	1.0	1.0
d	1.0	1.0	1.0	1.0	1.0	1.0
e	1.0	1.0	1.0	1.0	1.0	1.0
f	1.0	1.0	1.005	1.01	1.04	1.045
h	1.0	1.0	1.0	1.0	1.0	1.0
n	2.0	3.0	3.0	3.0	3.0	3.0
Coefficients						
k (10^{-4})	0.574	0.852	0.829	0.803	0.629	0.603
S	-0.755	-0.749	-0.753	-0.756	-0.777	-0.780
T	-0.719	-0.505	-0.510	-0.516	-0.554	-0.560
U	-3.901	-4.419	-3.885	-3.318	0.131	0.568
V	-8.620	-7.511	-7.113	-6.586	-0.553	0.817
Y	-1.061	0.792	0.698	0.518	-0.915	1.216
Error Sum,	60.5	54.0	4.4	34.1	14.1	0.98

TABLE 8.11

Comparison of Observed Rate Data with Computed Reaction Rates

	Partial Pressures of Components (at)					$r_{obs,m}$ moles/(g) (min) ($x10^{-4}$)	$r_{comp,m}$ moles/(g) (min) ($x10^{-4}$)	$r_{comp,m}$ moles/(g) (min) ($x10^{-4}$)
	CH_4	H_2O	CO	CO_2	H_2			
1	0.3070	0.6156	0.0009	0.0132	0.0553	1.412	1.554	1.529
2	0.2848	0.5724	0.0018	0.0249	0.1051	1.346	1.386	1.337
3	0.2664	0.5370	0.0033	0.0345	0.1478	1.265	1.267	1.200
4	0.2507	0.5070	0.0052	0.0427	0.1865	1.146	1.118	1.111
5	0.2232	0.4558	0.0084	0.0548	0.2447	0.906	0.941	0.876
6	0.2300	0.7018	0.0008	0.0114	0.0480	1.230	1.285	1.272
7	0.2124	0.6621	0.0015	0.0216	0.0914	1.115	1.152	1.125
8	0.1980	0.6295	0.0028	0.0301	0.1287	1.055	1.068	1.021
9	0.1857	0.6030	0.0040	0.0374	0.1618	0.969	1.002	0.954
10	0.1644	0.5542	0.0061	0.0488	0.2135	0.741	0.833	0.774
11	0.1839	0.7573	0.0007	0.0096	0.0405	1.045	1.081	1.072
12	0.1702	0.7214	0.0013	0.0184	0.0777	0.981	0.979	0.957
13	0.1584	0.6919	0.0022	0.0260	0.1106	0.894	0.908	0.875
14	0.1485	0.6679	0.0031	0.0326	0.1399	0.826	0.859	0.824
15	0.1307	0.6237	0.0049	0.0426	0.1851	0.649	0.719	0.675
16	0.1538	0.7944	0.0006	0.0083	0.0350	0.899	0.931	0.925
17	0.1420	0.7632	0.0011	0.0159	0.0668	0.840	0.846	0.828
18	0.1323	0.7367	0.0016	0.0227	0.0957	0.786	0.787	0.762
19	0.1241	0.7157	0.0025	0.0285	0.1213	0.731	0.750	0.720
20	0.1089	0.6731	0.0039	0.0379	0.1632	0.566	0.629	0.594
21	0.1319	0.8219	0.0005	0.0072	0.0304	0.794	0.813	0.809
22	0.1225	0.7935	0.0010	0.0138	0.0582	0.743	0.744	0.731
23	0.1140	0.7704	0.0014	0.0198	0.0834	0.687	0.693	0.674
24	0.1069	0.7521	0.0021	0.0249	0.1060	0.630	0.659	0.639
25	0.0935	0.7118	0.0034	0.0336	0.1447	0.511	0.554	0.529
26	0.1156	0.8431	0.0004	0.0063	0.0266	0.728	0.722	0.721
27	0.1075	0.8179	0.0008	0.0121	0.0507	0.683	0.664	0.653
28	0.1004	0.7977	0.0012	0.0172	0.0725	0.628	0.619	0.606
29	0.0945	0.7806	0.0016	0.0221	0.0932	0.581	0.594	0.577
30	0.0823	0.7441	0.0018	0.0298	0.1279	0.459	0.482	0.480

CHAPTER 9

CONCLUSIONS AND SUGGESTIONS FOR FUTURE WORK

9.1 CONCLUSIONS

9.1.1 Thermodynamics of Reforming.

The equilibrium outlet gas composition for a hydrocarbon-steam reformer may be calculated from a comprehensive digital computer program which allows for:

(i) any hydrocarbon of empirical formula $C_p H_q$

(ii) feed containing H_2O, CO_2, or O_2 individually or any combination of these

(iii) relevant operating temperatures and pressures.

In addition to evaluating the gas composition, the program also tests whether carbon deposition will occur by the Boudouard reaction and/or by methane pyrolysis. In fact, this feature was the primary reason for the program development in the present work. The developed program is capable of handling the situation of incomplete conversion of C_pH_q provided that the methane-steam and water gas shift reactions are assumed to be at equilibrium and that the only remaining hydrocarbons are methane and the given component C_pH_q.

It is emphasized that the results of the program assume that the conditions considered prevail at all radial and longitudinal positions within the catalyst bed, although in fact composition and temperature variations will exist.

Thus the program has the versatility of predicting compositions and selecting operating conditions for the production of rich gas, oxo-synthesis gas, Fischer-Tropsch gas and lean gas. However, it was not utilized in the present work for these purposes, but was used for a survey of the carbon deposition boundaries over a range of temperature, pressure and steam ratio for the hydrocarbons CH_4 to $CH_{1.9}$ giving the principal conclusions:

(i) as the ratio of $\frac{q}{p}$ decreases at given temperature and pressure, the minimum steam to avoid carbon deposition increases

(ii) the critical region for carbon deposition for different hydrocarbons shifts from high-temperature low-pressure operation for the larger $\frac{q}{p}$ values to low-temperature high-pressure operation for the smaller $\frac{q}{p}$ values.

9.1.2 Catalyst Properties.

Although the catalyst used was standard I.C.I. 46 - 1, which was formulated particularly for naphtha reforming, it was used in the present work for methane reforming, because the ultimate intention was to make comparative studies of the whole range of hydrocarbons from methane to heptane.

B.E.T. nitrogen adsorption isotherms for crushed pellets yielded:

(i) 32.05 m^2/g for fresh unreduced catalyst

(ii) 29.80 m^2/g for catalyst after reduction at 650° C

(iii) 25.29 m^2/g for catalyst reduced at 650° C and used for reforming at 540° C, 1 atm abs. pressure with a H_2O : CH_4 ratio of 3.0, for a period of 14 hours.

Pore radii distributions determined from desorption isotherms showed that:

(i) powdered (125 - 150 μ) unreduced catalyst had two thirds of the total B.E.T. area within the range 18 - 30 Å with some pores up to 330 Å, and on grinding there was no significant change

(ii) crushed reduced used catalyst had two thirds of the total B.E.T. area within the range 28 - 61 Å , thus showing a distinct increase in pore size by crystallite sintering ; at the same time the large pores which were present in the unreduced catalyst had been completely lost, presumably by carbon deposition in this size of pore to which the reactant gas would have preferential access.

9.1.3 Kinetic Steps.

The contributions made by the various rate processes have been examined on cylindrical pellets presenting a definite external area of contact to an up-flowing stream of reactant gas. The rate of flow of gas and the annular gap between catalyst and reactor wall have been varied so that the mass of catalyst per unit flowrate of gas and the external area of catalyst per unit flowrate of gas had a range of values. All experimental rate determinations were made on freshly reduced catalyst within a period of fourteen hours after activation, during which the existence of essentially constant activity was confirmed.

Gas-film diffusion limitations:

It was found that the conversion was clearly dependent on the external surface exposed to the gas, and hence, that pore diffusion limits the rate of reaction. Since there were variations in hydraulic mean diameter in these experiments, it was considered appropriate in attempting to detect the gas-film resistance to plot conversions against N_{Re} rather than versus velocity. It was established that gas-film resistance ceased to have any effect for $N_{Re} > 4$ at 540°C.

An Arrhenius type plot of observed rate against reciprocal temperature was used to confirm the onset of gas-film diffusion resistance at other temperatures; the transition value of N_{Re} increased with temperature.

Pore-diffusion limitations:

The effectiveness factor of the catalyst was found to be no more than approximately 0.1 at 540° C and even less at higher temperatures as the intrinsic kinetic rate increased.

Further experiments were performed on ground sized fractions of the catalyst material in order to obtain additional evidence on the pore diffusion limitations ; but owing to unexpected massive carbon

this line of investigation was discontinued.

Effect of pressure:

Conversions for given $\frac{W}{F_T}$ did not change with pressure within the range 1 - 13 atm abs. at 600 - 700° C. Hence the adsorption rate of none of the components is likely to be a controlling factor for the reaction.

Effect of initial concentrations :

From the shape of plots of initial reaction rates against initial methane mole fractions, one of the stages of the chemical reaction step is concluded to be rate controlling for the normal steam-methane operations ratios. For lower steam-methane ratios it is possible that the desorption of one of the products assumes control.

9.1.4 Kinetic Mechanism and Rate Equation.

On the assumption that the reaction is controlled solely by either an adsorption, a desorption or the actual chemical conversion step, it has been concluded that the former two are not rate controlling. No attempts to interpret the chemical conversion as an actual mechanism have been made, but evidence for the initial formation of carbon dioxide rather than carbon monoxide has been obtained.

However, empirical expressions for the initial rate and for the overall rate of reaction have been obtained by the least mean squares approximation. The initial rate data at 540° C and 1 atm abs. pressure were best fitted by:

$$r_{m,i} = 0.000673\ p_{CH_4,i}^{0.973}\ p_{H_2O,\,i}^{1.094}$$

In addition, several empirical initial rate expressions allowing for the retardation effect of methane and steam adsorption have been found satisfactory ; their general form is :

$$r_{m,i} = \frac{k\, p_{CH_4,i}\, p^2_{H_2O,i}}{[1 + S\, p_{CH_4,i} + T\, p_{H_2O,i}]^3}$$

The overall rate expression valid for 540° C, 1 atm abs., and steam : methane ratios between two and seven for the adsorption of reactants and products was selected from several reasonably good fits as a compromise between the lowest sum of squares of approximation errors and the retention of integer powers on the partial pressure terms. The chosen overall rate expression was :

$$r_m = \frac{k\, p_{CH_4}\, p^2_{H_2O}}{[1 + Sp_{CH_4} + Tp_{H_2O} + Up_{CO} + Vp_{CO_2} + Yp_{H_2}]^3}$$

9.2 SUGGESTIONS FOR FUTURE WORK.

The ability to predict the conversion and the product composition in relation to the space velocity and catalyst quantity is vital for the design of a reforming reactor. Therefore, in order that the type of kinetic results reported in this work may have practical significance, it is necessary that the work be extended to cover wider ranges of the operating variables and relevant factors. Suggestions are made below for the extension of the work along these lines and attention is finally drawn to several possible changes in experimental technique.

9.2.1 Operating Parameters.

The following scientific aspects of the reaction are those considered worthy of further investigation:

(i) Rate data collected over a range of temperatures must be combined with that presented in this work to arrive at a correlation applicable to the full operating range of reforming plant. This will serve also to establish the dependence on temperature of the apparent rate constant and of the coefficients in the adsorption term of the semi-empirical rate equation. Furthermore, the boundaries of the transition

into the bulk phase diffusion controlled regime should be determined more exactly at temperatures other than 540° C.

(ii) The effect of high pressures (greater than 30 atm) at very high temperatures (greater than 800° C) are worth investigation, since the tendency of the process deveopment is for reformer operating pressures to be gradually increased in order to obtain more favourable economics for the overall operating efficiencies.

(iii) The factors which may cause deviations from the plug flow assumption, i.e. radial and longitudinal dispersion, back-mixing effects, temperature and concentration gradients at any cross-section of the bed, could be investigated. This subject will have a great significance in the actual design of a reformer.

(iv) The factors which lead to the formation and build-up of kinetic carbon with regard to their effective operating boundaries, as well as the structural rearrangement of the catalyst crystal that accompanies the formation and adsorption of carbon should be determined.

(v) The change in the crystal structure of the catalyst after reduction alone, and after reduction and reforming operation for varying periods must be correlated with the change of the isotherm patterns and hysteresis loops. Techniques such as X-ray diffraction will be needed for such studies.

(vi) There should be an extension to higher hydrocarbons (C_3H_8 to C_7H_{16}) with testing of the catalyst effectiveness or determination of its effective thickness.

(vii) It is reported that small concentrations of hydrogen present in the feed, especially in the case of higher hydrocarbons than methane enhance the reaction and prevent the deposition of kinetic

carbon. Thus, future work may study the effects of hydrogen on the performance of the catalyst.

9.2.2 Improvement of the Experimental Technique.

(i) A more precise temperature control to restrict the temperature fluctuations to a narrower range, could be obtained by adding three small resistances around the reactor corresponding to the height of the catalyst bed, each governed by a separate, individual temperature controller. There would then be no need for the time-consuming temperature scan of the catalyst bed.

(ii) Improvement in quenching the reformed gas to eliminate any possible occurrence of homogeneous or wall-catalysed reactions after the reformed gas has left the catalyst bed is suggested. This could be partially achieved by switching off the reactor upper section heating element in combination with the operation of the three resistors proposed above, but would be done more effectively by a structural modification to the upper section incorporating forced air cooling.

(iii) Experimental data collected for adiabatic operation will complete the picture by the use of simultaneous heat and mass balances for given rates of conversion.

(iv) While the present scale of operation was found adequate for fundamental catalyst development work, a larger scale would be appropriate for scale-up purposes. The scale of operation was rather small for extrapolation to industrial scale, and was too large for a mechanistic study from an analysis of product distribution. Moreover, the precision of the gas chromatograph is considered to be insufficient for the detection of minute concentrations of unstable intermediates or even stable end products.

LIST OF SYMBOLS

a_i Activity of the component i.

A_a Apparent frequency factor.

A_p Area of pores having an average pore radius $\bar{r}_p$, m^2/g.

c Concentration, $mole/cm^3$.

c Constant of the B.E.T. equation.

c_i Concentration of the component i, $mole/cm^3$.

$c_{i,b}$ Concentration of the component i in the bulk gas phase, $mole/cm^3$.

$c_{i,s}$ Concentration of the component i at the surface of catalyst, $mole/cm^3$.

c_p Heat capacity of the reacting mixture at constant pressure, $cal/(g)(^oC)$.

c_s Concentration at outside particle surface, $mole/cm^3$.

d Inside diameter of the hollow cylindrical catalyst pellet, cm.

d_p Equivalent diameter (diameter of a sphere having the same surface area as the particle), cm.

D_c Outside diameter of the cylindrical catalyst pellet, cm.

D_d Radial ($D_{d,rad}$) or axial ($D_{d,ax}$) eddy diffusion (dispersion) coefficient, cm^2/sec.

D_{eff} Effective diffusion coefficient for a porous solid, based on total cross section normal to direction of diffusion, cm^2/sec.

$D_{i,m}$ Coefficient of molecular diffusion of species i in the multicomponent mixture m, cm^2/sec.

D_K	Diffusion coefficient for Knudsen flow, cm^2/sec.
D_{poi}	Diffusion coefficient for forced (Poiseuille) flow, cm^2/sec.
D_R	Reactor diameter, cm.
E_a	Apparent activation energy for the reaction, cal/mole.
F_i	Feedrate of the reactant component i, moles/min.
F_s	Dead-space-factor of B.E.T. apparatus.
F_T	Total feedrate of the reactant mixture, moles/min.
G^o	Standard free energy, cal/mole.
ΔG_T^o	Standard free energy change of a reaction at T deg K, cal/mole.
G	Superficial mass velocity of the bulk gas phase, based on total or superficial bed cross-section normal to the direction of mean flow, $g/(cm^2)(sec)$.
G_M	Molal superficial mass velocity, $mole/(cm^2)(sec)$.
h	Height of the cylindrical catalyst pellet, cm.
h	Heat transfer coefficient, $cal/(cm^2)(sec)(^oC)$.
ΔH	Enthalpy change of the reaction, cal/mole ($\Delta H < 0$ indicates exothermic reaction).
$I = \frac{1}{V_m c}$	Intercept term of B.E.T. equation.
j_D	Mass transfer factor, dimensionless.
j_H	Heat transfer factor, dimensionless.
k_B	Boltzman constant.
k_c	Mass transfer coefficient, based on concentration, cm/sec.

k_G Mass transfer coefficient, based on partial pressure; $k_G = k_c \frac{1}{R_g T}$.

k_s Intrinsic reaction rate constant based on total surface of catalyst.

k_v Intrinsic reaction rate constant based on volume of catalyst particle.

K Thermodynamic equilibrium constant in terms of partial pressures of reaction components.

K_a Thermodynamic equilibrium constant in terms of activities of reaction components.

K_A Equilibrium constant for adsorption of component A.

$\bar{L}$ Mean length of the pore, cm.

$L = \frac{V_c}{S_c}$ Length parameter of the catalyst defined as the ratio of the volume of particle to the external surface, cm.

m Order of the reaction.

M_i Molecular weight of the species i, g/mole.

N_i Number of moles of component i, moles.

N_o Avogadro's Number.

$N_{Pe} = \frac{d_p U}{D_d}$ Peclet number, dimensionless.

$N_{Pr} = \frac{c_p \mu}{\lambda}$ Prandtl number, dimensionless.

$N_{Re} = \frac{d_p G}{\mu}$ Reynolds number, dimensionless.

$N_{Sc} = \frac{\mu}{\rho D_{i,m}}$ Schmidt number, dimensionless.

N_T Total number of moles of the reaction mixture in the reactor, moles.

p_f Pressure film factor, atm.

p_i Partial pressure of the component i, atm.

$\frac{p}{p_o}$ Relative pressure (B.E.T. equation).

p_T Total pressure of the reaction mixture in the reactor, atm.

Q_t Rate of heat transfer, cal/(sec)(g of catalyst).

$\frac{q}{p}$ Ratio, atoms of hydrogen: atoms of carbon in the hydrocarbon feed.

r Reaction rate;
r_v=mole/(mole/(cm^3 of catalyst volume)(min);
r_m=mole/(g of catalyst)(min);
r_s=mole/(cm^2 of catalyst external surface)(min).

r_D Rate of bulk phase diffusion, mole/(cm^2 catalyst external surface)(min).

r_i Initial reaction rate.

$r_{obs.}$ Observed (experimentally determined) reaction rate.

r_p Radius of a pore, $\mathring{A}$.

$\bar{r}_p$ Mean radius pores, $\mathring{A}$.

R Radius of a spherical catalyst particle, cm.

R_g Universal gas constant, 1.987 cal/(mole)(^oK) or (8.3143)(10^7) ergs/(mole)(^oK).

$s=\frac{c-1}{V_m c}$ Slope of the B.E.T. equation.

S_c External surface area of the catalyst pellet, cm^2.

S_g Total surface area of the catalyst per unit mass (B.E.T. area), cm^2/g.

S_x External surface area of the catalyst particle per unit mass, accessible to reactant gas, cm^2/g.

$S_v=\rho_p S_g$	Total surface area of the catalyst per unit volume of the particle, cm^2/cm^3.
t	Multilayer thickness of the physically adsorbed layer built-up at pressure p, cm.
T	Absolute temperature, ^oK.
T_b	Bulk gas phase temperature, ^oK.
T_i	Temperature within the pore, ^oK.
T_s	Temperature at outside surface of catalyst.
V	Molal volume of liquid, cm^3/mole.
V_c	Volume of a catalyst pellet, cm^3.
V_g	Total pore volume per unit mass of catalyst, cm^3/g.
V_m	Volume of gas adsorbed in a mono-molecular layer, cm^3.
V_{mol}	Molal volume of gas, 22400 cm^3/mole at S.T.P.
V_R	Reactor volume, cm^3.
V_s	Volume of gas adsorbed at saturation pressure of adsorbate, cm^3.
u	Linear velocity of the bulk gas phase, cm/sec.
W	Mass of the catalyst charge, g.
x_i	Moles of component i reacted or formed per mole of total feed, mole per mole.
y_i	Mole fraction of component i, mole/mole.
Z.B.V.	Zero-bulk-volume of B.E.T. apparatus, cm^3.

GREEK LETTERS

α	steam : hydrocarbon molar ratio in the feed, $H_2O:C_pH_q$ mole/mole.
α'	Ratio, moles of steam : atoms of carbon of the hydrocarbon feed.
α	Condensation coefficient in adsorption kinetics.
β	carbon dioxide : hydrocarbon molar ratio in the feed, $CO_2:C_pH_q$ mole/mole.
$\beta=c_s\frac{(-\Delta H)(D_{eff})}{\lambda T_s}$	Heat generation function parameter, as defined by Weisz and Hicks.
γ	oxygen : hydrocarbon molar ratio in the feed, $O_2:C_pH_q$ mole/mole.
$\gamma=\frac{E}{R_gT_s}$	parameter, as defined by Weisz and Hicks.
β	Correction factor for non-ideality of nitrogen.
γ'	Volume change modulus, dimensionless.
ε	Void fraction of the catalyst bed, cm^3/cm^3.
ε_m	Void fraction of micro-pore region, cm^3/cm^3.
ε_M	Void fraction of macro-pore region, cm^3/cm^3.
λ	Thermal conductivity of porous structure, cal/(sec)(cm^2 total cross section)(^oC/cm).
λ_{eff}	Effective thermal conductivity of the reacting mixture, cal/(sec)(cm)(^oC).
η	Effectiveness factor, dimensionless.
μ_i	Viscosity of the component i, g/(cm)(sec).
μ_m	Viscosity of the reacting mixture, g/(cm)(sec).

ν_i	Stoichiometric coefficient of the reaction component i.
Ω	Collision integral for viscosity, evaluated by the Lennard-Jones intermolecular potential function for non-polar species.
ϕ	Thiele modulus, dimensionless.
ϕ_s	Thiele modulus for spherical geometry, dimensionless.
ϕ_L	Thiele modulus for flat plate (slab) geometry, dimensionless.
ϕ_{sp}	Thiele modulus for single pore model.
ϕ_s	Shape factor (sphericity), dimensionless.
ϕ_{ij}	Collision function of the species i and j.
$\Phi = \frac{L^2}{D_{eff}} \cdot \frac{1}{C_s} \cdot r_{obs}$	Modified Thiele modulus, as defined by Weisz and co-workers, dimensionless.
ρ	Density of the bulk gas phase, g/cm^3.
ρ_p	Apparent density of the catalyst.
ρ_t	True density of the catalyst.
σ	Surface tension, dyne/cm.
σ_i	Diameter of a molecule based on the assumption of a rigid spherical model, $\mathring{A}$.
τ	Tortuosity factor, dimensionless.
θ	Fraction of adsorbent surface which is covered by a mono-molecular layer of adsorbate molecules, cm^2/cm^2.
θ	Constant angle, ^{o}.
θ	Porosity of the catalyst, cm^3/cm^3.

SUBSCRIPTS

b	Bulk phase.
f	Final condition.
i	Initial condition.
i	Component i in the gaseous reacting mixture.
j	Component j in the gaseous reacting mixture.
p	Atoms of carbon in hydrocarbon molecule.
q	Atoms of hydrogen in hydrocarbon colecule.

REFERENCES

1. Adsetts, J.R., I.C.I. Agricultural Division, Billingham, Teeside, Private Communication (1971).

2. Akers, W.W., and D.P. Camp, A.I.Ch.E.J., 1, 471 (1955)

3. Akers, W.W.,and R.R. White, Chem. Eng. Prog., 44, 553 (1948)

4. Anderson, R.B., J. Catalysis, 3, 50 (1964).

5. Anderson, J.R., and B.G. Baker, Proc.Roy.Soc., A-271, 402 (1963)

6. Andrew, S.P.S., Inst. Fuel Proc., Eastbourne Conference, Vol.1, 235 (1965)

7. Andrew, S.P.S., Chem.Ind., 20, 826 (1965)

8. Andrew, S.P.S., Ind. Eng., Chem., Product Research & Development, 8, 321 (1969)

9. Aris, R., "Elementary Chemical Reactor Analysis", Prentice-Hall Inc. Englewood Cliffs, New Jersey, U.S.A. (1969)

10. Aris, R., Chem.Eng.Sci., 6, 262 (1957)

11. Arnold, M.R., K. Atwood, H.M. Baugh,& H.D. Smyser, Ind. Eng. Chem., 44, 999 (1952)

12. Baker, R.G., & W.L. Mercer, Inst. Gas Eng. J., 7, 36 (1967)

13. Balashova, S.A., T. Slovokhotova, & A.A. Balandin, Izv. Akad. Nauk. (U.S.S.R.), Old. Khim. Nauk. (1965); Engl. transl., Prull. Acad. Sci. U.S.S.R., 258 (1965)

14. Barrett, E.P., L.G. Joyner,& P.P. Halenda, J. Amer. Chem. Soc., 73, 373 (1951)

15. Belchetz, L., and E.K. Rideal, J. Amer. Chem. Soc., 57, 1168 (1935)

16. Bhatta, K.S.M.,and G.M. Dixon, Trans. Faraday Soc., 63, 2217 (1967)

17. Bhatta, K.S.M., and G.M. Dixon, Ind. Eng. Chem., Product Research and Development, 8, 3 (1969)

18. Binder, G.G.,and R.R. White, Chem. Eng. Prog., 46, 563 (1950)

19. Bischoff, K.B., A.I.Ch.E.J., 11, 351 (1965)

20. Bodrov, I.M.,and L.O. Apel'baum, Kinetika i Kataliz, engl.transl., 8, 326 (1967)

21. Bodrov, I.M., L.O. Apel'baum,and M.I. Temkin, Kinetika i Kataliz, engl. transl., 5, 614 (1964)

22. Bodrov, I.M., L.O. Apel'baum,and M.I. Temkin, Kinetika i Kataliz, engl. transl., 8, 696 (1967)

23. Bogue, R.H., "The Chemistry of Portland Cement", Reinhold Publishing Comp., New York, U.S.A. (1947)

24. Boudart, M., A.I.Ch.E.J., 2, 62 (1956)

25. Boudart, M., C.E. Heath,and V. Kevorkian, J.Phys.Chem., 64, 964 (1960)

26. Bridger, G.W.,Chem. Proc. Eng., 47, 39 (1966)

27. Bridger, G.W., and W. Wyrwas, Chem.Proc.Eng., 48, 101 (1967)

28. Brötz, W., "Fundamentals of Chemical Reaction Engineering", translated by D.A. Diener and J.A. Weaver, Addison-Wesley Publishing Co., Reading, Massachusetts, U.S.A. (1965)

29. Brunauer, S., P.H. Emmett, and E. Teller, J. Amer. Chem.Soc., 60, 309 (1938)

30. Cadle, P.J. and C.N. Satterfield, Ind. Eng. Chem., Fundamentals, 7, 189 (1968)
ibid., 7, 132 (1968)

31. Catalyst Handbook, Wolfe Scientific Books, London (1970)

32. Chambers, R.P.,and M. Boudart, J. Catalysis, 6, 141 (1966)

33. Chu, C., and O.A. Hougen, Chem.Eng. Sci., 17, 167 (1962)

34. Clark, A.A.H., G.F.I. Roberts, P.J. Savage,& E. Spivey, Inst. Gas Eng. J., 6, 20 (1966)

35. Cockerham, R.G., G. Percival,and T.A. Yarwood, Inst. Gas Eng. J., 5, 109 (1965)

36. Cooper, A.R. and G.V. Jeffreys, "Chemical Kinetics and Reactor Design" Oliver-Boyd, Edinburgh, (1971)

37. Corrigan, T.E., Chem. Eng., 61, 11, 236 (1954)
ibid., 61, 12, 198 (1954)
ibid., 62, 1, 199 (1955)
ibid., 62, 2, 195 (1955)
ibid., 62, 3, 201 (1955)
ibid., 62, 4, 198 (1955)
ibid., 62, 5, 203 (1955)
ibid., 62, 7, 227 (1955)

38. Coulson, J.M.,and J.F. Richardson, "Chemical Engineering", Vol. III, ed. by J. Richardson and D.G. Peacock, Pergamon Press, Oxford (1971)

39. Cranston, R.W.,and F.A. Inkley, Advan. Catalysis, IX, 143 (1957)

40. Cribb, G.S., Brit. Chem. Eng., 9, 366 (1964)

41. Cryder, D.S.,and D.J. Porter, Ind. Eng. Chem., 29, 1667 (1937)

42. Damköhler, G., Chemie-Ingenieur, III, 430 (1937)

43. Davies, H.S.,and K.J. Humphries, Inst. Gas Eng. J., 7, 708 (1967)

44. DeAcetis, J.,and G. Thodos, Ind. Eng. Chem., 52, 1003 (1960)

45. Dell, R.M.,and V.C. Wheeler, Trans. Faraday Soc., 58, 1590, (1962)

46. Denbigh, K.G.,and J.C.R. Turner, "Chemical Reactor Theory", 2nd ed., Cambridge University Press, Cambridge (1971)

47. Dent, F.J., L.A. Moignard, A.H. Eastwood, W.H. Blackburn and D. Hebden, 49th Report of the Joint Research Committee of the Gas Research Board and the University of Leeds (1949)

48. Dent, F.J., Gas and Coke, 13, 275 (1965)

49. Dirksen, M.A., H.R. Linden and E.S. Pettyjohn, Inst. Gas Techn. Research Bull., No. 4 (1953)

50. Dirksen, D.A., and C.H. Riesz, Ind. Eng. Chem., 45, 1562 (1953)

51. Dixon, G.M.,and F.E. Shephard, Inst. Gas Eng. J., 7, 383 (1967)

52. Dodge, B.F., Trans. Amer. Inst. Chem. Eng., 34, 529 (1938)

53. Dodge, B.F., "Chemical Engineering Thermodynamics", McGraw-Hill Book Co., New York, U.S.A. (1944)

54. Dowden, D.A., Ind. Eng. Chem., 44, 977 (1952)

55. Dowden, D.A., R.G. Schnell,and G.T.Walker, Paper presented to the Fourth International Congress on Catalysis, Moscow (1968)

56. Eisenberg, B. and H. Bliss, Chem. Eng. Symposium Series, No.72, Vol. 63, 3 (1967)

57. Faeth, P.A., "Adsorption and Vacuum Technique", The University of Michigan, Institute of Science and Technology, Ann Arbour, U.S.A. (1962)

58. Fischer and Porter, Flowmeter Handbook, 10-A-9010, Warminster, Pennsylvania, U.S.A.

59. Fox, J.M.,and J.C. Yarze, Ind. Chem., 65 (1964)

60. Frank-Kamenetskii,D.A. "Diffusion and Heat Exchange in Chemical Kinetics", engl. transl. by N. Thon, Princeton University Press, Princeton (1955)

61. Gadsby, J., C.N. Hinshelwood,and K.W. Sykes, Proc. Royal Soc., A-187, 129 (1946)

62. Galwey, A.K., Proc. Royal Soc., A-271, 218 (1963)

63. Geniesse, J.C.,and R. Reuter Ind. Eng. Chem., 24, 219 (1932)

64. Germain, J.E.,and C. Vaniscotte,Bull. Soc. Chim. France, 692 (1957) ibid., 319 (1958)

65. Gilliland, E.R., R.F. Baddour, and J.L. Russell, A.I.Ch.E.J., 4, 90 (1958)

66. Gilliland, E.R., and P. Harriott, Ind. Eng. Chem., 46, 2195 (1954)

67. Gordon, A.S., J. Amer. Chem. Soc., 70, 395 (1948)

68. Gordon, A.S., Ind. Eng. Chem., 44, 1857 (1952)

69. Goring, G.E., G.P. Curran, R.P. Tarbox, and E. Gorin, Ind. Eng. Chem., 44, 1051 (1952)

70. Greensfelder, B.S., and H.H. Voge, Ind. Eng. Chem., 37, 514 (1945)

71. Greensfelder, B.S., H.H. Voge, and G.M. Good, Ind. Eng. Chem., 37, 1168 (1945)

72. Grossman, L.M., Trans. Amer. Inst. Chem. Eng., 42, 535 (1946)

73. Gulbransen, E.A., and K.F. Andrew, Ind. Eng. Chem., 44, 1034 (1952)

74. Haley, A.J., J. Appl. Chem., 13, 392 (1963)

75. Hawk, C.O., P.L. Golden, H.H. Storch, and A.C. Fieldman, Ind. Eng. Chem., 24, 23 (1932)

76. Hebden, D., Trans. Inst. Gas Eng., 95, 602 (1945)

77. Hebden, D., and D.A. Percy, Inst. Gas Eng. J., 7, 719 (1967)

78. Hofer, L.J.E., E.M. Cohn, and W.C. Pebbles, J. Phys. Chem., 54, 1161 (1950)

79. Holland, D.R., and S.W.Wan, Chem.Eng. Prog., 59, 69 (1963)

80. Hollis, O.L., Advan. Gas Chromato., ed. by A. Zlatkis and L.S. Ettre, Preston Technical Abstracts Co., Evanston, U.S.A. (1966)

81. Hollis, O.L., and W.V. Hayes, J. Gas Chromato., 4, 235 (1966)

82. Hougen, O.A, and K.M. Watson, "Chemical Process Principles", Vol. 2, John Wiley, London (1954)

83. Hougen, O.A., and K.M. Watson, "Chemical Process Principles", John Wiley, London (1947)

84. Ipatieff, V.N., G.S. Monroe, and L.E. Fischer, Ind. Eng. Chem., 42, 92 (1950)

85. Ishiguro, T., Chem. Proc. Eng., 47, No.2, 87 (1968)

86. International Critical Tables of Numerical Data, National Research Council, U.S.A., ed. by E.W. Washburn, Vol. III, McGraw-Hill Book Co., New York, U.S.A. (1928)
ibid., Vol. III., (1928).

87. Johns, T., "Beckman Gas Chromatography Manual", Beckman Instruments, Inc.

88. Joy, A.S., Vacuum, 3, 254 (1963)

89. Kassel, L.S., J. Amer. Chem. Soc., 54. 3949 (1932)

90. Kemball, C., Proc. Royal Soc., A-207, 539 (1951)

91. Kemball, C., Catalysis Rev., 5, 33, (1972)

92. Kemball, C.,and H.S. Taylor, J. Amer. Chem. Soc., 70, 345 (1948)

93. Knox, J.H., "Gas Chromatography", Methuen, London (1962)

94. Kramers, H., Chem. Eng. Sci., 8, 45 (1958)

95. Landolt-Börnstein, "Zahlenwerte und Funktionen", 6th edition, Vol. II, Part 2a, Springer Verlag, Berlin (1960)

96. Lapidus, L., "Digital Computation for Chemical Engineers", McGraw-Hill Book Co., New York U.S.A. (1962)

97. Leibush, A.G.,and G.Ya. Bergo, J. Chem. Ind. U.S.S.R., 15, 41 (1938); Chem. Abstr. 32, 7698-8 (1938)

98. Leibush, A.G.,and M.A. Lyudkovskaya, Trudy Nauk. - Issledovatel i Proekt Inst. Azot, Prom., No.2, 62 (1952); Chem. Abstr., 52, 17919-g (1958)

99. Levenspiel, O., "Chemical Reaction Engineering", John Wiley, New York, U.S.A. (1962)

100. Lewis, W.K., E.R. Gilliland,and W.A. Reed, Ind. Eng. Chem., 41, 1227 (1949)

101. Lihou, D.A., Chem. Proc. Eng., 46, 487 (1965)

102. Marschner, R.F., Ind. Eng. Chem., 30, 554 (1938)

103. Masamune, S.,and J.M. Smith, A.I.Ch.E.J., 10, 246 (1964)

104. Mayland, B.J.,and G.E. Hays, Chem. Eng. Prog., 45, 452 (1949)

105. McD. Baker, M., and E.K. Rideal, Trans. Faraday Soc., 51, 1597 (1955)

106. McD. Baker, M., G.I. Jenkins,and E.K. Rideal, Trans.Faraday Soc., 51, 1592 (1955)

107. McKee, D.W., J. Amer. Chem. Soc., 84, 1109 (1962)

108. McKee, D.W., J. Amer. Chem. Soc., 84, 4427 (1962)

109. Mills, G.A., E.K. Boedeker,and A.G. Oblad, J. Amer. Chem.Soc., 72, 1554 (1950)

110. Mingle, J.O.,and J.M. Smith, Chem.Eng. Sci., 16, 31 (1961)

111. Montgomery, C.W., E.B. Weinberger,and D.S. Hoffman, Ind. Eng. Chem., 40, 601 (1948)

112. Morikawa, K., W.S. Benedict and H.S. Taylor, J. Amer. Chem. Soc., 58, 1445 (1936), ibid., 58, 1795 (1936).

113. Morikawa, K., N.R. Trenner,and H.S. Taylor, J. Amer. Chem. Soc., 59, 1103 (1937)

114. Nicklin, T., R.J. Whittaker,and G.M. Dixon, Nature, 212, 1367 (1966)

115. Nicklin, T., F. Farrington,and K.H. Burgess, Inst. Gas Eng. J., 8, 473 (1968)

116. Nicklin, T., F. Farrington and R.J. Whittaker, Inst. Gas Eng. J., 10, 151 (1970)

117. Nicklin, T.,and R.J. Whittaker, Inst. Gas Eng. J., 8, 15 (1968)

118. Padovani, C., Inst. Gas Eng. J., 4, 760 (1964)

119. Parkyns, N.D., Discussions of the paper "Further Developments in the Nickel-Urania- and-Alumina Catalyst System" by T. Nicklin, F. Farrington and R.J. Whittaker, Inst. Gas Eng. J. 10, 151 (1970)

120. Patai, S., E. Hofmann, and E. Rajbenbach, J. Appl. Chem., 2, 316 (1952)

121. Pease, R.N.,and P.R. Chesebro, J. Amer. Chem. Soc., 50, 1464 (1938)

122. Perry, J.H., "Chemical Engineers' Handbook", 4th edition, eds. R.H. Perry, C.H. Chilton and S.D. Kirkpatrick, McGraw-Hill Book Co., New York, U.S.A. (1963)

123. Petersen, E.E., "Chemical Reaction Analysis", Prentice-Hall, Inc., Englewood Cliffs, New Jersey, U.S.A. (1965)

124. Phillips, T.R., T.A. Yarwood, J. Mulhall,and G.E. Turner, J. Catalysis, 17, 28 (1970)

125. Phillips, T.R., J. Mulhall,and G.E. Turner, J. Catalysis, 15, 233 (1969)

126. Pierce, C., J. Phys. Chem., 57, 149 (1953)

127. Quibel, J., Chem. Proc. Eng., 50, No.6, 83 (1969)

128. Rakovskii, E.V., O.A. Burinova, and M.E. Rakovskii, Khim. Tverdogo Topliva, 8, 347 (1937); Chem. Abstr., 32, 1878-8 (1938)

129. Reid, R.C., and T.K. Sherwood, "The Properties of Gases and Liquids", 2nd edition, McGraw-Hill Book Co., New York, U.S.A. (1966)

130. Reitmeier, R.E., K. Atwood, H.A. Bennett, Jr., and H.M. Baugh, Ind. Eng. Chem., 40, 620 (1948)

131. Ribesse, J., and C. Van Maele, Inst. Gas Eng. J., I, 631 (1961)

132. Rice, F.O.,and K.F. Herzfeld, J. Amer. Chem. Soc., 56, 284 (1934)

133. Ries, H.E., R.A. van Nordstrand, M.F.L. Johnson,and H.O. Bauermeister, J. Amer. Chem. Soc., 67, 1242 (1945)

134. Riesz, C.H., H.A. Dirksen,and W.J. Pleticka, Bull. Inst. Gas Techn., 20 (1952)

135. Riesz, C.H., R. Lister, L.G. Smith,and V.I. Komarevsky, Ind. Eng. Chem., 40, 718 (1948)

136. Rittenhouse, G., J. Sed. Petrology, 13, 79 (1943)

137. Riverola, J.B.,and J.M. Smith, Ind. Eng. Chem. Fundamentals, 3, 308, (1964)

138. Roberts, G.W.,and C.N. Satterfield, Ind. Eng. Chem.,Fundamentals, 4, 288 (1965)

139. Roberts, G.W.,and C.N. Satterfield, Ind. Eng. Chem.,Fundamentals, 5, 317 (1966)

140. Rooke, D.E., Inst. Gas Eng. J., 7, 586 (1957)

141. Satterfield, C.N., "Mass Transfer in Heterogeneous Catalysis", Massachusetts Institute of Technology Press, Cambridge, Massachusetts, U.S.A. (1970)

142. Satterfield, C.N.,and P.J. Cadle, Ind. Eng. Chem., Fundamentals, 7, 202 (1968)

143. Schlaffer, W.G., C.R. Adams,and J.N. Wilson, J. Phys. Chem., 69, 1530 (1965)

144. Schlaffer, W.G., C.Z. Morgan,and J.N. Wilson, J. Phys. Chem., 61, 714 (1957)

145. Schneider, I.A., Z Physik. Chemie, 218, 338 (1961)
ibid.,220, 199 (1962)
ibid.,233, 234 (1963)

146. Schnell, C.R., J. Chem. Soc., (B). Phys. Org., 158 (1970)

147. Schwartz, C.E., and J.M. Smith, Ind. Eng. Chem., 45, 1209 (1953)

148. SenGupta, A.,and G. Thodos, Chem. Eng. Progr., 58, No.7, 58 (1962)

149. Sherwood, T.K., "A Course in Process Design", The M.I.T. Press, Cambridge, Massachusetts, U.S.A. (1963)

150. Shull, C.G., J. Amer. Chem. Soc., 70, 1405 (1948)

151. Slovokhotova, T.A., A.A. Balandin,and G.I. Usova, Vest. Mosk. Univ., Ser. II, Khim. 17, 26 (1962); Chem. Abstr., 58, 3283-c (1962)

152. Slovokhotova, T.A., and A.P. Ivanov, Vest. Mosk. Univ. Ser. Math. Mekh. Fiz. i Khim., 6, 125 (1951); Chem. Abstr., 46, 4340-a (1951)

153. Smith, J.M., "Chemical Engineering Kinetics", 2nd edition, McGraw-Hill Book Co., New York, U.S.A. (1970)

154. Somer, T.G., Brit. Chem. Eng., 8, 7 (1963)

155. Soonawala, H.D., Ph.D. Thesis, University of Birmingham (1969)

156. Spiers, H.M., "Technical Data on Fuel", 6th edition, The British National Committee, World Power Conference (1962)

157. Steacie, E.W.R., and I.E. Puddington, Can. J. Research, 16B, 176 (1938)
ibid., 16B, 260 (1938)
ibid., 16B, 411 (1938)

158. Storch, H.H., J. Amer. Chem. Soc., 54, 4188 (1932)

159. Storch, H.H., Ind. Eng. Chem., 37, 340 (1945)

160. Tamle, M.W., Disc. Faraday Soc., 8, 270 (1956)

161. Thiele, E.W., Ind. Eng. Chem., 31, 916 (1939)

162. Thomas, J.M., and W.J. Thomas, "Introduction to the Principles of Heterogeneous Catalysis", Academic Press, Inc., New York, U.S.A. (1967)

163. Tierney, J.W., R.M. Baird, and L.H.S. Roblee, A.I.Ch.E.J., 4, 460 (1958)

164. Topsøe, H., Inst. Gas Eng. J., 6, 401 (1966)

165. Wagman, D., J. Kilpatrick, W. Taylor, K. Pitzer, and F. Rossini, J. Research Nat. Bur. of Standards, 34, 143 (1945)

166. Wakao, N., and J.M. Smith, Chem. Eng. Sci., 17, 825 (1962)

167. Wakao, N., and J.M. Smith, Ind. Eng. Chem., Fundamentals, 3, 123 (1964)

168. Waterhouse, J., Gas World, 23rd Jan., 132 (1965)

169. Weekman, V.W.Jr., J. Catalysis, 5, 44 (1966)

170. Weekman, V.W.Jr., and R.L. Gorring, J. Catalysis, 4, 260 (1965)

171. Weisz, P.B., Z. Physik. Chem., Neue Folge, 11, 1 (1957)

172. Weisz, P.B., and J.S. Hicks, Chem. Eng. Sci., 17, 265 (1962)

173. Weisz, P.B., and C.D. Prater, Advan. Catalysis, Vol. VI, 143 (1954)

174. Weller, S., A.I.Ch.E.J., 2, 59 (1956)

175. Wheeler, A., "Catalysis", Vol. II, ed. H. Emmett, Reinhold Publishing Co., New York, U.S.A. (1955) ibid., Vol.III., ed. H. Emmett. Reinhold PublishingCo., New York, U.S.A. (1956)

176. Wicke, E., Chem.-Ing.-Tech., 29, 305 (1957)

177. Wilhelm, R.H., J. Pure Appl. Chem., 5, 403 (1962)

178. Wilhite, W.F., and O.L. Hollis, J. Gas Chromatog., 6, No. 2, 84 (1968)

179. Woodcock, C.J., Ph.D Thesis, Chem. Eng. Department, The University of Aston in Birmingham (1971)

180. Wright, P.G., P.G. Ashmore, and C. Kemball, Trans. Faraday Soc., 54, 1692 (1958)

181. Wright, M.M., and H.S. Taylor, Can. J. Research, 27 B, 303 (1949)

182. Yang, K.H., and O.A. Hougen, Chem. Eng. Prog., 46, 146 (1950)

183. Yarze, J.C. and T.E. Lockerbie, "Catalytic Steam Reforming of Light Liquid Hydrocarbons, The Kellogg Co., Research and Development Department, New Jersey, U.S.A. (1958)

184. Yoshida, F., D. Ramaswani, and O.A. Hougen, A.I.Ch.E.J., 8, 5 (1962)

185. Zel'dovitch, Y.B., Acta Physico-chim. U.S.S.R., 10, 583 (1939)

A P P E N D I C E S

LIST OF APPENDICES

LIST OF APPENDICES

A - 2.1

The Print-out of the Computer Program and of the Calculated Results of Equilibrium Gas Composition

Feedstocks	C_pH_q	(p = 1, q = 2)
	CH_4	(p = 1, q = 4)

```
JOB EQUILIBRIA,CESTF315,ATAMER,STREAM 4      RUN BY GEORGE 2/MK8C ON 08/07/70 AT 11.36
DISPLAY '  4EQUILIBRIA  '
LOG
MAXTIME 600
VOLUME 4000
VOLUME 14000
FORTRANUB ,,,,,,,T
PROGRAMLOAD XFAT,COMP,
CONSOLIDATE
RUN
****
```

```
FORTRAN COMPILATION BY #XFAT MK 2E    DATE  08/07/70  TIME  11/37/07
```

```
0001                MAP                                                          EQU  100
0002                PROGRAM  (EQUILIBRIUM  COMPOSITION)                          EQU  200
0003                INPUT 1=CR0                                                  EQU  300
0004                OUTPUT 2=LP0                                                 EQU  400
0005                TRACE 2                                                      EQU  500
0006                END                                                          EQU  600

0007                MASTER                                                       EQU  700
0008          C     EQUILIBRIUM  COMPOSITION  OF  STEAM REFORMED HYDROCARBONS    EQU  800
0009          C     T   = TEMPERATURE OF CATALYST   DEG.F                        EQU  900
0010          C     PT  = OPERATING PRESSURE   ATM.                              EQU 1000
0011          C     SR  = MOLS OF STEAM PER MOL OF HYDROCARBON FEED              EQU 1100
0012          C     PK1 = EQUILIBRIUM CONSTANT OF METHANE-STEAM REFORMING REACTION EQU 1200
0013          C     PK2 = EQUILIBRIUM CONSTANT OF WATER GAS SHIFT REACTION       EQU 1300
0014          C     PK3 = EQUILIBRIUM CONSTANT OF BOUDOUARD REACTION             EQU 1400
0015          C     PK4 = EQUILIBRIUM CONSTANT OF METHANE DECOMPOSITION          EQU 1500
```

```
0016          C     BASIS OF CALCULATION = 1MOL OF HYDROCARBON                                EQU 1600
0017                DIMENSION PT(10),T(8),PK1(8),PK2(8),PK3(8),PK4(8),X(8),Y(8),ER1(8) QU 1700
0018               1,ER2(8),P(13),Q(13),SR(13)                                              EQU 1800
0019          C     DATA INPUT                                                               EQU 1900
0020                READ(1,100)(PT(J),J=1,10)                                                EQU 2000
0021                READ(1,110)(T(I),PK1(I),ER1(I),PK2(I),ER2(I),PK3(I),PK4(I),I=1,8) EQU 2100
0022                WRITE(2,111)                                                             EQU 2200
0023                WRITE(2,112)(T(I),PK1(I),ER1(I),PK2(I),ER2(I),PK3(I),PK4(I),I=1,8) QU 2300
0024                READ (1,307) N                                                           EQU 2310
0025                READ (1,119) (P(L),Q(L),SR(L),L=1,N)                                     EQU 2400
0026                WRITE(2,120)(P(L),Q(L),SR(L),L=1,13)                                     EQU 2500
0027                READ(1,140)(X(M),Y(M),M=1,8)                                             EQU 2600
0028                WRITE(2,140)(X(M),Y(M),M=1,8)                                            EQU 2700
0029                LL=0                                                                     EQU 2800
0030          C     CHANGE OF PARAMETER  (SR)                                                EQU 2900
0031                DO 50 L = 1,N                                                            EQU 3000
0032          C     CHANGE OF PARAMETER  (T)                                                 EQU 3100
0033                DO 1 I=1,8                                                               EQU 3200
0034          C     INITIAL APPROXIMATIONS FOR A AND B                                       EQU 3300
0035                A=X(I)                                                                   EQU 3400
0036                B=Y(I)                                                                   EQU 3500
0037          C     CHANGE OF PARAMETER  (PT)                                                EQU 3600
0038                DO 2 J=1,10                                                              EQU 3700
0039          C     SOLUTION OF THE EQUATIONS BY NEWTON METHOD                               EQU 3800
0040                DO 3 K=1,50                                                              EQU 3900
0041                C=0.5*Q(L)-2.0*P(L)+3.0*A+4.0*B                                          EQU 4000
0042                D=P(L)-A-B                                                               EQU 4100
0043                R=SR(L)-A-2.0*B                                                          EQU 4200
0044                S=0.5*Q(L)-P(L)+SR(L)+2.0*A+2.0*B                                        EQU 4300
0045                DRS=D*R*S*S                                                              EQU 4400
0046                PSQ=PT(J)**2                                                             EQU 4500
0047                PAS=PSQ*A*C**3                                                           EQU 4600
0048                F=PAS-DRS*PK1(I)                                                         EQU 4700
0049                G=B*C-A*R*PK2(I)                                                         EQU 4800
0050                FA=PSQ*C*C*(C+9.0*A)-PK1(I)*S*(4.0*D*R-S*R-S*D)                          EQU 4900
0051                GA=3.0*R-PK2(I)*(R-A)                                                    EQU 5000
0052                FB=12.0*PSQ*A*C*C-PK1(I)*S*(4.0*D*R-S*R-2.0*S*D)                         EQU 5100
```

```
0053                GB=C+4.0*B+2.0*A*PK2(I)                                  EQU 5200
0054                DENOM=FA*GB-FB*GA                                        EQU 5300
0055                IF(DENOM)4,5,4                                           EQU 5400
0056              5 WRITE(2,200)                                             EQU 5500
0057                GO TO 2                                                  EQU 5600
0058              4 DELA=(G*FB-F*GB)/DENOM                                   EQU 5700
0059                DELB=(F*GA-G*FA)/DENOM                                   EQU 5800
0060                CH2=(B*C)/(A*R)                                          EQU 5900
0061                ERR2=ABS(PK2(I)-CH2)                                     EQU 6000
0062                IF (ER2(I)-ERR2)7,6,6                                    EQU 6100
0063              6 CH1=(PSQ*A*C**3)/DRS                                     EQU 6200
0064                ERR1=ABS(PK1(I)-CH1)                                     EQU 6300
0065                IF (ER1(I)-ERR1)7,15,15                                  EQU 6400
0066              7 A=A+DELA                                                 EQU 6500
0067              3 B=B+DELB                                                 EQU 6600
0068                LL=LL+1                                                  EQU 6700
0069                IF(LL-10)8,8,27                                          EQU 6800
0070              8 WRITE(2,210)A,B,F,G                                      EQU 6900
0071                GO TO 1                                                  EQU 7000
0072              C COMPOSITION OF THE REFORMED GAS ON DRY BASIS              EQU 7100
0073             15 SUM=A+B+C+D                                              EQU 7200
0074                PCD=100.0*D/SUM                                          EQU 7300
0075                PCA=100.0*A/SUM                                          EQU 7400
0076                PCB=100.0*B/SUM                                          EQU 7500
0077                PCC=100.0*C/SUM                                          EQU 7600
0078                TOT=A+B+C+D+R                                            EQU 7700
0079                D1=A+B                                                   EQU 7800
0080                D2=A+C                                                   EQU 7900
0081                D3=A+B+D                                                 EQU 8000
0082                A1=A/B                                                   EQU 8100
0083                A2=D2/D3                                                 EQU 8200
0084                A3=D1/D3                                                 EQU 8300
0085                A4=D2/B                                                  EQU 8400
0086                A5=A/C                                                   EQU 8500
0087                A6=D/D3                                                  EQU 8600
0088              C CHECK FOR CARBON DEPOSITION                              EQU 8700
0089                PK3COMP=(PT(J)*A*A)/(B*S)                                EQU 8800
```

```
0090                PK4COMP=(PT(J)*C*C)/(D*S)                                    EQU 8900
0091                WRITE(2,220)K                                                EQU 9000
0092                WRITE(2,230)T(I),PCD,D,PK1(I)                                EQU 9100
0093                WRITE(2,240)PT(J),PCA,A,CH1                                  EQU 9200
0094                WRITE(2,250)SR(L),PCB,B,PK2(I)                               EQU 9300
0095                WRITE(2,260)PCC,C,CH2                                        EQU 9400
0096                WRITE(2,270)R,PK3(I)                                         EQU 9500
0097                WRITE(2,280)TOT,PK3COMP                                      EQU 9600
0098                IF(PK3COMP-PK3(I))21,22,22                                   EQU 9700
0099             21 WRITE(2,290)                                                 EQU 9800
0100             24 WRITE(2,305)PK4(I)                                          EQU 9900
0101                WRITE(2,306)PK4COMP                                          EQU10000
0102                IF(PK4(I)-PK4COMP)23,25,25                                   EQU10100
0103             23 WRITE(2,290)                                                 EQU10200
0104                WRITE(2,601)DELA,A1,A2,A3                                    EQU10300
0105                WRITE(2,602)DELB,A4,A5,A6                                    EQU10400
0106                GO TO 40                                                     EQU10500
0107             22 WRITE(2,300)                                                 EQU10600
0108                GO TO 24                                                     EQU10700
0109             25 WRITE(2,300)                                                 EQU10800
0110                WRITE(2,601)DELA,A1,A2,A3                                    EQU10900
0111                WRITE(2,602)DELB,A4,A5,A6                                    EQU11000
0112             40 IF(J-1)11,11,2                                               EQU11100
0113             11 X(I)=A                                                       EQU11200
0114                Y(I)=B                                                       EQU11300
0115              2 CONTINUE                                                     EQU11400
0116              1 CONTINUE                                                     EQU11500
0117             50 CONTINUE                                                     EQU11600
0118            100 FORMAT(F10.2)                                               EQU11700
0119            110 FORMAT(F10.2,F15.6,F10.6,F10.4,F10.4,F10.6,F10.4)           EQU11800
0120            111 FORMAT(////,7X,4HT(I),12X,7HPK1 (I),8X,7HER1 (I),7X,7HPK2 (I),8X,7 QU11900
0121              1HER2 (I),8X,7HPK3 (I),8X,7HPK4 (I))                          EQU12000
0122            112 FORMAT(//,7F15.6)                                           EQU12100
0123            119 FORMAT(3F10.2)                                              EQU12200
0124            120 FORMAT(///,3X,3HP =,F6.2,6X,3HQ =,F6.2,10X,4HSR =F6.2)      EQU12300
0125            140 FORMAT(2F10.4)                                              EQU12400
0126            200 FORMAT(/,21H**JACOBIAN VANISHES**)                          EQU12500
```

```
0127                  210 FORMAT(/,23H**FAILED TO CONVERGE**,4(3X,F10.6))                    EQU12600
0128                  220 FORMAT(////,32X,14HPER CENT COMP.,12X,13HMOLS/MOL FEED,13X,16HEQUI QU12800
0129                     1L.CONSTANTS,8X,2HK=I2)                                            EQU12900
0130                  230 FORMAT(/,2X,3HT =,F8.2,1X,1HF,17X,3HCH4,F12.4,13X,F7.4,13X,3HKP1,2 QU13000
0131                     1X,E13.6,2X,5HGIVEN)                                               EQU13100
0132                  240 FORMAT(1X,4HPT =,F8.2,1X,3HATM,15X,2HCO,F13.4,13X,F7.4,13X,3HKP1,2 QU13200
0133                     1X,E13.6,2X,5HCHECK)                                               EQU13300
0134                  250 FORMAT(1X,4HSR =,F8.2,1X,4HMOLS,14X,3HCO2,F12.4,13X,F7.4,13X,3HKP2 QU13400
0135                     1,2X,E13.6,2X,5HGIVEN)                                             EQU13500
0136                  260 FORMAT(32X,2HH2,F13.4,13X,F7.4,13X,3HKP2,2X,E13.6,2X,5HCHECK)      EQU13600
0137                  270 FORMAT(32X,3HH2O,25X,F7.4,13X,3HKP3,2X,E13.6,2X,5HGIVEN)          EQU13700
0138                  280 FORMAT(32X,5HTOTAL,23X,F7.4,13X,3HKP3,2X,E13.6,2X,8HCOMPUTED)     EQU13800
0139                  290 FORMAT(80X,24H**NO CARBON DEPOSITION**)                           EQU13900
0140                  300 FORMAT(80X,21H**CARBON DEPOSITION**)                              EQU14000
0141                  305 FORMAT(80X,3HKP4,2X,E13.6,2X,5HGIVEN)                             EQU14100
0142                  306 FORMAT(80X,3HKP4,2X,E13.6,2X,8HCOMPUTED)                          EQU14200
0143                  307 FORMAT (I0)                                                       EQU14210
0144                  601 FORMAT(/,1X,5HDELA=,F6.4,12X,7HCO/CO2=,F9.5,10X,17HCO+H2/CO+CO2+CH QU14300
0145                     14=,F8.4,10X,18HCO+CO2/CO+CO2+CH4=,F6.4)                           EQU14400
0146                  602 FORMAT(1X,5HDELB=,F6.4,9X,10HCO+H2/CO2=,F9.5,21X,6HCO/H2=,F8.4,13X QU14500
0147                     1,15HCH4/CO+CO2+CH4=,F6.4)                                         EQU14600
0148                   27 STOP                                                            EQU14700
0149                      END                                                             EQU14800

 END OF SEGMENT, LENGTH   984, NAME  NONM

 0150                   FINISH

 END OF COMPILATION -  NO ERRORS

 S/C SUBFILE:    23 BUCKETS USED
```

Computer Print-Out

for

Two Sets of Calculated Results

Equilibrium Gas Composition

(Feedstock: CH_4)

Operating Conditions

First Set:

Temperature	:	1000°F (538°C)
Pressure	:	1 atm abs.
H_2O: CH_4 molar ratio, α	:	1.25

Second Set:

Temperature	:	1100°F (593°C)
Pressure	:	25 atm abs.
H_2O: CH_4 molar ratio, α	:	1.25

	PER CENT COMP.		MOLS/MOL FEED		EQUIL.CONSTANTS.	K= 4
T = 1000.00 F	CH4	30.1095	0.6685		KP1 0.488660E-01	GIVEN
PT = 1.00 ATM	CO	4.7700	0.1059		KP1 0.489478E-01	CHECK
SR = 1.25 MOLS	CO2	10.1621	0.2256		KP2 0.375020E 01	GIVEN
	H2	54.9584	1.2202		KP2 0.375183E 01	CHECK
	H2O		0.6929		KP3 0.154350E-01	GIVEN
	TOTAL		2.9130		KP3 0.170641E-01	COMPUTED
					CARBON DEPOSITION	
					KP4 0.846100E 00	GIVEN
					KP4 0.764550E 00	COMPUTED
					CARBON DEPOSITION	
DELA=-.0000	CO/CO2=	0.46938	CO+H2/CO+CO2+CH4=	1.3261	CO+CO2/CO+CO2+CH4=0.3315	
DELB=-.0001	CO+H2/CO2=	5.87754	CO/H2=	0.0868	CH4/CO+CO2+CH4=0.6685	

	PER CENT COMP.		MOLS/MOL FEED		EQUIL.CONSTANTS.	K= 3
T = 1100.00 F	CH4	56.0806	0.8605		KP1 0.408910E 00	GIVEN
PT = 25.00 ATM	CO	1.5303	0.0235		KP1 0.409295E 00	CHECK
SR = 1.25 MOLS	CO2	7.5596	0.1160		KP2 0.265410E 01	GIVEN
	H2	34.8294	0.5344		KP2 0.265459E 01	CHECK
	H2O		0.9945		KP3 0.792210E-01	GIVEN
	TOTAL		2.5290		KP3 0.469906E-01	COMPUTED
					NO CARBON DEPOSITION	
					KP4 0.194800E 01	GIVEN
					KP4 0.328116E 01	COMPUTED
					NO CARBON DEPOSITION	
DELA=-.0000	CO/CO2=	0.20243	CO+H2/CO+CO2+CH4=	0.5579	CO+CO2/CO+CO2+CH4=0.1395	
DELB=-.0000	CO+H2/CO2=	4.80973	CO/H2=	0.0439	CH4/CO+CO2+CH4=0.8605	

Computer Print-Out

for

Two Sets of Calculated Results

Equilibrium Gas Composition

Feedstock: C_pH_q (C_nH_{2n}) $p = 1$, $q = 2$

Operating Conditions

First Set:

Temperature : 1000°F (538°C)

Pressure : 1 atm abs.

H_2O: $CH_{q/p}$ ratio, α' : 1.50

Second Set:

Temperature : 1100°F (593°C)

Pressure : 25 atm abs.

H_2O: $CH_{q/p}$ ratio, α' : 1.50

	PER CENT COMP.	MOLS/MOL FEED	EQUIL.CONSTANTS, K= 5
T = 1000.00 F	CH4 26.2391	0.4944	KP1 0.488660E-01 GIVEN
PT = 1.00 ATM	CO 7.3332	0.1382	KP1 0.488661E-01 CHECK
SR = 1.50 MOLS	CO2 19.5001	0.3674	KP2 0.375020E 01 GIVEN
	H2 46.9276	0.8842	KP2 0.375020E 01 CHECK
	H2O	0.6270	KP3 0.154350E-01 GIVEN
	TOTAL	2.5112	KP3 0.206916E-01 COMPUTED
			CARBON DEPOSITION
			KP4 0.846100E 00 GIVEN
			KP4 0.629735E 00 COMPUTED
			CARBON DEPOSITION
DELA=-.0000 CO/CO2= 0.37606		CO+H2/CO+CO2+CH4= 1.0224	CO+CO2/CO+CO2+CH4=0.5056
DELB=-.0000 CO+H2/CO2= 2.78258		CO/H2= 0.1563	CH4/CO+CO2+CH4=0.4944

	PER CENT COMP.	MOLS/MOL FEED	EQUIL.CONSTANTS, K= 3
T = 1100.00 F	CH4 48.8404	0.6540	KP1 0.408910E 00 GIVEN
PT = 25.00 ATM	CO 3.3654	0.0451	KP1 0.409387E 00 CHECK
SR = 1.50 MOLS	CO2 22.4760	0.3010	KP2 0.265410E 01 GIVEN
	H2 25.3183	0.3390	KP2 0.265428E 01 CHECK
	H2O	0.8530	KP3 0.792210E-01 GIVEN
	TOTAL	2.1920	KP3 0.769522E-01 COMPUTED
			NO CARBON DEPOSITION
			KP4 0.194800E 01 GIVEN
			KP4 0.200432E 01 COMPUTED
			NO CARBON DEPOSITION
DELA=-.0000 CO/CO2= 0.14973		CO+H2/CO+CO2+CH4= 0.3841	CO+CO2/CO+CO2+CH4=0.3460
DELB=-.0000 CO+H2/CO2= 1.27619		CO/H2= 0.1329	CH4/CO+CO2+CH4=0.6540

Equilibrium Composition of the

Reformed Gas at Five

Different Temperature Levels

Feedstock : CH_4

Operating pressure : 1 atm abs.

H_2O: CH_4 molar ratio : 3.0

Compositon is given on the basis "per mole of methane reacted".

moles	°C (°F)	538 (1000)	593 (1100)	649 (1200)	704 (1300)	760 (1400)
CH_4		0.443	0.251	0.096	0.026	0.0063
H_2O		2.008	1.777	1.640	1.614	1.6384
CO		0.122	0.274	0.448	0.563	0.626
CO_2		0.435	0.475	0.456	0.412	0.368
H_2		2.106	2.721	3.168	3.335	3.349

A - 2.2

The Variation of Equilibrium Constants with Temperature

Reaction: $CH_4 + H_2O \rightleftarrows CO + 3H_2$

Temperature (^oC)	Thermodynamic Equilibrium Constant (*) (K)
500	$(9.442)\ (10^{-3})$
550	$(7.741)\ (10^{-2})$
600	$(5.029)\ (10^{-1})$
625	(1.189)
650	(2.686)
675	(5.821)
700	$(1.214)\ (10^{1})$
725	$(2.442)\ (10^{1})$
750	$(4.753)\ (10^{1})$
775	$(8.968)\ (10^{1})$
800	$(1.644)\ (10^{2})$
825	$(2.933)\ (10^{2})$
850	$(5.101)\ (10^{2})$
875	$(8.666)\ (10^{2})$
900	$(1.440)\ (10^{3})$

(**) $K = -28.08 - 22687.21\ (\frac{1}{T}) + 8.479\ \ln T - 0.005\ (T) - 0.469(10^{-6})\ T^2$

Reference: (*) Catalyst Handbook, Wolfe Scientific Books, London (1970)

(**) (179)

Fig: A 2.2.1 Equilibrium Constants of Reactions

$CH_4 + H_2O \rightleftharpoons CO + 3H_2$ and

$CH_4 + 2H_2O \rightleftharpoons CO_2 + 4H_2$

as a Function of Temperature

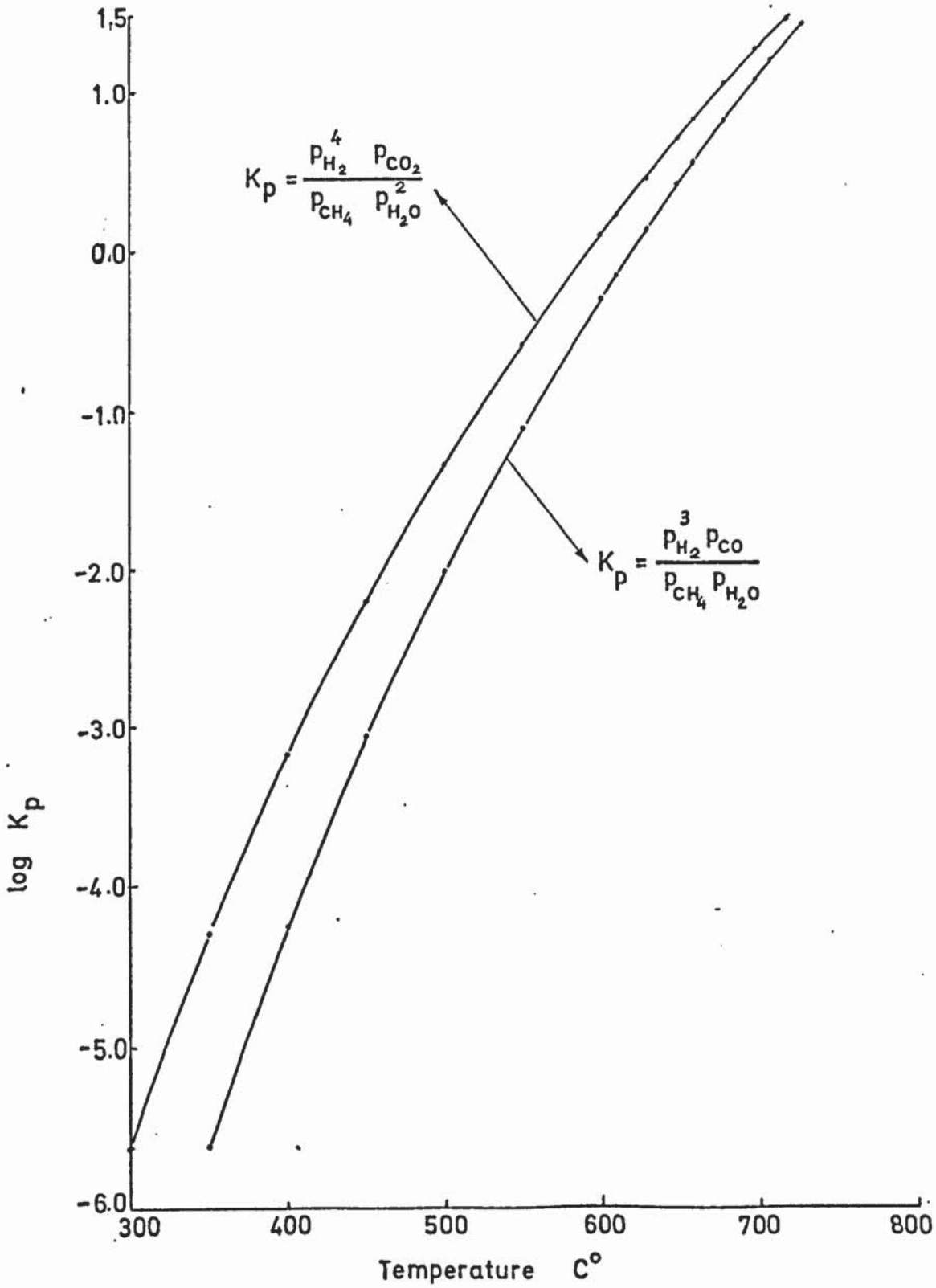

Reaction: $CO + H_2O \rightleftarrows CO_2 + H_2$

Temperature (^oC)	Thermodynamics Equilibrium Constant (*) (K)
500	4.878
550	3.434
600	2.527
625	2.199
650	1.923
675	1.706
700	1.519
725	1.361
750	1.228
775	1.113
800	1.015
825	$(9.295)\ (10^{-1})$
850	$(8.552)\ (10^{-1})$
875	$(7.901)\ (10^{-1})$
900	$(7.328)\ (10^{-1})$

(**) $K = -13.43 + 5405\ (\frac{1}{T}) + 1.208\ \ell n\ T$ (2)

Reference: (*) Catalyst Handbook, Wolfe Scientific Books, London (1970)

(**) Woodcock, C.J., Ph.D. Thesis, University of Aston in Birmingham (1971)

Fig: A - 2.2.2 Equilibrium Constants of Reactions

$CO + H_2O \rightleftharpoons CO_2 + H_2$ and

$CO_2 + H_2 \rightleftharpoons CO + H_2O$

as a Function of Temperature.

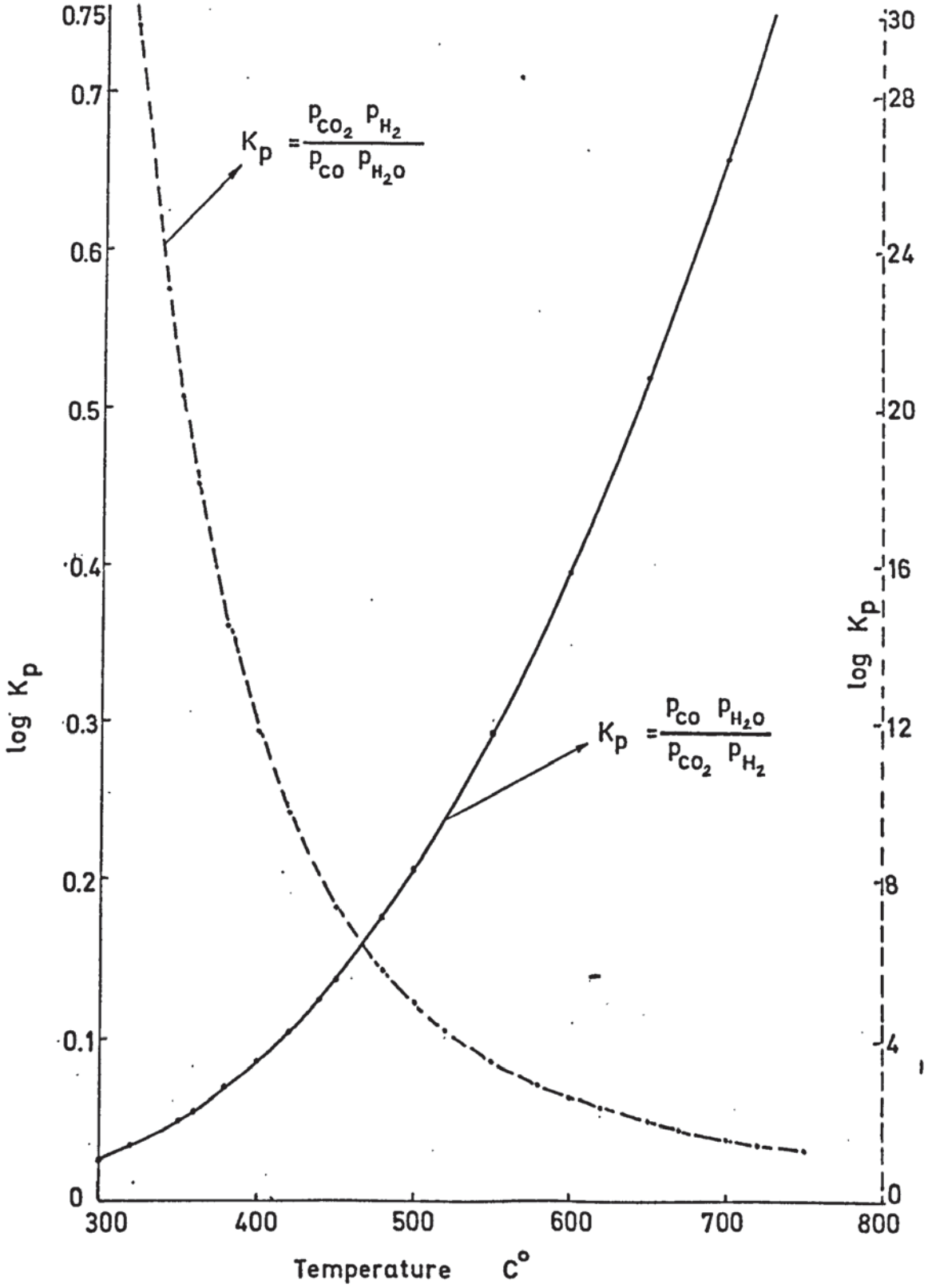

Reaction: $C + CO_2 \rightleftarrows 2CO$

Temperature (°C)	Thermodynamic Equilibrium Constant (*) (K)
327	$(1.868)\ (10^{-6})$
427	$(2.669)\ (10^{-4})$
482	$(2.355)\ (10^{-3})$
527	$(1.098)\ (10^{-2})$
538	$(1.543)\ (10^{-2})$
593	$(7.922)\ (10^{-2})$
627	$(1.926)\ (10^{-1})$
649	$(3.334)\ (10^{-1})$
704	1.187
727	1.900
760	3.668
816	$(1.007)\ (10^{1})$
827	$(1.220)\ (10^{1})$

(**) $K = -22.7164 + 21183.26(\frac{1}{T}) + 0.05212\ \ln T + (5.31)\ (10^{-4})\ T$

(for the reverse reaction)

Reference: (*) Wagman, D.H., J.E. Kilpatrick, W.J. Taylor, K.S. Pitzer, and F.D. Rossini, J. Research National Bureau of Standards, 34, 143 (1945).

(**) Woodcock, C.J., Ph.D. Thesis, University of Aston in Birmingham (1971)

Fig: A-2.2.3 Equilibrium Constant of Reaction

$$C + CO_2 \rightleftharpoons 2CO$$

as a Function of Temperature

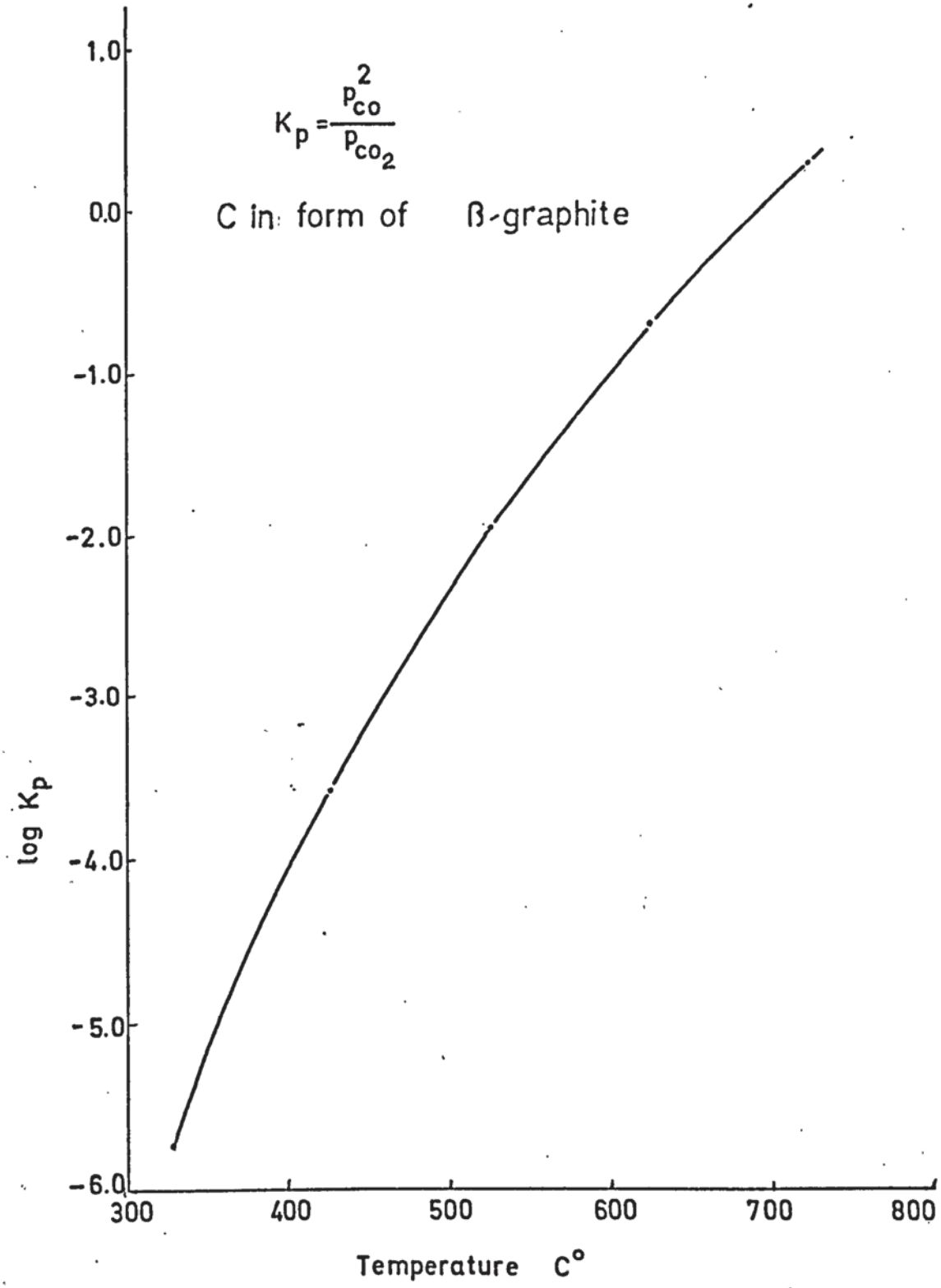

Fig. A-2.2.4 Equilibrium Constant of Reaction

$$C + 2H_2 \rightleftharpoons CH_4$$

as a Function of Temperature.

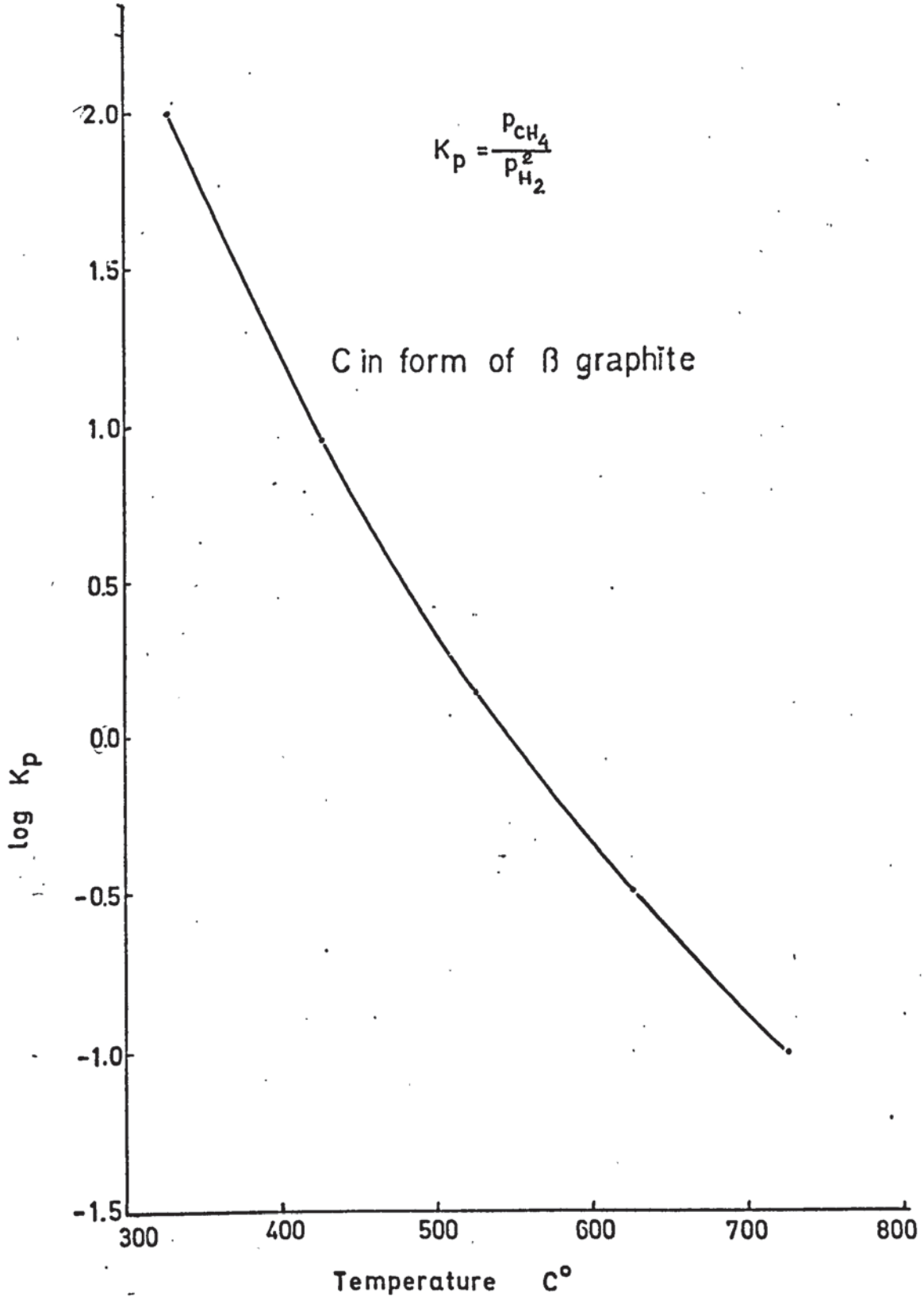

A - 4.1

SAMPLE CALCULATION FOR THE FISCHER AND PORTER FLOWMETERS

Combinations of tube sizes and float materials were used to obtain different gas flowrate ranges. For each combination used, a calibration curve was prepared, and in the case of the methane flowmeter, experimental checks were also performed.

The calibrations were carried out according to the computation procedure given in the Fischer and Porter Handbook, which involved calculation at tube scale readings for given operating conditions. The method for a given tube and float material may be summarized as follows:

(i) calculate the viscosity and density of the gas to be metered at the temperature and pressure of metering,

(ii) from the Fischer and Porter Handbook obtain the float density (ρ_f) and tube size factors (A) and (B)

(iii) calculate the viscous influence number (N), given by:

$$N = \frac{A}{\mu_{opt}} \sqrt{(\rho_f - \rho_{opt})\,\rho_{opt}}$$

(iv) from given float characteristic curves in the Fischer and Porter Handbook obtain the flow coefficients (C) at each tube scale reading, corresponding to the value of N.

(v) using the relationship

$$W = (C)(B)\sqrt{(\rho_f - \rho_{opt})\,\rho_{opt}}$$

calculate the gas flowrate W in g/min.

(vi) convert the flowrate W into units of moles/min.

Thus the flowrate versus scale reading calibration curve may be plotted from the calculated data.

Sample Calculation

Type: Triflat; 1/16 - 08 - G - 5/84

Tube and Float Data:

Tube diameter	:	1/16"
Scale calibration	:	0 - 8
Float material	:	stainless steel
Float density (ρ_f)	:	8.02 g/cm^3

Operating Conditions:

Pressure	:	0.7218 psig. (20" WG)
Temperature	:	71.6°F
Barometric pressure	:	755 mm Hg

Tube size Factors:

A	:	404
B	:	76.8

Fluid Properties: "Methane"

Viscosity at STP μ	:	0.01099 centipoise
Density at STP ρ	:	0.0006653 g/cm^3

(STP is 70°F and 14.7 psia).

Pressure correction : There was no need for a pressure correction, since any change of viscosity within the pressure range 1 - 15 atm was negligible (129)

Temperature correction is given by:

$$\mu_{opt} = \mu_{stp} + (\text{temp. coef})\ (t - 70)$$

Operating density:

$$\rho_{opt} = \rho_{stp}\ (R)$$

where $R = \left(\frac{p}{1}\right)\left(\frac{530}{460+t}\right)$

p = operating pressure, atm abs.

t = operating temperature, ^{o}F

Viscous influence number:

$$N = \frac{A}{\mu_{opt}} \sqrt{(\rho_f - \rho_{opt})\ \rho_{opt}} = 966$$

Flowrate of methane W g/min at operating temperature and pressure:

$$W = (C)\ (B) \sqrt{(\rho_f - \rho_{opt})\ \rho_{opt}} \quad g/min$$

or $F_{CH_4} = \frac{W}{16.04}$ moles/min.

From the float characteristic curve and using the value of N calculated, the following table was constructed:

Scale Reading	C	W (g/min)	F (moles/min)
3	0.0042	0.00425	$(0.265)(10^{-3})$
4	0.0160	0.01620	$(1.009)(10^{-3})$
5	0.0277	0.02805	$(1.748)(10^{-3})$
6	0.0450	0.04557	$(2.840)(10^{-3})$
7	0.0650	0.06582	$(4.102)(10^{-3})$
8	0.0890	0.09013	$(5.617)(10^{-3})$
10	0.1395	0.14127	$(8.805)(10^{-3})$

From the above data the calibration curves for methane are plotted for the barometric pressure, the amb ient (operating) temperature, the operating pressure, and for every type of flowmeter tube and float material.

Fig:A-4.1.1. Flow Rate of Methane

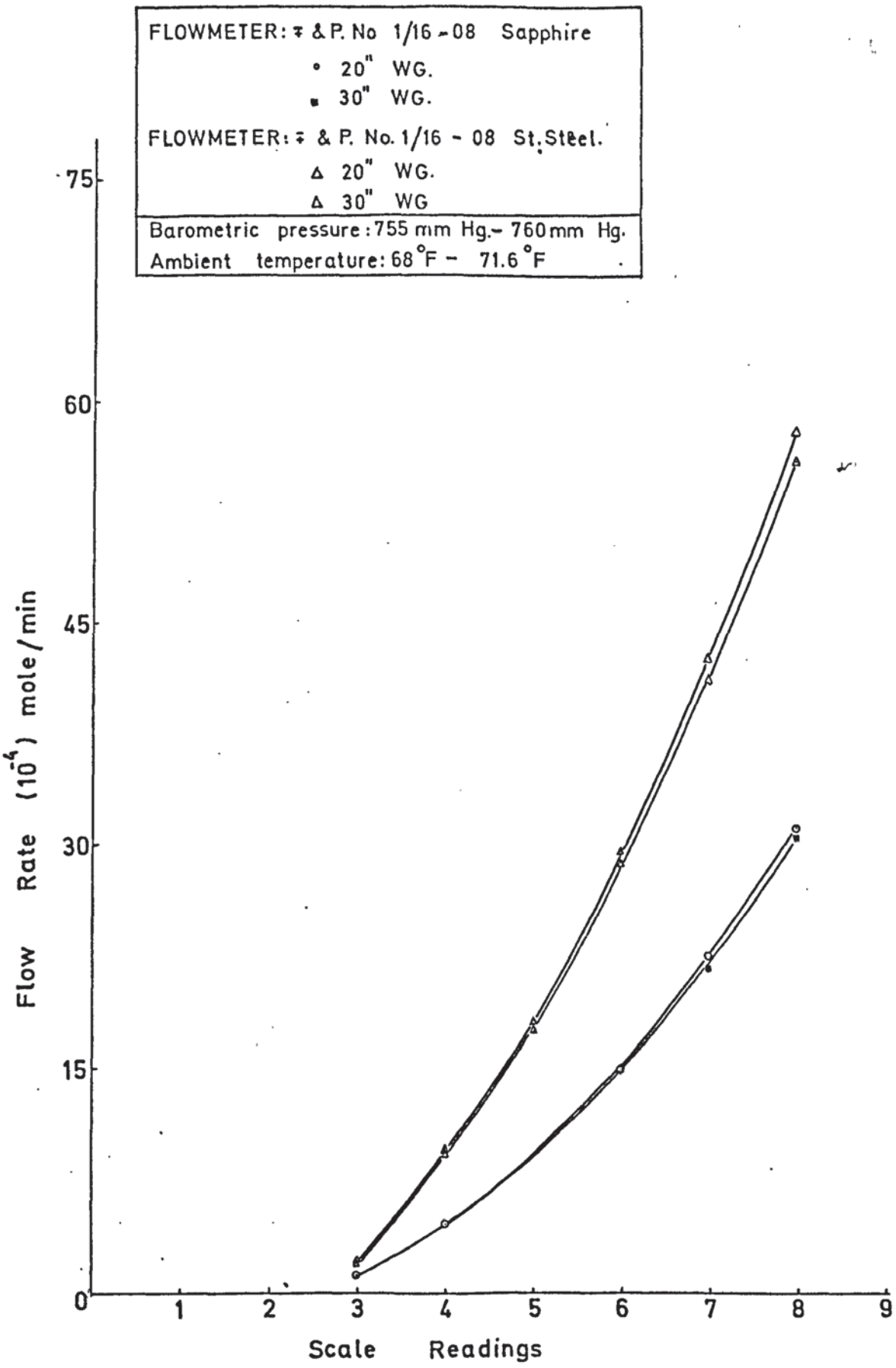

Fig:A-4.1.2. Flow Rate of Methane

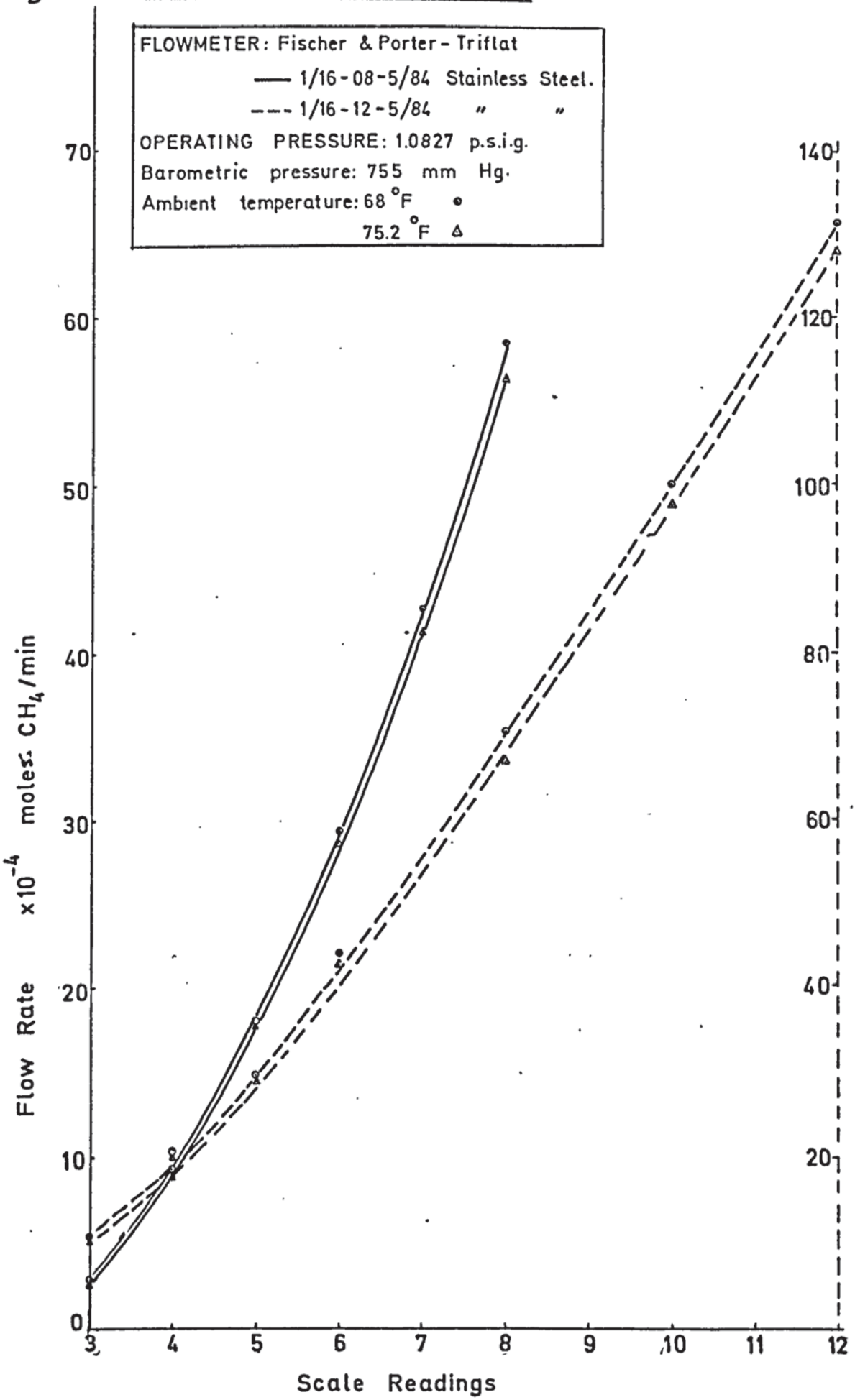

Fig:A-4.1.3. Flow Rate of Methane

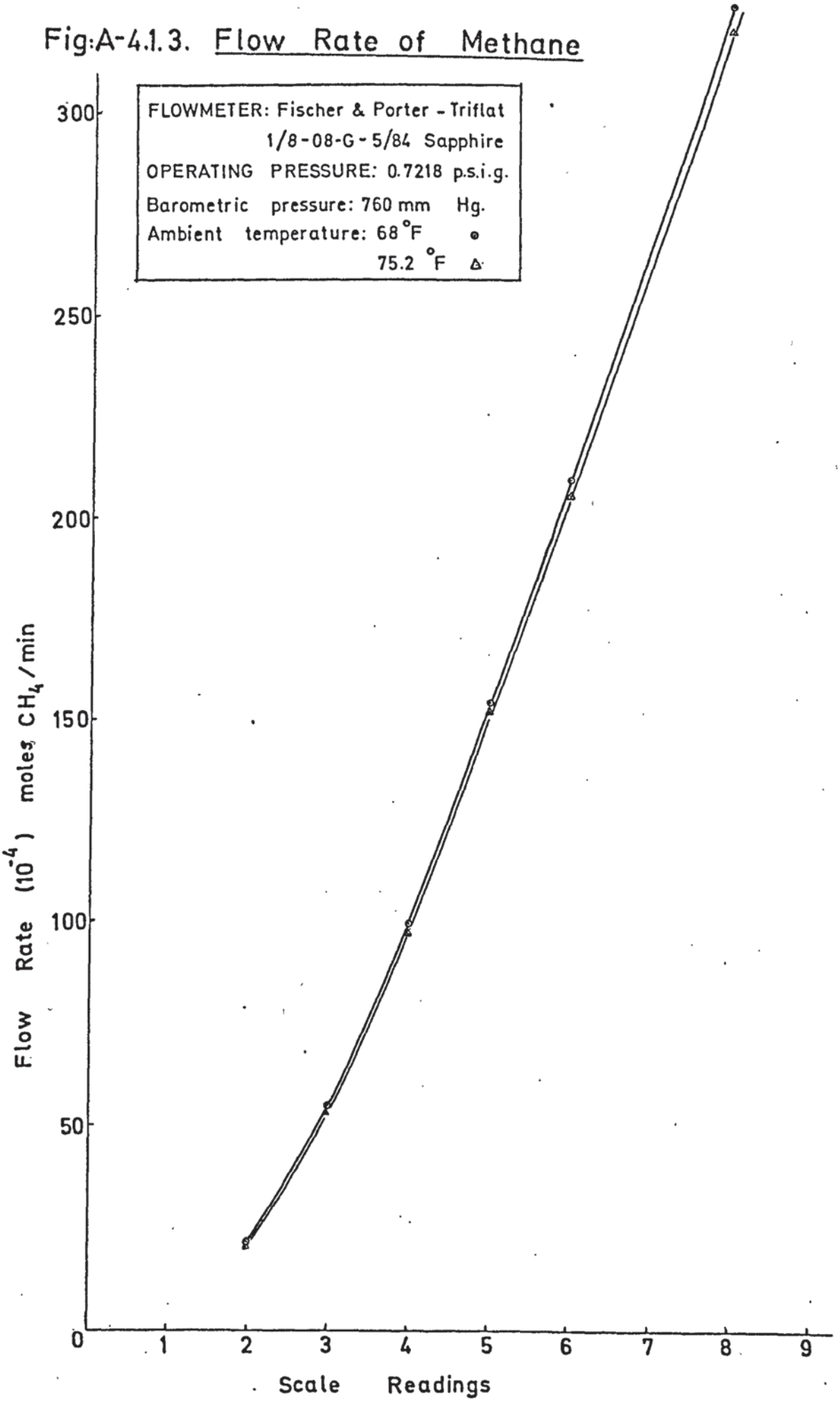

Fig.A-4.2 Feed Water Pump Discharge Rates.

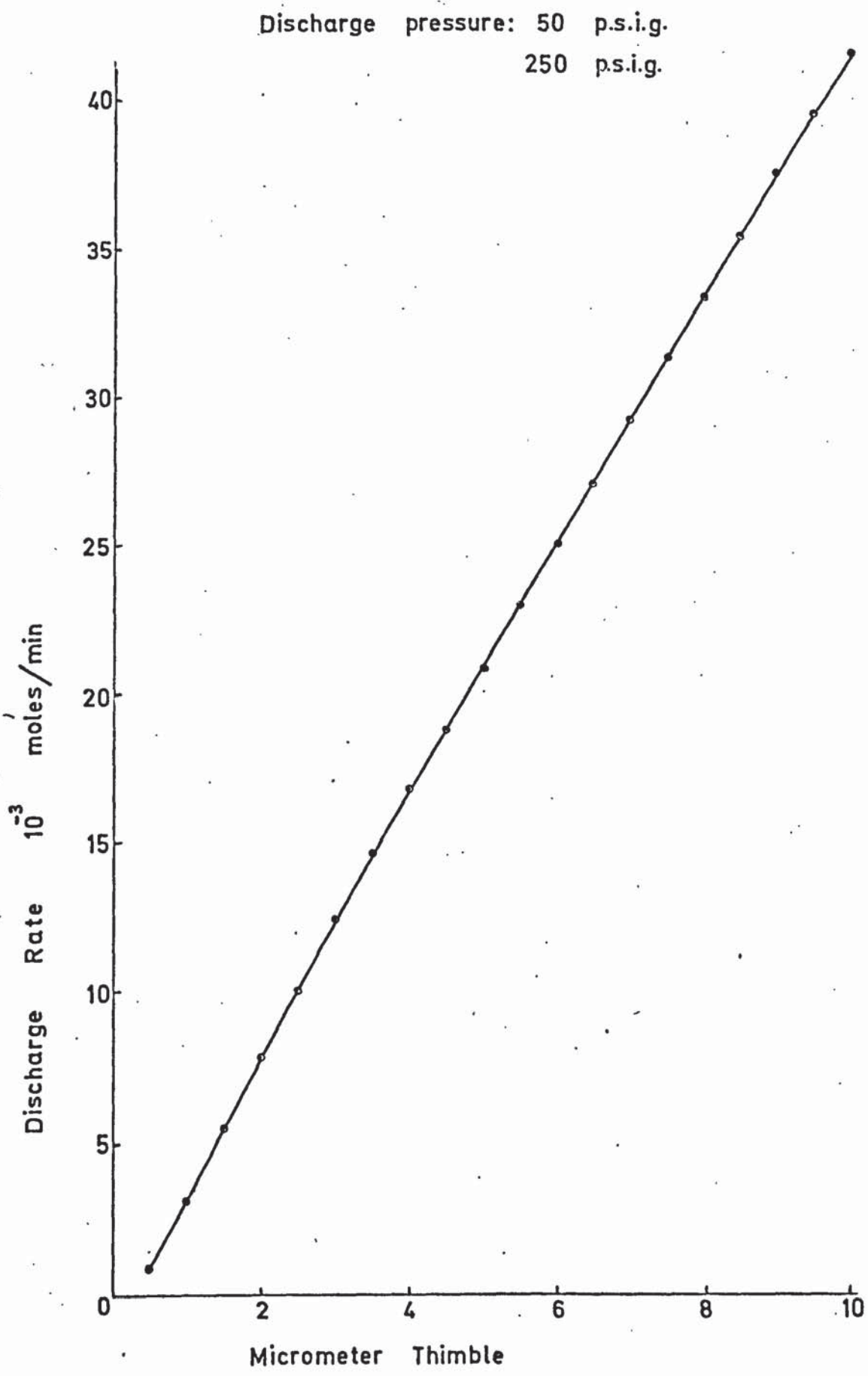

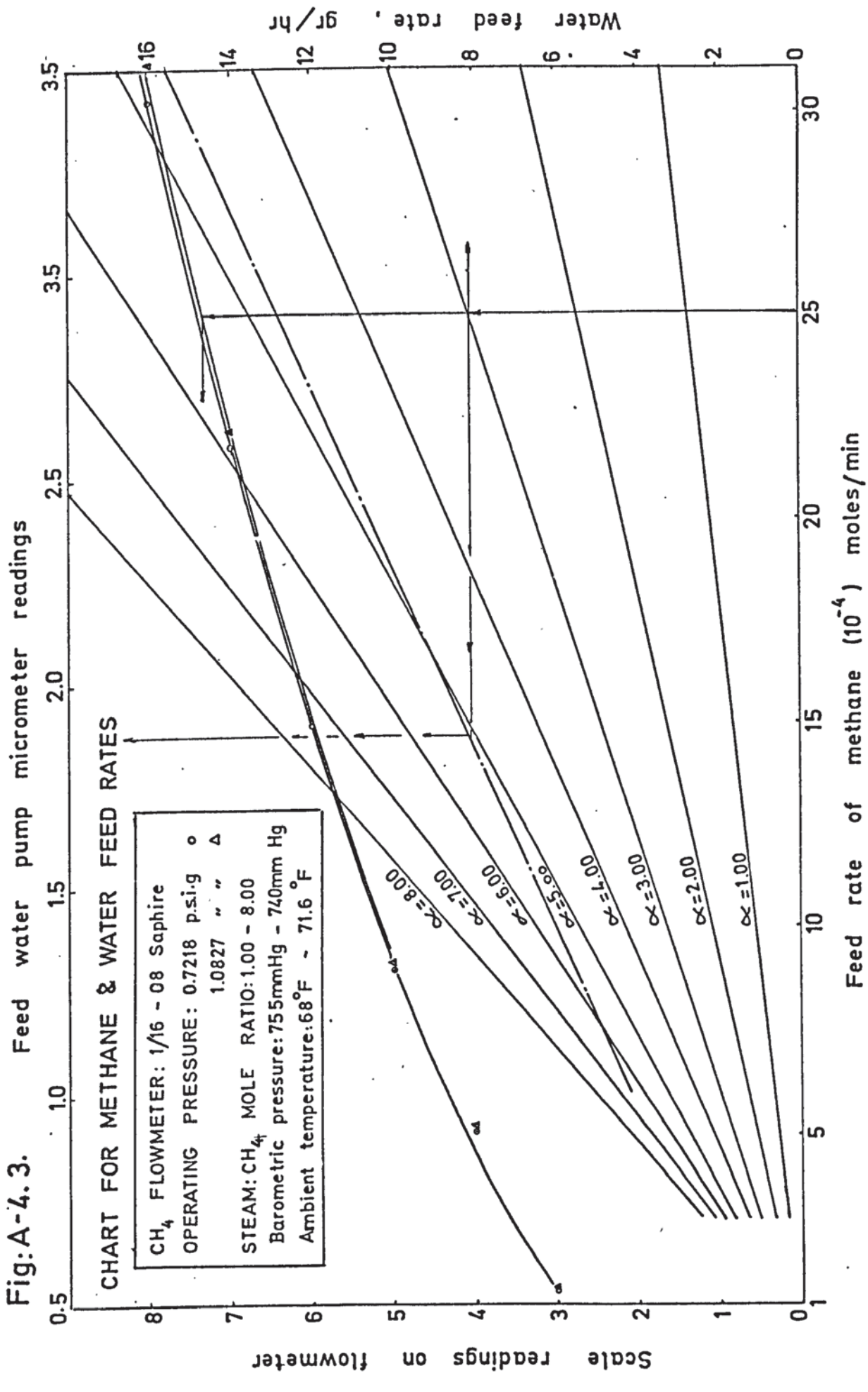

Fig: A-4.3. Feed water pump micrometer readings

A - 4.4

The Bulk Density of Ground Catalyst at Different Particle Size

Fractions (μ)	Measured Bulk Density (g/cm^3)
63- 75	0.864
90-106	0.835
106-125	0.934
125-150	1.073
150-355	1.257
251-295	1.195
295-355	1.201
355-425	1.327
355-600	1.340
425-699	1.368
600-850	1.350

Fig. A 4.5 Circuit Diagram for Reactor Controller

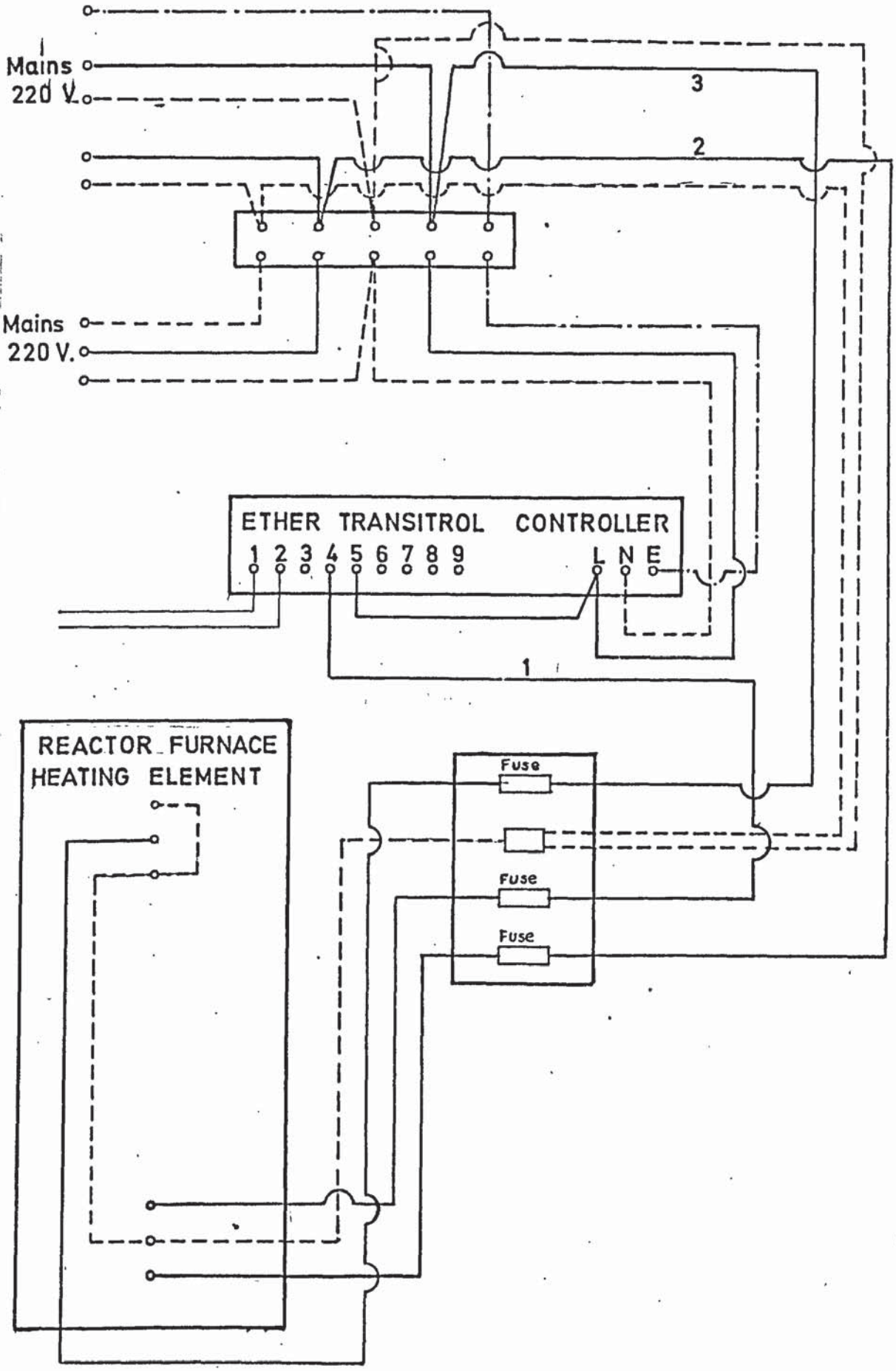

A - 4.6

Data Log Sheet used for

Reforming Runs

RUN NO: _____ DATE: _____

TIME-Start: _____
End : _____

Barometric pressure: _____ mm Hg
Ambient Temperature: _____ °F

CH_4

Pressure inlet flowmeter: _____ psig
Pressure exit flowmeter: _____ psig
Scale reading on flowmeter: _____
N = _____
C_1 = _____
w = _____
w = _____ gr/min
n = _____ mole/min

Corrected for:

H_2O

Pressure exit flowmeter: _____ psig
Pressure of plant inlet: _____ psig
Scale reading on flowmeter: _____
Pump micrometer: _____
Burette - end: _____
- start: _____
Feed rate: _____ ml/H
n = _____ moles/min

H_2 or N_2

Pressure inlet flowmeter: _____ psig
Pressure exit flowmeter: _____ psig
Scale reading on flowmeter _____
N = _____
C_1 = _____
w = _____
w = _____ gr/min.
n = _____ moles/min.

Corrected for:

PRESSURES -psig-

Steam generator exit: _____
Reactor inlet: _____
Reactor exit (I): _____
Reactor exit (II): _____

TEMPERATURES -°C-

CH_4-preheater(1) : _____
Steam generator inlet : _____
Superheater (2) : _____
Linecheater (3) : _____
Reactor (top) : _____
Reactor (middle) : _____
Reactor (bottom) : _____
Reactor outside wall (4) : _____
Reactor outside wall (5) : _____
Reactor (6) : _____
Reactor (7) : _____

REACTOR EXIT GAS

Relief Valve-Dome pressure-: _____ psig
Temperature : _____ °F
Pressure bef. flowmeter : _____ in.WG.
Scale reading on flowmeter : _____
ρ _____ gr/min _____
μ _____ centipoise _____

CHROMATOGRAPH

Sample loop:
Time :
H_2 ( )
CO ( )
CH_4 ( )
CO_2 ( )

VARIAC SETTINGS

Feed Water heating tape: _____
Feed preheater : _____
Steam generator (main) : _____
Steam generator (bottom) : _____
Superheater (main) : _____
Superheater (bottom) : _____
Linecheater : _____
Reactor (bottom) : _____
Reactor (middle) : _____
Reactor (top) : _____

H_2O coll. at cond. exit: _____ ml.

REMARKS

_____

Table A - 5.1

GAS CHROMATOGRAPH

ATTENUATOR SETTINGS FOR GAS COMPONENTS

GAS	per cent composition	Attenuator setting for 5 ml sample loop	Attenuator setting for 1 ml sample loop
pure H_2	100	(out of recorder scale)	200
pure CO	100	50	20
pure CH_4	100	50	20
pure CO_2	100	5,2	1
Standard Gas I			
H_2	50.2	200	100
CO	4.9	5	2
CH_4	34.5	50	20,10
CO_2	10.4	2,1	1
Standard Gas II			
H_2	37.6	200	100
CO	23.4	20	5
CH_4	19.6	20	10
CO_2	19.4	2	1
Reformed Gas			
H_2		200, 100	100,50,20
CO		2,1	1
CH_4		50	20
CO_2		1	1

A - 5.2

Sample Calculation for the Composition of a Reformed Gas

Operating Parameters:

CH_4 - flowrate	:	(9.70) (10^{-3}) moles/min
H_2O - flowrate	:	(29.14) (10^{-3}) moles/min
H_2O : CH_4 ratio	:	3.0
Total feedrate	:	(38.84) (10^{-3}) moles/min
Reactor temperature	:	650°C
Operating pressure	:	0.987 atm abs.

Gas Chromatographic Data:

Carrier gas	:	Argon
Carrier gas pressure	:	30.5 psig.
Carrier gas flowrate	:	125 ml (STP)/min
Detector current	:	200 mAmp
Column temperature	:	40° C
Sample loop	:	1 ml (nominal)

Hydrogen peak:

attenuator setting	:	100
peak height	:	19.18 cm
width at the peak mid-height	:	0.33 cm
peak area	:	6.3294 cm^2
reduced peak area	:	3.1647 cm^2

corr. calibration coefficient	:	10.854
H_2, %	:	34.35

Carbon monoxide peak:

attenuator setting	:	1
peak height	:	6.42 cm
width at the peak mid-height	:	0.36 cm
peak area	:	2.3112 cm^2
reduced peak area	:	0.01156 cm^2
corr. calibration coefficient	:	125.65
CO, %		1.45

Methane peak:

attenuator setting	:	20
peak height	:	18.46 cm
width at the peak mid-height	:	0.59 cm
peak area	:	10.8914 cm^2
reduced peak area	:	1.08914 cm^2
corr. calibration coefficient	:	52.14
CH_4, %		56.79

carbon dioxide peak:

attenuator setting	: 1
peak height	: 4.95 cm
width at the peak mid-height	: 1.04 cm
peak area	: .5.1480 cm^2
reduced peak area	: 0.02574 cm^2
corr. calibration coefficient	:287.98
CO_2, %	7.41

Mass balance check

H_2 %	: 34.35%
(3)(CO%) + (4)(CO_2%)	: 34.01%
Difference	:+ 0.34%

A - 5.3

Mass Balance Calculation for

an Experimental Run

Mass balance based on stoichiometry:

Basis of calculation: 1 mole of methane,

and α moles of steam

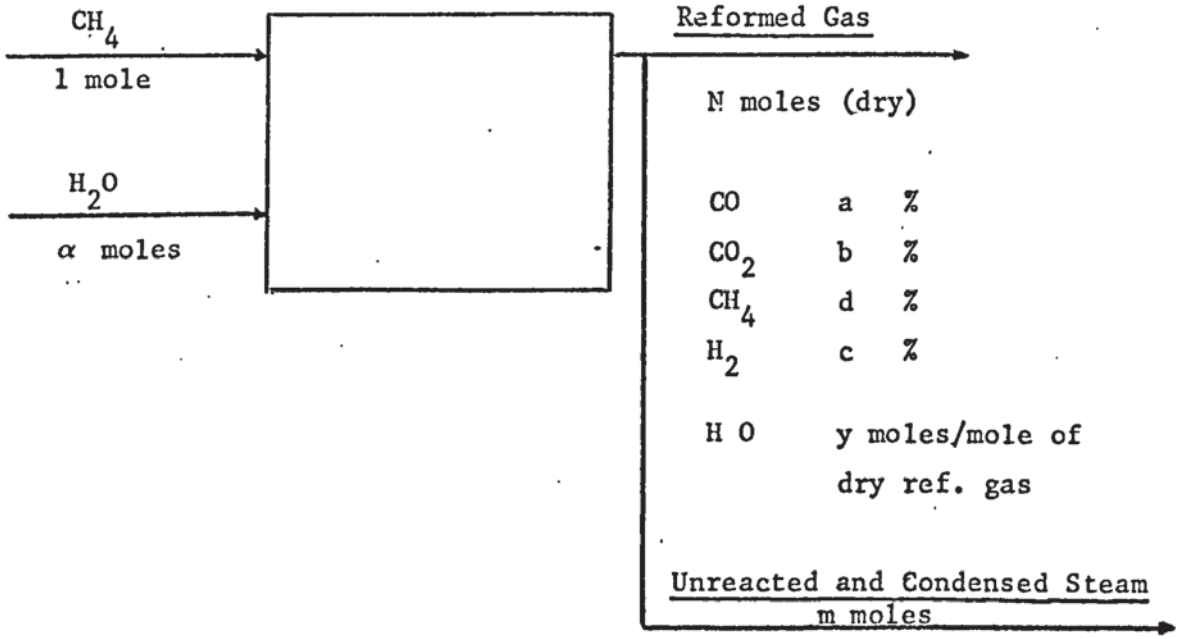

On the basis that no carbon formation by the pyrolysis of methane takes place during the operation, three element balances can be set up. The reformed gas is saturated with water vapour at the temperature of the water condenser (t ^{o}C). The quantity of water vapour present in N moles of dry reformed gas is, from Dalton's law,:

$$y = N \frac{p'_{H_2O}}{P_T - p'_{H_2O}}$$

where:

p_T = total pressure of the dry reformed gas after cooling.

p'_{H_2O} = vapour pressure of liquid water at t ^oC.

The temperature of the reformed gas leaving the condenser was a maximum of 25^oC. Since the pressure of the gas was only 2 - 4" WG, p_T was assumed to be 760 mm Hg.

Thus p'_{H_2O} = 23.756 mm Hg

p_T = 760 mm Hg.

and $p'_{H_2O} : (p_T - p'_{H_2O})$ = 0.0322

This value was very small, and therefore, the reformed gas leaving the condenser was assumed to be dry in the subsequent calculations.

The water vapour in the gas was considered to be condensed and collected.

Hence the three element balances were set up as follows:

I. Carbon balance:

$$1 = \frac{N}{100} (a+b+d)$$

$$N = \frac{100}{(a+b+d)}$$

II. Hydrogen balance:

$$2 \pm \alpha = \frac{N}{100} (2d+c) + m$$

III. Atomic oxygen balance:

$$\alpha = \frac{N}{100} (a+2b) + m$$

m can be eliminated from Equations II and III, solving the resulting equation for N and substituting in Equation I yields

$$c = 3a + 4b$$

Thus a quantitative check of the analytical results by a mass balance would simply be carried out by:

$$H_2\ \% = (3)\ (CO\ \%) + (4)\ (CO\ \%)$$

If c was found to be greater than 3a + 4b, it would have indicated an excess of hydrogen in the reformed gas originating from pyrolysis of methane, whereby carbon appeared to be deposited. The reverse was indicated an excess of the oxides of carbon, which implied a reaction of deposited carbon with steam.

This method of checking the experimental results by the mass balance was found superior to the direct determination of the reformed gas quantity by a gas meter and to the measurement of the condensed water collected at the exit of the water condenser, since it prevented the interference of additional experimental errors or reading inaccuracies.

For an experimental run to be considered valid, the mass balance check had to be within the limits of $\pm$ 2%, and results outside these limits were discarded.

The flowrates of various reaction components leaving the catalyst contact were calculated according to the mass balance relationships:

CH_4 : $\left(\frac{d}{a + b + d}\right)\ (F_{CH_4})$ moles/min (FCH4)

H_2O (calculated independently by the oxygen balance and by the hydrogen balance):

(i) $(\alpha - \frac{a + 2b}{a + b + d})\ (F_{CH_4})$ moles/min (FH201)

(ii) $(\alpha + \frac{2(a + b) - c}{a + b + d})\ (F_{CH_4})$ moles/min (FH202)

CO : $(\frac{a}{a + b + d})\ (F_{CH_4})$ moles/min (FCO)

CO_2 : $(\frac{b}{a + b + d})\ (F_{CH_4})$ moles/min (FCO2)

H_2 : $(\frac{c}{a + b + d})\ (F_{CH_4})$ moles/min (FH2)

The total reactor gas was the sum of the components.

In the calculation of the mole fractions and partial pressures of each component, the above procedure was repeated.

Mass balance check : $3a + 4b$ (BALN)

Conversion % : $(\frac{a + b}{a + b + d})\ (100)$ (CONV)

Conversion x_{CH} : $(\frac{a + b}{a + b + d})\ (\frac{1}{1 + \alpha})$ (SCH4)

(in terms of "moles of CH_4 reacted per mole of total feed")

Moles of H_2O reacted per mole of total feed, and moles CO, CO_2, H_2 formed per mole of total feed were calculated in similar manner.

Volume of reformed gas leaving the catalyst bed at the operating conditions were calculated as follows:

(i) VOLRG = $(\frac{273 + t}{273})\ (\frac{1}{p_T})$ $\left[\begin{matrix}\text{sum of the moles of} \\ \text{components}\end{matrix}\right]$ cm^3/min

(a) Moles of unreacted steam based on oxygen balance

(b) Moles of unreacted steam based on hydrogen balance

(ii) VOLRGO = $(\frac{273 + t}{273})\ (\frac{1}{p_T})$ $\left[\begin{matrix}\text{moles of methane and} \\ \text{steam in}\end{matrix}\right]$ cm^3/min

(iii) VOLRR = Arithmetic average of the gas leaving the reactor (VOLRG) and entering the reactor (VOLRGO)

Linear velocity of the reacting gas : (cm/min)

VOLRR/free area of the annulus

Contact time : (10^{-3} min)

height of the bed/linear velocity

The quantity of condensed water was computed by the hydrogen and by the oxygen balances and was used as a check for the actual collected quantity. The figures for computed and collected amounts of unreacted H_2O checked within $\pm$ 50% at low flowrates. This was due to the incomplete draining of the pressure knock-out vessel at the exit of the condenser and to the time period of an experimental run ($\approx$ 30 min).

Viscosity of the reacting components was calculated from the equation:

$$\mu_i = 0.00002669 \sqrt{\frac{(M_i)\quad(T)}{\sigma^2\ \Omega}} \qquad g/cm/sec$$

where Ω is the Lennard-Jones potential parameter for non-polar components, and Stockmayer potential for polar components, and M_i is the molecular weight.

The values for σ and Ω were calculated from data given by Sherwood and Reid (129). A set of constants are given below:

	σ (Å)	ϵ_0/k ($^\circ$K)	Ω
for 650°C			
CH_4	3.758	148.6	0.8828
CO	3.690	91.7	0.8235
CO_2	3.941	195.2	0.9370
H_2	2.827	59.7	0.7740

	σ	ϵ/k	Ω
H_2O (polar)	2.52	775	1.677

The viscosity of the mixture was calculated according to the equations given in Chapter 8.

The superficial mass velocity based on the free area of annulus was calculated:

(i) on the feedrate of methane and steam (G), and

(ii) on the flowrate of the sum of the reacting components at the exit of the catalyst bed (G1 and G2)

The Reynolds number of the gas was computed according to G and G1 from the equation

$$N_{Re} = \frac{(D_R - D_c)G}{\mu_m}$$

In the calculation of the following ratios:

$$\text{K-SHIFT} = = \frac{P_{CO_2} \; P_{H_2}}{P_{CO} \; P_{H_2O}} .$$

$$\text{K-SHIFT REV.} = \frac{P_{H_2O} \; P_{CO}}{P_{CO_2} \; P_{H_2}}$$

$$\text{K-BOUDOUARD} = \frac{P_{CO}^2}{P_{CO_2}}$$

$$\text{K-METHANE} = \frac{P_{CH_4}}{P_{H_2}^2}$$

$$\text{K-REFORMING} = \frac{P_{CO}\ P_{H_2}^3}{P_{CH_4}\ P_{H_2O}}$$

$$\text{K-COMB.REFOR.} = \frac{P_{CO_2}\ P_{H_2}^4}{P_{CH_4}\ P_{H_2O}^2}$$

to follow the approach to the equilibrium, two values of H_2O partial pressure were used.

A - 5.4

The Print-out of the Computer Program for the Evaluation of Experimental Runs and One Set of Calculated Results

Operating Parameters of the Run

Feedstock : CH_4

Temperature : $540^{o}C$

```
JOB DATAEVALTN,CESTF315,ATAMER,STREAM 1      RUN AT ASTON UNIV.   ON 19/05/72 AT 10.45
                                             PRINTED AT  10/53

FORTRAN
****


      LIST(LP)
      SEND TO (ED,ASTD-DEFAULT(0))
      WORK(ED,WORK FILE    (0))
      MAP                                                                    DAT  100
      PROGRAM  (DATA)                                                        DAT  200
      INPUT 1=CR0                                                            DAT  300
      OUTPUT 2=LP0                                                           DAT  400
      TRACE 2                                                                DAT  500
      END                                                                    DAT  600


      MASTER                                                                 DAT  700
C     DATA EVALUATION                                                        DAT  800
      DIMENSION W(28),ACAT(28),HEI(28),AFR(28),AHYD(28),ACMO(28),AMET(       DAT 5700
     128),ACDO(28),CHYD(28),CCMO(28),CMET(28),CCDO(28),FMET(28),FWAT(28      DAT 5833
     2),PCH4(28),PH2O1(28),PH2O2(28),PCO(28),PCO2(28),PH2(28),PATM(28),      DAT 5834
     3VMIX1(28),VMIX2(28),VMIX3(28),VMIX4(28),VMIX5(28),VISC(28),            DAT 5838
     4D(28),G(28),G1(28),G2(28),REYN(28),REYN1(28),                          DAT 5839
     5HYD(28),CH4(28),CMO(28),CDO(28),SUM(28),CSUM(28),H2(28),CO(28),        DAT 6000
     6CMT(28),CO2(28),TOT(28),BAL1(28),BAL2(28),RAT1(28),TOTC(28),           DAT 6001
     7CONV(28),FTOT(28),WFT(28),ACFT(28),ALPHA(28),FCH4(28),FH2O1(28),       DAT 6002
     8FH2O2(28),FCO(28),FCO2(28),FH2(28),TOTRG1(28),TOTRG2(28),YCH4(28),      AT 6003
     9YH2O1(28),YH2O2(28),YCO(28),YCO2(28),YH2(28),DEN(28),SCH4(28),         DAT 6004
     1SH2O(28),SCO(28),SCO2(28),SH2(28),ECH4(28),EH2O1(28),EH2O2(28),        DAT 6005
     2ECO(28),ECO2(28),EH2(28),VOLRG(28),VEL(28),TAU(28),RECTAU(28),         DAT 6006
     3RHO(28),REA(28),REB(28),REC(28),COLWAT(28)                             DAT 6007
C     DATA INPUT                                                             DAT 6100
      DO 1 I=1,8                                                             DAT 6150
      READ(1,100)(W(I),ACAT(I),HEI(I),AFR(I),PATM(I),D(I))                   DAT 6200
```

```
100 FORMAT(F10.4,F10.4,F10.2,F10.4,F10.3,F10.3)                          DAT 6300
    WRITE(2,101)(W(I),ACAT(I),HEI(I),AFR(I),PATM(I),D(I))               DAT 6400
101 FORMAT(////////,4X,8HWEIGHT =,F7.4,5X,9HSURFACE =,F8.4,5X,8HHEIGHT AT 6500
   1 =,F5.2,5X,11HFREE AREA =,F8.4,6X,10HOPE.PRES.=,F6.3,4X,7HCAT.D.=, AT 6600
   2F5.3)                                                               DAT 6601
    READ(1,110)(AHYD(I),ACMO(I),AMET(I),ACDO(I),FMET(I),FWAT(I))        DAT 6700
110 FORMAT(F10.5,F10.5,F10.5,F10.5,F10.3,F10.3)                          DAT 6800
    READ(1,120)(CHYD(I),CCMO(I),CMET(I),CCDO(I))                        DAT 6900
120 FORMAT(F10.3,F10.3,F10.3,F10.3)                                      DAT 7000
    IF(AHYD(I))2,3,2                                                    DAT 7200
  2 IF(ACMO(I))4,5,4                                                    DAT 7300
  4 IF(AMET(I))6,7,6                                                    DAT 7400
  6 IF(ACDO(I))8,9,8                                                    DAT 7500
  8 HYD(I)=AHYD(I)*CHYD(I)                                              DAT 7600
    CMO(I)=ACMO(I)*CCMO(I)                                              DAT 7700
    CH4(I)=AMET(I)*CMET(I)                                              DAT 7800
    CDO(I)=ACDO(I)*CCDO(I)                                              DAT 7900
    GO TO 10                                                            DAT 8000
  3 CMO(I)=ACMO(I)*CCMO(I)                                              DAT 8100
    CH4(I)=AMET(I)*CMET(I)                                              DAT 8200
    CDO(I)=ACDO(I)*CCDO(I)                                              DAT 8300
    HYD(I)=100.0-CMO(I)-CH4(I)-CDO(I)                                   DAT 8450
    GO TO 10                                                            DAT 8500
  5 HYD(I)=AHYD(I)*CHYD(I)                                              DAT 8600
    CH4(I)=AMET(I)*CMET(I)                                              DAT 8700
    CDO(I)=ACDO(I)*CCDO(I)                                              DAT 8800
    CMO(I)=100.0-HYD(I)-CH4(I)-CDO(I)                                   DAT 8900
    GO TO 10                                                            DAT 9000
  7 HYD(I)=AHYD(I)*CHYD(I)                                              DAT 9100
    CMO(I)=ACMO(I)*CCMO(I)                                              DAT 9200
    CDO(I)=ACDO(I)*CCDO(I)                                              DAT 9300
    CH4(I)=100.0-HYD(I)-CMO(I)-CDO(I)                                   DAT 9400
    GO TO 10                                                            DAT 9500
  9 HYD(I)=AHYD(I)*CHYD(I)                                              DAT 9600
    CMO(I)=ACMO(I)*CCMO(I)                                              DAT 9700
    CH4(I)=AMET(I)*CMET(I)                                              DAT 9800
    CDO(I)=100.0-HYD(I)-CMO(I)-CH4(I)                                   DAT 9900
 10 SUM(I)=HYD(I)+CMO(I)+CH4(I)+CDO(I)                                  DAT10000
```

```
      WRITE(2,150)(HYD(I),CMO(I),CH4(I),CDO(I),SUM(I))                    DAT10100
  150 FORMAT(///,8X,4HH2 =,F5.2,12X,4HCO =,F5.2,13X,4HCH4=,F5.2,11X,4HCO AT10200
     12=,F5.2,15X,6HTOTAL=,F6.2)                                          DAT10300
      CSUM(I)=100.0/SUM(I)                                                DAT10400
      H2(I)=CSUM(I)*HYD(I)                                                DAT10500
      CO(I)=CSUM(I)*CMO(I)                                                DAT10600
      CMT(I)=CSUM(I)*CH4(I)                                               DAT10700
      CO2(I)=CSUM(I)*CDO(I)                                               DAT10800
      TOT(I)=H2(I)+CO(I)+CMT(I)+CO2(I)                                    DAT10900
      WRITE(2,160)(H2(I),CO(I),CMT(I),CO2(I),TOT(I))                      DAT11000
  160 FORMAT(/,8X,4HH2 =,F5.2,12X,4HCO =,F5.2,13X,4HCH4=,F5.2,11X,4HCO2= AT11100
     1,F5.2,15X,6HTOTAL=,F6.2)                                            DAT11200
      BAL1(I)=3.0*CMO(I)+4.0*CDO(I)                                       DAT11300
      BAL2(I)=3.0*CO(I)+4.0*CO2(I)                                        DAT11400
      WRITE(2,170)(BAL1(I),BAL2(I))                                       DAT11500
  170 FORMAT(6X,6HBAL1 =,F5.2,10X,6HBAL2 =,F5.2)                          DAT11600
      RAT1(I)=CO2(I)/(CO(I)+CO2(I))                                       DAT11700
      WRITE(2,180)(RAT1(I))                                               DAT11800
  180 FORMAT(6X,6HRAT1 =,F7.4)                                            DAT11900
      TOTC(I)=CO(I)+CMT(I)+CO2(I)                                         DAT12000
      CONV(I)=100.0*(CO(I)+CO2(I))/TOTC(I)                                DAT12100
      WRITE(2,190)(CONV(I))                                               DAT12200
  190 FORMAT(6X,6HCONV =,F5.2)                                            DAT12300
      FTOT(I)=FMET(I)+FWAT(I)                                             DAT12400
      WRITE(2,195)(FTOT(I),FMET(I),FWAT(I))                               DAT12410
  195 FORMAT(6X,6HFTOT =,F7.3,8X,6HFMET =,F7.3,10X,5HFWAT=,F7.3)          DAT12420
      WFT(I)=W(I)/FTOT(I)                                                 DAT12500
      ACFT(I)=ACAT(I)/FTOT(I)                                             DAT12600
      ALPHA(I)=FWAT(I)/FMET(I)                                            DAT12700
      WRITE(2,200)(WFT(I),ACFT(I),ALPHA(I))                               DAT12800
  200 FORMAT(6X,6HW/FT =,F7.3,8X,6HAC/FT=,F7.3,9X,6HALPHA=,F7.3)          DAT12900
      FCH4(I)=CMT(I)*FMET(I)/TOTC(I)                                      DAT13000
      FH201(I)=(ALPHA(I)-((CO(I)+2.0*CO2(I))/TOTC(I)))*FMET(I)            DAT13100
      FH202(I)=(ALPHA(I)+(2.0*CO(I)+2.0*CO2(I)-H2(I))/TOTC(I))*FMET(I)    DAT13200
      FCO(I)=CO(I)*FMET(I)/TOTC(I)                                        DAT13300
      FCO2(I)=CO2(I)*FMET(I)/TOTC(I)                                      DAT13400
      FH2(I)=H2(I)*FMET(I)/TOTC(I)                                        DAT13500
      TOTRG1(I)=FCH4(I)+FH201(I)+FCO(I)+FCO2(I)+FH2(I)                    DAT13600
```

```
      TOTRG2(I)=FCH4(I)+FH2O2(I)+FCO(I)+FCO2(I)+FH2(I)                    DAT13700
      WRITE(2,210)(FCH4(I),FH2O1(I),FH2O2(I),FCO(I),FCO2(I),FH2(I))      DAT13800
  210 FORMAT(6X,6HFCH4 =,F7.3,8X,6HFH2O1=,F7.3,9X,6HFH2O2=,F7.3,6X,6HFCO AT13900
     1  =,F6.3,6X,6HFCO2 =,F6.3,6X,6HFH2  =,F6.3)                       DAT14000
      WRITE(2,220)(TOTRG1(I),TOTRG2(I))                                  DAT14100
  220 FORMAT(4X,15HTOTAL REF.GAS1=,F7.3,14X,15HTOTAL REF.GAS2=,F7.3)     DAT14200
      YCH4(I)=FCH4(I)/TOTRG1(I)                                          DAT14300
      YH2O1(I)=FH2O1(I)/TOTRG1(I)                                        DAT14400
      YH2O2(I)=FH2O2(I)/TOTRG2(I)                                        DAT14500
      YCO(I)=FCO(I)/TOTRG1(I)                                            DAT14600
      YCO2(I)=FCO2(I)/TOTRG1(I)                                          DAT14700
      YH2(I)=FH2(I)/TOTRG1(I)                                            DAT14800
      PCOR=1.0/PATM(I)                                                   DAT14210
      PCH4(I)=YCH4(I)/PCOR                                               DAT14220
      PH2O1(I)=YH2O1(I)/PCOR                                             DAT14222
      PH2O2(I)=YH2O2(I)/PCOR                                             DAT14224
      PCO(I)=YCO(I)/PCOR                                                 DAT14226
      PCO2(I)=YCO2(I)/PCOR                                               DAT14228
      PH2(I)=YH2(I)/PCOR                                                 DAT14230
      WRITE(2,225)(PCH4(I),PH2O1(I),PH2O2(I),PCO(I),PCO2(I),PH2(I))      DAT14232
  225 FORMAT(6X,6HPCH4 =,F6.4,9X,6HPH2O1=,F6.4,10X,6HPH2O2=,F6.4,7X,6HPC AT14234
     10  =,F6.4,6X,6HPCO2 =,F6.4,6X,6HPH2  =,F6.4)                       DAT14236
      WRITE(2,230)(YCH4(I),YH2O1(I),YH2O2(I),YCO(I),YCO2(I),YH2(I))      DAT14900
  230 FORMAT(6X,6HYCH4 =,F6.4,9X,6HYH2O1=,F6.4,10X,6HYH2O2=,F6.4,7X,6HYC AT15000
     10  =,F6.4,6X,6HYCO2 =,F6.4,6X,6HYH2  =,F6.4)                       DAT15100
      YTOT1=YCH4(I)+YH2O1(I)+YCO(I)+YCO2(I)+YH2(I)                       DAT15101
      YTOT2=YCH4(I)+YH2O2(I)+YCO(I)+YCO2(I)+YH2(I)                       DAT15102
      PTOT1=PCH4(I)+PH2O1(I)+PCO(I)+PCO2(I)+PH2(I)                       DAT15103
      PTOT2=PCH4(I)+PH2O2(I)+PCO(I)+PCO2(I)+PH2(I)                       DAT15104
      WRITE(2,232)(YTOT1,YTOT2,PTOT1,PTOT2)                              DAT15105
  232 FORMAT(6X,6HYTOT1=,F6.4,9X,6HYTOT2=,F6.4,10X,6HPTOT1=,F6.4,7X,6HPT AT15106
     1OT2=,F6.4)                                                         DAT15107
      DEN(I)=(1.0+ALPHA(I))*TOTC(I)                                      DAT15200
      SCH4(I)=(CO(I)+CO2(I))/DEN(I)                                      DAT15300
      SH2O(I)=(CO(I)+2.0*CO2(I))/DEN(I)                                  DAT15400
      SH2O2=(H2(I)-2.0*CO(I)-2.0*CO2(I))/DEN(I)                          DAT15401
      SCO(I)=CO(I)/DEN(I)                                                DAT15500
```

```
      SCO2(I)=CO2(I)/DEN(I)                                                  DAT15600
      SH2(I)=H2(I)/DEN(I)                                                    DAT15700
      WRITE(2,231)(SCH4(I),SH2O(I),SH2O2,SCO(I),SCO2(I),SH2(I))              DAT15800
  231 FORMAT(6X,6HSCH4 =,F6.4,9X,6HSH2O1=,F6.4,10X,6HSH2O2=,F6.4,7X,6HSC     AT15900
     10  =,F6.4,6X,6HSCO2 =,F6.4,6X,6HSH2  =,F6.4)                          DAT16000
      ECH4(I)=22.36*FCH4(I)                                                  DAT16100
      EH2O1(I)=22.386*FH2O1(I)                                               DAT16200
      EH2O2(I)=22.386*FH2O2(I)                                               DAT16300
      ECO(I)=22.404*FCO(I)                                                   DAT16400
      ECO2(I)=22.264*FCO2(I)                                                 DAT16500
      EH2(I)=22.428*FH2(I)                                                   DAT16600
      TCOR=(273.0+540.0)/273.0                                               DAT16700
      VOLRG(I)=TCOR*PCOR*(ECH4(I)+EH2O1(I)+ECO(I)+ECO2(I)+EH2(I))            DAT16900
      VOLRGAS2=TCOR*PCOR*(ECH4(I)+EH2O2(I)+ECO(I)+ECO2(I)+EH2(I))            DAT16901
      VOLRGO=TCOR*PCOR*(22.36*FMET(I)+22.386*FWAT(I))                        DAT16910
      VOLRR=(VOLRG(I)+VOLRGO)/2.0                                            DAT16920
      WRITE(2,240)(VOLRG(I),VOLRGAS2,VOLRGO,VOLRR)                           DAT17000
  240 FORMAT(6X,29HVOLUME OF REFORMED GAS      =,F8.2,10X,F8.2,10X,F8.2,     AT17100
     110X,F8.2,2X,11HCM3 PER MIN)                                            DAT17101
      VEL(I)=VOLRR/AFR(I)                                                    DAT17200
      TAU(I)=HEI(I)*1000.0/VEL(I)                                            DAT17300
      RECTAU(I)=VEL(I)/HEI(I)                                                DAT17400
      WRITE(2,250)(VEL(I),TAU(I),RECTAU(I))                                  DAT17500
  250 FORMAT(6X,30HLIN VELOCITY OF REACTING GAS =,F8.2,14X,16HCONTACT        DAT17600
     1TIME =,F5.2,4X,3HMIN,8X,16HSPACE  VELOCITY=,F6.2)                      DAT17700
      RHO(I)=(FMET(I)*16.042+FWAT(I)*18.016)/VOLRR                           DAT17800
      WRITE(2,260)(RHO(I))                                                   DAT17900
  260 FORMAT(6X,30HDENSITY OF REFORMED GAS      =,F6.4)                      DAT18000
      REA(I)=2.0+ALPHA(I)                                                    DAT18100
      REB(I)=(2.0*CMT(I)+H2(I))/TOTC(I)                                      DAT18200
      REC(I)=REA(I)-REB(I)                                                   DAT18300
      COLWAT(I)=REC(I)*FMET(I)*1.08096                                       DAT18400
      COLWAT1=FH2O1(I)*1.08096                                               DAT18401
      WRITE(2,270)(COLWAT(I),COLWAT1)                                        DAT18500
  270 FORMAT(6X,17HCOLLECTED WATER =,F6.2,7X,F6.2,2X,9HML PER HR)            DAT18600
      VCH4=(0.00002669*((16.042*813.0)**0.5))/((3.758**2.0)*0.9109)          DAT18610
      VH2O=(0.00002669*((18.016*813.0)**0.5))/((2.520**2.0)*1.790)           DAT18617
      VCO=(0.00002669*((28.01*813.0)**0.5))/((3.690**2.0)*0.8386)            DAT18624
```

```
 VCO2=(0.00002669*((44.01*813.0)**0.5))/((3.941**2.0)*0.9615)          DAT18631
 VH2=(0.00002669*((2.016*813.0)**0.5))/((2.827**2.0)*0.7884)           DAT18638
 PHI12=((1.0+((VCH4/VH2O)**0.5)*((18.016/16.042)**0.25))**2.0)/((8. AT19620
10*(1.0+(16.042/18.016)))**0.5)                                        DAT19621
 PHI13=((1.0+((VCH4/VCO)**0.5)*((28.01/16.042)**0.25))**2.0)/((8.0* AT19622
1(1.0+(16.042/28.01)))**0.5)                                           DAT19623
 PHI14=((1.0+((VCH4/VCO2)**0.5)*((44.01/16.042)**0.25))**2.0)/((8.0 AT19624
1*(1.0+(16.042/44.01)))**0.5)                                          DAT19625
 PHI15=((1.0+((VCH4/VH2)**0.5)*((2.016/16.042)**0.25))**2.0)/((8.0* AT19626
1(1.0+(16.042/2.016)))**0.5)                                           DAT19627
 PHI21=(VH2O/VCH4)*(16.042/18.016)*PHI12                               DAT19628
 PHI23=((1.0+((VH2O/VCO)**0.5)*((28.01/18.016)**0.25))**2.0)/((8.0* AT19629
1(1.0+(18.016/28.01)))**0.5)                                           DAT19630
 PHI24=((1.0+((VH2O/VCO2)**0.5)*((44.01/18.016)**0.25))**2.0)/((8.0 AT19631
1*(1.0+(18.016/44.01)))**0.5)                                          DAT19632
 PHI25=((1.0+((VH2O/VH2)**0.5)*((2.016/18.016)**0.25))**2.0)/((8.0* AT19633
1(1.0+(18.016/2.016)))**0.5)                                           DAT19634
 PHI31=(VCO/VCH4)*(16.042/28.01)*PHI13                                 DAT19635
 PHI32=(VCO/VH2O)*(18.016/28.01)*PHI23                                 DAT19636
 PHI34=((1.0+((VCO/VCO2)**0.5)*((44.01/28.01)**0.25))**2.0)/((8.0*( AT19637
11.0+(28.01/44.01)))**0.5)                                             DAT19638
 PHI35=((1.0+((VCO/VH2)**0.5)*((2.016/28.01)**0.25))**2.0)/((8.0*(1 AT19639
1.0+(28.01/2.016)))**0.5)                                              DAT19640
 PHI41=(VCO2/VCH4)*(16.042/44.01)*PHI14                                DAT19641
 PHI42=(VCO2/VH2O)*(18.016/44.01)*PHI24                                DAT19642
 PHI43=(VCO2/VCO)*(28.01/44.01)*PHI34                                  DAT19643
 PHI45=((1.0+((VCO2/VH2)**0.5)*((2.016/44.01)**0.25))**2.0)/((8.0*( AT19644
11.0+(44.01/2.016)))**0.5)                                             DAT19645
 PHI51=(VH2/VCH4)*(16.042/2.016)*PHI15                                 DAT19646
 PHI52=(VH2/VH2O)*(18.016/2.016)*PHI25                                 DAT19647
 PHI53=(VH2/VCO)*(28.01/2.016)*PHI35                                   DAT19648
 PHI54=(VH2/VCO2)*(44.01/2.016)*PHI45                                  DAT19649
 VMIX1(I)=(VCH4*YCH4(I))/(YCH4(I)+(YH2O1(I)*PHI12)+(YCO(I)*PHI13)+( AT19650
1YCO2(I)*PHI14)+(YH2(I)*PHI15))                                        DAT19651
 VMIX2(I)=(VH2O*YH2O1(I))/(YH2O1(I)+(YCH4(I)*PHI21)+(YCO(I)*PHI23)+ AT19652
1(YCO2(I)*PHI24)+(YH2(I)*PHI25))                                       DAT19653
 VMIX3(I)=(VCO*YCO(I))/(YCO(I)+(YCH4(I)*PHI31)+(YH2O1(I)*PHI32)+(YC AT19654
102(I)*PHI34)+(YH2(I)*PHI35))                                          DAT19655
```

```
      VMIX4(I)=(VCO2*YCO2(I))/(YCO2(I)+(YCH4(I)*PHI41)+(YH2O1(I)*PHI42)+ AT19656
     1(YCO(I)*PHI43)+(YH2(I)*PHI45))                                    DAT19657
      VMIX5(I)=(VH2*YH2(I))/(YH2(I)+(YCH4(I)*PHI51)+(YH2O1(I)*PHI52)+(YC AT19658
     10(I)*PHI53)+(YCO2(I)*PHI54))                                      DAT19659
      VISC(I)=VMIX1(I)+VMIX2(I)+VMIX3(I)+VMIX4(I)+VMIX5(I)              DAT18660
      WRITE(2,360)(VMIX1(I),VMIX2(I),VMIX3(I),VMIX4(I),VMIX5(I))       DAT18676
  360 FORMAT(12X,5F18.8)                                                DAT18677
      WRITE(2,370)(VISC(I))                                             DAT18678
  370 FORMAT(6X,22HVISCOSITY OF REF GAS =,F10.8)                        DAT18679
      G(I)=((FMET(I)*16.042)+(FWAT(I)*18.016))/(60.0*AFR(I))            DAT18680
      G1(I)=((FCH4(I)*16.042)+(FH2O1(I)*18.016)+(FCO(I)*28.01)+(FCO2(I)* AT18681
     144.01)+(FH2(I)*2.016))/(60.0*AFR(I))                              DAT18682
      G2(I)=((FCH4(I)*16.042)+(FH2O2(I)*18.016)+(FCO(I)*28.02)+(FCO2(I)* AT18683
     144.01)+(FH2(I)*2.016))/(60.0*AFR(I))                              DAT18684
      WRITE(2,380)(G(I),G1(I),G2(I))                                    DAT18685
  380 FORMAT(6X,21HSUP.MASS VEL. (10+3)=,F10.5,10X,F10.5,10X,F10.5)     DAT18686
      REYN(I)=(1.830-D(I))*G(I)/(1000.0*VISC(I))                        DAT18687
      REYN1(I)=(1.830-D(I))*G1(I)/(1000.0*VISC(I))                      DAT18688
      WRITE(2,390)(REYN(I),REYN1(I))                                    DAT18689
  390 FORMAT(6X,17HREYNOLDS NUMBER =,F8.2,16X,F8.2)                     DAT18690
      CSHIFT1=(PCO2(I)*PH2(I))/(PCO(I)*PH2O1(I))                        DAT20000
      CSHIFT2=(PCO2(I)*PH2(I))/(PCO(I)*PH2O2(I))                        DAT20010
      CSHIREV1=1.0/CSHIFT1                                              DAT20020
      CSHIREV2=1.0/CSHIFT2                                              DAT20030
      WRITE(2,280)(CSHIFT1,CSHIFT2,CSHIREV1,CSHIREV2)                   DAT20040
  280 FORMAT(//,6X,17HKSHIFT REACTION =,F8.4,10X,F8.4,10X,12HKSHIFT REV. AT20050
     1=,F8.4,10X,F8.4)                                                  DAT20051
      CBOUD=(PCO(I)**2.0)/PCO2(I)                                       DAT20060
      WRITE(2,282)(CBOUD)                                               DAT20070
  282 FORMAT(6X,17HKBOUDOUARD REAC.=,F10.7)                             DAT20080
      CMETH=PCH4(I)/(PH2(I)**2.0)                                       DAT20090
      WRITE(2,284)(CMETH)                                               DAT20100
  284 FORMAT(6X,17HKMETHANE   REAC.=,F11.8)                             DAT20110
      CREF1=(PCO(I)*(PH2(I)**3.0))/(PCH4(I)*PH2O1(I))                   DAT20120
      CREF2=(PCO(I)*(PH2(I)**3.0))/(PCH4(I)*PH2O2(I))                   DAT20130
      WRITE(2,286)(CREF1,CREF2)                                         DAT20140
  286 FORMAT(6X,17HREFORMING  REAC.=,F10.7,16X,F10.7)                   DAT20150
      CREFCOM1=(PCO2(I)*(PH2(I)**4.0))/(PCH4(I)*(PH2O1(I)**2.0))        DAT20160
```

```
      WRITE(2,288)(CREFCOM1)                                          DAT20170
  288 FORMAT(6X,17HCOMB.REFOR.REAC.=,F10.7)                           DAT20180
    1 CONTINUE                                                        DAT18700
      STOP                                                            DAT18800
      END                                                             DAT18900

END OF SEGMENT, LENGTH  3418, NAME  NONM



      FINISH                                                          DAT19000
END OF COMPILATION -  NO ERRORS

S/C SUBFILE:      64 BUCKETS USED
```

WEIGHT = 5.2133 SURFACE = 8.5477 HEIGHT = 1.79 FREE AREA = 0.8156 OPE.PRES.= 0.980

CAT.D.=1.520

H2 =42.39 CO = 1.65 CH4=46.62 CO2= 9.23 TOTAL= 99.88

H2 =42.44 CO = 1.65 CH4=46.68 CO2= 9.24 TOTAL=100.00

BAL1 =41.85 BAL2 =41.90

RAT1 = 0.8486

CONV =18.91

FTOT = 13.011 FMET = 3.260 FWAT= 9.751

W/FT = 0.401 AC/FT= 0.657 ALPHA= 2.991 ✓ $\Delta = \pm 0.64$

FCH4 = 2.643 FH201= 8.611 FH202= 8.581 FCO = 0.093 FCO2 = 0.523 FH2 = 2.403

TOTAL REF.GAS1= 14.275 TOTAL REF.GAS2= 14.244

PCH4 =0.1815 PH201=0.5912 PH202=0.5904 PCO =0.0064 PCO2 =0.0359 PH2 =0.1650

YCH4 =0.1852 YH201=0.6033 YH202=0.6024 YCO =0.0065 YCO2 =0.0367 YH2 =0.1684

YTOT1=1.0000 YTOT2=0.9992 PTOT1=0.9800 PTOT2=0.9792

SCH4 =0.0474 SH201=0.0876 SH202=0.0899 SCO =0.0072 SCO2 =0.0402 SH2 =0.1847

VOLUME OF REFORMED GAS = 970.96 968.89 884.84 927.90 CM3 PER MIN

LIN VELOCITY OF REACTING GAS = 1137.69 CONTACT TIME = 1.57 MIN SPACE VELOCITY=635.58

DENSITY OF REFORMED GAS =0.2457

COLLECTED WATER = 9.28 9.31 ML PER HR

0.00004979 0.00018845 0.00000288 0.00002050 0.00001662

VISCOSITY OF REF GAS =0.00027825

SUP.MASS VEL. (10+3)= 4.65855 4.65980 4.64864

REYNOLDS NUMBER = 5.19 5.19

KSHIFT REACTION = 1.5639 1.5661 KSHIFT REV.= 0.6394 0.6385

KBOUDOUARD REAC.= 0.0011439

KMETHANE REAC.= 6.66614739

REFORMING REAC.= 0.0002684 0.0002688

COMB.REFOR.REAC.= 0.0004197

Fig: A-6.1. The Correction Factor, β, for the Nonideality of Nitrogen at Liquid-nitrogen Temperatures (After. P.A. Faeth [57])

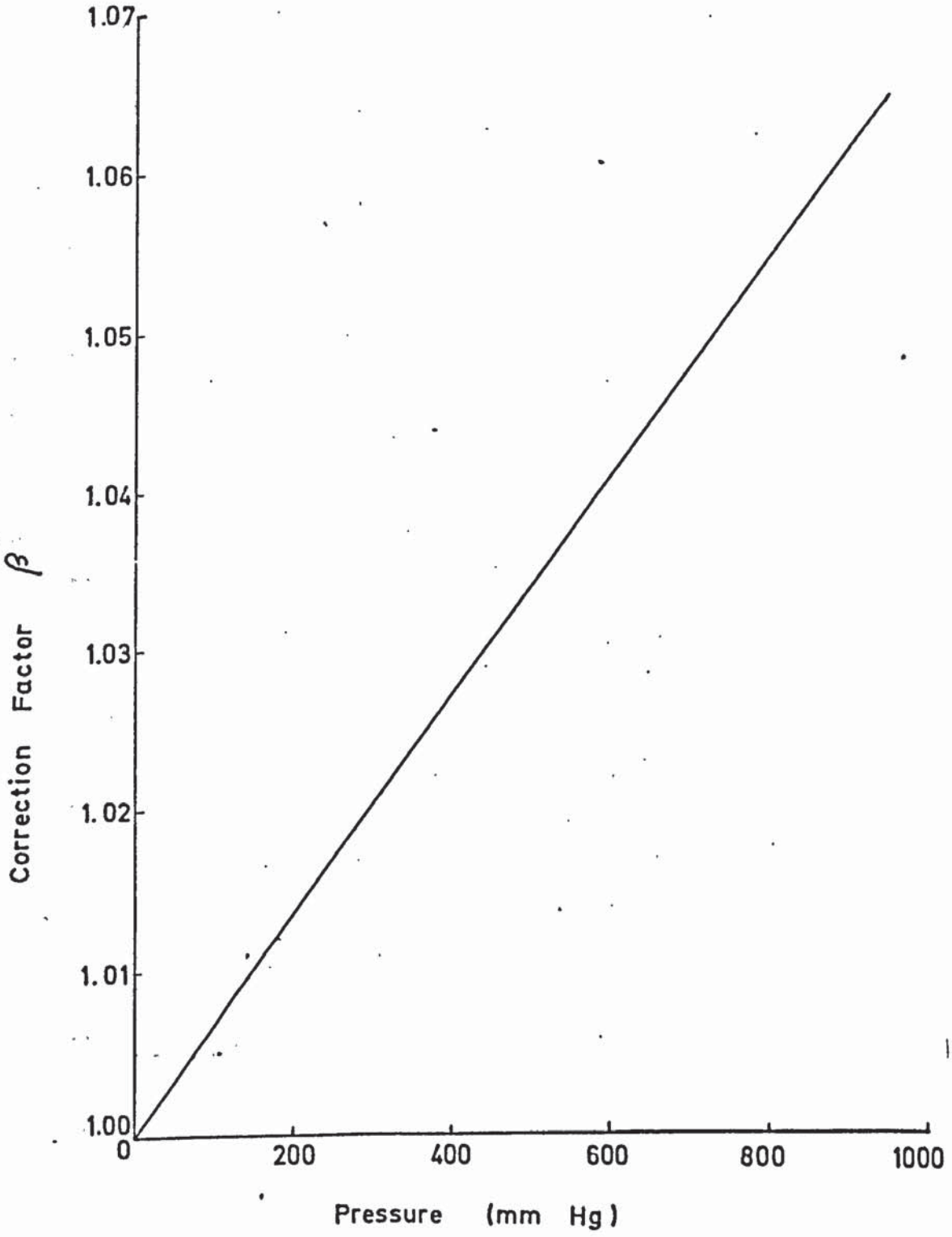

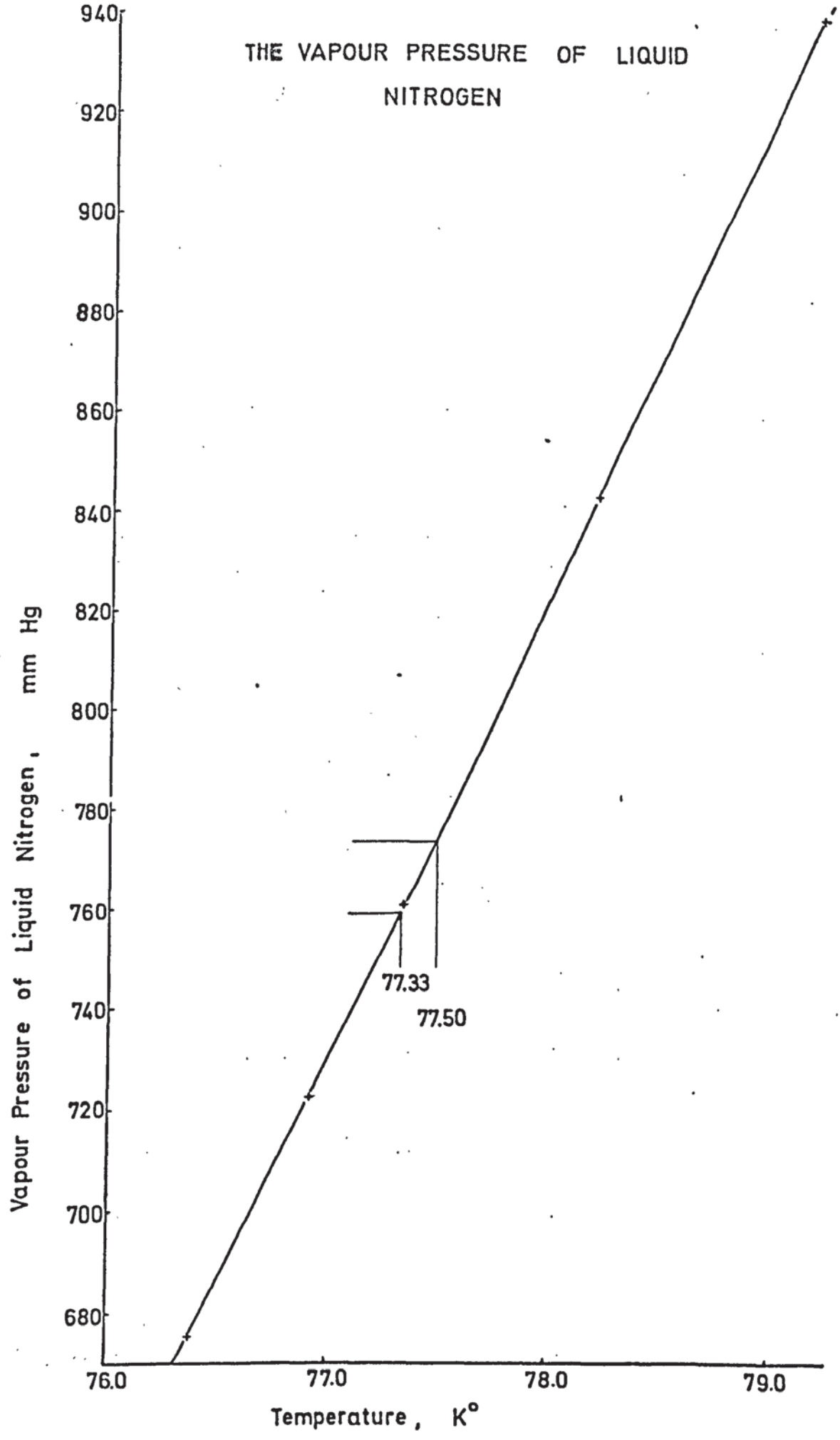
THE VAPOUR PRESSURE OF LIQUID NITROGEN
940
920
900
880
860
840
820
800
780
760
740
720
700
680
Vapour Pressure of Liquid Nitrogen, mm Hg
77.33
77.50
76.0
77.0
78.0
79.0
Temperature, K°

Fig. A-6.2

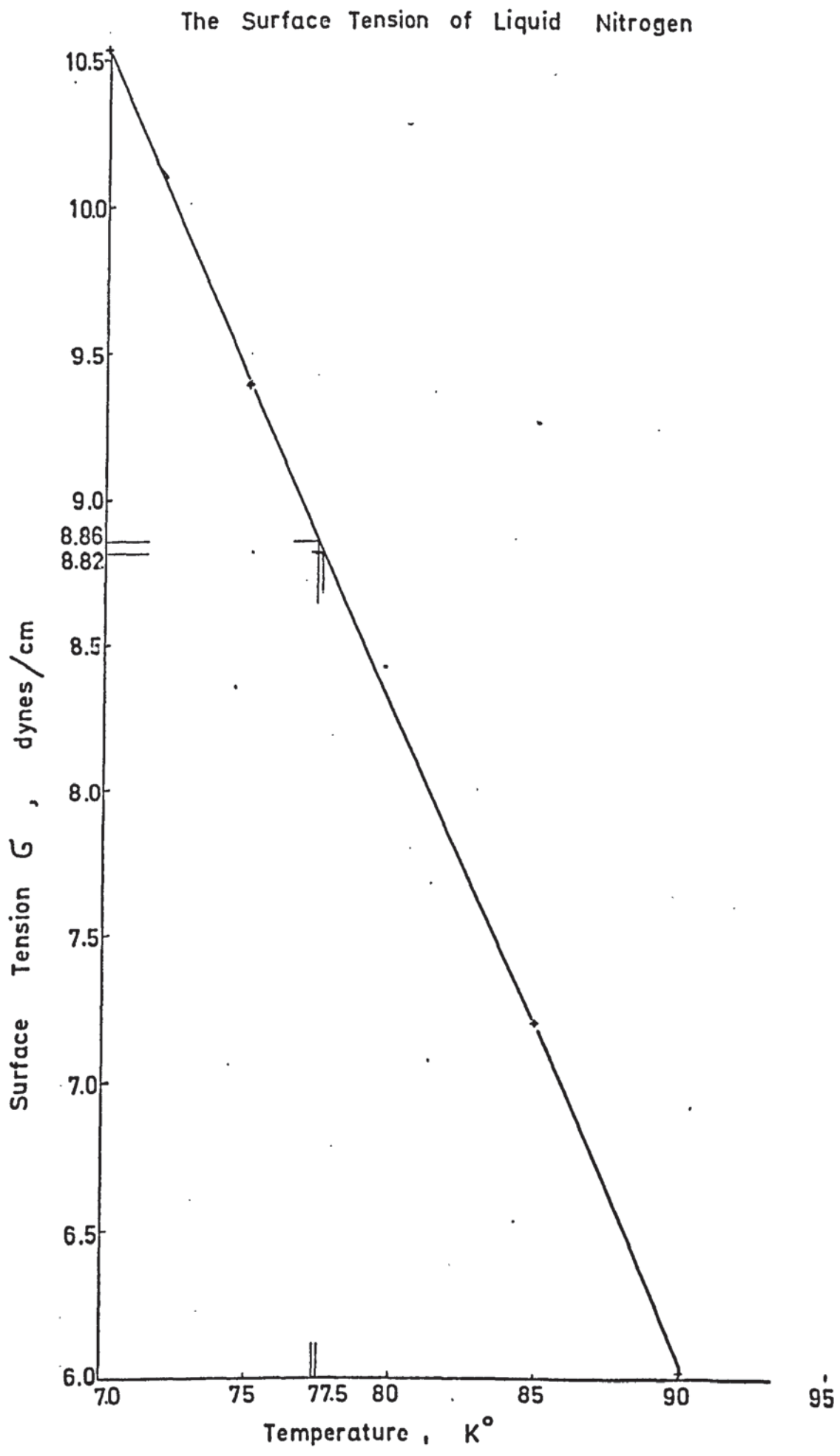
The Surface Tension of Liquid Nitrogen
Surface Tension G , dynes/cm
10.5
10.0
9.5
9.0
8.86
8.82
8.5
8.0
7.5
7.0
6.5
6.0
7.0
75
77.5
80
85
90
95
Temperature , K°

Fig. A-6.3.

TABLE A - 6.1

INDIVIDUAL and CUMULATIVE BULB VOLUMES

of B.E.T. - APPARATUS

Burette B	Individual Volume (ml)	Cumulative Volume (ml)
1	3.481	3.481
2	5.242	8.723
3	9.089	17.812
4	17.343	35.155
5	52.717	87.872

Burette B'	Individual Volume (ml)	Cumulative Volume (ml)
1	1.924	1.924
2	1.999	3.923
3	3.423	7.346
4	2.697	10.043
5	8.147	18.190

CUMULATIVE BULB VOLUMES (ml)

FOR ANY BURETTE - BULB COMBINATION

Zero-Bulb	Zero-Bulb 11.690	B'1 13.614	B'2 15.613	B'3 19.036	B'4 21.733	B'5 29.880
B1	15.171	17.095	19.094	22.517	25.214	33.361
B2	20.413	22.337	24.336	27.759	30.456	38.603
B3	29.502	31.426	33.425	36.848	39.545	47.692
B4	46.845	48.769	50.768	54.191	56.888	65.035
B5	99.562	101.486	103.485	106.908	109.605	117.752

TABLE A - 6.2

DETERMINATION OF ZERO-BULB-VOLUME (Z.B.V.)

Mercury level in manometer C as base line : 80.0 mm

Burette and Bulb used	Bulb Volume Y (ml)	Pressure reading at Z.B.V. P_1 (mm)	Pressure readings P_2 (mm)	(P_1-P_2) (mm)	$\frac{P_2}{P_1-P_2}$	Zero-Bulb-Volume at STP ZBV=(Y) $\frac{P_2}{P_1-P_2}$
*Z.B.V.		226.8				
B3	17.812		90.2	136.6	0.6603	11.729
B2	8.723		130.2	96.6	1.3478	11.725
B1	33.781		174.8	52.0	3.3615	11.670
B1+B'	10.827		117.8	109.0	1.0807	11.669
B1+B'	13.524		105.2	121.6	0.8651	11.668
B1+B'	21.671		80.2	146.6	0.5471	11.824
B1+B'	13.524		105.2	121.6	0.8651	11.668
B1+B'	10.827		117.8	109.0	1.0807	11.669
B1+B'	7.404		138.8	88.0	1.5772	11.646
B1	3.481		175.0	51.8	3.3783	11.728
**Z.B.V.		228.6				
B1	3.481		175.8	52.8	3.3295	11.562
B3	17.812		90.6	138.0	0.6565	11.665
B4	35.155		57.2	171.4	0.3337	11.703
					Av.	11.690 ml

* Temperature of the burettes : $15^{\circ}C$ (constant)

D_{15} = 13.5581 g/cm^3

D_o = 13.5951 g/cm^3

**Second run for control:

Temperature of the burettes : $13^{\circ}C$ (constant)

D_{13} = 13.5630 g/cm^3

D_o = 13.5951 g/cm^3

TABLE A - 6.3

BULB FACTORS*

	Zero-Bulb	B'1	B'2	B'3	B'4	B'5
Zero-Bulb	4.202	4.893	5.612	6.842	7.811	10.739
B1	5.453	6.144	6.863	8.093	9.062	11.991
B2	7.337	8.028	8.747	9.977	10.946	13.875
B3	10.604	11.295	12.014	13.244	14.213	17.141
B4	16.837	17.528	18.247	19.477	20.447	23.375
B5	35.784	36.476	37.194	38.424	39.394	42.322

(* for t = 20^{o}C)

TABLE A - 6.4

THE DETERMINATION OF THE DEAD-SPACE-FACTOR (D.S.F.) IN B.E.T. MEASUREMENTS

(for only one measurement)

Stopcock 6	Burette and Bulb used	Bulb Factor $F_v = V_1 (\frac{T_o}{P_o})$	Pressure Readings P_1 (mm Hg)	$(\frac{1}{T_1})(\frac{D_T}{D_o})$	Volume of He at STP $V_o = V_1 (\frac{T_o}{P_o})(\frac{P}{T_1})(\frac{D_T}{D_o})$	Average Value V_{av}	Corrected Pressure $p = p_1 (\frac{D_T}{D_o})$	Volume of He in the sample tube $V_s = V_{av} - V_o'$	D.S.F. $F_s = \frac{V_s}{P_c}$
closed	B5	35.784	217.2	0.003473	26.993				
"	B5+B'2	37.194	208.6	"	26.946				
"	B5+B'2	38.424	202.4	"	27.005				
"	B5+B'4	39.394	197.2	"	26.980				
"	B5+B'5	42.322	183.2	"	26.928				
"	B4+B'5	23.375	331.8	"	26.936	26.964			
				$(\frac{1}{T_1})$	$V_o' = V_1 (\frac{T_o}{P_o})(\frac{P_1}{T_1})$				
open	B3+B'5	17.141	365.8	0.003482	21.833		364.85	5.131	0.01406
"	B2+B'3	9.977	553.0	"	19.211		551.56	7.753	0.01405
"	B3+B'3	13.244	449.2	"	20.715		448.03	6.249	0.01395
"	B4+B'3	19.477	330.8	"	22.434		329.94	4.530	0.01373
"	B3+B'5	17.141	367.8	"	21.952		366.84	5.012	0.01366
"	B2+B'5	13.875	435.0	"	21.016		433.87	5.948	0.01371
"	B2+B'4	10.946	517.8	"	19.735		516.45	7.229	0.01399
"	B2+B'3	9.977	555.4	"	19.295		553.96	7.669	0.01384
"	B4+B'3	19.477	331.0	"	22.440		330.14	4.526	0.01368

Temperature of the burettes during measurement = $14^{\circ}C$ ($T = 287.16^{\circ}K$)

$D_{14} = 13.5606\ g/cm^3$

$D_o = 13.5951\ g/cm^3$

Average value for D.S.F. = 0.01385 $cm^3/mm\ Hg$.

TABLE A - 6.5

CALCULATION TABLE FOR THE B.E.T. AREA

1	2	3	4	5	6	7	8	9
	Stopcock 6	Burette and Bulb	bulb factor (F_v)	Temp. (°C)	Pressure Readings (P_1) (mm)	$(\frac{1}{T_1})(\frac{D_T}{D_o})$	Volume of N_2 at 0°C and 760 mm $V_o = F_v(\frac{P_1}{T_1})(\frac{D_T}{D_o})$	Average value for N_2, V_T	DSF (F_s)
	closed	B5+B'4	39.394	12	149.2	0.003499	20.566		
	"	B5+B'3	38.424	"	152.9	"	20.557	(Average of 10 Readings)	
	"	B5+B'2	37.194	"	157.6	"	20.510		
	"	B4+B'2	18.247	"	321.3	"	20.514		
	"	B5+B'5	42.322	"	139.6	"	20.672	20.537	
							Volume of N_2 at 0°C and 760 mm remained in the burette V_R		
1	open	B5+B'5	42.322	"	100.2	"	14.838		0.0154
2	"	B5+B'4	39.394	"	106.6	"	14.694		"
3	"	B5+B'3	38.424	"	108.8	"	14. 627		"
4	"	B5+B'1	36.476	"	113.6	"	14.499		"
5	"	B5+B'0	35.784	"	115.8	"	14.499		"
6	"	B4+B'5	23.375	"	163.8	"	13.397		"
7	"	B4+B'4	20.447	12.6	182.0	0.003491	12.991		"
8	"	B4+B'3	19.477	13	188.8	0.003486	12.819		"
9	"	B5+B'2	37.194	12	111.9	0.003499	14.563		"

TABLE A - 6.5

CALCULATION TABLE FOR THE B.E.T. AREA

	10	11	12	13	14	15
	Non-ideal. Corr. (β)	$V_s = P_1 (\frac{D_T}{D_o}) (F_s) (\beta)$	$V_a = V_T - V_R - V_S$	Pressure in Mano. I (P_o)	Relative pressure (P_1/P_o)	$\frac{P_1}{V_a(P_o - P_1)}$
1	1.0065	1.550	4.149	775.6	0.127	0.0357
2	1.0070	1.650	4.193	"	0.137	0.0380
3	1.0072	1.684	4.226	775.3	0.140	0.0386
4	1.0077	1.759	4.279	774.2	0.146	0.0402
5	1.0079	1.793	4.245	"	0.150	0.0413
6	1.0175	2.561	4.579	"	0.212	0.0586
7	1.0120	2.830	4.716	"	0.235	0.0651
8	1.0125	2.937	4.781	"	0.244	0.0675
9	1.0075	1.732	4.242	775.3	0.144	0.0396

Weight of the sample $w = 0.5497$ g

Intercept (by graphical extrapolation) : $I = 0.0014$

Slope: 0.266

$$V_m = \frac{1}{I + s} = 3.7397 \text{ cm}^3$$

$$\text{B.E.T. area, } S_g = \frac{V_m}{w} (K) = \frac{3.7397}{0.5497} (4.38) = 29.8 \text{ m}^2/\text{g}$$

TABLE A - 6.5

CALCULATION TABLE FOR THE NITROGEN ISOTHERM

	1 Stopcock 6	2 Burette and Bulb used	3 Bulb Factor (F_V)	4 Temp. (°C)	5 Pressure Readings (P_1)	6 $(\frac{1}{T})(\frac{D_T}{D_o})$	7 Volume of N_2 at 0°C and 760 mm $V_o=F_V(\frac{P_1}{T_i})(\frac{D_T}{D_o})$	8 Average Value for N_2 (V_T)	9 D.S.F (F_s)
	closed	B5+B'3	38.424	13.2	357.0	0.003483	47.777		
	"	B4+B'3	19.477	"	703.8	"	47.744		
	"	B4+B'2	18.247	"	751.8	"	47.780		
	"	B4+B'2	17.528	"	782.5	"	47.772		
	"	B5+B'1	36.476	"	376.0	"	47.769		
	"	B5+B'3	38.424	"	357.0	"	47.777		
	"	B5+B'4	39.394	"	348.2	"	47.776		
	"	B5+B'5	42.322	"	324.0	"	47.760	47.769	
							Volume of N_2 at 0°C and .760 mm remained in the burette (V_R)	$P_c=P_1(\frac{D_T}{D_o})$	
1	open	B5+B'5	42.322	13.2	262.0	0.003483	38.621	261.37	0.0150
2	"	B4+B'5	23.375	"	422.4	"	34.390	421.39	"
3	"	B4+B'4	20.447	"	465.0	"	33.116	463.88	"
4	"	B3+B'4	14.213	13.0	577.2	0.003486	28.598	575.81	"
5	"	B3+B'3	13.244	"	596.4	"	27.535	594.97	"
6	"	B2+B'3	9.977	"	654.0	"	22.746	652.43	"

TABLE A - 6.5 (cont.)

CALCULATION TABLE FOR THE NITROGEN ISOTHERM

	10	11	12	13	14	15
	Non-ideal. Correction (β)	$V_s = P_1 (\frac{D_T}{D_o})(F_s)(\beta)$	$V_a = V_T - V_R - V_s$	Pressure in Manometer I (P_o)	Relative Pressure (P_1/P_o)	N_2 absorbed per gram of catalyst sample = 0.6358 g
1	1.0172	3.988	5.160	774.0	0.339	8.116
2	1.0275	6.495	6.884	773.5	0.546	10.827
3	1.0307	7.172	7.481	"	0.601	11.766
4	1.0385	8.970	10.201	"	0.746	16.044
5	1.0397	9.279	10.955	771.5	0.771	17.230
6	1.0435	10.212	14.811	771.3	0.846	23.295

TABLE A - 6.5 (cont.)

	1	2	3	4	5	6	7	8	9
7	open	B2+B'2	8.747	13.0	673.0	0.003486	20.521	671.38	0.0150
8	"	B1+B'2	6.863	"	699.8	"	16.742	698.12	"
9	"	B1+B'1	6.144	"	709.0	0.003483	15.185	707.30	"
10	"	B0+B'1	4.893	13.2	728.0	"	12.407	726.25	"
11	"	B0+B'1	4.893	"	727.0	"	12.390	725.26	"
12	"	B0+B'0	4.202	"	739.0	"	10.816	737.23	"
13	open	B1+B'0	5.453	13.2	710.2	0.003483	13.489	708.49	"
14	"	B1+B'1	6.144	"	696.6	"	14.907	694.93	"
15	"	B2+B'1	8.028	13.0	654.2	0.003486	18.308	652.63	"
16	"	B2+B'2	8.747	"	641.0	"	19.545	639.46	"
17	"	B3+B'2	12.014	"	580.8	"	24.303	579.40	"
18	"	B3+B'3	13.244	"	569.6	"	26.297	568.23	"
19	"	B4+B'3	19.477	"	473.5	"	32.121	472.36	"
20	"	B4+B'4	20.447	"	459.2	"	32.703	458.10	"
21	"	B5+B'4	39.394	"	277.6	"	38.087	276.93	"
22	"	B5+B'5	42.322	"	261.8	"	38.624	261.17	"

TABLE A - 6.5 (Cont.)

	10	11	12	13	14	15
7	1.0450	10.524	16.724	771.3	0.870	26.304
8	1.0470	10.964	20.063	"	0.905	31.556
9	1.0475	11.113	21.471	771.0	0.917	33.770
10	1.0485	11.422	24.940	"	0.941	37.653
11	1.0482	11.403	23.976	772.2	0.940	37.710
12	1.0490	11.600	25.353	776.3	0.955	39.876
13	1.0475	11.132	23.148	774.6	0.917	36.408
14	1.0468	10.912	21.950	775.4	0.898	34.523
15	1.0435	10.215	19.246	775.4	0.844	30.271
16	1.0427	10.001	18.223	772.8	0.829	28.662
17	1.0388	9.050	14.416	771.6	0.753	22.673
18	1.0380	8.847	12.625	771.6	0.732	19.857
19	1.0310	7.305	8.343	771.6	0.613	13.122
20	1.0305	7.081	7.986	771.6	0.594	12.560
21	1.0188	4.232	5.450	769.6	0.361	8.571
22	1.0172	3.985	5.160	769.3	0.340	8.116

Nomenclature for Table A - 6.5

V_T = The total volume of adsorbate gas (N_2) admitted into the burette system, cm^3.

V_R = The volume of adsorbate gas remaining in the burettes at equilibrium pressure, cm^3.

These volumes are calculated from Eq. (6.9)

$V_s = (p_c)(F_s)(\beta)$ = the volume of adsorbate gas present in the sample tube and not adsorbed, cm^3.

p_c = The equilibrium gas pressure corrected to 0^oC, mm Hg

F_s = The dead-space-factor, cm^3/mm Hg

β = The correction factor for non-ideality of nitrogen. A plot of the correction factor as a function of the pressure at liquid nitrogen temperatures is reproduced in Fig. A - 6.1.

$V_a = V_T - V_R - V_s$ = the volume of adsorbate adsorbed, cm^3

p = the equilibrium gas pressure of the bur ette system as indicated on manometer C, mm Hg.

p_o = the vapour pressure of nitrogen at the temperature of the liquid nitrogen bath, mm Hg

p/p_o = The relative pressure

TABLE A - 6.6

CALIBRATION OF THE SAMPLE FLASK FOR TRUE DENSITY DETERMINATION BY HELIUM DISPLACEMENT

Stopcock 6	Burette and Bulb used	Volume V_1, ml	Temp. of burette system	Temp. of sample tube	Pressure observed P_1	P_2	$\frac{P_1-P_2}{P_2}$	$V_1\frac{(P_1-P_2)}{P_2}$
closed	B4+B*0	46.845	18.0	18.0	388.6			
"	B3+B*0	29.502	19.0	19.0	617.0			
"	B5+B*0	106.908	19.0	19.0	170.7			
"	B5+B*4	109.605	19.0	19.1	166.4			
"	B5+B*5	117.752	19.1	19.1	155.8			
"	B4+B*5	65.035	18.0	18.2	279.6			
open	B4+B*5	65.035	18.0	18.2		201.2	0.3896	25.342
	B5+B*5	117.752	19.2	19.2		128.2	0.2153	25.351
	B5+B*4	109.605	19.0	19.1		135.2	0.2308	25.293
	B5+B*0	106.908	19.0	19.0		138.0	0.2369	25.333
	B3+B*0	29.502	19.0	19.0		332.0	0.8584	25.325
	B4+B*0	46.845	19.0	19.0		252.2	0.5408	25.335

Average value for the sample flask volume:

V_c = 25.335 ml

A - 8.1

DEVELOPMENT OF THE SYSTEM OF LINEAR EQUATIONS FOR THE COMPUTER PROGRAM IN CORRELATING THE INTEGRAL RATE DATA

The suggested rate equation is of the form:

$$RR_i = \frac{(RC)\ (P_i)^A\ (Q_i)^B}{\left[1 + (S)(P_i)^C + (T)(Q_i)^D + (U)(PC_i)^E + (V)(PD_i)^F + (Y)(PH_i)^H\right]^\alpha}$$

$$RC = \frac{1}{R}$$

$$RR_i = \frac{(P_i)^A\ (Q_i)^B}{\left[R + (S)(R)(P_i)^C + (T)(R)(Q_i)^D + (U)(R)(PC_i)^E + (V)(R)(PD_i)^F + (Y)(R)(PH_i)^H\right]^\alpha}$$

Substituting

$$(S)(R) = \beta$$

$$(T)(R) = \gamma$$

$$(U)(R) = \varepsilon$$

$$(V)(R) = \phi$$

$$(Y)(R) = \lambda$$

$$R + (\beta)\ (P_i)^C + (\gamma)\ (Q_i)^D + (\varepsilon)\ (PC_i)^E + (\phi)(PD_i)^F + (\lambda)(PH_i)^H = \left[\frac{(P_i)^A\ (Q_i)^B}{RR_i}\right]^{\frac{1}{\alpha}}$$

To minimize the sum of the squares of the approximation errors

$$\$ = \sum_{i=1}^{n} \left\{ \left[\frac{(P_i)^A (Q_i)^B}{RR_i}\right]^{\frac{1}{\alpha}} - \left[(R+\beta P_i{}^C + \gamma Q_i{}^D + \varepsilon PC_i{}^E + \phi PD_i{}^F + \lambda PH_i{}^H)\right] \right\}^2$$

The function $\$ = \$\ (R, \beta, \gamma, \varepsilon, \phi, \lambda\ )$ is differentiated with respect to the unknown parameters:

$$\frac{\partial \phi}{\partial R} = 2 \sum_{i=1}^{n} \left\{ \left[\frac{(P_i)^A (Q_i)^B}{RR_i} \right]^{1/a} - \left[(R + \beta P_i^C + \gamma Q_i^D + \varepsilon PC_i^E + \phi PD_i^F + \lambda PH_i^H) \right] \right\} (-1) = 0$$

$$\frac{\partial \phi}{\partial \beta} = 2 \sum_{i=1}^{n} \left\{ \quad " \quad " \right\} (-1)(P_i^C) = 0$$

$$\frac{\partial \phi}{\partial \gamma} = 2 \sum_{i=1}^{n} \left\{ \quad " \quad " \right\} (-1)(Q_i^D) = 0$$

$$\frac{\partial \phi}{\partial \varepsilon} = 2 \sum_{i=1}^{n} \left\{ \quad " \quad " \right\} (-1)(PC_i^E) = 0$$

$$\frac{\partial \phi}{\partial \phi} = 2 \sum_{i=1}^{n} \left\{ \quad " \quad " \right\} (-1)(PD_i^F) = 0$$

$$\frac{\partial \phi}{\partial \lambda} = 2 \sum_{i=1}^{n} \left\{ \quad " \quad " \right\} (-1)(PH_i^H) = 0$$

Substituting for:

$$\left[\frac{(P_i)^A (Q_i)^B}{RR_i} \right]^{1/a} = AA_i$$

$$P_i^C = BB_i$$

$$Q_i^D = DD_i$$

$$PC_i^E = EE_i$$

$$PD_i^F = FF_i$$

$$PH_i^H = HH_i$$

and rearranging gives:

$$1.\ \sum_{i=1}^{n} AA_i = R\sum_{i=1}^{n} 1 + \beta\sum_{i=1}^{n} BB_i + \gamma\sum_{i=1}^{n} DD_i + \varepsilon\sum_{i=1}^{n} EE_i + \phi\sum_{i=1}^{n} FF_i + \lambda\sum_{i=1}^{n} HH_i$$

$$2.\ \sum_{i=1}^{n} (AA_i)(BB_i) = R\Sigma BB_i + \beta\Sigma(BB_i)^2 + \gamma\Sigma(DD_i)(BB_i) + \varepsilon\Sigma(EE_i)(BB_i) + \phi\Sigma(FF_i)(BB_i) + \lambda\Sigma(HH_i)(BB_i)$$

$$3.\ \sum_{i=1}^{n} (AA_i)(DD_i) = R\Sigma DD_i + \beta\Sigma(BB_i)(DD_i) + \gamma\Sigma(DD_i)^2 + \varepsilon\Sigma(EE_i)(DD_i) + \phi\Sigma(FF_i)(DD_i) + \lambda\Sigma(HH_i)(DD_i)$$

$$4.\ \sum_{i=1}^{n} (AA_i)(EE_i) = R\Sigma EE_i + \beta\Sigma(BB_i)(EE_i) + \gamma\Sigma(DD_i)(EE_i) + \varepsilon\Sigma(EE_i)^2 + \phi\Sigma(FF_i)(EE_i) + \lambda\Sigma(HH_i)(EE_i)$$

$$5.\ \sum_{i=1}^{n} (AA_i)(FF_i) = R\Sigma FF_i + \beta\Sigma(BB_i)(FF_i) + \gamma\Sigma(DD_i)(FF_i) + \varepsilon\Sigma(EE_i)(FF_i) + \phi\Sigma(FF_i)^2 + \lambda\Sigma(HH_i)(FF_i)$$

$$6.\ \sum_{i=1}^{n} (AA_i)(HH_i) = R\Sigma HH_i + \beta\Sigma(BB_i)(HH_i) + \gamma\Sigma(DD_i)(HH_i) + \varepsilon\Sigma(EE_i)(HH_i) + \phi\Sigma(FF_i)(HH_i) + \lambda\Sigma(HH_i)^2$$

Indicating:

$\sum_{i=1}^{n} AA_i = SA$ $\qquad$ $\sum_{i=1}^{n} 1 = SN$

$\Sigma BB_i = SB$ $\qquad$ $\Sigma (BB_i)^2 = SBB$

$\Sigma DD_i = SD$ $\qquad$ $\Sigma (DD_i)^2 = SDD$

$\Sigma EE_i = SE$ $\qquad$ $\Sigma (EE_i)^2 = SEE$

$\Sigma FF_i = SF$ $\qquad$ $\Sigma (FF_i)^2 = SFF$

$\Sigma HH_i = SH$ $\qquad$ $\Sigma (HH_i)^2 = SHH$

$\sum_{i=1}^{n} (AA_i)(BB_i) = SAB$

$\Sigma (BB_i)(DDi) = \Sigma (DD_i)(BB_i) = SBD$

$\Sigma (BB_i)(EE_i) = \Sigma (EE_i)(BB_i) = SBE$

$\Sigma (BB_i)(FF_i) = \Sigma (FF_i)(BB_i) = SBF$

$\Sigma (BB_i)(HH_i) = \Sigma (HH_i)(BB_i) = SBH$

$$\sum_{i=1}^{n}(AA_i)(DD_i) = SAD$$

$$\Sigma(DD_i)(EE_i) = \Sigma(EE_i)(DD_i) = SDE$$

$$\Sigma(DD_i)(FF_i) = \Sigma(FF_i)(DD_i) = SDF$$

$$\Sigma(DD_i)(HH_i) = \Sigma(HH_i)(DD_i) = SDH$$

$$\sum_{i=1}^{n}(AA_i)(EE_i) = SAE$$

$$\Sigma(EE_i)(FF_i) = \Sigma(FF_i)(EE_i) = SEF$$

$$\Sigma(EE_i)(HH_i) = \Sigma(HH_i)(EE_i) = SEH$$

$$\sum_{i=1}^{n}(AA_i)(FF_i) = SAF$$

$$\Sigma(FF_i)(HH_i) = \Sigma(HH_i)(FF_i) = SFH$$

$$\sum_{i=1}^{n}(AA_i)(HH_i) = SAH$$

Rewriting the system of linear equations:

$$1\quad R(SN) + \beta(SB) + \gamma(SD) + \varepsilon(SE) + \phi(SF) + \lambda(SH) = SA$$
$$2\quad R(SB) + \beta(SBB) + \gamma(SBD) + \varepsilon(SBE) + \phi(SBF) + \lambda(SBH) = SAB$$
$$3\quad R(SD) + \beta(SBD) + \gamma(SDD) + \varepsilon(SDE) + \phi(SDF) + \lambda(SDH) = SAD$$
$$4\quad R(SE) + \beta(SBE) + \gamma(SDE) + \varepsilon(SEE) + \phi(SEF) + \lambda(SEH) = SAE$$
$$5\quad R(SF)\ \ \beta(SBF) + \gamma(SDF) + \varepsilon(SEF) + \phi(SFF) + \lambda(SFH) = SAF$$
$$6\quad R(SH)\ \ \beta(SBH) + \gamma(SDH) + \varepsilon(SEH) + \phi(SFH) + \lambda(SHH) = SAH$$

$$SA = B(1)$$
$$SAB = B(2)$$
$$SAD = B(3)$$
$$SAE = B(4)$$
$$SAF = B(5)$$
$$SAH = B(6)$$

This set of equations were solved by the digital computer ICL-1905 using a library program FH-ACSL issued by the International Computers Ltd.